

## STATUS OF THESIS

Title of thesis

**Studies Separation of Gas Mixtures by Membrane Processes**

I, FAROOQ AHMAD, here by allow my thesis to be placed at the Information Resource Center (IRC) of Universiti Teknologi PETRONAS (UTP) with the following conditions:

1. The thesis becomes the properties of UTP.
2. The IRC of UTP may make copies of the thesis for academic purposes only.
3. This thesis is classified as

Confidential

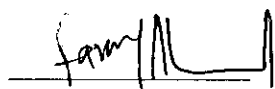
Non-confidential

If this thesis is confidential, please state the reason:

The contents of the thesis will remain confidential for years.

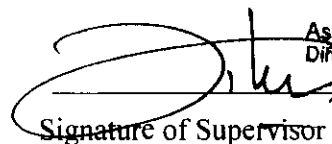
Remarks on disclosure:

Endorsed by



Signature of Author

Farooq Ahmad,  
Village and P.O.  
Tootkilli Distt &  
Teh; Mardan  
N.W.F.P Pakistan



Signature of Supervisor

Assoc Prof Dr Hilmi Mukhtar

Assoc. Prof. Dr. Hilmi Mukhtar  
Director, Undergraduate Studies

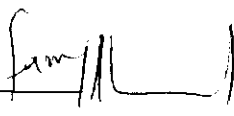
Date :

Date : 24/7/08

**UNIVERSITI TEKNOLOGI PETRONAS**

Approval by Supervisor (s)

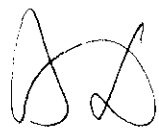
The undersigned certify that they have read, and recommend to The Postgraduate Studies Programme for acceptance, a thesis entitled “**Studies Separation of Gas Mixtures by Membrane Processes**” submitted by **Farooq Ahmad** for the fulfillment of the requirements for the degree of Doctor of Philosophy in Chemical Engineering.

24/7/08   
Date

Signature:   
Assoc. Prof. Dr. Hilmi Mukhtar  
Director, Undergraduate Studies

Main supervisor: Assoc Prof Dr Hilmi Mukhtar

Date: 24/7/08

Signature:    
Dr. Zakaria bin Man Senior Lecturer  
Chemical Engineering Programme  
Prof. Binay K. Dutta Professor  
Chemical Engineering Department  
UNIVERSITI TEKNOLOGI PETRONAS  
Co-Supervisors: Dr Zakaria Man, Prof. Binay Kanti Dutta

Date: 24/07/08

**UNIVERSITI TEKNOLOGI PETRONAS**

**Studies Separation of Gas Mixtures by Membrane  
Processes**

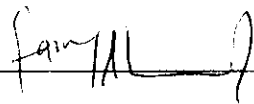
**By  
Farooq Ahmad**

**A THESIS  
SUBMITTED TO THE POSTGRADUATE STUDIES  
PROGRAMME AS A REQUIREMENT FOR THE  
DEGREE OF DOCTOR OF PHILOSOPHY IN  
CHEMICAL ENGINEERING  
BANDAR SERI ISKANDAR,  
PERAK**

**July 2008**

## DECLARATION

I hereby declare that the thesis is based on my original work except for quotations and citations which have been duly acknowledged. I also declare that it has not been previously or concurrently submitted for any other degree at UTP or other institutions.

Signature: 

Name : FAROOQ AHMAD

Date : 24/7/08

## ACKNOWLEDGEMENT

First and foremost, I would like to give my sincere thanks to ALLAH SWT, the Almighty, the source of my life and hope for giving me the strength and wisdom to complete the research.

I am most grateful to my supervisor Assoc. Prof. Dr. Hilmi Mukhtar for giving me an opportunity to pursue a PhD degree. Many times, his patience and constant encouragement has steered me to the right direction. I would also like to thank my co-supervisors Dr. Zakaria Man, Prof Binay Kanti Dutta for their suggestions and helps.

Again, I am most grateful to Prof. Binay for his support and help in my PhD work. Many times his help and ideas helped me a lot in completing my work on time. He always spared much time to help me.

I would like also express my gratitude to all technologists from UTP, En. Jailani, En Fauzi, En.Yusuf, En.Zaaba, En. Anwar, En. Shahafizan, En. Zikrullah, En. Mahadhir, Cik. Norhazneyza and Cik.Azimah for their effort in helping and providing me with the all chemicals and other experimental tools that I need for this research. Special thanks also to my postgraduate friends for their encouragement and friendship. My sincere thanks also to postgraduate office staffs, Pn.Norma, Pn.Haslina, Pn.Kamaliah, En. Fadhil and En. Borhan for their assistance during my study.

At last and most importantly, I would like to thank my family for their open-mindedness and endless support. They are always close to my heart.

## ABSTRACT

Gas separation using membrane process is getting more attention since the last decade. This is due to the advantages offered by the membrane process, such as, compactness, simplicity and energy savings.

The present work focuses on the study of permeability and selectivity characteristics of both porous and non-porous membranes for separation of carbon dioxide and other gases from natural gas. Pore flow model with capillary condensation mechanism have been used to explore the separation of carbon dioxide, hydrogen sulfide, propane, butane and nitrogen from its binary mixture with methane by a nano-porous membrane. The carbon dioxide from  $\text{CO}_2/\text{CH}_4$  binary mixture, hydrogen sulfide from  $\text{H}_2\text{S}/\text{CH}_4$  binary mixture, propane from  $\text{C}_3\text{H}_8/\text{CH}_4$  and butane from  $\text{C}_4\text{H}_{10}/\text{CH}_4$  binary mixture was found to preferentially permeate through the membrane pores thus blocking the flow of methane. The methane left on the permeate side was found to be slightly soluble in the condensed phase. In case of  $\text{N}_2/\text{CH}_4$  binary mixture, methane was found to be preferentially permeated through the membrane pores. The nitrogen left was found to be slightly soluble in the condensed methane. The Kelvin equation has been used to analyze the condensation phenomena. The highest permeability of  $1150 \text{ gmol/m}^2\cdot\text{s}\cdot\text{bar}$  for condensed carbon dioxide in  $\text{CO}_2/\text{CH}_4$  binary mixture was found followed by  $800 \text{ gmol/m}^2\cdot\text{s}\cdot\text{bar}$  for condensed methane in  $\text{N}_2/\text{CH}_4$ ,  $700 \text{ gmol/m}^2\cdot\text{s}\cdot\text{bar}$  for condensed hydrogen sulfide in  $\text{H}_2\text{S}/\text{CH}_4$  binary mixtures respectively. In case of C3 and C4 highest permeability of  $700 \text{ gmol/m}^2\cdot\text{s}\cdot\text{bar}$  were achieved for propane in  $\text{C}_3\text{H}_8/\text{CH}_4$  binary mixture, followed by  $500 \text{ gmol/m}^2\cdot\text{s}\cdot\text{bar}$  for butane in  $\text{C}_4\text{H}_{10}/\text{CH}_4$  binary mixture, respectively. The data obtained from the computed results were compared reasonably well with the published experimental data.

The separation factor of  $\text{N}_2/\text{CH}_4$  was found to be the highest with 439 followed by the separation of  $\text{H}_2\text{S}/\text{CH}_4$  and  $\text{CO}_2/\text{CH}_4$ , respectively. In case of lower hydrocarbons, C3 and C4, a highest selectivity of 140 was achieved in  $\text{C}_4\text{H}_{10}/\text{CH}_4$  binary mixture followed by 75 in  $\text{C}_3\text{H}_8/\text{CH}_4$  binary mixture, respectively.

Experimental work was conducted to study the permeability and selectivity of pure carbon dioxide, methane and its binary mixture at various feed pressure, temperature and composition through non-porous silicone rubber membranes. The permeability of pure methane and carbon dioxide was found to increase with pressure, where as such plots for carbon dioxide become convex towards pressure axis at higher pressure (17 bars) due to reduction in free volume of the polymer. The experimental results showed that for binary mixture of carbon dioxide and methane, permeability was found to be not only dependent on the feed gas pressure but also dependent on the molar composition of feed gas. The permeation flux was found to increase with pressure difference, and the enhancement of the proportion of the carbon dioxide in the feed gas. Experimental results showed that the selectivities estimated from pure gas varied slightly with an increase in the feed pressure but reached to a maximum value of 11.4. With 20 % CO<sub>2</sub> in the feed stream, the selectivity was found to be lower by a factor of two to three times than that of pure components over the whole pressure range. High selectivities were obtained at 80% CO<sub>2</sub> in the feed stream.

An analytical model expressed in terms of pressure and feed composition was derived from permeability behavior of pure carbon dioxide and methane to predict quantitatively the permeability of binary mixtures. It was indicated that the model could be used to evaluate the separation properties and to choose the optimal feed compositions for the membrane separation systems of carbon dioxide and methane.

## ABSTRAK

Pemisahan gas menggunakan proses membran semakin mendapat perhatian Sejak sedekad yang lalu. Ini disebabkan kelebihan yang ditawarkan oleh proses membran seperti penggunaan tenaga, kepadatan, mudah pakai dan penjimatan.

Penyelidikan ini memfokuskan kajian terhadap ke atas penelapan dan ciri-ciri pemisahan oleh kedua-dua membran berliang dan tidak berliang untuk pemisahan karbon dioksida dan gas-gas lain dari gas asli. Model aliran liang dengan mekanisme kondensasi kapilari telah digunakan untuk memeriksa dengan teliti pemisahan karbon dioksida, hidrogen sulfida, propana, butana dan nitrogen dari campuran binari dengan metana menggunakan membran berliang nano. Karbon dioksida dari campuran binari  $\text{CO}_2/\text{CH}_4$ , hidrogen sulfida dari campuran binari  $\text{H}_2\text{S}/\text{CH}_4$ , propana dari campuran binari  $\text{C}_3\text{H}_8/\text{CH}_4$  dan butana dari campuran binari  $\text{C}_4\text{H}_{10}/\text{CH}_4$  lebih utama meresapi menerusi liang membran, lantas menyekat pengaliran metana. Metana yang tertinggal di bahagian tidak terlelap terlarut sedikit di dalam fasa terpeluwap dan oleh itu kuantiti gas yang kecil meresapi melalui liang. Dalam kes campuran binari  $\text{N}_2/\text{CH}_4$ , metana lebih utama meresapi melalui liang membran. Nitrogen yang tertinggal terlarut sedikit di dalam metana yang terpeluwap. Persamaan Kelvin telah digunakan untuk menganalisa fenomena kondensasi tersebut. Kadar penelapan komponen yang terpeluwap dengan komponen tidak terpeluwap yang terlarut telah dikira untuk pelbagai parameter sistem seperti saiz liang, suhu, tekanan dan faktor pemisah telah dinilai untuk komposisi suapan yang berbeza. Telapan tertinggi  $1150 \text{ gmol/m}^2\cdot\text{s}\cdot\text{bar}$  untuk karbon dioksida terpeluwap dalam campuran binari  $\text{CO}_2/\text{CH}_4$  telah diperolehi diikuti oleh  $800 \text{ gmol/m}^2\cdot\text{s}\cdot\text{bar}$  untuk metana terpeluwap dalam  $\text{N}_2/\text{CH}_4$ ,  $700 \text{ gmol/m}^2\cdot\text{s}\cdot\text{bar}$  untuk hidrogen sulfida terpeluwap dalam campuran binari  $\text{H}_2\text{S}/\text{CH}_4$  secara berurutan. Bagi hydrocarbon rendah C3 dan C4, penelapan tertinggi  $700 \text{ gmol/m}^2\cdot\text{s}\cdot\text{bar}$  telah dicapai untuk propana dalam campuran binari  $\text{C}_3\text{H}_8/\text{CH}_4$ , diikuti  $500 \text{ gmol/m}^2\cdot\text{s}\cdot\text{bar}$  untuk butana dalam campuran binari  $\text{C}_4\text{H}_{10}/\text{CH}_4$  secara berurutan. Data yang diperolehi dari keputusan melalui pengiraan adalah sepadan dengan data eksperimen yang diterbitkan. Pemisahan  $\text{N}_2/\text{CH}_4$  didapati adalah yang tertinggi dengan 439 diikuti oleh pemisahan  $\text{H}_2\text{S}/\text{CH}_4$  dan  $\text{CO}_2/\text{CH}_4$  masing-masing. Bagi hydrocarbon

rendah C3 dan C4, kepemilihan tertinggi 140 telah dicapai di dalam campuran binari  $C_4H_{10}/CH_4$  diikuti dengan 75 di dalam campuran binari  $C_3H_8/CH_4$  secara berurutan.

Eksperimen telah dijalankan untuk mengkaji kebolehtelapan dan kepemilihan karbon dioksida tulen, metana dan campuran binarinya pada pelbagai tekanan, suhu dan komposisi suapan menerusi membran getah silikon tidak berliang. Kebolehtelapan metana tulen dan karbon dioksida didapati meningkat dengan tekanan di mana lakaran graf untuk karbon dioksida melengkung ke arah paksi tekanan pada tekanan tinggi (17 bar) disebabkan oleh pengurangan isipadu bebas polimer. Keputusan eksperimen menunjukkan bahawa untuk campuran binari karbon dioksida dan metana, kebolehtelapan bukan sahaja bergantung kepada tekanan gas suapan tetapi juga kepada komposisi molar gas suapan. Fluks penelapan meningkat dengan peningkatan perbezaan tekanan, dan penambahan nisbah kandungan karbon dioksida di dalam gas suapan. Keputusan eksperimen menunjukkan bahawa kepemilihan yang dianggarkan dari gas tulen berbeza sedikit dengan peningkatan di dalam tekanan suapan tetapi mencapai nilai maksima 11.4. Dengan 20%  $CO_2$  di dalam aliran suapan, kepemilihan adalah dua hingga tiga kali ganda lebih rendah dari kepemilihan komponen tulen pada keseluruhan julat tekanan. Kepemilihan tinggi diperolehi untuk 80%  $CO_2$  di dalam aliran suapan.

Sebuah model analitikal yang dinyatakan dari segi tekanan dan komposisi suapan telah diterbitkan dari perilaku penelapan karbon dioksida tulen dan metana untuk meramal kebolehtelapan campuran binari secara kuantitatif. Ia menunjukkan bahawa model tersebut boleh digunakan untuk menilai ciri-ciri pemisah dan untuk memilih komposisi suapan optima bagi sistem pemisahan membran untuk karbon dioksida dan metana.

## TABLE OF CONTENTS

STATUS OF THESIS	i
APPROVAL PAGE	ii
TITLE PAGE	iii
DECLARATION	iv
ACKNOWLEDGEMENT	v
ABSTRACT	vi
ABSTRAK	viii
TABLE OF CONTENTS	1
LIST OF TABLES	5
LIST OF FIGURES	8
NOMENCLATURES	13
<b>CHAPTER 1: INTRODUCTION</b>	<b>16</b>
1.1 Natural Gas	16
1.2 Natural Gas in Malaysia	17
1.3 Carbon Dioxide in Natural Gas	18
1.4 Recent Technologies for Natural Gas Purification	19
1.4.1 Absorption	19
1.4.2 Adsorption	22
1.4.3 Cryogenic Technology	23
1.4.4 Membrane Technology	24
1.5 Comparison between Membrane process and Conventional Processes for Natural Gas Purification	27
1.6 Problem Statement	29
1.7 Objective of Study	30
1.8 Scope of Study	31

1.8.1	Development of Simulation Model	32
1.8.2	Permeability of Pure CO <sub>2</sub> , CH <sub>4</sub> and its Binary Mixture CO <sub>2</sub> /CH <sub>4</sub> Through Silicon Rubber Membranes	32
1.9	Organization of Thesis	32
<b>CHAPTER 2: LITERATURE REVIEW</b>		<b>34</b>
2.1	Membrane Types and Applications	34
2.1.1	Porous Membrane	34
2.1.2	Non-porous Membrane	35
2.2	Gas Transport Through Membrane	36
2.2.1	Gas Transport Through Porous Membrane	36
2.2.2	Gas Transport Thorough Non- Porous Membrane	43
2.3	Theory of Gas Permeation Through Polymer Membranes	44
2.3.1	Introduction	44
2.3.2	Gas Permeation in Glassy Polymers	46
	2.3.2.1 Sorption of Gases in Glassy Polymer	47
	2.3.2.2 Diffusion of Gases in Glassy Polymer	48
2.3.3	Gas Permeation in Rubbery Polymers	49
	2.3.3.1 Sorption	49
	2.3.3.2 Diffusion	49
	2.3.3.3 Mixed Gas Sorption	49
	2.3.3.4 Mixed Gas Diffusion	50
2.3.4	Gas Permeability Through Silicone Rubber	50
2.4	Effects of Operating Conditions on Polymer Permeability	50
2.4.1	Effect of Temperature on Permeability	50
2.4.2	Effect of Pressure and Concentration on Permeability	52
2.5	Mixed Gas Permeability from Pure Gases by Analytical Model	54
		57
<b>CHAPTER 3: DEVELOPMENT OF MEMBRANE MODEL</b>		
3.1	Introduction	57

3.2	Theory	59
3.3	Assumptions Used in Simulation Model	61
3.4	Algorithm Used in Simulation Model	62
3.5	Validation of the Model	65
3.6	Results and Discussions	67
3.6.1	Methane/Carbon Dioxide System	67
3.6.2	Methane/Propane System	68
3.6.3	Methane/Butane System	70
3.6.4	Methane/Hydrogen Sulfide System	72
3.6.5	Methane/Nitrogen System	74
3.6.7	Selectivity of Nano-Porous Membranes	76
	<b>CHAPTER 4: MATERIALS AND METHODS</b>	<b>85</b>
4.1	Materials	85
4.2	Membrane Characterization	85
4.2.1	Scanning Electron Microscopy (SEM)	85
4.2.2	Energy Dispersive X-ray Spectroscopy (EDX)	86
4.2.3	Thermo Gravimetric Analysis (TGA)	86
4.2.4	Differential Scanning Calorimetry (DSC)	87
4.3	Methods	87
4.3.1	Experimental Set Up	87
4.3.2	Experimental Procedures	90
4.3.3	Analysis of Experimental Results	91
	<b>CHAPTER 5: RESULTS AND DISCUSSIONS</b>	<b>93</b>
5.1	Membrane Characterizations	93
5.2	Permeability of Pure Gases	96
5.2.1	Effect of Feed Pressure on Permeability	96

5.2.2	Effect of Temperature on Permeability	99
5.3	Permeability of Binary Mixture of CO <sub>2</sub> /CH <sub>4</sub>	103
5.3.1	Effect of Pressure, Temperature and Feed Composition	103
5.4	Separation Study Through Silicone Rubber Membranes	110
5.4.1	Effect of Pressure, Temperature and Feed Composition on Selectivity	110
5.5	Interpretation of Experimental Data Using Analytical Model	114
 <b>CHAPTER 6: CONCLUSIONS AND RECOMMENDATIONS</b>		132
6.1	Conclusions	132
6.2	Recommendations	134
 <b>REFERENCES</b>		135
APPENDIX A	Physical Properties of Acid gases, C <sub>3</sub> and C <sub>4</sub> at different Temperature.	146
APPENDIX B	Pure Gas Permeability of CO <sub>2</sub> and CH <sub>4</sub> at Different Pressure and at Constant Temperature of 25°C.	149
APPENDIX C	Pure Gas Permeability of CO <sub>2</sub> and CH <sub>4</sub> at Different Temperature and at Constant Pressure of 8 bar.	154
APPENDIX D	Permeability of CO <sub>2</sub> and CH <sub>4</sub> in Binary Mixture (CO <sub>2</sub> +CH <sub>4</sub> ) at Different Pressure and at Constant Temperature 25°C.	159
APPENDIX E	Permeability of CO <sub>2</sub> and CH <sub>4</sub> in Binary Mixture ( CO <sub>2</sub> +CH <sub>4</sub> ) at Different Temperature and at Constant Pressure of 8 bar.	176
APPENDIX F	Papers Published and Presented in International Journals and Conferences.	192

## LIST OF TABLES

Table 1.1	Composition of raw natural gas.	16
Table 1.2	Typical impurities composition allowed in natural gas for the delivery to the U.S pipe line.	17
Table 1.3	Pipe line composition of natural gas.	18
Table 1.4	Composition of carbon dioxide in some natural gas wells.	19
Table 1.5	Status of membrane for gas separation process.	26
Table 1.6	Industrial membranes for CO <sub>2</sub> separation from natural gas.	27
Table 1.7	Comparisons of the absorption process and membrane process for CO <sub>2</sub> removal.	29
Table 3.1	The selected operating conditions and separation strategy for binary systems.	63
Table 3.2	Solubility for methane / carbon dioxide system.	77
Table 3.3	Solubility for methane /propane system.	78
Table 3.4	Solubility for methane / butane system.	80
Table 3.5	Comparison of the computed equilibrium data with the experimental data of Kohn and Kurata (1958).	81
Table 3.6	Solubility for methane /hydrogen sulfide system.	82
Table 3.7	Solubility for methane/nitrogen system.	83
Table 4.1	Capabilities of the gas membrane unit.	88
Table 4.2	Summary of the Selected operating conditions for experimental study.	91
Table 5.1	Selectivity of CO <sub>2</sub> over CH <sub>4</sub> through silicone rubber membrane M <sub>1</sub> at different pressure.	111
Table 5.2	Selectivity of CO <sub>2</sub> over CH <sub>4</sub> through silicone rubber membrane M <sub>2</sub> at different pressure.	112
Table 5.3	Selectivity of CO <sub>2</sub> over CH <sub>4</sub> through silicone rubber membrane M <sub>3</sub> at different pressure.	112
Table 5.4	Selectivity of CO <sub>2</sub> over CH <sub>4</sub> through silicone rubber membrane M <sub>1</sub> at different temperature.	113
Table 5.5	Selectivity of CO <sub>2</sub> over CH <sub>4</sub> through silicone rubber membrane M <sub>2</sub> at different temperature.	113

Table 5.6	Selectivity of CO <sub>2</sub> over CH <sub>4</sub> through silicone rubber membrane M <sub>3</sub> at different temperature.	114
Table 5.7	Linear fitting equations for pure CO <sub>2</sub> and pure CH <sub>4</sub> permeability at different pressure across silicone rubber membrane M, M <sub>1</sub> , M <sub>3</sub> .	115
Table 5.8	Permeability of carbon dioxide at its partial pressure through silicone rubber membrane M <sub>1</sub> .	115
Table 5.9	Permeability of methane at its partial pressure through silicone rubber membrane M <sub>1</sub> .	116
Table 5.10	Polymath results for co-efficients <i>m</i> , <i>n</i> , and <i>l</i> for silicone rubber membrane M <sub>1</sub> for CO <sub>2</sub> permeability.	116
Table 5.11	Percentage error between experimental permeability and calculated permeability of carbon dioxide through silicone rubber membrane M <sub>1</sub> .	118
Table 5.12	Permeability of carbon dioxide at its partial pressure through silicone rubber membrane M <sub>2</sub> .	119
Table 5.13	Permeability of methane at its partial pressure through silicone rubber membrane M <sub>2</sub> .	120
Table 5.14	Permeability of carbon dioxide at its partial pressure through silicone rubber membrane M <sub>3</sub> .	121
Table 5.15	Permeability of methane at its partial pressure through silicone rubber membrane M <sub>3</sub> .	122
Table 5.16	Polymath results for co-efficients <i>m</i> , <i>n</i> , and <i>l</i> for CO <sub>2</sub> permeability through silicone rubber membrane M <sub>2</sub> .	122
Table 5.17	Polymath results for co-efficients <i>m</i> , <i>n</i> , and <i>l</i> for CO <sub>2</sub> permeability through silicone rubber membrane M <sub>3</sub> .	123
Table 5.18	Percentage error between experimental permeability and calculated permeability of carbon dioxide through siliconerubber membrane M <sub>2</sub> .	125
Table 5.19	Percentage error between experimental permeability and calculated permeability of carbon dioxide through siliconerubber membrane M <sub>3</sub> .	125
Table 5.20	Polymath results for co-efficients <i>m</i> , <i>n</i> , and <i>l</i> for CH <sub>4</sub> permeability through silicone rubber membrane M <sub>1</sub> .	126
Table 5.21	Percentage error between experimental permeability and calculated. Permeability of methane through silicone rubber membrane M <sub>1</sub> .	127
Table 5.22	Polymath results for co-efficients <i>m</i> , <i>n</i> , and <i>l</i> for CH <sub>4</sub> permeability	128

through silicone rubber membrane M<sub>2</sub>.

Table 5.23	Polymath results for co-efficients $m$ , $n$ , and $l$ for CH <sub>4</sub> permeability through silicone rubber membrane M <sub>3</sub> .	128
Table 5.24	Percentage error between experimental permeability and calculated permeability of methane through silicone rubber membrane M <sub>2</sub> .	129
Table 5.25	Percentage error between experimental permeability and calculated permeability of methane through silicone rubber membrane M <sub>3</sub> .	130

## LIST OF FIGURES

Figure 1.1	Schematic representation of membrane process.	24
Figure 2.1	Schematic presentation of mechanisms for permeation of gases through membranes.	37
Figure 2.2	Six flow modes of Lee and Hwang (1986) for flow of condensable gases through small pores.	44
Figure 2.3	Solution-diffusion mechanism.	53
Figure 2.4	Pressure dependencies of various penetrant-polymer systems.	55
Figure 3.1	Schematic of condensation flow through a nano pore.	59
Figure 3.2	Algorithm to find capillary condensation pressure, permeability and selectivity for model binary systems ( $\text{CO}_2/\text{CH}_4$ , $\text{C}_3\text{H}_8/\text{CH}_4$ , $\text{C}_4\text{H}_{10}/\text{CH}_4$ , $\text{H}_2\text{S}/\text{CH}_4$ , $\text{N}_2/\text{CH}_4$ ).	64
Figure 3.3	Comparison of experimental condensation pressure (bar) for methanol hydrogen separation by Sperry et al (1991) with data predicted using Kelvin equation.	66
Figure 3.4	Comparison of the experimental separation factor for methanol–hydrogen system by Sperry et.al (1991) with the model prediction.	66
Figure 3.5	Condensation pressure of carbon dioxide at constant temperature of 190K for different pore size.	67
Figure 3.6	Condensation pressure of carbon dioxide for different pore size and at different temperature.	68
Figure 3.7	Permeability of carbon dioxide at various pore size for different temperature.	68
Figure 3.8	Condensation pressure of propane with pore size at constant temperature at 360K.	69
Figure 3.9	Condensation pressure of propane with pore size at different temperature.	69
Figure 3.10	Permeability of propane with pore size at different temperature.	70
Figure 3.11	Condensation pressure of butane with pore size at constant temperature 360K.	71
Figure 3.12	Condensation pressure of butane with pore size at different temperature.	71
Figure 3.13	Permeability of butane with pore size at different temperature.	72

Figure 3.14	Condensation pressure of hydrogen sulfide with pore size at constant temperature 190K.	73
Figure 3.15	Condensation pressure of hydrogen sulfide with temperature for different pore size.	73
Figure 3.16	Permeability of hydrogen sulfide with temperature for different pore size.	74
Figure 3.17	Condensation pressure of Methane with pore size at constant temperature 190K.	75
Figure 3.18	Condensation pressure of methane with pore size at different temperature.	75
Figure 3.19	Permeability of methane with temperatures for different pore size.	76
Figure 3.20	Selectivity for different CO <sub>2</sub> -CH <sub>4</sub> model binary system at different temperature.	77
Figure 3.21	Selectivity of methane/propane binary mixtures with temperature.	79
Figure 3.22	Selectivity of methane / butane binary mixtures with temperature.	79
Figure 3.23	Selectivity of H <sub>2</sub> S/CH <sub>4</sub> binary mixture at different temperature.	81
Figure 3.24	Selectivity of N <sub>2</sub> /CH <sub>4</sub> binary mixtures at various temperatures.	82
Figure 4.1	Schematic diagram of the membran separation unit.	88
Figure 4.2	Membrane Separation Unit	89
Figure 5.1	SEM image of silicone rubber membrane.	93
Figure 5.2	TGA analysis showing thermal degradation temperature of silicone rubber membrane.	94
Figure 5.3	DSC analysis of silicone rubber membrane showing glass transition temperature of silicone rubber membrane.	95
Figure 5.4	Permeability of pure CO <sub>2</sub> and pure CH <sub>4</sub> permeability through M <sub>1</sub> silicone rubber membrane with different pressure at 25°C.	97
Figure 5.5	Permeability of pure CO <sub>2</sub> and pure CH <sub>4</sub> permeability through M <sub>2</sub> siliconerubber membrane with different pressure at 25°C.	97
Figure 5.6	Permeability of pure CO <sub>2</sub> and pure CH <sub>4</sub> permeability through M <sub>3</sub> silicone rubber membrane with different pressure at 25°C.	98
Figure 5.7	Comparison of CO <sub>2</sub> permeability against pressure across silicone rubber membranes M <sub>1</sub> , M <sub>2</sub> and M <sub>3</sub> .	99
Figure 5.8	Comparison of CH <sub>4</sub> permeability against pressure across silicone rubber membranes M <sub>1</sub> , M <sub>2</sub> and M <sub>3</sub> .	99
Figure 5.9	Permeability of pure CO <sub>2</sub> and CH <sub>4</sub> through M <sub>1</sub> silicone rubber membrane	100

against temperature at 8 bar.

Figure 5.10	Permeability of pure CO <sub>2</sub> and CH <sub>4</sub> through M <sub>2</sub> silicone rubber membrane against temperature at 8 bar.	101
Figure 5.11	Permeability of pure CO <sub>2</sub> and CH <sub>4</sub> through M <sub>3</sub> silicone rubber membrane against temperature at 8 bar.	101
Figure 5.12	Comparison of CO <sub>2</sub> permeability against temperature across silicone rubber membranes M <sub>1</sub> , M <sub>2</sub> and M <sub>3</sub> .	102
Figure 5.13	Comparison of CH <sub>4</sub> permeability against temperature across silicone rubber membranes M <sub>1</sub> , M <sub>2</sub> and M <sub>3</sub> .	102
Figure 5.14	Permeability of CO <sub>2</sub> through silicone rubber membrane M <sub>1</sub> in binary mixture of CO <sub>2</sub> /CH <sub>4</sub> against pressure at 25°C.	103
Figure 5.15	Permeability of CO <sub>2</sub> through silicone rubber membrane M <sub>2</sub> in binary mixture of carbon dioxide and methane against pressure at 25°C.	103
Figure 5.16	Permeability of CO <sub>2</sub> through silicone rubber membrane M <sub>3</sub> in binary mixture of carbon dioxide and methane against at 25°C.	104
Figure 5.17	Permeability of CO <sub>2</sub> through M <sub>1</sub> silicone rubber membrane in binary mixture of carbon dioxide and methane against temperature at 8 bar.	104
Figure 5.18	Permeability of CO <sub>2</sub> through M <sub>2</sub> silicone rubber membrane in binary mixture of carbon dioxide and methane against temperature at 8 bar.	105
Figure 5.19	Permeability of CO <sub>2</sub> through M <sub>3</sub> silicone rubber membrane in binary mixture of carbon dioxide and methane against temperature at 8 bar.	105
Figure 5.20	Permeability of CH <sub>4</sub> through M <sub>1</sub> silicone rubber membrane in binary mixtures of carbon dioxide and methane against pressure at 25°C.	106
Figure 5.21	Permeability of CH <sub>4</sub> through M <sub>2</sub> silicone rubber membrane in binary mixtures of carbon dioxide and methane against pressure at 25°C.	106
Figure 5.22	Permeability of CH <sub>4</sub> through M <sub>3</sub> silicone rubber membrane in binary mixtures of carbon dioxide and methane against pressure at 25°C.	107
Figure 5.23	Permeability of CH <sub>4</sub> through M <sub>1</sub> silicone rubber membrane in binary mixture of carbon dioxide and methane against temperature at 8 bar.	107
Figure 5.24	Permeability of CH <sub>4</sub> through M <sub>2</sub> silicone rubber membrane in binary mixture of carbon dioxide and methane against temperature at 8 bar.	108
Figure 5.25	Permeability of CH <sub>4</sub> through M <sub>3</sub> silicone rubber membrane in binary mixture of carbon dioxide and methane with different temperature at 8 bar	108

Figure 5.26	Comparison of CO <sub>2</sub> permeability against pressure in binary mixture (60% CO <sub>2</sub> - 40%CH <sub>4</sub> ) across silicone rubber membranes M <sub>1</sub> , M <sub>2</sub> and M <sub>3</sub> .	109
Figure 5.27	Comparison of CO <sub>2</sub> permeability against temperature in binary mixture (60% CO <sub>2</sub> - 40%CH <sub>4</sub> ) across silicone rubber membranes M <sub>1</sub> , M <sub>2</sub> and M <sub>3</sub> .	109
Figure 5.28	Comparison of CH <sub>4</sub> permeability against pressure in binary mixture (60% CO <sub>2</sub> - 40%CH <sub>4</sub> ) across silicone rubber membranes M <sub>1</sub> , M <sub>2</sub> and M <sub>3</sub> .	110
Figure 5.29	Comparison of CH <sub>4</sub> permeability against temperature in binary mixture (60% CO <sub>2</sub> - 40%CH <sub>4</sub> ) across silicone rubber membranes M <sub>1</sub> , M <sub>2</sub> and M <sub>3</sub> .	110
Figure 5.30	Comparison of experimental and calculated permeabilities of CO <sub>2</sub> through M <sub>1</sub> silicone rubber membrane in binary mixtures of methane and carbon dioxide at different pressure.	117
Figure 5.31	Comparison of experimental and calculated permeabilities of CO <sub>2</sub> through M <sub>1</sub> silicone rubber membrane in binary mixture (40% CO <sub>2</sub> -60% CH <sub>4</sub> ) at different pressure.	118
Figure 5.32	Comparison of experimental and calculated permeabilities of CO <sub>2</sub> through M <sub>2</sub> silicone rubber membrane in binary mixtures of methane and carbon dioxide at different pressure.	123
Figure 5.33	Comparison of experimental and calculated permeabilities of CO <sub>2</sub> through M <sub>3</sub> silicone rubber membrane in binary mixtures of methane and carbon dioxide at different pressure.	123
Figure 5.34	Comparison of experimental and calculated permeabilities of CO <sub>2</sub> through M <sub>2</sub> silicone rubber membrane in binary mixture (40% CO <sub>2</sub> -60% CH <sub>4</sub> ) at different pressure.	124
Figure 5.35	Comparison of experimental and calculated permeabilities of CO <sub>2</sub> through M <sub>3</sub> silicone rubber membrane in binary mixture (40%CO <sub>2</sub> -60% CH <sub>4</sub> ) at different pressure.	124
Figure 5.36	Comparison of experimental and calculated permeabilities of CH <sub>4</sub> through M <sub>1</sub> silicone rubber membrane in binary mixture of methane and carbon dioxide at different pressure.	126
Figure 5.37	Comparison of experimental and calculated permeabilities of CH <sub>4</sub> through M <sub>1</sub> silicone rubber membrane in binary mixture (40% CO <sub>2</sub> -60% CH <sub>4</sub> ) at different pressure.	127

- Figure 5.38 Comparison of experimental and calculated permeabilities of CH<sub>4</sub> through M<sub>2</sub> silicone rubber membrane in binary mixture of methane and carbon dioxide at different pressure. 128
- Figure 5.39 Comparison of experimental and calculated permeabilities of CH<sub>4</sub> through M<sub>3</sub> silicone rubber membrane in binary mixture of methane and carbon dioxide at different pressure. 129
- Figure 5.40 Comparison of experimental and calculated permeability of CH<sub>4</sub> through M<sub>2</sub> silicone rubber membrane in binary mixture (40% CO<sub>2</sub>-60% CH<sub>4</sub>) at different pressure. 130
- Figure 5.41 Comparison of experimental and calculated permeability of CH<sub>4</sub> through M<sub>3</sub> silicone rubber membrane in binary mixture (40% CO<sub>2</sub>-60% CH<sub>4</sub>) at different pressure. 131

## NOMENCLATURES

$A'$	Membrane area	(m)
$A$	Root for compressibility factor	(-)
$a$	Attractive parameter	$(\text{Jm}^3/\text{mol}^2)$
$B$	Root for compressibility factor	(-)
$b$	Excluded volume parameter	$(\text{m}^3/\text{mol})$
$b'$	Hole affinity constant	(1/bar)
$C_s$	Concentration of gas molecule	(mol/L)
$C_D$	Concentration by normal dissolution	(mol/L)
$C_H$	Concentration by hole filling	(mol/L)
$D$	Diffusivity Coefficient	$(\text{cm}^2/\text{s})$
$D_o$	Pre-exponential factor	$(\text{cm}^2/\text{s})$
$D_S$	Surface diffusivity Co-efficient	$(\text{cm}^2/\text{s})$
$d$	Diameter of pore	(m)
$E_D$	Activation energy	(kJ/mol K)
$f$	Equilibrium loading factor	$(\text{m}^3/\text{kg})$
$f^l$	Liquid fugacity	(bar)
$f^v$	Vapor fugacity	(bar)
$G_{vis}$	Viscous gas flux	$(\text{m}^3/\text{m}^2.\text{s})$
$J$	Gas flux	$(\text{m}^3/\text{m}^2.\text{s})$
$K_d$	Constant Parameter	(mol.m)
$K_D$	Henry's law dissolution constant	$(\text{bar.cm}^3/\text{mol})$
$l$	Membrane thickness	(m)
$L$	Pore length	(m)
$M$	Molecular weight	(kg/gmol)
$m,n,l$	Co-efficients	(-)
$P$	Permeability	(barrer)
$P_{\text{surface}}$	Permeability due to surface diffusion	(barrer)
$P_{\text{Knudsen}}$	Permeability due to Knudsen diffusion	(barrer)
$p$	Pressure	(bar)
$P_t$	Apparent permeability	$(\text{gmol}/\text{m}^2.\text{s}.\text{bar})$

$P_{CO_2 \text{ mix}}$	Permeability of CO <sub>2</sub> at its partial pressure	(barrer)
$p_{CH_4 \text{ pure}}$	Permeability of CH <sub>4</sub> at its partial pressure	(barrer)
$P_1$	Partial pressure of the gas on the feed side	(bar)
$P_2$	Partial pressure of the gas on the permeate side	(bar)
$P_0$	Vapor pressure	(bar)
$p_o$	Pre-exponential factor for permeability	(barrer)
$P_{con}$	Condensation pressure	(bar)
$Q$	Volumetric flow rate	(cm <sup>3</sup> /s)
$Q_{stp}$	Volumetric flow rate at standard temperature and pressure	(cm <sup>3</sup> (STP)/s)
$p$	Pressure	(bar)
$R$	Universal gas constant	(kJ/mol.K)
$r$	Pore radius	(nm)
$S$	Henry's law solubility coefficient	(cm <sup>3</sup> (STP)/cm <sup>3</sup> .atm)
$T$	Temperature	(°C or K)
$T_g$	Glass transition temperature	(°C or K)
$Tr$	Reduced temperature	(-)
$T_c$	Critical temperature	(K)
$t$	Thickness of the adsorbed layer	(nm)
$t_1$	Thickness of the adsorbed layer at upstream end of the pore	(nm)
$t_2$	Thickness of the adsorbed layer at downstream end of the pore	(nm)
$t_m$	Membrane thickness	(mm)
$V_m$	Molar volume	(cm <sup>3</sup> /mol)
$X$	Mol fraction	(-)
$Z_l$	Liquid compressibility factor	(-)
$Z_v$	Vapor compressibility factor	(-)
$Z$	Parameter	(-)

## GREEK SYMBOLS USED

$\alpha$	Selectivity	(-)
$(\Delta H)_s$	Partial molar enthalpy of sorption	(J/mol)
$(\Delta H)_{condensation}$	Partial molar enthalpy of condensation	(J/mol)
$(\Delta H)_{mixing}$	Partial molar enthalpy of mixing	(J/mol)
$\theta$	Contact angle between the liquid and the pore wall	(°)
$\omega$	Acentric factor for species	(-)
$\lambda$	Mean free path	(m)
$\mu$	Viscosity	(Pa.s)
$\rho_m$	Membrane density	(g/cm <sup>3</sup> )
$\varepsilon$	Membrane porosity	(-)
$\sigma$	Interfacial tension	(N.m)
$\alpha''$	Constant parameter	(-)

## CHAPTER 1

### INTRODUCTION

#### 1.1. Natural Gas

Natural gas is a fuel that burns cleaner than many other fossil fuels (Pascoli et al, 2001). It is used for heating, cooling, and production of electricity and it finds many uses in industry. Natural gas is more environmentally attractive than other fossil fuels because when burns it emits lower quantities of green house gases than do other fossil fuels (Pascoli et al, 200). The composition of raw natural gas varies from one location to another (Rojey et al, 1997). Basically, methane is the major component in raw natural gas, comprising typically 75-90% of the total component (Baker, 2004). Natural gas also contains significant amount of ethane, propane, butane and other higher hydrocarbons (Mohammed Awad, 2004). In addition, natural gas may also contain undesirable impurities such as carbon dioxide, hydrogen sulfide and nitrogen (Baker 2004). Table 1.1 shows composition of raw natural gas and implication of impurities in natural gas (Ahmad et al, 2006).

**Table 1.1** Composition of raw natural gas.

Component	Composition	Remarks
CH <sub>4</sub>	<90%	Major combustible constituent
C <sub>2</sub> H <sub>6</sub>	>3%	Lower hydrocarbon causing an increase in dewpoint of natural gas
C <sub>3</sub> H <sub>8</sub>	>0.505	
C <sub>4+</sub>	>0.20%	
CO <sub>2</sub>	More than 2%	Corrosion ,Acidic, Lower heating value (Dotmundt, 1999)
N <sub>2</sub>	4% Nitrogen	Undesirable constituent , must be reduced to pipe line quality
H <sub>2</sub> S	Traces	Toxic and corrosive (Spillman, 1989)

All these impurities need to be separated from natural gas in order to meet the pipeline specification for natural gas delivery. Typical impurities composition allowed in US for the delivery of natural gas to the pipeline are shown in the Table 1.2 (Baker, 2004).

**Table 1.2** Typical impurities composition allowed in natural gas for the delivery to the U.S pipeline.

Component	Specification
CO <sub>2</sub>	< 2 mole %
H <sub>2</sub> O	< 120 ppm
H <sub>2</sub> S	< 4 ppm
Total inerts ( N <sub>2</sub> , He, Ar etc.)	< 4 mole %

## 1.2. Natural Gas in Malaysia

As one of the natural gas producers in the world, Malaysia produces about 53.9 billion cubic metres of natural gas from the total worldwide production of about 2691.6 cubic metres in 2004 (Gas Malaysia, 2003). In addition, during the last decades, Malaysia's proven reserves of natural gas have increased quite significantly from 1.39 trillion cubic metres to 2.4 6 trillion cubic metres in 2004 (Gas Malaysia, 2005). This huge reserve of natural gas is an important asset for Malaysian government to meet the growing demand of energy in the future.

Gas Malaysia Bhd. has more strict limits than US for pipe line composition of natural gas. Table 1.3 below shows the required quality (pipe line quality) of treated natural gas as suggested by (Spillman, 1989) as well as that stipulated by Gas Malaysia.

**Table 1.3** Pipe line quality of natural gas.

Component	Composition % (Spillman et al, 1989)	Composition % (Gas Malaysia, 2005)
CH <sub>4</sub>	93.60	92.73
C <sub>2</sub> H <sub>6</sub>	3.00	4.03
C <sub>3</sub> H <sub>8</sub>	0.50	0.77
C <sub>4+</sub>	0.20	0.15
CO <sub>2</sub>	2.00 max	1.83 max
He	0.06	Trace
H <sub>2</sub>	0.04	Trace
O <sub>2</sub>	Trace	Trace
Hg	Trace	Trace
N <sub>2</sub>	Trace	Trace
H <sub>2</sub> S	Trace	Trace

### 1.3. Carbon Dioxide in Natural Gas

One of these impurities that need to be separated from natural gas is carbon dioxide. Carbon dioxide composition in natural gas varies between gas fields. Table 1.4 shows the composition of carbon dioxide in some natural gas wells in the world (Roje et al, 1997). Some gas fields only has trace amount of CO<sub>2</sub> such as in Xinjiang, China while in other places such as in Natuna, Indonesia, extremely high CO<sub>2</sub> content (71mole %) is discovered (Suhartanto et al, 2001). It is well known that carbon dioxide in the presence of water is highly corrosive that can rapidly destroy the pipeline and equipment system. Specifically for LNG plant, the natural gas is cooled down to very low temperature that can make CO<sub>2</sub> become solid. However, for pipeline transportation, the solidification of CO<sub>2</sub> must be prevented as it may block the pipeline system and cause transportation problem.

**Table 1.4** Composition of carbon dioxide in some natural gas wells (Rojey et al, 1997).

Location	CO <sub>2</sub> (mg/l)
Lacq (France)	9.3%
Frigg (Norway)	0.3%
Uch (Pakistan)–	46.2%
Kapuni (New Zealand)–	43.8%
Uthmaniyah (Saudi Arabia)	8.9%
Terengganu (Malaysia)	7%
Lacq (France)	9.3%
Frigg (Norway)	0.3%
Duri, Indonesia	23.0

In addition, the presence of CO<sub>2</sub> will also reduce the heating value of natural gas and eventually the selling price of natural gas will be lowered. Therefore, CO<sub>2</sub> removal from natural gas is necessary in order to improve the quality of natural gas produced (Dortmundt et al, 1999).

#### **1.4. Recent Technologies for Natural Gas Purification**

A wide range of technologies are currently available for natural gas purification. These include amine-based or hot potassium carbonate-based absorption process, adsorption technology and membrane technology. However, each of these technologies has some limitation for purifying natural gas. Most commercial processes to remove acid gas in bulk quantity involve the use of amine, usually alkanolamines, as chemical solvent in absorption technology due to its outstanding performance (Kohl et al, 1979).

##### **1.4.1. Absorption**

Absorption, is a physical or chemical phenomenon or a process in which atoms, molecules, or ions enter some bulk phase - gas, liquid or solid material. This is a different process from adsorption, since the molecules are taken up by the volume, not

by surface. A more general term is sorption which covers both adsorption and absorption. Monoethanolamine (MEA) and diethanolamine (DEA) are two types of alkanolamines that have been most widely used to remove acid gases from natural gas (Jou et al, 1983). Recently, methyldiethanolamine (MDEA) was found to be a potential chemical in separating acid gases from natural gas. The choice of type of amine solutions used are primarily dependent on the partial pressure of acid gas in the feed gas stream and on the level of acid gas desired in the treated gas (Sartori et al, 1983). MEA is normally required for low feed pressure gas stream and for stringent outlet gas specifications. DEA is suitable for medium and high pressure feed stream treatment while MDEA has better interaction to  $H_2S$  than  $CO_2$ , which makes it preferable to be used for high  $H_2S$  content treatment (Kohl et al, 1979).

The removal of acid gases using amines is usually carried out at elevated pressure and lower temperature. The natural gas containing acid gases is contacted with amine solution on an absorber column. Some set of chemical reactions will take place between the amine solution and acid gases. If MEA ( $RNH_2$ ) or DEA ( $R_2NH$ ) is used as absorbent, the absorption of  $CO_2$  can not exceed 0.5 mol of  $CO_2$ /mol of amine due to formation of carbamic acid ( $R_2NCOOH$ ) (Sartori,1983). This is one of the disadvantages of using MEA or DEA in  $CO_2$  removal from natural gas. However, the formation of carbamic acid can be prevented by choosing MDEA to strip off  $CO_2$  from natural gas. Due to the absence of carbamic acid in the reaction, one mol of  $CO_2$  will react with one mol of MDEA following its stoichiometric reaction (Polasek et al, 1994).

MDEA has smaller enthalpy reaction that makes it favorable in terms of regeneration cost as compared to MEA or DEA. However, MDEA reacts very slowly with  $CO_2$  which makes it less economical and less practical to remove high  $CO_2$  concentration as larger number of trays or an increased height of packing must be built. In general, absorption technology has some disadvantages. Absorbents such as amines are corrosive (Polasek et al, 1994). Consequently, anti corrosion agent must be frequently injected in order to avoid corrosion. In addition, disposal of used amine solution can cause environmental issue (Bord et al, 2004). Even though amine solutions are regenerated by steam stripping after being used to strip  $CO_2$  or  $H_2S$ , not all of the amines can be recycled back to the absorber column. Consequently, some amount of

reused amine solution must be treated properly before being disposed into the environment.

Foaming is one of the most severe operational problems in acid gas treating plants that remove carbon dioxide (CO<sub>2</sub>) and hydrogen sulfide (H<sub>2</sub>S) from petroleum gas streams by using a principle of gas absorption into aqueous solutions of alkanolamines. On the basis of plant experiences, (Stewart et al, 1994; Abidi et al, 2001) foaming occurred during plant start up and operation in both absorber and regenerator. It was caused by high gas velocities, sludge deposits on gas contactors, and process contaminants entering the process with feed gas and makeup water or generated within the process through reactions of alkanolamine degradation. These process contaminants were condensed or dissolved hydrocarbons, suspended solids, organic acids, water-soluble surfactants, degradation products of alkanolamine, additives (e.g., corrosion inhibitors and antifoam agents), grease, and inorganic chemicals in make up water.

Foaming was reported to cause a number of adverse impacts on the integrity of plant operation, reflecting significant extra expenditures in capital investment and operation. Such impacts include excessive loss of absorption solvents, premature flooding, reduction in plant throughput, off-specification of products, and high absorption solvent carryover to downstream plants. To cope with foaming problems, preventive and control measures, including mechanical filtration, carbon adsorption, solution reclamation (distillation), and antifoam addition, have been applied. The antifoam addition is the least preferable among the three measures because it does not physically remove process contaminants from the system and thus does not permanently remedy foaming problems (Abdi et al, 2001). Apart from the above plant experiences, there were several research works systematically carried out to reveal behavior and mechanism of foaming in gas treating plants (Mandal et al 2003, Rooney et al 2000, Bhurisa et al, 2008).

### 1.4.2. Adsorption

Adsorption process uses solid medium called adsorbent to remove acid gases from the gas mixtures. Typical adsorbents for this process are zeolites, carbon molecular sieve, silica gel, and alumina (Scott et al, 1998). CO<sub>2</sub> is sorbed into the adsorbent until it becomes fully loaded and then it is regenerated to release CO<sub>2</sub> from the adsorbent. The regeneration process is necessary in adsorption process as it will affect CO<sub>2</sub> sorption capacity of adsorbent.

There are two types of adsorption processes in term of regeneration methods i.e. Thermal Swing Adsorption (TSA) and Pressure Swing Adsorption (PSA). In TSA process, desorption takes place at temperatures much higher than adsorption. Increasing temperature is required to shift the adsorption equilibrium and cause the regeneration of the adsorbent. The gas is passed through the adsorbent bed at pressure,  $p_1$ , and relatively low temperature until the bed is fully loaded,  $n_1$ . Bed temperature is then raised causing the adsorption equilibrium to change so that the partial pressure of the gas increases  $p_2$ . The differences in the gas partial pressure between the adsorbent and fluid across the adsorbent creates the driving force for desorption to occur. Once the desorption process stops, the bed temperature is cooled down in which new equilibrium loading is attained,  $n_2$ . The difference between loading at low temperature,  $n_1$ , and loading after desorption,  $n_2$ , represents the net removal capacity or maximum loading that can be achieved by TSA at one cycle (Perry et al, 1999).

TSA process is primarily applicable for separation or purification of small concentration of impurities on feed gas such as gas drying operation and natural gas sweetening from H<sub>2</sub>S, mercaptans, organic sulfide, and disulfide (Kohl et al, 1997). PSA process is quite similar to TSA except the regeneration of adsorbent is done by applying reduced pressure of system. Feed gas is passed through at relatively high pressure until the bed is fully loaded at  $n_1$ . By reducing the total pressure, the adsorbed gas will be released until it reaches a new equilibrium,  $n_2$ . The net removal capacity of PSA bed is equal to the difference between loading at  $n_1$  and  $n_2$  (Perry et al, 1997). Major uses for PSA process are mainly for bulk separation where contaminants are present at higher concentration. This process is widely used for

hydrogen separation, air separation and air drying (Kohl, et al, 1997). New application such as carbon dioxide removal from natural gas is still under development.

The selection of regeneration methods of absorption process depend on economical and technical factor. TSA needs long cycle time as time required to heat, desorb, and cool a bed is usually in the range of a few hours to over a day. Therefore, TSA is exclusively used to remove small concentrations of impurities from feeds due to this cycle time limitation (Keller et al, 1987). Besides long cycle time, TSA also requires high energy supply and suffer from large heat loss. On the contrary, PSA has short cycle time as time required to load, depressurize, regenerate, and repressurize a bed is usually a few minutes and can in some cases be only a few seconds. This short cycle time makes PSA become attractive for bulk removal of impurities from feeds (Keller et al, 1987). However, PSA has some disadvantages due to high pressure and vacuum pressure requirements which contribute to the high operating cost.

#### **1.4.3. Cryogenic Technology**

Cryogenic separation is a process commonly used to liquefy and purify gas at very low temperature (below 0°C). This type of separation sometime is also called low temperature distillation. The main principle of this separation is based on freezing point differences of each component. Nevertheless, the separation into pure components is influenced by the composition of the gas being cooled (Mc Kee, 2002). Cryogenic method generally has good economies of scale for bulk separation (>10% of CO<sub>2</sub>). This separation requires no additional water and chemicals, thus no further separation is required. For natural gas sweetening, the liquid CO<sub>2</sub> produced is ready for easy transportation and does not require compression (Mc Kee, 2002).

However, the main disadvantage of cryogenic separation is its high energy consumption mainly required for the refrigerant compressor; therefore this process is not cost effective for purification purposes. This process requires the removal of water and other condensable gases, before the gas stream is cooled to avoid freezing and eventual blockage of process equipment. Additional separation is also required in the

sweetening stage since about 10% of hydrocarbon components are also present together with CO<sub>2</sub>. These two additional separation steps incurred extra cost, which contribute to the high cost of installing the system (Mc Kee, 2002).

#### 1.4.4. Membrane Technology

Existing Natural gas purification technologies such as amine stripping, PSA and TSA are still suffering from several shortcomings. Adsorption technologies consume large space, high capital and operating cost and amine absorption process require solvent recovery and environmental problems (Dortmundt et al, 1999). Since the last two decades, membrane technology has been developed to face these challenges. This technology is based on the ability of CO<sub>2</sub> and other components of natural gas in passing through a thin membrane barrier. The mixture of gases will be separated into permeate and retentate stream. The highly permeating component will diffuse through the membrane and separated from the non-permeable component. Membrane process in removing CO<sub>2</sub> and other gases from natural gas can be illustrated in Figure 1.1

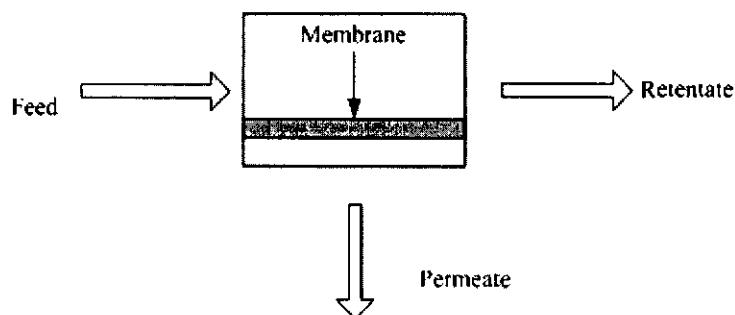


**Figure 1.1** Schematic representation of membrane process (Mulder, 1996).

However, the application of membrane for gas separation, particularly for CO<sub>2</sub> removal, is relatively new as compared to other existing technologies. Unlike other gas separation using membrane technology such as hydrogen separation from methane and nitrogen or nitrogen enrichment from air, CO<sub>2</sub> removal using membrane technology still requires much improvement in term of stability and separation performance in order to be able to compete with current CO<sub>2</sub> removal technologies.

Table 1.5 shows the current status for gas separation membrane including CO<sub>2</sub> removal. From Table 1.5 it can be seen that the application of membrane, particularly for CO<sub>2</sub> removal from natural gas is still under developing process. A few membrane companies such as UOP and ProSep Technologies, Inc. have installed cellulose acetate and polyimide membrane units for CO<sub>2</sub> removal at gas processing plant in several countries such as Pakistan and Egypt (Dortmundt et al, 1999). UOP company with their commercial membranes namely Separex have been successfully installed in Qadirpur and Kadanwari, Pakistan to remove CO<sub>2</sub> from natural gas. In Kadanwari, two stage-units of UOP's Separex cellulose acetate membranes are designed to treat 210 MMSCFD of feed gas at 90 bars with the CO<sub>2</sub> content to be reduced from 12% to less than 3%. In addition, the largest membrane-based natural gas plant in the world is Separex membrane system installed in Qadirpur, Pakistan. It is designed to process 265 MMSCFD of natural gas at 59 bars. The CO<sub>2</sub> content is reduced from 6.5% to less than 2% (Dortmundt et al, 1999).

In addition, some gas fields with smaller feed flow rate have been using Grace cellulose acetate and Medal Polyimide membrane from ProSep Technologies, Inc. to remove CO<sub>2</sub> from natural gas (ProSep, 2000). Grace cellulose acetate membranes from ProSep, Inc have been reported successful to remove 3.1 % CO<sub>2</sub> content on natural gas to pipeline gas specification (less than 2% of CO<sub>2</sub>). The Grace CA membrane is designed to process 60 MMSCFD of natural gas without hydrocarbon losses. Another commercial membrane from ProSep namely Medal Polyimide membranes are also used to remove 50% CO<sub>2</sub> content to below 10% CO<sub>2</sub> (ProSep,2000 ). Recently, some companies are interested to develop membrane for gas separation especially for CO<sub>2</sub> removal from natural gas. Table 1.6 provides an overview of the industrial membranes for CO<sub>2</sub> separation from several major membrane companies.

**Table 1.5** Status of membrane for gas separation process.

Process		Applications	Comments	References
Established Process	O <sub>2</sub> /N <sub>2</sub>	Nitrogen enrichment from air	Processes are all well developed, only incremental improvement in performance are required	(Baker,2004)
	H <sub>2</sub> /CH <sub>4</sub>	Hydrogen recovery		
	H <sub>2</sub> /N <sub>2</sub>	Ammonia purge gas		
	H <sub>2</sub> /CO <sub>2</sub>	Synthesis gas ratio adjustment		
Developing Processes	CO <sub>2</sub> /CH <sub>4</sub>	Carbon dioxide removal from natural gas	Better membranes need to be developed for high CO <sub>2</sub> content	(Nunes, 2001)
	VOC/air	Air pollution control application	Several applications are being developed, significant growth expected as the process becomes accepted	(Nunes, 2001)
To be developed processes	H <sub>2</sub> S/CH <sub>4</sub>	Natural gas treatment	Niche applications, difficult for membranes to compete with existing technology	(Baker,2004)
	Organic vapor mixtures	Separation of organic mixtures in refineries and petrochemical plants	Requires better membranes and modules. Potential size of application is large	(Baker,2004)

**Table 1.6** Industrial membranes for CO<sub>2</sub> separation from natural gas.

Commercial Membrane	Material	Companies	References
Separex	Cellulose acetate	UOP	(Dotmundt,1999)
Cynara	Cellulose acetate	NATCO group	(NATCO. 2002)
Grace membrane	Cellulose acetate	ProSep Tech.Inc	(ProSep. 2000)
Medal membrane	Polyimide	ProSep Tech.Inc	

### **1.5. Comparison between Membrane Process and Conventional Technologies for Natural Gas Purification**

Meyer et al (1991) and Cooley (1990) reported that gas permeation already applied industrially to remove CO<sub>2</sub> from natural gas. So far, these units have only been used for small capacities and they can be justified economically with commercially available membrane units capacity only if the inlet CO<sub>2</sub> concentration is high. Membranes are currently used for CO<sub>2</sub> removal from natural gas processing at processing rates from 1 MMSCFD to 250 MMSCFD (Echt, 2002). New units are in design to handle volumes up to 500 MMSCFD (Echt, 2002). It has been observed for many years that non- porous polymer films exhibit a higher permeability towards some gases than others. The mechanism for gas permeation is independent of membrane configuration and is based on the principle that certain gases permeate more rapidly than others.

Single stage membrane units are recommended for low flow rates while a recycle loops should be considered for higher flow rates to minimize the loss of hydrocarbons due to incomplete separation. Separation of carbon dioxide from hydrocarbon is most cost competitive at low flow rates, for high carbon dioxide concentration or for offshore platforms.

As mentioned in the preceding paragraphs that membranes were restricted to either small natural gas streams or those with very high CO<sub>2</sub> content, such as in the enhanced oil recovery CO<sub>2</sub> floods. However, as the technology matures, the technology spreads into a wider variety of natural gas sweetening application. Now that the technology becomes better known, one can stand back and can see the relative strength and weaknesses of the process versus the more established absorption technology. Table 1.7 below shows some key areas for comparison between amine absorption and membrane gas separation (Echt, 2002). There are no hard and fast rules applied to the comparison made in Table 1.7 because all CO<sub>2</sub> removal systems are by nature is site specific. The system differs according to the natural gas being processed, the location of the installation and the economic parameters used by the end customers. For example, membrane systems can be easily installed on platforms due to its light weight for CO<sub>2</sub> removal in enhanced oil recovery CO<sub>2</sub> floods.

**Table 1.7** Comparisons between membrane process and adsorption process for CO<sub>2</sub> removal.

<i>Operating issues</i>		
Issues	Absorption	Membrane
User comfort	Very familiar	Still new
Hydrocarbon losses	Very low	Loses depends upon conditions
Meets low CO <sub>2</sub> specification	Yes ppm levels	NO, Less than 2% is challenging
Energy consumption	Moderate to high	Low
Operating cost	Moderate	Low
Maintenance cost	Low to moderate	Low
Ease of operation	Relatively complex	Relatively simple
Environmental impact	Moderate	Low
<i>Capital cost issues</i>		
Delivery Time	Long for large systems	Modular construction is faster
Installation Time	Long	Short for skid-mounted equipment
Pre-treatment	Low	Low to moderate
Recycle Compression	Not used	Depends upon conditions

### 1.6. Problem Statement

Raw natural gas contains many impurities such as acid gases i.e. carbon dioxide and hydrogen sulfide, lower hydrocarbons i.e. propane and butane and also nitrogen. CO<sub>2</sub> composition in natural gas may vary from 2-80% depending on the geographical location of the well. The presence of lower and heavy hydrocarbon causes the condensation of natural gas in the low temperature ranges (Mohammed Awad, 2004).

Studies performed by the Gas Research Institute reveal that 14% of known reserves in the United States are sub-quality due to high nitrogen content (Hugman, 1993). Nitrogen-contaminated natural gas has a low Btu value and has to be upgraded by removing the nitrogen.

Currently, amine adsorption is used for the removal of carbon dioxide and hydrogen sulfide from natural gas. As discussed in Section 1.5 amine absorption process have limitations to remove carbon dioxide and hydrogen sulfide from natural gas. Regeneration of solvent is one of the limitations and the process becomes uneconomical if the acid gas concentration is high as large amount of solvent is required. In addition amine also faces foaming problems. Alternative methods to overcome these problems need to be explored. On the other hand, other technologies or processes are required to be coupled with amine absorption process for the removal of nitrogen and lower hydrocarbons from natural gas.

Membrane process is known for its agile and compactness. Although organic membrane are already commercially available but they are still subjected to a lot of improvements. Basically, the performance of a membrane is assessed according to its permeability and selectivity. High permeability leads to higher productivity and lower cost while high selectivity contributes to more efficient separation and higher recovery. One of the limitation in gas separation using membrane process is that the difficulty to achieve both high permeability and selectivity at the same time. At present high permeability membrane is usually followed by low selectivity and vice versa. More understanding in terms of various transport mechanisms for different membrane types, porous and non-porous; need to be explored and understood for optimum operation. Therefore, both experimental and modeling study is required to understand the true behaviour of membrane process so that it becomes a viable technology in future.

### **1.7. Objective of Study**

The main objectives of this research are:

- i. To develop a simulation model for predicting the separation of carbon dioxide, lower hydrocarbon, nitrogen and hydrogen sulfide from natural gas using nano-

porous membrane.

- ii. To model the effect of pore size and temperature on permeability of condensed component in binary mixture using nano-porous membrane.
- iii. To investigate the effect of pressure, temperature on the permeability and ideal selectivity of pure CO<sub>2</sub> over CH<sub>4</sub> through silicon rubber membranes.
- iv. To study the effect of pressure, temperature and various compositions of CO<sub>2</sub>/CH<sub>4</sub> on permeability and selectivity of silicon rubber membranes.
- v. To apply analytical model for mixed gas permeability using experimental permeability of pure gases.

## **1.8. Scope of Study**

The scope of this research is divided into the following section:

### **1.8.1 Development of Simulation Model**

Pore flow model with capillary condensation mechanism has been developed to explore the separation of carbon dioxide, lower hydrocarbon, nitrogen and hydrogen sulfide from methane by a nano-porous membrane. The carbon dioxide, lower hydrocarbons, hydrogen sulfide preferentially permeate through the membrane pores thus blocking the flow of methane in case of methane/carbon dioxide, methane/lower hydrocarbons, methane/hydrogen sulfide binary mixtures respectively. The methane left on the permeate side is slightly soluble in the respective condensed phase, and thus a small quantity of gas permeates the pores. In case of methane/nitrogen binary system, methane preferentially condenses through the membrane pores and thus blocking the flow of nitrogen.

The Kelvin equation has been used to analyze the effect of pore size and temperature on condensation pressure. Comparison with limited data has been provided. The permeation rates of condensed component with dissolved non-condensed component has been calculated for a wide range of system parameters such as pore size (1-50 nm), temperature, pressure and selectivities are evaluated for different feed composition.

### **1.8.2 Permeability of Pure CO<sub>2</sub>, CH<sub>4</sub> and its Binary Mixture CO<sub>2</sub>/CH<sub>4</sub> Through Silicon Rubber Membranes**

Three Silicon rubber membranes of different thickness were used to study the permeability of the pure and binary mixture of gases through silicon rubber membrane. The performance of silicon rubber membranes were evaluated by determining the pure CO<sub>2</sub> and CH<sub>4</sub> permeability, CO<sub>2</sub>/CH<sub>4</sub> ideal selectivity as well as binary mixture of CO<sub>2</sub>/CH<sub>4</sub> at different feed pressure and temperature.

The data collected were then analyzed with the analytical model. Using Poly math a multiple linear regression was carried to predict the binary mixture permeability from pure gas permeability. Comparisons between actual and calculated permeabilities were made.

### **1.9 Organization of Thesis**

This thesis is divided into following chapters. Chapter 1 describes the research background related to common problems in natural gas treating process with regard to the presence of acid gases particularly for CO<sub>2</sub>. The advantages and disadvantages of existing CO<sub>2</sub> separation technology such amine-based absorption, adsorption and membrane technology were also presented in this chapter. This chapter also presents problem statement, objectives of research and scope of study of this work.

Chapter 2 reviews the past and current research work pertaining to gas transport through porous and non-porous membrane. It covers information on variuos transport mechanism through porous and non-porous membranes.

Chapter 3 describes in detail on the deveopment of simulation model for predicting the separation of carbon dioxide and other gaes from natural gas using nano-porous membrane.. This chapter also presents results from simulation model.

Chapter 4 discusses the materials and method applied in this study in order to study permeability and selectivity study through silicone rubber membranes. It also describes various charaterization techniques such as SEM, DSC and TGA used for the characterization of silicone rubber membranes. This chapter covers the testing

procedure to study gas separation performance in terms of  $\text{CO}_2$ ,  $\text{CH}_4$  permeability and  $\text{CO}_2/\text{CH}_4$  selectivity at various feed pressures, temperature and feed composition.

Chapter 5 discusses all the experimental results obtained in this work. It includes membrane performance in terms of pure  $\text{CO}_2$ ,  $\text{CH}_4$  permeability and ideal selectivity of  $\text{CO}_2/\text{CH}_4$  at various feed pressure and temperature. It also covers binary mixture permeability at different pressure, feed composition and temperature. This chapter also includes the characterization results of membrane.

Chapter 6 contains concluding remarks along with the recommendations for future work.

## CHAPTER 2

### LITERATURE REVIEW

Membrane is defined as selective barrier between two phases that has ability to transport one component than the other (Mulder, 1996). Membrane based separation processes are attractive for several reasons, namely; the process is simple; there are diverse applications, which can be studied by the same basic formulations; there is no phase change involved, which is measured in commercial applications as energy savings; the process is generally carried out at atmospheric conditions which, besides being energy efficient, can be important for sensitive applications encountered in pharmaceutical and food industry and finally modules can be added and optimized in a process design to achieve the desired separation (Dortmundt, 1999). The diversity of membrane based separation systems makes it difficult to categorize them clearly. The systems are typically labeled either on the basis of type of membrane employed, or on the driving force applied to assist penetrant transport through the membrane.

#### 2.1. Membrane Types and Applications

The types of membranes used for gas separation are classified as porous, non-porous. With each type of membrane used, further classification is based on the type of applied driving force for the penetrant.

##### 2.1.1. Porous Membranes

A porous membrane is a rigid highly void structure with randomly interconnected pores (Veen et al, 1996). The separation of material by porous membranes is mainly a function of the permeate character and membrane properties like the pore size and pore size distribution (Wang et al, 1996). A porous membrane is very similar in its structure and function to a conventional filter. In general only those molecules that differs considerably in size can be separated by porous membrane. Porous membranes for gas separation exhibit high flux but low selectivity.

Gas separation by porous membranes is mainly dominated by the inorganic membrane but organic polymeric membranes are also tried with success (Baker et al, 2004). Currently, typical and prevalent porous inorganic membranes used for gas separation are carbon membrane, vycor glass, silica, alumina, zirconia and porous ceramic structures (Veen et al, 1996). Air Products and Chemicals developed carbon nano-porous membrane for gas separation (Rao et al, 1992). Ceramic membranes are also tried for gas separation (Veen et al, 1996). Their thermal stability makes them advantageous in all the processes at high temperature. Selectivities of the carbon membranes are much greater than those of other inorganic membranes and the polymeric membranes. The selectivities of typical highly selective carbon membranes are 10–20 times larger than Vycor glass and silica membranes. In addition, the average permeabilities are an order of magnitude higher than that of Vycor glass membranes (Wang et al, 1996).

There are several ways to prepare porous membranes such as solution casting, sintering stretching, track etching and phase separation. The final morphology of the membrane obtained greatly varies depending on the properties of the material and the process condition utilized (Rao et al, 1992).

### **2.1.2. Non-Porous Membranes**

Non-porous membranes primarily consist of polymer membranes. The non-porous structure of the polymer is related to the non-continuous passages present in the polymer chain matrix. These passages are created and destroyed due to thermally induced motion of the chains. Therefore, the transport of a penetrant is based on its movement through these passages. The effects of penetrant activity (driving force) and operating conditions then play an important role in governing the gas transport rate and separation property of the membrane. The first non-porous membrane used for separation purposes was natural rubber (Stannett, 1978). With the capability of controlling the chemical structure and properties of synthetic polymers, new possibilities were opened to improve the transport and separation properties of membranes. The gas transport is based on gas dissolution in a membrane, followed by diffusion of the gas through the membrane, under the influence of the applied driving force. The relative sorption and diffusion rates of gases then lead to

separation of the gas mixture. Production of high purity industrial gases like oxygen, nitrogen, natural gas etc. are few of the many applications of this process. Thus, with wide range of possible applications, the research in the membrane separation area is directed towards exploring new membrane materials, as well as an understanding of the gas transport through membrane.

## **2.2. Gas Transport Through Membrane**

Various transport models are presented in literature explaining the observed transport phenomena through membranes. Some models are based on thermodynamic and statistical mechanical principles, where as others are based on correlations between the observed transport phenomena and the physical properties of the membrane material. Gas transport through membrane has been investigated for 40 years (Ismail and Lorna, 2002) and several methods have been introduced to explain the transport phenomena through membrane. Solution-diffusion has been widely accepted to describe the mechanism of separation through non-porous dense membranes.

### **2.2.1. Gas Transport Through Porous Membrane**

Different mechanism may be involved in the transport of gases across the porous membrane. The property of gas flow in porous membrane depends on the ratio of the number of gas molecule - molecule collisions to that of the molecule-wall collisions. The Knudsen number is a characteristic parameter defining different regions of this ratio. There are four types of flow that predominate the transport of gas molecules through in the pores, namely viscous diffusion, Knudsen diffusion, surface diffusion and capillary condensation. In porous membrane, each of these mechanisms may contribute to the total transport mechanism of the permeating gas. Figure 2.1 gives a schematic representation of the mechanisms for the permeation of gases through porous as well as non-porous membranes.

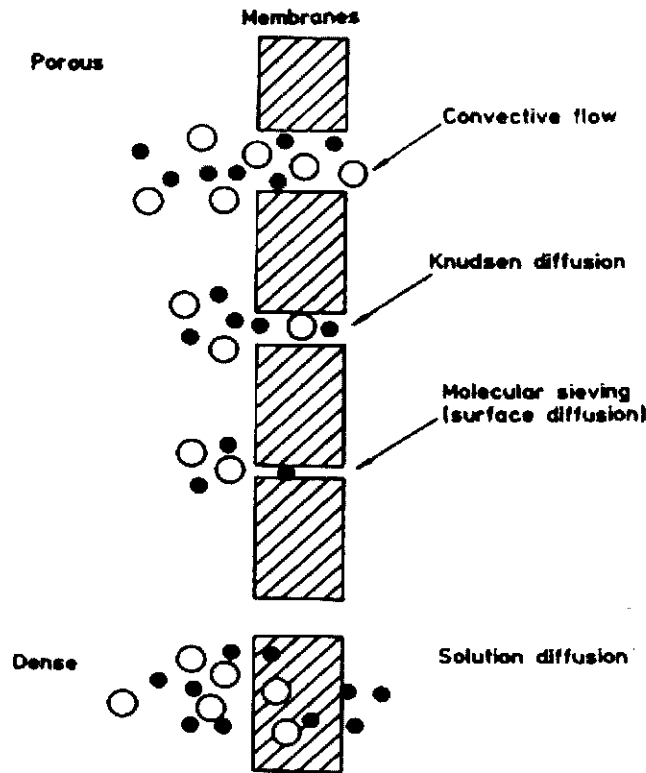


**Figure 2.1.** ‘Schematic presentation of mechanisms for permeation of gases through membranes (Baker, 1995).

### i) Viscous Diffusion

Viscous diffusion mechanism often occurs in larger pore size,  $r > 10\text{nm}$  (Mulder, 1996). Viscous diffusion occurs when the mean free path of the molecule is smaller than the pore size. If a pressure gradient is applied in such pore regimes bulk (laminar) flow occurs. Such transport is often referred to as poiseuille flow or molecular diffusion (Javaid, 2005). The assumption that the pore resembles a perfect cylinder is necessary to model the viscous flow in cylinders (Bird et al, 1960). The proportions of Knudsen to Poiseuille flow is governed by the ratio of the pore radius ( $r$ ) to the mean free path ( $\lambda$ ) of the gas molecules. The mean free path is given by

$$\lambda = \frac{3\mu}{2p} \left[ \frac{\pi RT}{2M} \right]^{1/2} \quad (2.1)$$

where,  $\mu$  is viscosity of gas molecule,  $M$  is the molecular weight of the gas,  $p$  is the

pressure,  $R$  is the universal gas constant and  $T$  is the temperature. If  $\lambda/r \ll 1$  viscous or Poiseuille flow predominate and the gas flux,  $G_{vis}$  through the pore is described by the following expression

$$G_{vis} = \frac{r^2 (P_1 - P_2)}{16 L \mu R T} \quad (2.2)$$

where  $G_{vis}$  is the viscous gas flux through the pore,  $r$  is the pore radius,  $P_1$ , partial pressure of the gas on the feed side,  $P_2$ , partial pressure of the gas on the permeate side,  $L$  is the pore length

## ii) Knudsen Diffusion

Knudsen diffusion mechanism occurs when the mean free path of the gas molecules is greater than the pore size of the membrane. In this situation, the collisions between gas molecules are less frequent than the collisions between gas molecules and pore wall. At every collision with the pore walls the gas molecules are momentarily adsorbed and are then reflected in a random direction. As there is less number of collisions among molecules than the pore walls, each molecule will move independent of others. Hence, the separation of a gas mixture is achieved because different gas species move at different velocities.

If pores are substantially smaller than the mean free path Knudsen flow  $Q$ , prevails and is given by the following equation,

$$Q = \frac{4d(P_1 - P_2)}{3L(2M\pi RT)^{1/2}} \quad (2.3)$$

where  $d$  is pore diameter

As this flow is molecular weight dependant, ideal separation occurs when down stream pressure is negligibly small. Thus for a gas mixture 1 and 2, Knudsen flow for the species 1 and 2 are given as follow.

$$Q_1 = \frac{4dP_1}{3l(2M_1\pi RT)^{1/2}} X \quad (2.4)$$

$$Q_2 = \frac{4d(P_1 - P_2)}{3l(2M_2\pi RT)^{1/2}} (1 - X) \quad (2.5)$$

where X is the mol fraction of gas 1 in feed. Selectivity of component 2 over component 1 is defined as

$$\alpha = \frac{Q_1/Q_2}{X/(1-X)} = \left( \frac{M_2}{M_1} \right)^{1/2} \quad (2.6)$$

For Knudsen flow, the selectivity ratio or the separation factor for binary gas mixtures can be estimated from the square root of the ratio of the molecular weights (Mulder, 1996). The actual separation factor, however, is found to be smaller. This is attributed to back diffusion, to non-separative diffusion, concentration polarization on the feed or on the permeate side and the occurrence of viscous flow in large pores.

### iii) Surface Diffusion

This mechanism occurs when the pore size of membrane is so small that the gas molecules can not pass freely through the membrane pore. In this mechanism, the permeating gas molecules exhibit a strong affinity for the membrane surface and adsorb along the pore walls. In practical situations, there will be a distribution of pore sizes in the membrane, and thus the gas permeability is actually influenced by a combination of transport mechanisms. From a practical standpoint, as the pore size decreases, the membrane porosity is expected to decrease, resulting in a lower gas flow through the membrane. Therefore, the pore size and porosity must be balanced to produce an efficient membrane. Surface diffusion exhibits high selectivity and high permeability for the smaller components of a gas mixture (Keizer et al, 1988). For relatively low surface concentrations, the surface flux,  $J_s$ , for a single gas is generally described by the two dimensional Fick, s law (Burgarraf and Cot, 1996).

$$J_s = -2 \frac{t_m \varepsilon^2}{r_p \tau} (1 - \varepsilon) D_s \frac{dC_s}{dZ} \quad (2.7)$$

Burgarraf and Cot (1996) formulate the surface permeability as follow.

$$P_{surface} = 2 \frac{t_m \varepsilon^2}{r_p \tau} (1 - \varepsilon) D_s \rho_m f \quad (2.8)$$

where  $\varepsilon$  is membrane porosity,  $t_m$  is membrane thickness,  $D_s$  is surface diffusivity co-efficient and  $f$  is equilibrium loading factor

#### iv) Capillary Condensation

In capillary condensation the pores are partially or completely blocked by the adsorbed vapor, preventing the flow of non-condensed gases through membrane. In experiments with condensable and non condensable gases, adsorption of the condensable gas component can restrict or even completely block the permeation of the non condensable gas. Condensable gases can be transported through porous media as a gas or as a liquid. Under certain conditions both phases might be present, rendering the quantitative description of the transport into a challenging problem (Uchytíl et al, 2005). Gas separation can also be affected by partial condensation for some component of a gas mixture in the pores, with the exclusion of others, and the subsequent transport of the condensed molecules across the pore. Selective adsorption of the more strongly adsorbed components of a gas mixture on the pore surface followed by the surface diffusion of the adsorbed molecule across the pore can also facilitate the separation of gases. Capillary condensation requires the pore size of the membrane to be in the mesoporous size range (diameter  $>30\text{Å}$ ) so that condensation of the component of a gas mixture can take place.

Although the literature for gas separation with micro porous membrane is dominated by inorganic membrane, but the polymer membranes were also be tried with some success.e.g; substituted oxyacetylene have high free volume (Baker et al, 1995). Membrane made from these materials appears to function as finely micro porous membrane, with pores of 5-15Å diameters. This extremely high free volume provides a sorption capacity as much as 10 times higher than the conventional glassy polymer (poly dimethyl siloxane, for many years known as the best permeable polymer. These high free volume polymers also have unusual permeability characteristics with

mixtures of condensable and non condensable gases. For example the permeability of nitrogen is reduced 20 times in the presence of as little as 1200 ppm of condensable vapors such as per fluorocarbons FC77 through PTMSP (Poly[1-Trimethylsilyl-1Propyne]). When the condensable gas is removed from the feed gas, the nitrogen permeability rapidly returns to its original value. The best explanation for this is that condensable vapors adsorbs in the 5-15 Å diameter pores of the membrane, blocking the flow of non condensable nitrogen gas (Uchytel et al, 2005). Although there are published work on gas transport through capillary condensation but it is not fully understood yet. There is still no agreement on how to predict permeability if capillary condensation in small pores occur. The six different flow modes proposed by Lee and Hwang (1986) are widely used for the description of condensable gases through small pores of the membranes. In the following section, a brief summary of Lee and Hwang (1986) six flow regimes are given below.

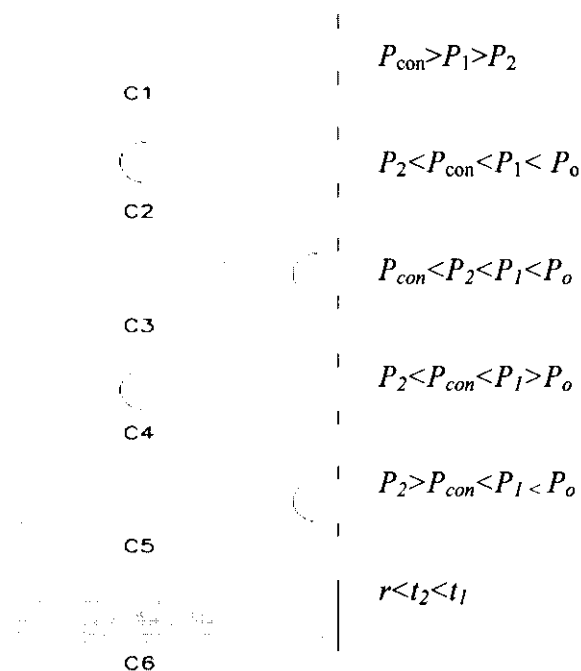


**Figure 2.2:** Six flow modes of Lee and Hwang (1986) for flow of condensable gases through small pores (Uchytel et al, 2005).

In case  $C_1$  there is no condensation in the pores and the total flux is the sum of Knudsen and surface diffusion. In this case the condensation pressure ( $P_{con}$ ) is higher than feed pressure ( $P_1$ ) and permeate pressure ( $P_2$ ).

So the apparent permeability ( $P_t$ ) is,

$$P_i = P_{Knudsen} + P_{surface} \quad (2.9)$$

In case of C<sub>2</sub> capillary condensation take place at the upstream end of the pore but not at the downstream end. Condensation flow occurs at the upstream end of the pore and Knudsen and surface flow occurs at the downstream side of the pore. So in this case the apparent permeability is,

$$P_i = \frac{K_d \rho RT}{\mu z M (P_1 - P_2)} \times \left[ -\frac{(r-t_1)^2}{r^2} \ln \frac{P_1}{P_0} - \frac{(r-t_1)^2}{r^2} \ln \frac{P_{con}}{P_0} \right] \quad (2.10)$$

where,  $K_d = \rho \pi r^4 / 8M$ ,  $\rho$  is the density of condensate,  $t$  is the thickness of the adsorbed layer at up stream face of pore and  $z$  is a parameter determined as,

$$z = \frac{L}{1 + \frac{3\pi \rho R^3 2\pi M RT (P_1 - P_2)}{64 M \mu (P_{con} - P_2)}} \quad (2.10a)$$

In case of C<sub>3</sub>, the entire pore is filled with the capillary condensate and apparent permeability is given by the following equation,

$$P_i = \frac{K_d \rho RT}{\mu M (P_1 - P_2)} \times \left[ \frac{(r-t_1)^2}{r^2} \ln \frac{P_1}{P_0} - \frac{(r-t_2)^2}{r^2} \ln \frac{P_2}{P_0} \right] \quad (2.11)$$

In case of C<sub>4</sub>, the condensation occurs at the upstream end of the pore. The meniscus is located somewhere inside the capillary. The apparent permeability for this case is,

$$P_i = -\frac{K_d \rho RT L (r-t_1)^2}{\mu z (P_1 - P_2) r^2} \ln \left( \frac{P_{con}}{P_0} \right) \quad (2.12)$$

In case of C<sub>5</sub>, the upstream end of the pore is filled with a bulk condensate and a capillary condensation occurs at the downstream side. The entire pore is filled with condensate. The apparent permeability equation

$$P_i = \frac{-k_d \rho RT}{\mu M (P_1 - P_2)} \times \frac{(r-t_2)^2}{r^2} \times \ln \left( \frac{P_2}{P_0} \right) \quad (2.13)$$

In case of  $C_6$ , the entire pore is filled with a bulk condensate and no meniscus exist in the pore. The apparent permeability thus becomes,

$$P_i = \frac{K_d}{\mu} \quad (2.14)$$

We will follow only one case  $C_3$ , which corresponds to a pore entirely filled with condensate i.e. both upstream and downstream. This case is a representative condition that would be used for the separation of  $\text{CO}_2$  and other gases from  $\text{CH}_4$  by this approach.

A very high selectivity of separation of the condensable component can be achieved by this mechanism but the extent of removal of that component from the gas mixture is limited by the condensation partial pressure of the component at the system temperature, the pore size and the geometry of the membrane (Ahmad et al, 2008). However, not many attempts have been done to study capillary condensation phenomenon for the separation of gas mixtures. Selective adsorption provides the most flexible and attractive choice for the practical separation of gas mixtures, because the separation selectivity is determined by the preferential adsorption of certain components of the gas mixture on the surface of the membrane pores as well as by the selective diffusion of the absorbed molecules. In nano, meso- and microporous media, like in the inorganic membranes, as the relative pressure is increased, the adsorbed and capillary condensed materials permeate together, and the porous media becomes more like a semi-permeable membrane through which the sorbable component will flow freely while the weakly sorbed component will be blocked (Uchytel et al, 2005).

### **2.2.2. Gas Transport Through Non –Porous Membrane**

The solution-diffusion mechanism is widely used to describe transport phenomena through non-porous membrane. This mechanism consists of three steps:

- i) Sorption is the ability of a gas molecule to be dissolved into the membrane interface.
- ii) Diffusion is the ability of gas to penetrate through the membrane.
- iii) De-sorption is the ability of the penetrant gas to be released at the opposite

interface of the membrane.

Figure 2.3 illustrate the solution - diffusion mechanism.

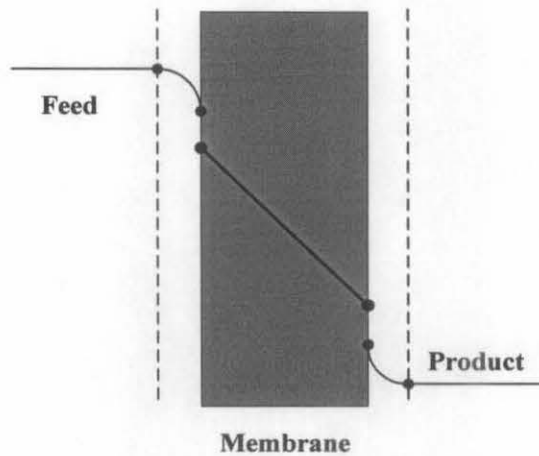


**Figure 2.3** Solution-diffusion mechanisms.

Based on solution-diffusion mechanism, the quantitative measure of mass transported through membrane, which is known as permeability ( $P$ ), is a result from sorption and diffusion of gas molecule. Sorption ( $S$ ) is a thermodynamic factor and measures the amount of gas absorbed into the membrane while diffusion ( $D$ ) is a kinetic factor, which indicates how fast a gas could diffuse from one side of the membrane to the other. The relationship between permeability, solubility and diffusivity can be described as follows

$$P = DS \quad (2.15)$$

This relationship can only be applied if  $D$  and  $S$  are constant throughout the experiment.

## 2.3 Theory of Gas Permeation Through Polymer Membranes

### 2.3.1. Introduction

In 1829 Thomas Graham observed the inflation of a wet pig bladder with  $\text{CO}_2$  (Stannett, 1978; Boddeker, 1995) It was the first study on gas permeation. In 1866, Graham formulated the “Solution diffusion process”, where he postulated that the permeation process involved the dissolution of penetrant, followed by transmission of

the dissolved species through the membrane. The other important observations made at that time were:

- i) Pressure has no effect on permeation.
- ii) With increase in temperature, penetrant solubility decreases, but made the membrane more permeable.
- iii) Prolonged exposure to high temperature affected the retention capacity of the membrane.
- iv) Differences in the permeability could be exploited for application in gas separations.
- v) Variation in membrane thickness altered the permeation rate but not the separation characteristics of the polymer.

Fick in 1855, by analogy to Fourier's law of heat conduction, proposed the law of mass diffusion where the penetrant flux  $J$ , for one dimensional diffusion, is represented as

$$J = -D \frac{\partial C}{\partial x} \quad (2.16)$$

Here  $D$  is the gas diffusion coefficient;  $\partial C/\partial x$  is the concentration gradient applied across the membrane and  $C$  is concentration of the dissolved gas, given as the amount of gas per cubic centimeter of the membrane. In late 1870's, Stefan and Exner showed that gas permeation through membrane was proportional to the product of solubility coefficient ( $S$ ) and Fick's diffusion coefficient ( $D$ ). These results were extended by Wroblewski to present a quantitative solution to the Graham's solution-diffusion model (Stannett, 1978). The dissolution of gas was based on Henry's law of solubility, where the concentration of the gas in the membrane was directly proportional to the applied gas pressure. as shown in equation 2.17.

$$C = S p \quad (2.17)$$

Wroblewski further showed that under steady state conditions, and assuming diffusion and solubility coefficients to be independent of concentration, the gas permeability can be expressed as

$$P = \frac{Jl}{\Delta p} \quad (2.18)$$

where  $(\Delta p/l)$  is the applied pressure gradient across the membrane thickness  $l$ ,  $P$  is defined as the gas permeability of the membrane. The conventional unit for expressing  $P$  is Barrers, where 1 Barrer =  $10^{-10} \text{cm}^3$  (STP)/cm. sec. cmHg). Although, the study of gas permeation is 150 years old, significant advances have been made only in the last three decades. The interest in the field was generated from the developments of new synthetic polymeric materials. The study of gas transport and separation through polymer membranes is based on the morphology of the polymer. The gas transport through amorphous polymers is further divided into gas transport study through rubbery and glassy polymers. Even though the gas transport behavior is similar for each classification, each category is being dealt separately in the following subsections in order to bring out their salient features.

### 2.3.2. Gas Permeation in Glassy Polymers

Gas transport through glassy polymers has been the focus of intense research because of favorable separation properties observed with these polymers. However, full characterization of the gas transport and separation properties of glassy polymer is limited by the time dependent changes of the polymer's physical properties. These changes are important in evaluating the performance of the polymer during its anticipated service life. Attempts have been made to explain the observed time-dependent transport behavior at a molecular level. Models have been proposed to describe the observed transport behavior based upon statistical, mechanical-structural, and thermodynamic considerations (Stern, 1994). These explanations fall into three basic theories, namely

- i) The "hole" vacancy theory, where certain work is assumed to be done on the polymer matrix to create or expand a hole for the gas molecule. The successful creation and expansion leads to the diffusion of gas molecule through the membrane.
- ii) The activated complex theory, which describes the movement of gas molecules with sufficient energy through the matrix by overcoming a potential energy barrier.

iii) The fluctuation theory, which is based on thermal fluctuations in the matrix leading to an emergence of excess space which then permits the passage of gas molecules. All three explanations presented above are originally derived from the free volume molecular theory. This theory postulates that the movement of gas molecules is dependent upon the available free volume in the polymer matrix, as well as, sufficient energy of the gas molecules to overcome attractive forces between chains. All these descriptions are conceptually valid in explaining the gas transport through glassy polymers. But without experimental data, nothing can be said with confidence regarding the true gas transport process through glassy polymers. Therefore, for all practical purposes, phenomenological models are used instead to describe the observed gas permeation process.

### **2.3.2.1. Sorption of Gases in Glassy Polymer**

The permeation behavior in glassy polymers is again viewed with respect to the diffusion - solution model. The failure of Henry's law to explain the higher sorption capability in glassy polymers is explained in terms of the presence of two or more modes for sorption. The concept of two or more modes for sorption of penetrants was initially applied by Matthes, in 1944, to study water sorption in cellulose (Stannett, 1978). The first attempt to explain solubility of small molecules in glassy polymers, using this model, was presented by Meares in 1954. The mechanism was then modeled in its final form by Barrer, Michaels and Vieth, as dual sorption model. The model assumes that a polymer consists of a continuous chain matrix, along with microvoids (holes), frozen in the matrix. These microvoids, present in discrete as well as continuous domains, are caused by the non equilibrium thermodynamic state of glassy polymers.

The dual sorption mechanism is defined in terms of Henry's law of solubility (dissolution in continuous chain matrix) and Langmuir-type of sorption (sorption in microvoids). The basic assumptions during modeling are (Vieth et al, 1976):

- i) The two modes are always in equilibrium.
- ii) The penetrants sorbed under Langmuir mode are completely immobilized.
- iii) Diffusion occurs only in the dissolved mode.

iv) The diffusion coefficient is independent of concentration.

The gas concentration in the polymer, for an applied pressure (p) is then given as

$$C = C_D + C_H = K_D p + \frac{C_H b' p}{(1 + bp)} \quad (2.19)$$

where  $C$  = concentration,

$C_D$  = concentration by normal dissolution,

$C_H$  = concentration by hole filling,

$K_D$  = Henry's law dissolution constant,

$b'$  = hole affinity constant,  $p$ : pressure.

The above model provides a conceptual reference for studying gas sorption in glassy polymers but it fails to correlate the sorption parameters to known properties of the polymer and the gas (Banerjee, 1994). Also, the presence of just two distinct modes is an oversimplification when considering the presence of sorption site size distribution. A study by (Jordan and Koros, 1995) has attempted to answer these issues with partial success under some restrictions, namely low sorption level and spherical geometry of the molecule.

### 2.3.2.2. Diffusion of Gases in Glassy Polymer

The diffusion of gas molecules through glassy membranes is based on Fick's law of diffusion. According to Fick's law the permeation flux is given by

$$J = -D_D \left( \frac{\partial C_D}{\partial X} \right) \quad (2.20)$$

where,  $D_D$  is the diffusion coefficient for the Henry's law mode sorbed gas molecules. Petropoulos (Petropoulos, 1970) has modified equation 2.20 and suggested that the Langmuir mode adsorbed molecules could also have some mobility. Petropoulos incorporated this mobility in terms of dual mode transport model (Petropoulos, 1985; Petropoulos, 1988). The proposed modification to the Fick's law for diffusion, defined in equation 2.20, was done by introducing a new diffusion coefficient  $D_H$  for the mobility of the Langmuir mode species. The total permeation flux is then given

$$J = -D_D \left( \frac{\partial C_D}{\partial X} \right) - D_H \left( \frac{\partial C_H}{\partial X} \right) \quad (2.21)$$

In conclusion, the excellent agreement between the experimental data and the theoretical explanation presented by the dual mode sorption model (Nguyen et al, 2007; Galiatsatou et al, 2006; Huang et al, 2006; Hu et al, 2003) is one of the main reasons for its popularity. This descriptive model has also been successful in predicting the synergistic effects of gases on mixed gas transport (Dhingara and Mirand, 1998). The model, however, fails to address the diffusional coupling effects on mixed gas transport through glassy polymers.

### **2.3.3. Gas Permeation Through Rubbery Polymers**

#### **2.3.3.1. Sorption**

Gas solubility in rubbery polymers is well defined in terms of Henry's law of solubility shown in equation 2.17 (Crank and Park, 1968). The model is valid for low molecular weight gases and at low gas pressures. Positive deviations to this model have been observed due to the swelling of polymer matrix in the presence of penetrants. The strong synergistic interactions primarily occur with vapors and water sorption. Non-ideal gas phase effects are sometimes corrected by replacing the gas pressure terms with corresponding fugacities (Vieth, 1991).

#### **2.3.3.2. Diffusion**

The gas transport through rubbery materials is described in terms of Fick's law for diffusion. The diffusion coefficient is shown to be concentration independent whenever, Henry's law of solubility is applicable.

#### **2.3.3.3. Mixed Gas Sorption**

The solubility of a gas mixture into a rubbery polymer is also evaluated in terms of Henry's law. The partial pressure and Henry's law solubility coefficient value of the gases are used to calculate the partial solubility of the gas (Alexopoulos, 1969). The effects from the second gases are assumed negligible.

#### **2.3.3.4 Mixed Gas Diffusion**

The permeate flux measured during mixed gas permeation is shown to be sum of the permeate flux of individual gases, based on the partial pressure of gases. Therefore, the diffusion coefficient value remained the same as that for single gas transport through rubbery membrane (Alexopoulos, 1969). Thus, gas-gas interactions, as well as, gas-polymer interactions does not affect the diffusion coefficient of the gases in rubbery polymer. In conclusion, the gas transport phenomena for rubbery polymers are well defined in terms of Henry's Law of solubility and Fick's laws of diffusion. The relative solubility of the gases is the controlling factor in the selectivity of the rubbery membrane.

#### **2.3.4 Gas Permeability Through Silicone Rubber**

The penetration mechanism of gas in polymer can also be applied to silicone rubber to help understand gas permeability. Free volume or "holes" exists in the rubber matrix. "Holes" thermally form and disappear with the movement of polymer chains. Gases are soluble in rubber like substance. When rubber is exposed to a gas, solution occurs at the surface and the dissolved gas molecules diffuse into the interior. The diffusion of gas molecules in the rubber membrane is a process in which the gas molecules migrate from "holes" (free volume) to "holes" (free volume). The permeation of gas through a membrane involves in solution on one side, diffusion through the membrane to the other side, and finally evaporation out of membrane. The rate of permeation is a specific function of a given gas and rubber (Lebaron and Pinnavaia, 2001). The rate of permeation depends on both solubility and the diffusion rate.

### **2.4. Effects of Operating Conditions on Polymer Permeability**

#### **2.4.1. Effect of Temperature on Permeability**

The thermal effects on solubility and diffusion show opposite trends. Generally, for gas adsorption, solubility decreases with increase in temperature as the condensability of the penetrant decreases with temperature. The solubility dependence with temperature is typically written in terms of the van't Hoff relationship (Kesting and Fritzsche, 1993).

$$S = S_o \exp \left[ \frac{-\Delta H_s}{RT} \right] \quad (2.22)$$

where  $S_o$  is a constant and  $\Delta H_s$  is the partial molar enthalpy of sorption. The solubility in thermodynamic terms is said to be a two step process (Ghosal and Freeman, 1994). The first step involves the condensation of the gas molecule in a polymer, followed by creation of a molecular scale gap for accommodating this gas molecule. These individual steps then contribute to the total enthalpy of sorption and are mathematically represented as

$$\Delta H_s = \Delta H_{\text{condensation}} + \Delta H_{\text{mixing}} \quad (2.23)$$

For low molecular weight super critical gases, low condensibility causes the mixing step to control the sorption property of a polymer. For the case of weak interactions between the gas molecule and the polymer, the change in enthalpy of mixing is positive, which then leads to an increase in solubility with increase in temperature. For the case of condensable gases and vapors, the enthalpy change for condensation is negative and dominant, thereby showing a decrease in solubility with increasing temperature.

Temperature dependence on gas diffusion is well expressed in term of an Arrhenius type relationship, as movement of gas molecules through a membrane is considered as thermally activated process (Kesting and Fritzsche, 1993). Mathematically, the temperature dependence of diffusion is given as,

$$D = D_o \exp \left[ \frac{-E_D}{RT} \right] \quad (2.24)$$

where,  $D_o$  is the pre exponential factor and  $E_D$  is the activation energy of diffusion. Studies on the thermal effects during gas transport have shown that the activation energy term is dependent on the size of the penetrant and not on its mass (Crank Park, 1968). Diffusion is the most temperature sensitive transport parameter, in comparison to solubility and permeability (Koros, 1987). Combining the temperature dependence

equations for the diffusion and sorption coefficients, the temperature effects on gas permeability is then given as,

$$p = p_o \exp\left[\frac{-E_p}{RT}\right] \quad (2.25)$$

where  $E_p$  is the activation energy of permeation and is an algebraic sum of  $E_D$  and  $\Delta H_s$ .

In general, permeability increases with increasing temperature. However, there are exceptions, especially near the glass transition temperature of the polymer, where opposite trends have been observed. Experiments with CO<sub>2</sub> permeation through a polyimide membrane showed decrease in permeability with increase in temperature (Costello and Koros, 1995). The same behavior was also observed for butane permeation through the same polyimide. This observation was explained in terms of pressure effects on the polymer under isothermal operating conditions. The high stress caused by the applied gas pressure was said to cause a transition in the polymer from a rubbery state to a glassy state.

#### **2.4.2. Effect of Pressure and Concentration on Permeability**

This review has so far presented the gas transport phenomena based on ideal operating conditions. However, marked deviations are observed between the theoretical predictions and the experimental gas transport parameter values, particularly at elevated pressures. The affect of pressure and therefore, the gas concentration in the membrane is a major challenge in effective modeling of the gas transport process. Change in the pressure of penetrant contacting with the polymer may cause large permeability variations. Four typical patterns of response are observed in permeability versus pressure relationships (Koros and Chern, 1987), as seen in Figure 2.3

(a) Linear, with slope close to 0. This represents the ideal case that satisfies the assumption of diffusion and solution being independent of gas pressure (i.e., low sorbing penetrants, such as He or N<sub>2</sub> in rubbery or glassy polymers).

(b) Nearly linear increase of permeability with increasing pressure. This often describes the permeability of an organic vapor into a rubbery polymer.

(c) A decreasing trend of permeability with increasing pressure. This is typically observed with highly soluble gases such as CO<sub>2</sub> in glassy polymers.

(d) Concave upwards. This can be perceived as a combination of (b) and (c), and is typical of a plasticizing penetrant such as organic vapor in a glassy polymer.

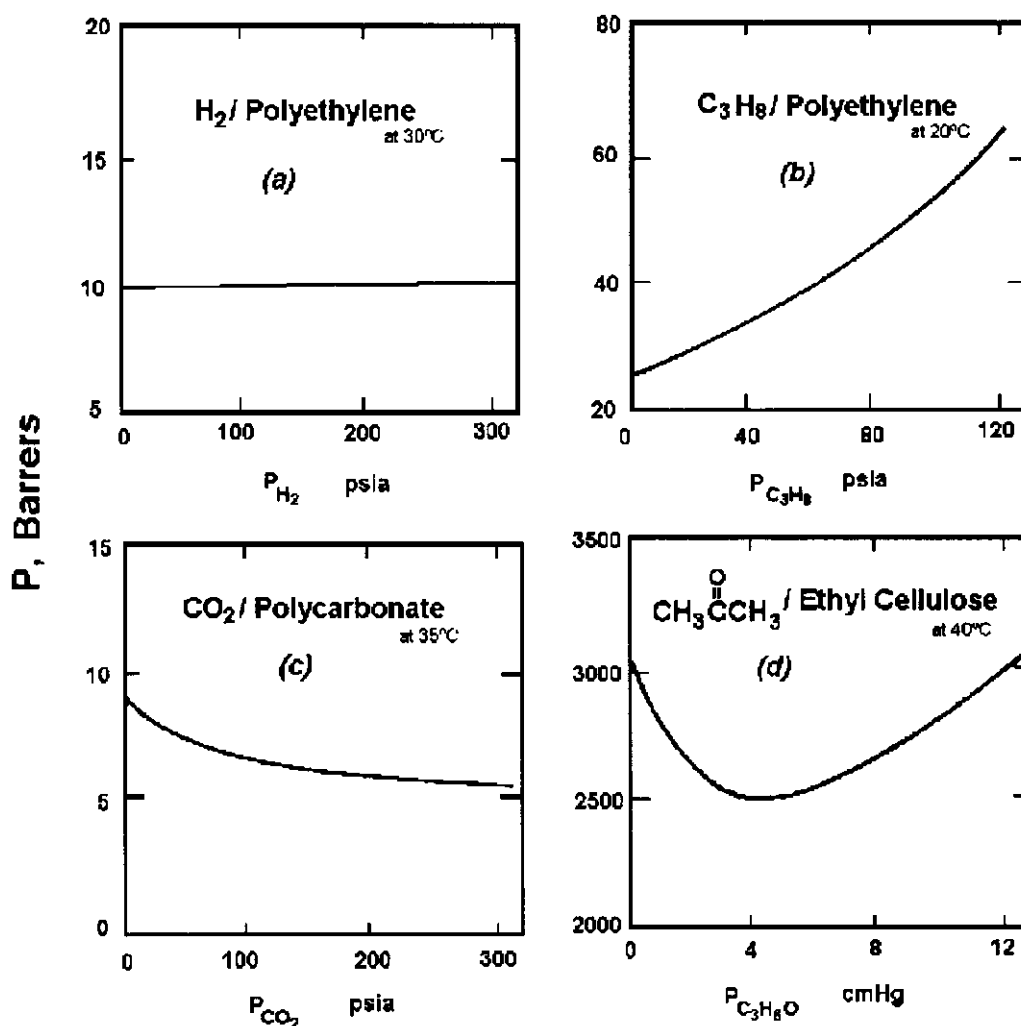


Figure 2.4: Pressure dependencies of various penetrant-polymer systems.

## **2.5. Mixed Gas Permeability from Pure Gases Permeabilities by Analytical Model**

Polymeric membranes have been successfully used in many gas separation applications. Their success has been largely based on their mechanical and thermal stability, along with good gas separation properties (Wu et al, 2006). Understanding the transport behavior of the target gases through membranes is the foundation of realizing effective separation of mixed gases and selecting the appropriate feed conditions (Dhingra and Marand, 1998). Generally, the permeation behavior of pure gas through membrane depends mainly on the properties of the gas and membrane as well as on the feed conditions. As for gas mixture, the transport behavior of one component through membrane is affected by the presence of other penetrants so that it deviates from that of pure. Therefore, using the permeation data of pure gas to estimate the separation properties of gas mixture may lead to wrong results (Dhingra and Marand, 1998). There have been extensive studies on the comparison of the difference between pure and mixed gas permeation behavior (Ettouney and Majeed 1997; Yeom et al 2000; Stern 1994; Hughes and Jiang 1995; Jordan and Koros 1990; Merkel et al 2000). The coupling effects (solubility coupling and diffusion coupling) is an important factor that makes the transport behavior of mixed gas deviated from pure gas (Dhingra and Marand 1998). This deviation in permeability of pure and mixed gases is more significant in glassy polymer than rubbery polymer. Moreover, plasticization also affects the transport phenomena through membrane, particularly in mixtures containing carbon dioxide and organic vapors. In plasticization of polymer, the penetrant interaction with the polymer causing swelling of the polymer matrix and thus its permeability is increased (Jordan et al, 1987).

In real industrial membrane separation, to optimize the separation design and to determine the proper feed conditions, it is necessary to establish a mathematical model based on the available experimental data. The model can be used as a powerful tool to evaluate or predict the performance of membrane at various feed conditions for a specific gas pair- membrane system. However, as far we know, there are a few models being applied to predict practical performance of the membrane as a function of the experimental parameters. Ettouney and Majeed (1997) developed permeability functions to describe the permeation behavior of pure and mixture of  $N_2$ ,  $O_2$ ,  $CH_4$  and

CO<sub>2</sub> through cellulose acetate and silicone rubber membranes. Permeability functions are developed for the N<sub>2</sub>, O<sub>2</sub>, CH<sub>4</sub> and CO<sub>2</sub> species in polysulfone and silicone rubber membranes. For each species all data collected for the pure and mixture gases are used to obtain the permeability functions. The functions are expressed in terms of linear dependence on species partial pressures on the feed side. The resulting permeability functions are given by

$$P = a_i + b_i P_{CO_2} + c_i P_{N_2} + d_i P_{CO_2} + e_i P_{CH_4} \quad (2.26)$$

where  $a_i$ ,  $b_i$ ,  $c_i$  and  $d_i$  are the fitting co-efficients.

Prabhkar et al (2005) developed a self consistent model to describe the dependence of vapor and gas permeability on the concentration and temperature in rubbery polymers. The variation of the propane permeability with the permeate pressure was accurately predicted in their models. Cornesa et al (1999) investigated H<sub>2</sub> – N<sub>2</sub> binary gas mixtures transport across ceramic membranes, and derived a mathematical model based on mass balance to calculate successfully the composition of the penetrants as a function of the different experimental parameters.

Wu et al (2006) developed an analytical model to predict transport of pure O<sub>2</sub>, N<sub>2</sub> and CO<sub>2</sub> and its mixture through PDMS membrane in which the permeability of a species is expressed in a linear relationship with the partial pressure of the component. The resulting analytical model is

$$J = U\Delta P + V \quad (2.27)$$

where  $J$  is the flux,  $\Delta P$ , the pressure difference and  $U$  and  $V$  are the constants.

In this study based on permeation behavior of pure CO<sub>2</sub>, CH<sub>4</sub> and its binary mixtures through silicone rubber membranes at various feed conditions a simple and practical mathematical model expressed in terms of pressure and composition was derived to predict quantitatively the permeability of the permeated stream. There are two feed variables (pressure, and feed composition). The intrinsic transport parameters such as diffusion coefficient and solubility co-efficient are not introduced into the model,

due to the difficulty in obtaining the accurate values of them in practical applications. The variation of intrinsic parameters could be considered as embodied in the change of feed variables such as temperature and pressure.

## CHAPTER 3

### DEVELOPMENT OF MEMBRANE MODEL

#### 3.1. Introduction

This chapter focuses on the development of capillary condensation model for predicting separation of acid gases, lower hydrocarbon and nitrogen from natural gas using nano-porous membranes. There are different mechanisms of the gas transport through porous membranes. The mass transport through nano-porous membranes is more complex. In case of gas flow through porous membranes with very small pores (size of about several nanometers), Knudsen diffusion is usually the dominant mechanism of the transport. The separation factor for this case is proportional to the ratio of the reciprocal square roots of molecular weights of the substances (Jaguste and Bhatia, 1995). It is also well known that the transport through small pores is influenced by the interactions of permeating molecules with the pore walls. These interactions could lead to their sorption on the pore surface. The sorbed layer of molecules might not be immobile and the transport of sorbed molecules can occur from one site to another in the direction of decreasing loading. Adsorbable gases have higher permabilities in porous material than predicted from the equations for Knudsen and Poiseuille flow. This additional contribution to the transport is called surface diffusion (Uchytel et al, 2003). Adsorbate-adsorbate interactions are responsible for the possible formation of multilayer.

Multi-layer adsorption occurs and is followed by capillary condensation. The condensed phase undergoes Poiseuille flow. The phenomenon has been treated in details in several articles (Harya et al, 1986; Shindo et al, 1986; Rhim and Hwang, 1975). Under certain combinations of pore diameter and vapor pressure of a gas capillary condensation occurs in a porous membrane. The potential of this phenomenon has been explored by Rhim and Hwang by developing a model for the flow of capillary condensation (Rhim and Hwang, 1975). They measured individual permeation rates of  $C_2H_6$ ,  $n-C_4H_{10}$  and  $CO_2$  through Vycor glass membrane. Later on, Lee and Hwang (1986) studied the permeation of Freon-113 and  $H_2O$  through Vycor glass membrane and compared their experimental results with their improved model.

Uchytel et al (2003) conducted experimental studies of both 'permanent gases' and 'condensable gases' (butane, propane and Freon 112) through a Vycor glass membrane of an average diameter of 4 nm and reported an increased permeability of butane at a higher mean pressure of the gas. A comparison of the steady state and dynamic (in which the downstream pressure was allowed to vary) permeation experiments was reported very recently by Uchytel et al (2005). The experimental flux data indicated condensation of the gas in smaller pores but not in the bigger ones. Thus pore size distribution shows an expected effect on the permeability. Stepanek et al (2007) reported an interesting study on the calculation of pore size distribution and pore morphology from the simulated results of capillary condensation in a porous medium. A different approach to the problem of condensation and permeation through fine pores based on statistical mechanics has been reported in several recent articles. Elkamel and Noble (1991) used the local density approximation (LDA) theory for the calculation of capillary condensation and separation of methane from a mixture with nitrogen. Separation factors as high as 12 to 2400 were predicted. Neimark et al (2003) used the non-local density functional theory (NLDFT) to model capillary condensation in extremely small pores (~ 1 nm) that matches the augmented Laplace-Kelvin equation for pore size one order of magnitude larger. The density functional approach has been used recently by Bryk et al (2007) to analyze the effect of surface roughness of pores on capillary condensation. However, not many attempts have been done to study capillary condensation phenomenon for separation of gas mixtures.

In present work, capillary condensation and pore flow model have been used to explore the separation of carbon dioxide, hydrogen sulfide, propane, butane and nitrogen from its binary mixtures with methane by a nano-porous membrane. The hydrogen sulfide, propane, butane preferentially permeates through the membrane pores thus blocking the flow of methane. The methane left on the permeate side is slightly soluble in the condensed phase and thus a small quantity of gas permeates through the pores. In case of methane/nitrogen binary mixtures, methane preferentially permeate through the membrane pores and nitrogen is left on the permeate side. The nitrogen left on the permeate side is slightly soluble in the condensed phase. The Kelvin equation has been used to analyze the condensation phenomena. The permeation rate of condensed phase with dissolved non-condensed

component has been calculated for a wide range of system parameters such as pore size, temperature, pressure and separation factors are evaluated for different feed composition.

### 3.2. Theory

In capillary condensation the pores are partially or completely blocked by the adsorbed vapor, preventing the flow of non-condensed gases through membrane (Baker et al, 2004). Condensable gases can be transported through porous media as a gas or as a liquid. Under certain conditions both phases might be present, rendering the quantitative description of the transport a challenging problem (Sidhu et al 2000). Despite numerous published work on gas transport by capillary condensation the phenomena is not fully understood. There is a lack of agreement on how to predict permeability if capillary condensation occurs in small pores. The technique presented by Lee and Hwang (1986) are widely used for the description of condensable gases through small pores of the membrane. As described in Chaper-2 they investigated the transport of condensable vapors through micro-porous membrane and predict six flow regimes depending on the pressure distribution and the thickness of the adsorbed layer. Here we consider the case of complete filling of a pore, with condensate in both upstream and downstream face of pore. For the condensation to occur in pore at both upstream and downstream face of membrane the condensation pressure ( $P_{con}$ ) should be lesser than both upstream pressure (feed pressure  $P_1$ ) and downstream pressure (Permeate pressure  $P_2$ ) across the membrane at certain feed temperature greater than the critical temperature of the non-permeating species and lesser than the critical temperature of the permeating species. This situation is schematically shown in Figure 3.1.

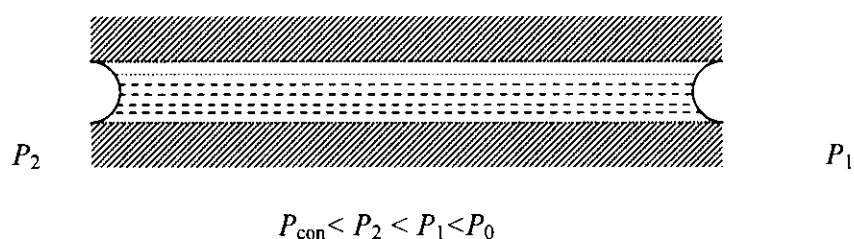


**Figure 3.1:** Schematic of condensation flow through a nano pore.

In this case the entire pore is filled with the capillary condensate and apparent permeability is given by the equation (2.13). The condition of capillary condensation is described by Kelvin equation (Uchytel, 2005). Kelvin equation describes the change of vapour pressure over liquid curved with a radius  $r$ .

$$\frac{\rho RT}{M} \ln\left(\frac{P_{\text{con}}}{P_0}\right) = -\frac{2\sigma \cos\theta}{r} \quad (3.1)$$

where  $\sigma$  is the interfacial tension,  $r$  is the pore radius and  $\theta$  is the contact angle between the liquid and the pore wall.

In order to calculate the solubility of non-condensed phase in condensed phase an equation of state is used. An equation of state is a constitutive equation describing the state of matter under a given set of physical conditions. The Soave equation of state and the Peng-Robinson equation of state can describe the PVT behavior of condensed phases as well. In the present work Peng-Robinson equation of state (EOS) is used to calculate the solubilities of non condensed phase in condensed phase. This equation gives good estimate for the solubilities of gases in the condensed phase (Sandler 1989). The Peng-Robinson equation of state is

$$P = \frac{RT}{V_m - b} - \frac{a\alpha}{V_m^2 + 2bV_m - b^2} \quad (3.2)$$

where

$$a = \frac{0.45724R^2 T_c^2}{P_c} \quad (3.2a)$$

$$b = \frac{0.07780RT_c}{P_c} \quad (3.2b)$$

$$\alpha' = (1 + (0.37464 + 1.54226\omega - 0.26992\omega^2)(1 - T_r^{0.5}))^2 \quad (3.2c)$$

$$T_r = \frac{T}{T_c} \quad (3.2d)$$

where,  $T_r$  = reduced temperature,  $T_c$  = critical temperature where  $\omega$  is the acentric factor for the species.

$$PV = ZnRT \quad (3.3)$$

where  $Z$  = compressibility factor

At vapor liquid equilibrium, fugacity of a component in vapor phase equals that of a component in liquid phase, The vapor phase fugacity (Sandler 1989) is given by

$$\ln f_i^v(T,P,y_i) = \frac{B_i}{B}(Z^v - 1) - \ln(Z^v - B) - \frac{A}{\sqrt{2}B} \left[ \frac{2\sum_j y_j A_{ij}}{A} - \frac{B_i}{B} \right] \ln \left[ \frac{Z^v + (\sqrt{2} + 1)B}{Z^v - (\sqrt{2} - 1)B} \right] \quad (3.4)$$

where,  $A = aP/(RT)^2$ ,  $B = bP/RT$ ,  $Z^v$  = Compressibility factor for vapor phase

The expression for liquid fugacity according to Peng – Robinson equation of state is written as under. It follows the same development as that of vapor fugacity expression except that the liquid compressibility factor ( $Z^l$ ) is used in calculation

$$\ln f_i^l(T,P,y_i) = \frac{B_i}{B}(Z^l - 1) - \ln(Z^l - B) - \frac{A}{\sqrt{2}B} \left[ \frac{2\sum_j y_j A_{ij}}{A} - \frac{B_i}{B} \right] \ln \left[ \frac{Z^l + (\sqrt{2} + 1)B}{Z^l - (\sqrt{2} - 1)B} \right] \quad (3.5)$$

where,  $Z^l$  = Compressibility factor for liquid phase

Equations (3.4) and (3.5) can be solved by an iterative numerical technique in conjunction with the equation of state given by equation (3.2-3.4). In every separation process, flux and selectivity are the two important parameters to determine the suitability of a membrane. In order to calculate the separation factors, we first evaluate the solubilities of the non condensed phase in condensed phase. As stated earlier Peng-Robinson equation of state (EOS) is used to calculate the solubilities of non-condensed phase in condensed phase. The solubility data obtained are used for the calculation of selectivity of condensed phase over non-condensed phase by using the following formula at various temperatures.

$$\alpha = \frac{x_{\text{condensed phase}}}{x_{\text{non - condensed phase}}} \bigg/ \frac{y_{\text{condensed phase}}}{y_{\text{non - condensed phase}}} \quad (3.6)$$

where  $x$  is the mol fraction in the pore, and  $y$  is the mol fraction in the bulk

### 3.3. Assumptions Used in Simulation Model

The following assumptions are made for the computation of capillary condensation pressure, permeability and selectivity of binary systems ( $\text{CO}_2/\text{CH}_4$ ,  $\text{C}_3\text{H}_8/\text{CH}_4$ ,  $\text{C}_4\text{H}_{10}/\text{CH}_4$ ,  $\text{H}_2\text{S}/\text{CH}_4$ ,  $\text{N}_2/\text{CH}_4$ ) ( Ahmad et al, 2008).

- i) In computation of permeability using equation (2.13) it is assumed that thickness of the adsorbed layer at upstream face of the membrane is equal to thickness of the adsorbed layer at downstream face of the membrane.
- ii) It is also assumed that the thickness of the adsorbed layer is equal to molecular diameter of the permeating species.
- iii) Pore length ( $L$ ) is assumed as ten times the molecular diameter of permeating species.
- iv) Effects that are ignored in the computation of capillary condensation pressure are the non-ideality of condensable vapors, compressibility of the condensate and adsorption on the pore walls
- v) The interaction between the pore wall and condensate are ignored and curvature effects are taken into account for the computation of capillary condensation pressure.
- vi) Selectivity is calculated on the basis of equilibrium solubility of non-condensed component in the condensed component of binary mixture. In reality such a system operating at steady state will be away from equilibrium and a higher separation factor will be achieved.

### 3.4. Algorithm Used in Simulation Model

Algorithm to find capillary condensation, permeability and selectivity of binary mixture of gases are shown in Figure 3.4. The physical properties used in the computation of capillary condensation pressure, permeability and selectivity are shown in Appendix-A. MATLAB software version 7.1 is used to solve equation 3.1 and 2.11 to compute the effect of pore size on capillary condensation pressure and permeability at different temperature.

For the computation of solubility equation 3.2 to 3.6 are used. Physical properties used in the equation are taken from (Sandler, 1989) and are reported in appendix-E. Equations 3.2 to 3.5 were solved by using the programming code developed by (Sandler, 1989). This code solves equations 3.4 and 3.5 by an iterative numerical technique in conjunction with the equation of state given by equation (3.2) and (3.3).

Based on the solubility of non-condensed component in condensed component, selectivity is computed using equation 3.6. The pressure, temperature ranges and separation strategy used in the computation of capillary condensation pressure, permeability and selectivity are shown in the following Table 3.1.

**Table 3.1** The selected operating conditions and separation strategy for selected binary systems.

System	Pressure ranges	Temperature ranges	Separation Strategy	Basis of Strategy
CO <sub>2</sub> /CH <sub>4</sub>	$P_1 = 8.85$ to 32.2 bar $P_2 = 8.7$ to 32.01 bar	$T_1 = 230$ to 270K	CO <sub>2</sub> preferentially condenses compared to CH <sub>4</sub>	$P_{con}$ for CO <sub>2</sub> is lower than $P_{con}$ for CH <sub>4</sub>
C <sub>3</sub> H <sub>8</sub> /CH <sub>4</sub>	$P_1 = 0.2003$ to 35.430 bar $P_2 = 0.2000$ to 35.41 bar	$T_1 = 200$ to 360 K	C <sub>3</sub> H <sub>8</sub> preferentially condenses compared to CH <sub>4</sub>	$P_{con}$ for C <sub>3</sub> H <sub>8</sub> is lower than $P_{con}$ for CH <sub>4</sub>
C <sub>4</sub> H <sub>10</sub> /CH <sub>4</sub>	$P_1 = 0.2003$ to 35.43 bar $P_2 = 0.2000$ to 35.41 bar	$T_1 = 200$ to 360K	C <sub>4</sub> H <sub>10</sub> preferentially condenses compared to CH <sub>4</sub>	$P_{con}$ for C <sub>4</sub> H <sub>10</sub> is lower than $P_{con}$ for CH <sub>4</sub>
H <sub>2</sub> S/CH <sub>4</sub>	$P_1 = 0.2600$ to 72.10 bar $P_2 = 0.2599$ to 71.09 bar	$T_1 = 190$ to 350 K	H <sub>2</sub> S preferentially condenses compared to CH <sub>4</sub>	$P_{con}$ for H <sub>2</sub> S is lower than $P_{con}$ for CH <sub>4</sub>
N <sub>2</sub> /CH <sub>4</sub>	$P_1 = 0.3000$ to 44.99 bar $P_2 = 0.2800$ to 44.800 bar	$T_1 = 100$ to 190K	CH <sub>4</sub> preferentially condenses compared to N <sub>2</sub>	$P_{con}$ for CH <sub>4</sub> is lower than $P_{con}$ for N <sub>2</sub>

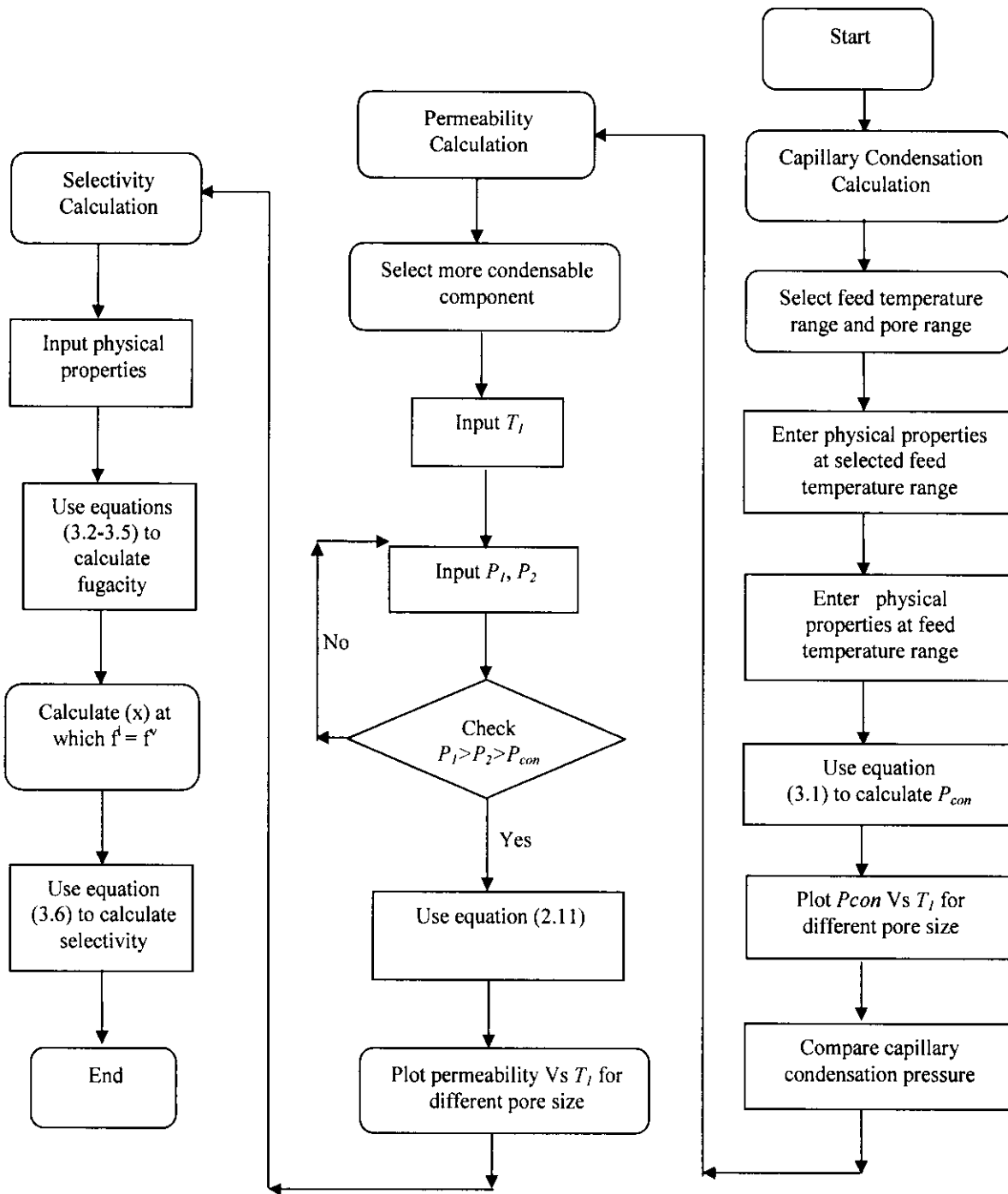


**Figure 3.2:** Algorithm to find capillary condensation pressure, permeability and selectivity for model binary systems ( $\text{CO}_2/\text{CH}_4$ ,  $\text{C}_3\text{H}_8/\text{CH}_4$ ,  $\text{C}_4\text{H}_{10}/\text{CH}_4$ ,  $\text{H}_2\text{S}/\text{CH}_4$ ,  $\text{N}_2/\text{CH}_4$ ).

### 3.5. Validation of the Model

The computed results obtained from the simulation model are verified by the experimental data of other similar system ( $\text{CH}_3\text{OH}/\text{H}_2$ ) (Sperry et al, 1991). They found that capillary condensation of  $\text{CH}_3\text{OH}$  took place significantly below than that predicted by Kelvin equation. The comparison between experimental condensation pressure given by Sperry et al (1991) and predicted values by the Kelvin equation has been shown in Figure 3.3 (Ahmad et al 2008). The computed results and experimental data compare well at least up to a temperature of 420K (147°C). This establishes the validity of the model up to a reasonably high temperature for gas separation applications. It is found that Kelvin equation predicts little reduction in vapor pressure. This is consistent with previous studies for other fluid system. Deetz et al (1987) found that the Kelvin equation predicts only 1% reduction in saturated pressure in 0.22  $\mu\text{m}$  diameters pores. However, his experimentally measured vapor pressure reduction was approximately an order of magnitude greater than that predicted by the Kelvin equation. Based on experimental observation of Deetz et al (1987) and Sperry et al (1991) it appears that if condensation pressure calculated in this study is measured experimentally in a nano-porous membrane, the vapor pressure reduction may be appreciably greater than predicted in this study using Kelvin equation. Effects that are ignored in the Kelvin equation are the non-ideality of condensable vapors, compressibility of the condensate (Melrose, 1966) and adsorption on the pore walls (Satterfield, 1980). It is due to this reason that the reduction of condensation pressure shown in Figure 3.3 using Kelvin equation is lesser. The Kelvin equation includes curvature effects but not effects due to the interactions between the liquid and the pore wall (Elkamel and Noble, 1991).

In order to test the validity of the model, the modeling approach has been applied to the similar experimental system of separation of a mixture of methanol and hydrogen reported by Sperry et al (1991). The selectivity computed by using the present model are found to compare reasonably well with the experimental results of Sperry et al (1991) and are shown in Figure 3.4. The reason behind the deviation of the experimental values is that the selectivity is calculated on the basis of equilibrium solubility of hydrogen in the condensed phase of methanol. In reality such a system operating at steady state will be away from equilibrium and a higher selectivity will be achieved (Ahmad et al, 2008).

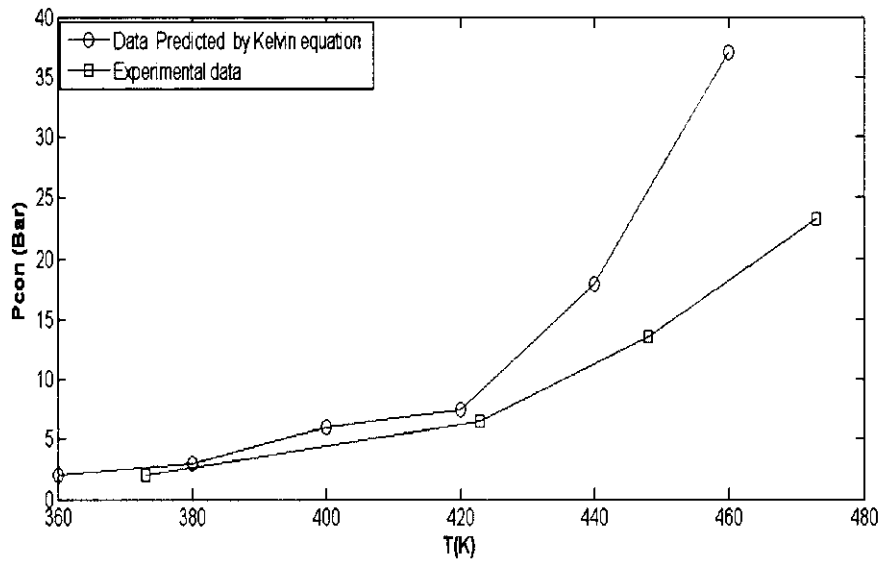


**Figure 3.3:** Comparison of experimental  $P_{con}$  for methanol-hydrogen separation by Sperry et al (1991) with  $P_{con}$  predicted using Kelvin equation.

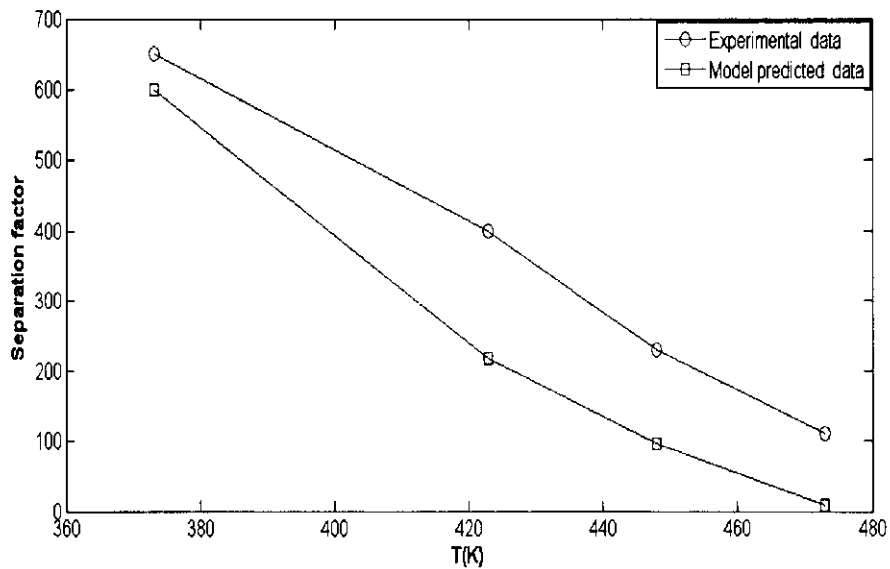


**Figure 3.4:** Comparison of the experimental selectivity for methanol-hydrogen system by Sperry et al (1991) with the model prediction.

### 3.6. Results and Discussions

The algorithm described in section 3.5 has been applied to model binary systems of  $\text{CO}_2/\text{CH}_4$ ,  $\text{C}_3\text{H}_8/\text{CH}_4$ ,  $\text{C}_4\text{H}_{10}/\text{CH}_4$ ,  $\text{N}_2/\text{CH}_4$ ,  $\text{H}_2\text{S}/\text{CH}_4$  in order to predict their permeability and selectivity.

#### 3.6.1. Methane / Carbon dioxide System

In Figure 3.5 the typical variation of condensation pressure of carbon dioxide at different pore size and at constant temperature is shown. It shows that as the pore size is increased, condensation pressure is increased and we need more pressure or lower temperature to cause condensation inside the pore. The variation in condensation pressure with temperatures for different pore size is shown in Figure 3.6 (Ahmad et al, 2006). The permeability of condensed carbon dioxide of methane/carbon dioxide binary mixture has been calculated using equation (2.11) at different temperatures for various pore sizes and is shown in Figure 3.7. Since the selected pore diameters are small, condensation occurs at temperature well above the normal condensation temperature at the prevailing pressure. This makes the pore flow separation more attractive than the cryogenic separation process. A wide range of pore size and temperature were selected for computation of permeability and selectivity. The computed results are presented below.

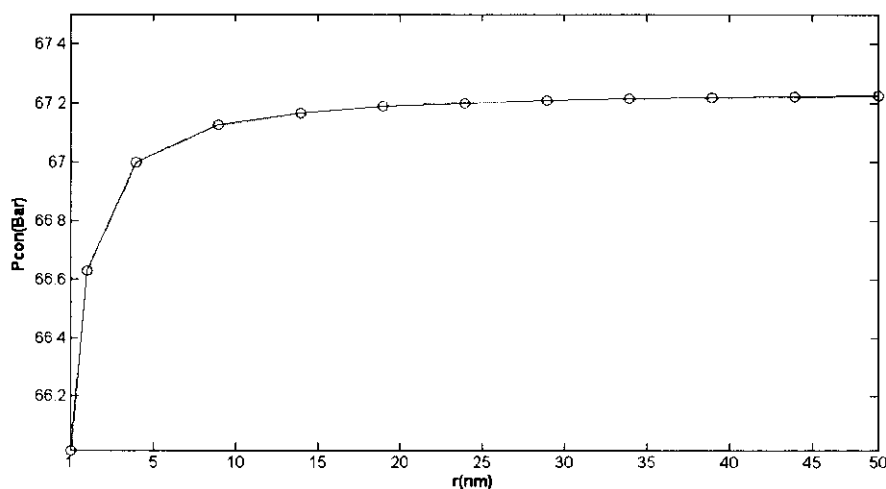


**Figure 3.5:** Condensation pressure of carbon dioxide at constant temperature of 190K for different pore size.

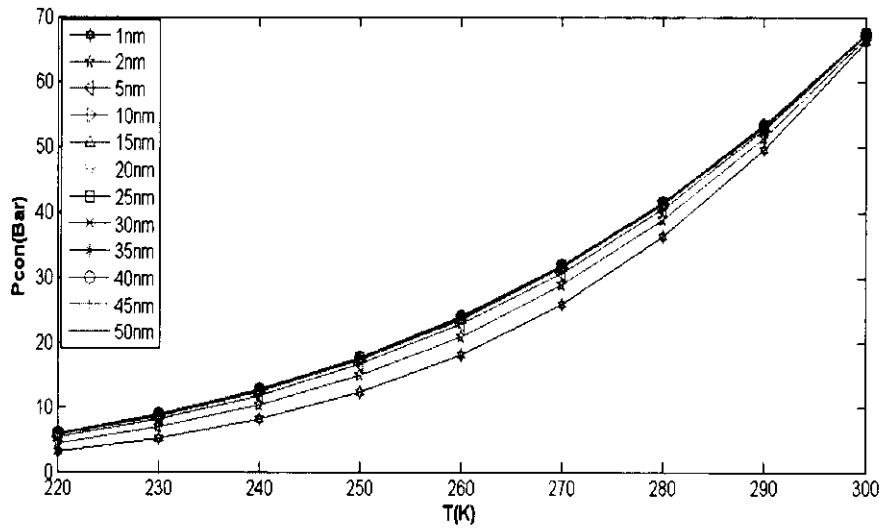


**Figure 3.6:** Condensation pressure of carbon dioxide for various pore size at different temperature.

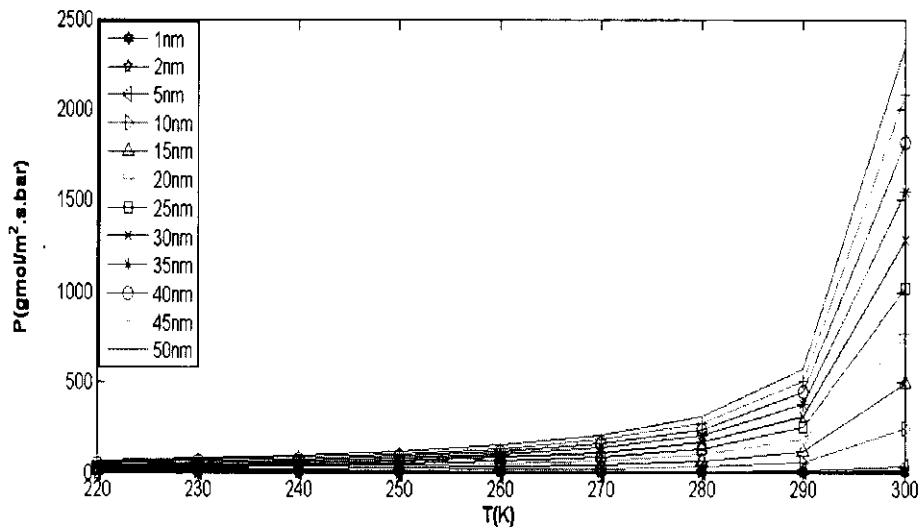


**Figure 3.7:** Permeability of carbon dioxide at various pore size at different temperature.

### 3.6.2. Methane / Propane System

In Figure 3.8 the variation of condensation pressure of propane with various pore size and at constant temperature is shown. It shows that as the pore size is increased, condensation pressure is increased and we need more pressure or lesser temperature to cause condensation inside the pore. The variation in condensation pressures with pore size at different temperature are shown in Figure 3.9. The permeability of condensed

propane of methane/propane binary mixture has been calculated using equation (2.11) at various temperatures for different pore size and are shown in Figure 3.10. A wide range of pore size and temperature were selected for computation of permeability. The computed results are presented below. The condensation pressure is more sensitive to temperature than the pore size. The variation in condensation pressure at 5nm and 40 nm are significant while at 10nm, 15nm, 20nm, 25nm, 30nm, 35nm pore size the condensation pressures are merged and the variation is not significant (Ahmad et al, 2007).

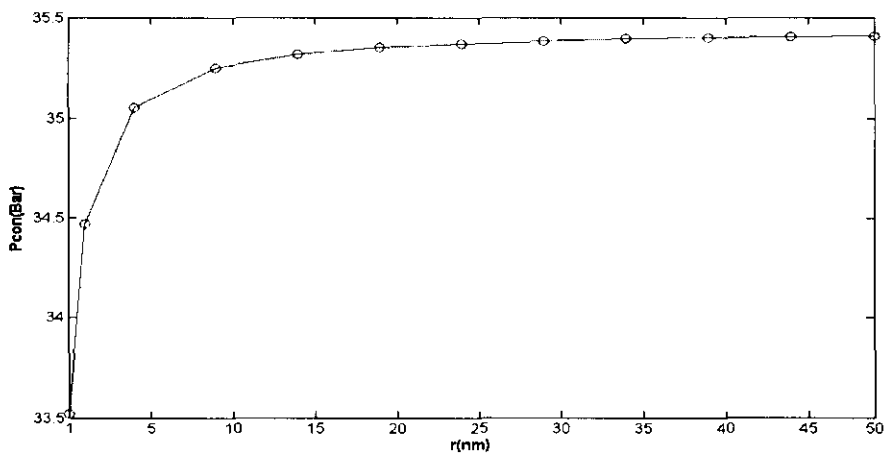


**Figure 3.8:** Condensation pressure of propane with pore size pore size at constant temperature at 360K.

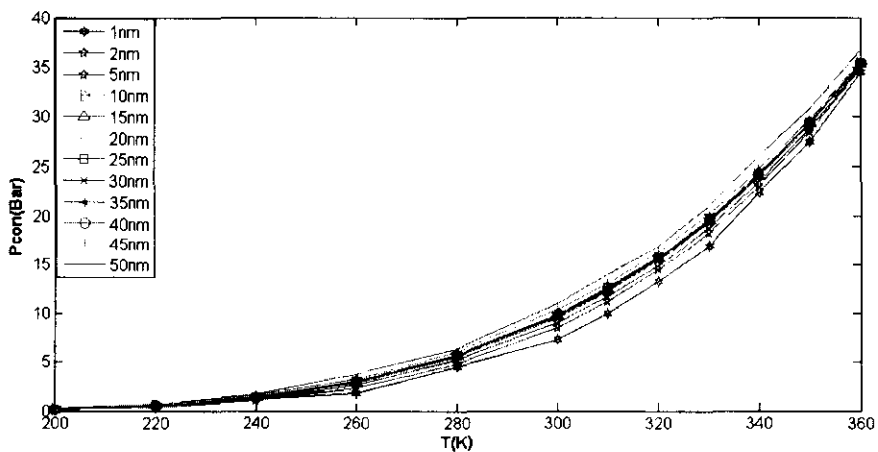


**Figure 3.9:** Condensation pressure of propane with pore size at different temperature.

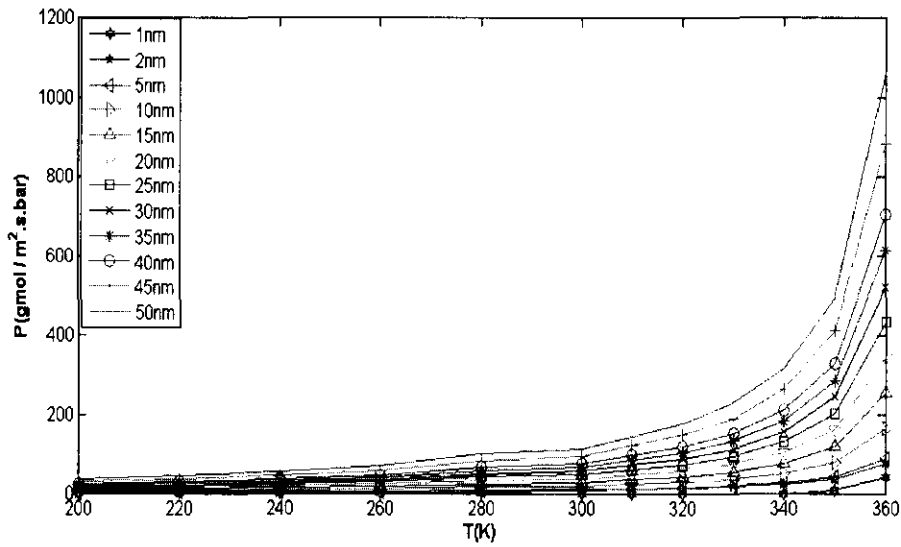


**Figure 3.10:** Permeability of propane with pore size at different temperature.

### 3.6.3 Methane/Butane System

In methane/butane binary mixtures, the butane preferentially condenses and blocks the flow of methane. The typical variation of condensation pressure with pore size is shown in Figure 3.11. It shows that condensation pressure for butane increases with increase in pore size, the effect of pore size on condensation pressure is shown in Figure 3.12. At pore size of 30 nm and 40 nm the changes in condensation pressures are insignificant (Ahmad et al, 2007). In Figure 3.13 the permeability variation with temperature for different pore is shown. A higher permeability is obtained at higher pore size.

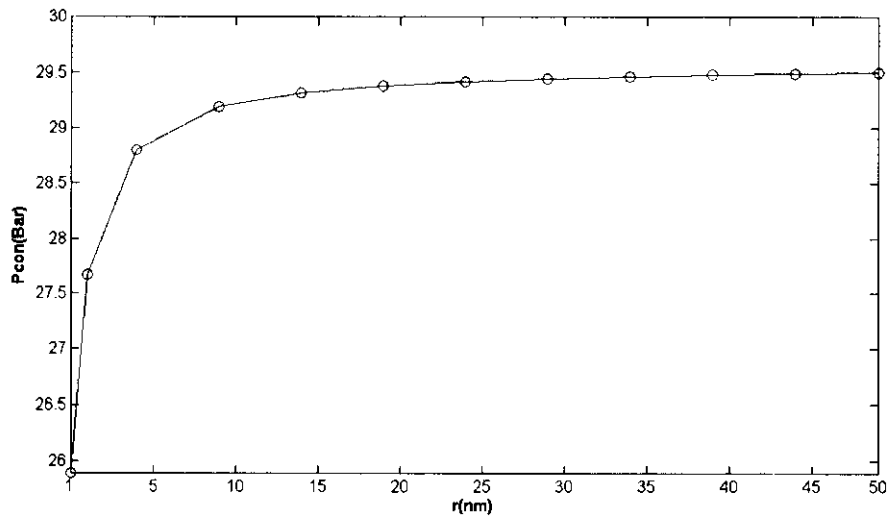


**Figure 3.11:** Condensation pressure of butane with pore size at constant temperature at 410K.

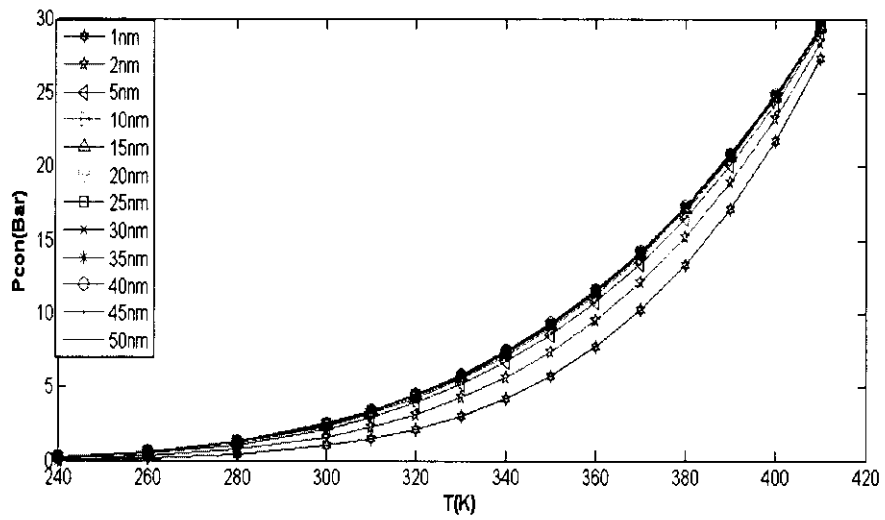


**Figure 3.12:** Condensation pressure of butane with various pore size at different temperature.

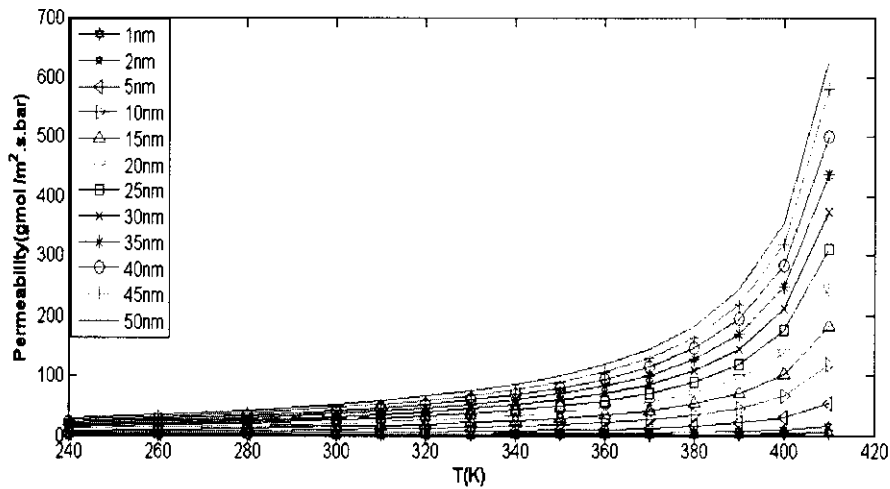


**Figure 3.13:** Permeability of butane with pore size at different temperature.

### 3.6.4 Methane/ Hydrogen sulfide System

In Figure 3.14 the typical variation of condensation pressure of hydrogen sulfide at different pore size and at constant temperature is shown. It shows that as the pore size is increased, condensation pressure is increased and we need more pressure or lower temperature to cause condensation inside the pore. The variation in condensation pressure with temperatures for different pore size is shown in Figure 3.15 (Ahmad et al, 2008). The permeability of condensed hydrogen sulfide of methane/hydrogen sulfide binary mixture has been calculated using equation (2.11) at different temperatures for various pore sizes and is shown in Figure 3.16. Since the selected pore diameters are small, condensation occurs at temperature well above the normal condensation temperature at the prevailing pressure. This makes the pore flow separation more attractive than the cryogenic separation process. A wide range of pore size and temperature were selected for computation of permeability and selectivity. The computed results are presented below.

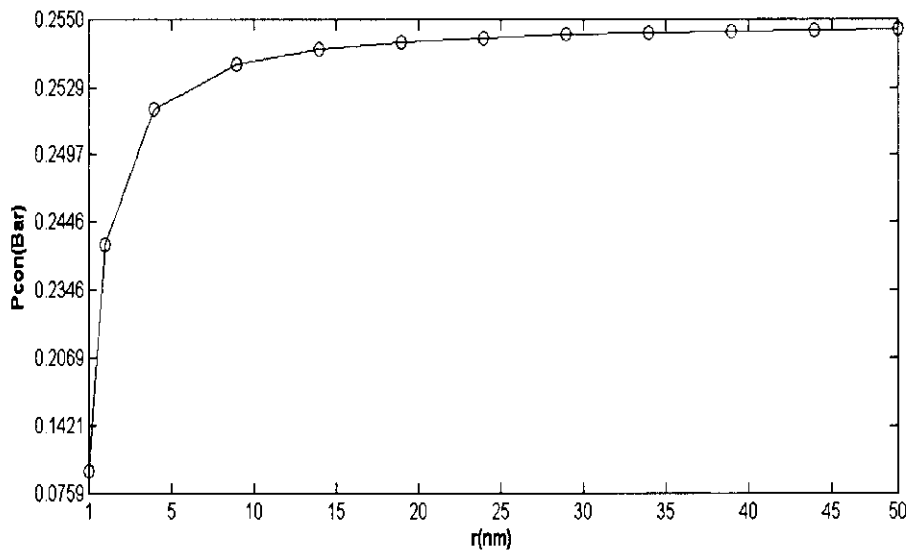


**Figure 3.14:** Condensation pressure of hydrogen sulfide with pore size at constant temperature 190K.

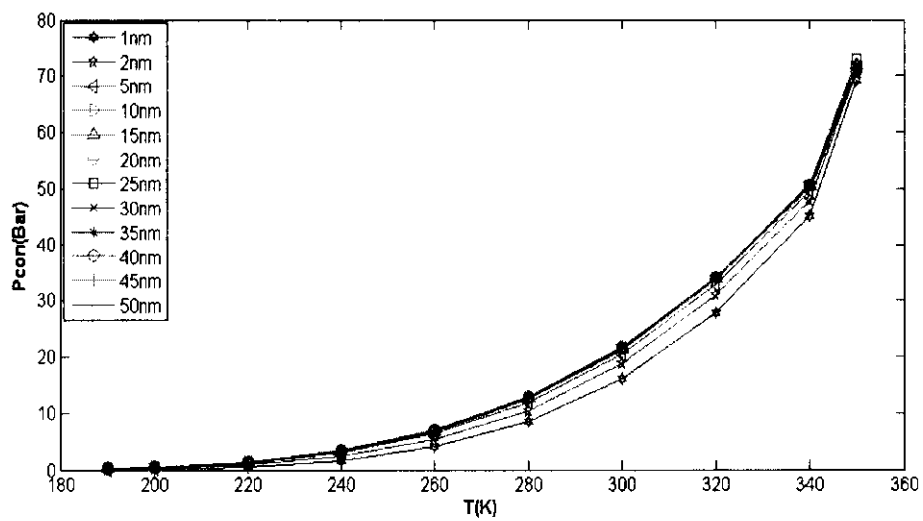


**Figure 3.15:** Condensation pressure of hydrogen sulfide with temperature for different pore size.

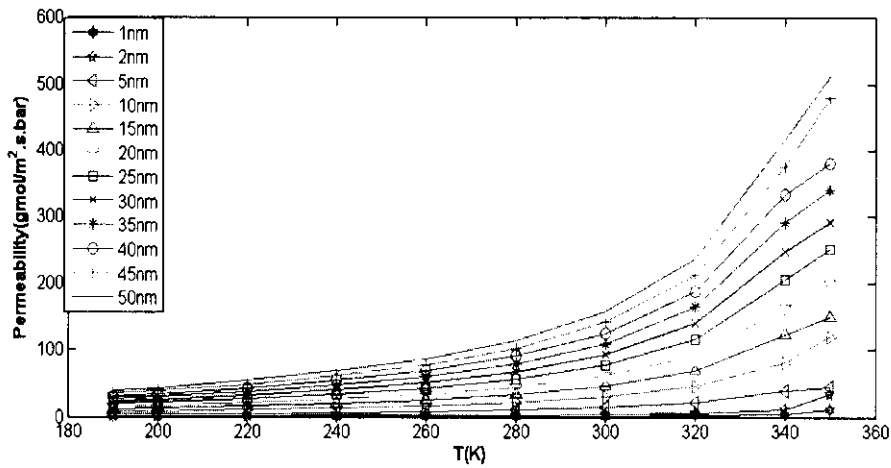


**Figure 3.16:** Permeability of hydrogen sulfide with temperature for different pore size.

### 3.6.5. Methane / Nitrogen System

In Figure 3.17 the typical variation of condensation pressure of methane at different pore sizes and at constant temperature is shown. It shows that as the pore size is increased, condensation pressure is increased and we need more pressure or lower temperature to cause condensation inside the pore. The variation in condensation pressure with temperatures for different pore size is shown in Figure 3.18. The variation in condensation pressure at 5nm, 30nm and 50 nm are significant while at 10nm, 20 nm pore size the condensation pressures are merged and the variation is not significant. The condensation pressure at 40 nm is merged with the condensation pressure at 50nm and thus the variation is not significant. The permeability of condensed methane of methane/nitrogen binary mixture has been calculated using equation (2.11) at different temperatures for various pore size and are shown in Figure 3.19. A wide range of pore size and temperature were selected for computation of permeability and selectivity. The computed results are presented below.

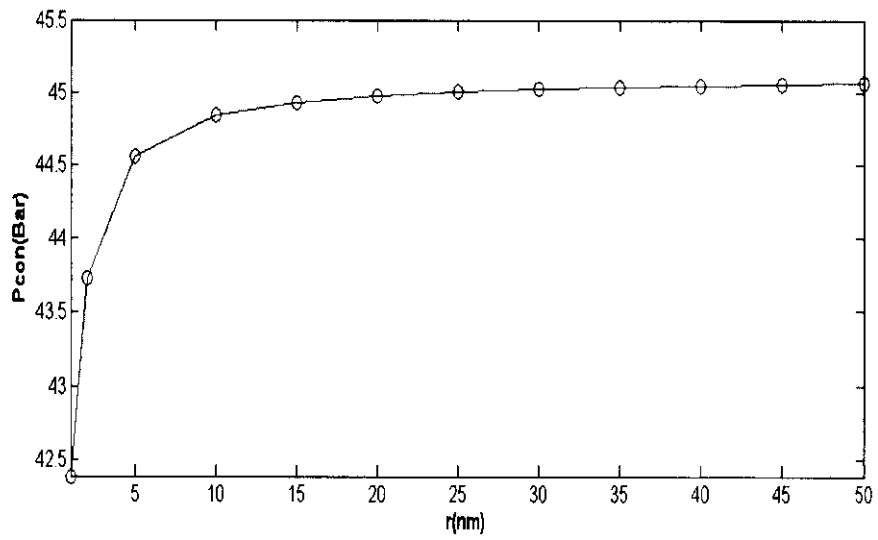


**Figure 3.17:** Condensation pressure of methane with various pore size at constant temperature 190K.

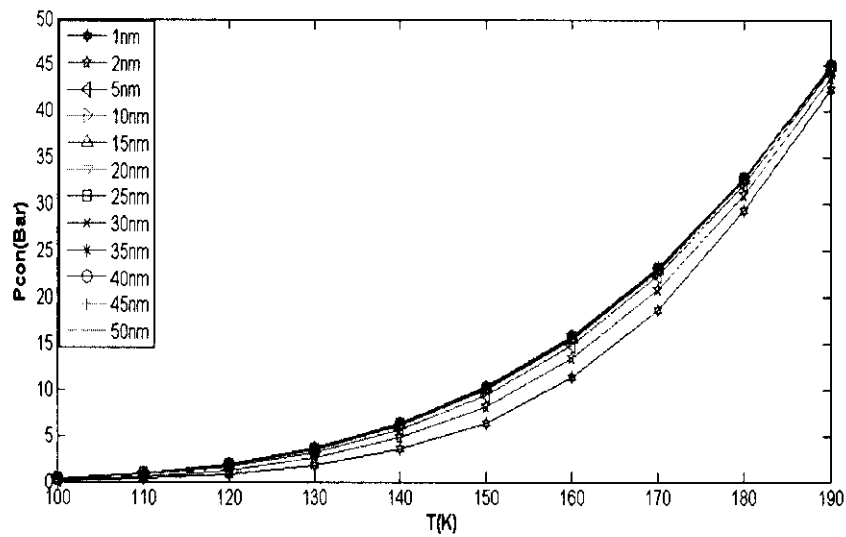


**Figure 3.18:** Condensation pressure of methane with pore size at different temperature.

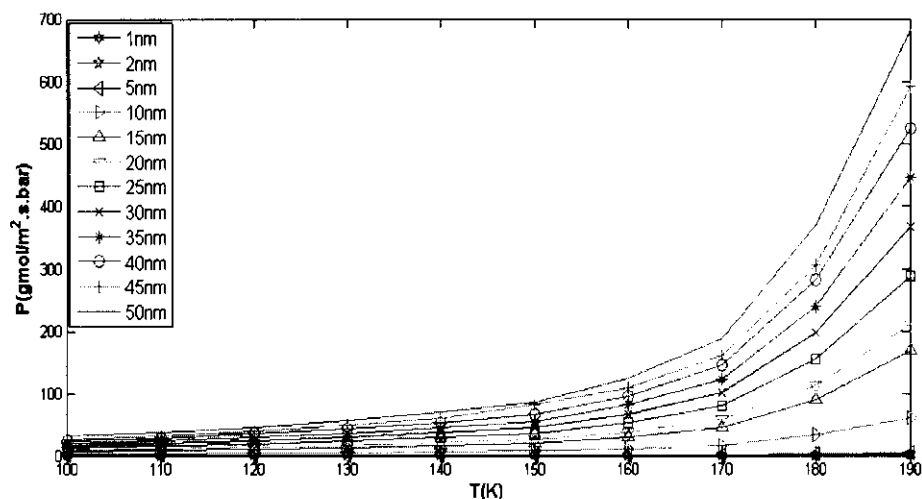


**Figure 3.19:** Permeability of methane with temperatures for different pore size.

The above computed values of permeability compare reasonably well with the experimental data of Lee and Hwang (1986). Experimental results for methanol-hydrogen separation in (Speery et al, 1991) were also compared with our calculated permeabilities and it was observed that our calculated permeabilities show the same trends. These calculations as well as those of Lee and Hwang were performed for straight pore. For tortuous pores the increased path length will cause the permeability to decrease (Elkamel and Noble 1991). With increasing temperature permeability is increased, because at higher temperature more pressure is required to cause capillary condensation inside the pore.

### 3.6.6. Selectivity of Nano-Porous Membranes.

The vapor liquid equilibrium data and selectivity of binary mixtures of methane/carbon dioxide, methane/propane, methane/butane, methane/hydrogen sulfide and methane/nitrogen has been calculated by using equation (3.3 to 3.6) and is shown in Tables 3.2 to 3.7 and in Figures 3.20 to 3.24 respectively.

**Table 3.2** Solubility for Methane / Carbon dioxide System.

Composition of CO <sub>2</sub> in the bulk phase ( y CO <sub>2</sub> )	Composition of CH <sub>4</sub> in the bulk phase ( y CH <sub>4</sub> )	P <sub>1</sub> (Bar)	T(K)	Composition of CH <sub>4</sub> in the pore ( x CH <sub>4</sub> )	Composition of CO <sub>2</sub> in the pore ( x CO <sub>2</sub> )
0.2	0.8	8.7	230	0.023	0.977
		12.7	240	0.033	0.967
		17.8	250	0.051	0.949
		24.3	260	0.084	0.916
		32.01	270	0.13	0.870
0.4	0.6	8.7	230	0.023	0.977
		12.7	240	0.033	0.967
		17.8	250	0.051	0.949
		24.3	260	0.084	0.916
		32.01	270	0.13	0.870
0.6	0.4	8.7	230	0.01515	0.98485
		12.7	240	0.0210	0.97900
		17.8	250	0.0322	0.96780
		24.3	260	0.0515	0.94850
		32.0	270	0.074	0.92600
0.8	0.2	8.7	230	0.008	0.992
		12.7	240	0.011	0.9890
		17.8	250	0.016	0.9840
		24.3	260	0.025	0.9850
		32.0	270	0.034	0.9660

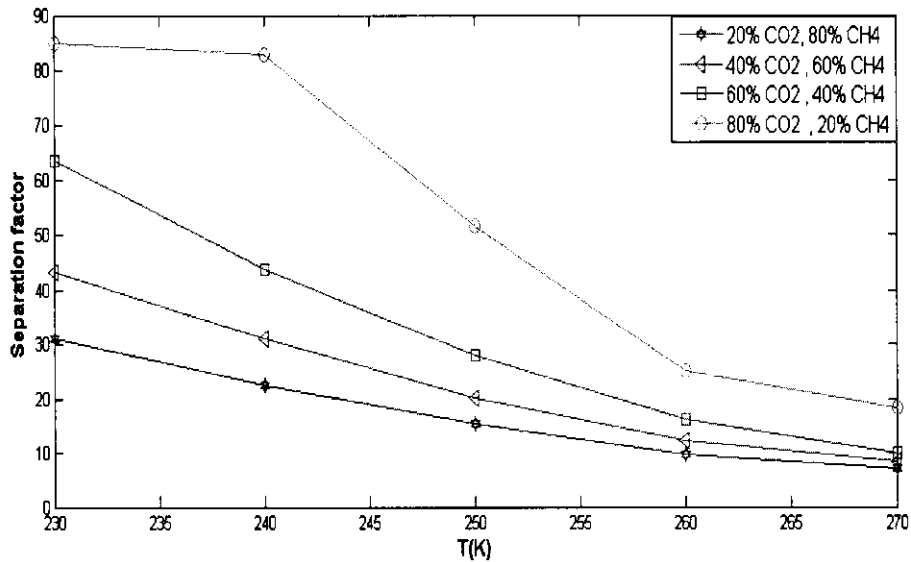


**Figure 3.20:** Selectivity of CO<sub>2</sub> over CH<sub>4</sub> for different CO<sub>2</sub>-CH<sub>4</sub> model binary system at different temperature (K).

**Table 3.3** Solubility for Methane / Propane system.

Composition of C <sub>3</sub> H <sub>8</sub> in the bulk phase (yC <sub>3</sub> H <sub>8</sub> )	Composition of CH <sub>4</sub> in the bulk phase (yCH <sub>4</sub> )	P <sub>1</sub> (Bar)	T(K)	Composition of CH <sub>4</sub> in the pore (xCH <sub>4</sub> )	Composition of C <sub>3</sub> H <sub>8</sub> in the pore (xC <sub>3</sub> H <sub>8</sub> )
0.2	0.8	0.200	200	0.00330	0.9970
		0.600	220	0.00690	0.9931
		1.460	240	0.01180	0.98820
		3.09	260	0.0230	0.9770
		5.800	280	0.0380	0.9620
		9.900	300	0.0610	0.9390
		15.90	320	0.1200	0.8800
0.15	0.85	0.200	200	0.00340	0.9966
		0.600	220	0.00733	0.99267
		1.460	240	0.01395	0.98605
		3.090	260	0.02450	0.9755
		5.800	280	0.04050	0.95950
		9.900	300	0.06400	0.93600
		15.90	320	0.12700	0.87200
0.10	0.90	0.200	200	0.00364	0.99636
		0.600	220	0.00780	0.99220
		1.460	240	0.01400	0.98775
		3.090	260	0.02480	0.97520
		5.800	280	0.04300	0.95700
		9.900	300	0.06600	0.92900
		15.90	320	0.13800	0.96200
0.05	0.95	0.200	200	0.00388	0.9962
		0.600	220	0.00825	0.9915
		1.460	240	0.01410	0.9859
		3.090	260	0.02500	0.9750
		5.800	280	0.04350	0.9565
		9.900	300	0.07200	0.9280
		15.90	320	0.13900	0.8610

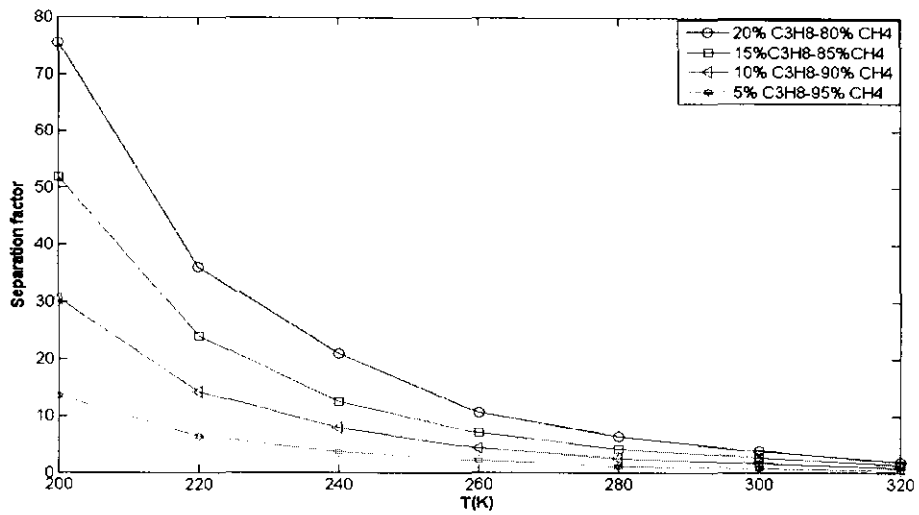


**Figure 3.21:** Selectivity of  $C_3H_8$  over  $CH_4$  for different  $C_3H_8/CH_4$  model binary system at different temperature.

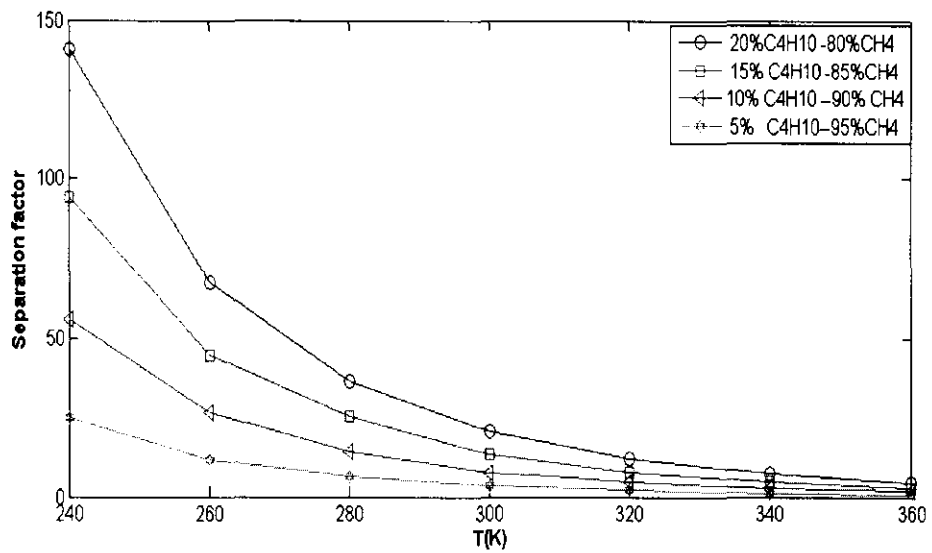


**Figure 3.22:** Selectivity of  $C_4H_{10}$  over  $CH_4$  for different  $C_4H_{10}/CH_4$  model binary system at different temperature.

**Table 3.4** Solubility for Methane / Butane system.

Composition of C <sub>4</sub> H <sub>10</sub> in the bulk phase (yC <sub>4</sub> H <sub>8</sub> )	Composition of CH <sub>4</sub> in the bulk phase (yCH <sub>4</sub> )	P <sub>1</sub> (Bar)	T(K)	Composition of CH <sub>4</sub> in the pore (xCH <sub>4</sub> )	Composition of C <sub>3</sub> H <sub>8</sub> in the pore (xC <sub>4</sub> H <sub>10</sub> )
0.2	0.8	0.2410	240	0.001770	0.998230
		0.6100	260	0.003690	0.996310
		1.3000	280	0.006788	0.993200
		2.5600	300	0.01200	0.98800
		4.5000	320	0.020000	0.980000
		7.5000	340	0.033000	0.967000
		11.600	360	0.052600	0.947400
0.15	0.85	0.2410	240	0.0018800	0.9981200
		0.6100	260	0.0039100	0.9961900
		1.3000	280	0.0069000	0.9921000
		2.5600	300	0.0130400	0.9869600
		4.5000	320	0.0213000	0.9787000
		7.5000	340	0.0348800	0.9651200
		11.600	360	0.0562000	0.9438000
0.10	0.90	0.2410	240	0.001990	0.998010
		0.6100	260	0.004150	0.995850
		1.3000	280	0.007600	0.992400
		2.5600	300	0.013600	0.986400
		4.5000	320	0.022700	0.977300
		7.5000	340	0.036900	0.963100
		11.600	360	0.060090	0.939910
0.05	0.95	0.2410	240	0.002100	0.997900
		0.6100	260	0.004380	0.995620
		1.3000	280	0.008100	0.991900
		2.5600	300	0.014400	0.985600
		4.5000	320	0.023800	0.976200
		7.5000	340	0.040500	0.959500
		11.600	360	0.063300	0.936700

**Table 3.5** Comparison of the computed equilibrium data with the experimental data of Kohn and Kurata (1958).

Temperature ( $T$ )K	Pressure ( $P_1$ ) Bar	Composition of CH <sub>4</sub> in the bulk phase $y$ CH <sub>4</sub>	Composition of methane in the pore, $x$ CH <sub>4</sub> , Theoretical	Composition of methane in the pore, $x$ CH <sub>4</sub> , Experimental
277.5K	13.7	0.140	0.0044	0.005
	20.6	0.392	0.019	0.021
	27.5	0.513	0.0334	0.035
	34.4	0.580	0.048	0.049
	41.3	0.632	0.058	0.062
	48.2	0.655	0.0785	0.071
	55.1	0.690	0.097	0.090
310K	27.5	0.012	0.00086	0.001
	34.4	0.180	0.0165	0.013
	41.3	0.280	0.0312	0.025
	48.2	0.342	0.0443	0.038
	55.1	0.405	0.062	0.051

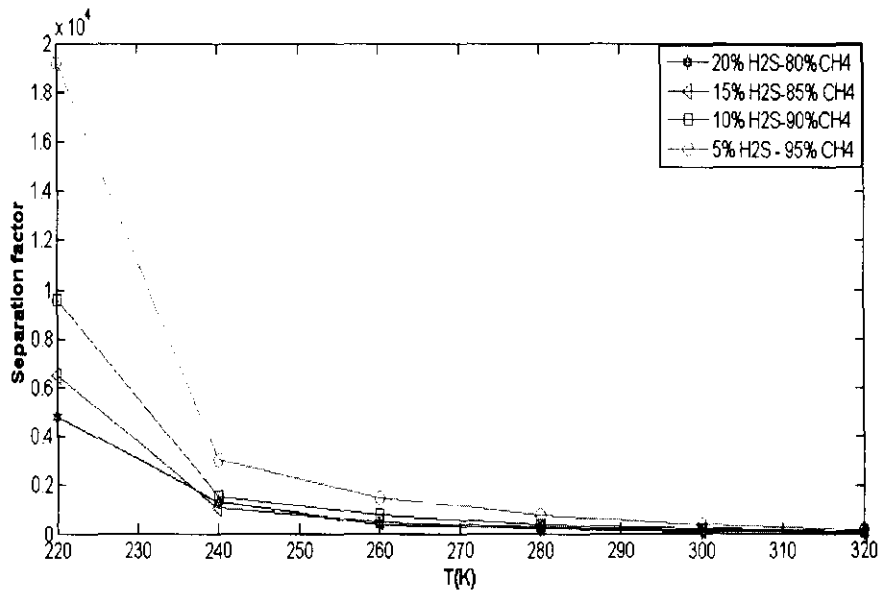


**Figure 3.23:** Selectivity of H<sub>2</sub>S over CH<sub>4</sub> for different H<sub>2</sub>S/CH<sub>4</sub> model binary system at different temperature.

**Table 3.6:** Solubility for Methane /Hydrogen sulfide system.

Composition of CH <sub>4</sub> in the bulk phase ( $y$ CH <sub>4</sub> )	Composition of H <sub>2</sub> S in the bulk phase ( $y$ H <sub>2</sub> S)	$P_1$ (Bar)	$T(K)$	Composition of CH <sub>4</sub> in the pore ( $x$ CH <sub>4</sub> )	Composition of H <sub>2</sub> S in the pore ( $x$ H <sub>2</sub> S)
0.96	0.04	0.4880	200	0.00125	0.99876
		3.4000	240	0.00784	0.99216
		6.9999	260	0.01586	0.98414
		12.880	280	0.03100	0.96900
		21.77	300	0.06100	0.93900
0.92	0.08	0.4880	200	0.00120	0.9988
		3.4000	240	0.00720	0.99280
		6.9999	260	0.01500	0.98500
		12.88	280	0.02980	0.97020
		21.77	300	0.05700	0.94300
0.88	0.12	0.4880	200	0.001130	0.99887
		3.4000	240	0.007000	0.99300
		6.9999	260	0.01448	0.98552
		12.88	280	0.02800	0.97200
		21.77	300	0.05400	0.94600
34.10	320	0.13350	0.86650		
0.84	0.16	0.4880	200	0.00109	0.99891
		3.4000	240	0.00039	0.99961
		6.9999	260	0.01375	0.98625
		12.880	280	0.02670	0.97330
		21.77	300	0.05100	0.94900

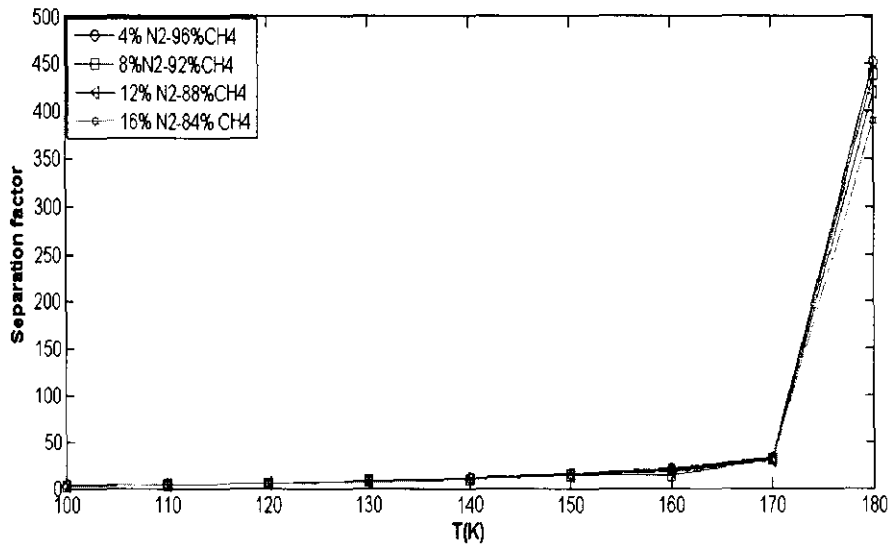


**Figure 3.24.** Selectivity of CH<sub>4</sub> over N<sub>2</sub> for different CH<sub>4</sub>/N<sub>2</sub> model binary system at different temperature.

**Table 3.7: Solubility for Methane/Nitrogen System.**

Composition of $N_2$ in the bulk phase ( $y N_2$ )	Composition of $CH_4$ in the bulk phase ( $y CH_4$ )	$P_1$ (Bar)	T(K)	Composition of methane in the pore ( $x CH_4$ )	Composition of $N_2$ in the pore ( $x N_2$ )
0.04	0.96	0.300	100	0.99910	0.00090
		0.800	110	0.99855	0.00145
		1.800	120	0.99770	0.00230
		3.500	130	0.99680	0.00320
		5.999	140	0.99560	0.00440
		10.10	150	0.99380	0.00620
		15.20	160	0.99180	0.00820
		23.10	170	0.98900	0.01100
		32.50	180	0.98250	0.01750
0.08	0.92	0.300	100	0.0018	0.9982
		0.800	110	0.0028	0.9972
		1.800	120	0.0045	0.9955
		3.500	130	0.0064	0.9936
		5.999	140	0.0088	0.9912
		10.10	150	0.0122	0.9878
		15.20	160	0.0165	0.9835
		23.10	170	0.0230	0.9770
		32.50	180	0.0365	0.9635
0.12	0.88	0.300	100	0.00031	0.99969
		0.800	110	0.00440	0.99560
		1.800	120	0.00800	0.79600
		3.500	130	0.01000	0.99000
		5.999	140	0.01350	0.98650
		10.10	150	0.01680	0.98320
		15.20	160	0.02500	0.97500
		23.10	170	0.03600	0.96400
		32.50	180	0.04990	0.95010
0.16	0.84	0.300	100	0.00042	0.99580
		0.800	110	0.00590	0.99410
		1.800	120	0.00900	0.99100
		3.500	130	0.01300	0.98700
		5.999	140	0.01700	0.98300
		10.10	150	0.02500	0.97500
		15.20	160	0.03399	0.96601
		23.10	170	0.04800	0.95200
		32.50	180	0.05800	0.94200

The solubilities of binary systems methane/carbon dioxide, methane/propane ethane/carbon dioxide, methane/propane, methane/butane methane/hydrogen sulfide and methane/nitrogen systems has been calculated by using equation 3.2 to 3.5 and

is shown in Tables 3.2 to 3.7. For the binary system of methane/hydrogen sulfide system the calculated data match satisfactorily with the experimental data for this system reported by Kohn and Kurata (1958). Based on solubility the selectivity of binary mixtures has been calculated by using equation (3.6) and is shown in Figures 3.20 to 3.24. Figures 3.10, 3.13, 3.16, 3.19 give the permeability of condensed component in binary mixtures with temperature for different pore size. With increasing temperature permeation rate is increased, because at higher temperature more pressure is required to cause capillary condensation inside the pore. The permeation rate increases with pore size, but at larger pore size more condensation pressure is required and we require higher pressure or lesser temperature at the feed side to cause condensation inside the pore.

The above computed values of permeability compare reasonably well with the experimental data of Lee and Hwang (1986). The permeability increases with temperature and the selectivity decreases. Therefore, a balance should be struck between the two to decide upon the optimum operating temperature. These calculation and as well as those of Sperry et al (1991) and Lee and Hwang (1986) were performed for straight pore. For tortuous pores the increased path length will cause the permeability to decrease (Ahmad et al, 2008).

## CHAPTER 4

### MATERIALS AND METHODS

This chapter focuses on the materials and methodology used in this work

#### 4.1 Materials

Carbon dioxide, methane and silicone rubber membranes were used as the material in this study. Carbon dioxide, 99.8% pure and methane, 99.5% pure were provided by Malaysian Oxygen Company (MOX). The binary mixture of CO<sub>2</sub>/CH<sub>4</sub> was obtained by blending appropriate composition of pure CO<sub>2</sub> and CH<sub>4</sub>.

Silicone rubber was chosen as a material for study carbon dioxide and methane permeability in this study. It is a commercially available membrane and is provided by the manufacturer (Bibby-Sterilin, UK) in the form of flat sheets. The silicone rubber membrane was chosen due to its availability and its capability to with stand at high pressure of 25 bar. Three silicone rubber membranes of different thickness have been used in this study. The thickness of membrane M<sub>1</sub>, M<sub>2</sub> and M<sub>3</sub> are 0.762mm, 0.9 mm and 2.7mm respectively. The density of the membrane is 0.0074g/cm<sup>3</sup> at 25°C.

#### 4.2. Membrane Characterization

Various analytical instruments were used to characterize the physical properties of silicone rubber membranes. These include scanning electron microscopy (SEM), energy dispersive x-ray spectroscopy (EDX), and thermogravimetric analysis (TGA) and differential scanning calorimetry (DSC).

##### 4.2.1. Scanning Electron Microscopy (SEM)

Scanning electron microscopy was used to characterize the structure of surface and sub-layer of silicone rubber membrane. Images obtained from SEM shows detailed 3-dimensional at much higher magnifications than is possible with a light microscope. The SEM used in this study is LEO SUPRA 50 VP FESEM model.

In this work, surface and cross-section of the silicone rubber membranes were chosen randomly and was then cut carefully using a sharpened razor blade. Samples were then coated with gold using a sputter coater. After coating, membrane samples were observed using SEM with magnification range from 300 to 1500 X. Magnification of images were created by electrons instead of light waves as in conventional light microscope, which uses a series of glass lenses to bend the light waves

#### **4.2.2. Energy Dispersive X-ray Spectroscopy (EDX)**

(EDS or EDX) was used for the elemental analysis of silicone rubber membrane. EDX systems used in the present analysis were connected with SEM. Scanning electron microscopes were equipped with a cathode and magnetic lenses to create and focus a beam of electrons. A detector was used to convert X-ray energy into voltage signals; this information is sent to a pulse processor, which measures the signals and passes them onto an analyzer for data display and analysis. Its characterization capabilities are due in large part to the fundamental principle that each element has a unique atomic structure allowing x-rays that are characteristic of an element's atomic structure to be identified uniquely from each other.

To stimulate the emission of characteristic x-rays from a specimen, an high energy beam of charged particles such as electrons or protons, or a beam of x-rays, was focused into the sample being studied. At rest, an atom within the sample contains ground state (or unexcited) electrons in discrete energy levels or electron shells bound to the nucleus. The incident beam may excite an electron in an inner shell, ejecting it from the shell while creating an electron hole. An electron from an outer, higher-energy shell then fills the hole, and the difference in energy between the higher-energy shell and the lower energy shell is released in the form of an x-ray. The x-ray released by the electron was then detected and analyzed by the energy dispersive spectrometer. These x-rays were characteristic of the difference in energy between the two shells, and of the atomic structure of the element from which they were emitted.

#### **4.2.3 Thermogravimetric Analysis (TGA)**

Thermogravimetric analysis (TGA) was used to evaluate the surface degradation temperature of silicone rubber membrane. The TGA used in the present analysis is

from Pekin Elmer having model Pyris-1 TGA. This instrument simply measures weight vs. temperature as a sample is heated in a nitrogen atmosphere.

Silicone rubber membranes samples (2 - 10 mg) were heated from 150 °C to 800 °C at a fixed rate of 10 °C/min. in nitrogen environment. The weight loss versus temperature was recorded using Perkin-Elmer TGA apparatus.

#### **4.2.4. Differential Scanning Calorimetry (DSC)**

DSC was used for the determination of the glass transition temperature of the silicone rubber. The model used in this study is Perkin Elmer Model Pyris -1 DSC. The sample was quenched to below -55 °C in nitrogen environment before the measurement began.

### **4.3. Methods**

This section focuses on the description of the experimental set up as well as procedure used to determine the permeability of pure CO<sub>2</sub>, CH<sub>4</sub> and its binary mixture.

#### **4.3.1. Experimental Set Up**

Existing membrane separation unit available in the Unit operation laboratory Universiti Teknologi Petronas was used in the experiment. The unit was capable to investigate the permeability of pure CO<sub>2</sub> and CH<sub>4</sub>, and also a binary mixture of CO<sub>2</sub>/CH<sub>4</sub> in various compositions. The schematic diagram is shown in Figure 4.1. The equipment has the following capabilities.

**Table 4.1** Capabilities of the gas membrane unit.

Parameter	Ranges	Instrument
Feed Pressure	1-90 bar	Pressure transducer
Feed Temperature	25-400°C	Thermocouple
Volumetric flow rate	0-5500 ml/min	Mass flow controller
Concentration of CO <sub>2</sub> and CH <sub>4</sub>	0-100 vol%	Infra red gas analyzer
Mixed gas composition	Can mix the pure gases to the desired binary mixture composition	Inline mixer

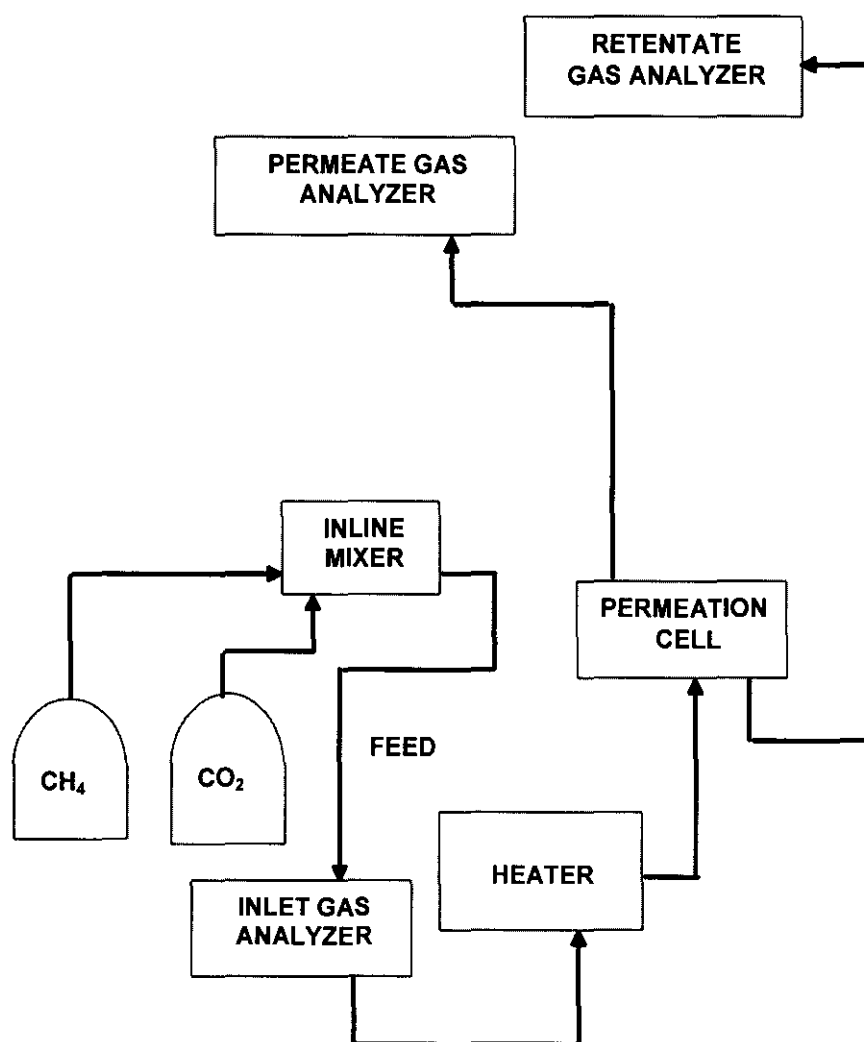


**Figure 4.1:** Schematic diagram of the membrane separation unit.



**Figure 4.2:** Membrane Separation Unit

### 4.3.2. Experimental Procedure

- i. The computer linked to the system was turned on. The Lab view software was activated. Line tracing and necessary valves positioning was implemented to ensure that the flow of the feed gas into the membrane is not obstructed.
- ii. Gas permeation measurements were performed using pure CO<sub>2</sub> and pure CH<sub>4</sub> in unit operation laboratory, Universiti Teknologi Petronas (UTP), Tronoh Malaysia. Before performing the experiment, the gas permeation test unit was evacuated to less than 0.1 bar by vacuum pump for 1 hour to remove all residual gases remaining in the equipment.
- iii. The operating conditions, feed flow rate, pressure, feed gas pressure and temperature was selected using the data acquisition system. The selected operating conditions used in the experiments are listed in Table 4.1.
- iv. The main gas supply was opened and adjusted to the desired pressure using pressure regulator.
- v. The set point of the desired pressure was put into the lab view software.
- vi. The system was allowed to reach steady state. The system is reached steady state when there is no fluctuation in the reading. When the system reached steady state, the permeate flow rate, retentate flow rate and feed flow rate were automatically recorded. For pure gas permeability, the effect of pressure was studied from 2 to 24 bar. Where as , for mixed gases the pressure was varied from 2 to 14 bar. The reason is the difficulty in maintaining the composition at pressure greater than 14 bar
- vii. For mixed gas permeability measurements, the pure gases from the feed gas cylinder were mixed in the inline mixer. In order to achieve the desired volume percent composition of the binary mixture, the flow rate of the component gases were manipulated until the desired binary mixture composition was obtained.
- viii. After the desired mixture was achieved, then steps (iii) to (vi) were repeated to achieve the permeate flow rate, composition of components gases in the permeate and retentate flow rate. The experiment was repeated three times

for every set of reading and the average permeate flow rate was used in the permeability calculation.

**Table 4.2** Summary of the selected operating conditions for experimental study.

Operating condition	Ranges
Feed Pressure	2 to 24 bar for Pure and 2 to 14 for mixed gases
Feed Temperature	25 to 150°C
Volumetric feed flow rate	100-5000 ml/min
Concentration of mixed gas (CO <sub>2</sub> /CH <sub>4</sub> )	20-80 vol%

### 4.3.3 Analysis of Experimental Results

In order to determine the permeability, the permeate flow rate need to be corrected to STP. The volumetric flow rate  $Q$  was then corrected to STP conditions (0 °C and 1 atm) using the following equation

$$Q_{STP} = \frac{T_{STP}}{T} \times Q \quad (4.1)$$

in which  $T_{STP}$  and  $Q_{STP}$  referred to temperature (K) and volumetric of permeate gas (cm<sup>3</sup>/s) at STP condition. After conversion into STP condition, gas permeability  $P$  was then calculated using the following formula (Baker, 2004)

$$P = \frac{Q_{sp} l}{A' \times \Delta p} \quad (4.2)$$

where  $l$  is length of membrane and  $\Delta p$  and  $A$  are trans-membrane pressure and effective membrane area, respectively. The CO<sub>2</sub>/CH<sub>4</sub> ideal selectivity (unitless),  $\alpha_{CO_2/CH_4}$ , of silicone rubber membrane can be determined by dividing CO<sub>2</sub> permeability,  $P_{CO_2}$ , over CH<sub>4</sub> permeability,  $P_{CH_4}$ .

$$\alpha_{CO_2/CH_4} = \frac{P_{CO_2}}{P_{CH_4}} \quad (4.3)$$

For mixed gases the permeate flow rate is multiplied by vol percent of the component gas in the mixture. Let  $x$  is the volume percent of the carbon dioxide in the permeate stream and  $1-x$  is the volume percent of methane in the permeate stream. Then the permeate flow rate of  $CO_2$ ,  $Qx$  and permeate flow rate of  $CH_4$  is  $Q(1-x)$ . After correcting permeate flow rate for both gases to STP conditions ( $0^\circ C$  and 1 atm), the permeability for  $CO_2$  and  $CH_4$  was then calculated using the following formula.

$$P'_{CO_2} = \frac{Q_{sp} x l}{A' \times \Delta p} \quad (4.4)$$

$$P'_{CH_4} = \frac{Q_{sp} (1-x) l}{A' \times \Delta p} \quad (4.5)$$

The selectivity based on mixed gas permeability is then given by

$$\alpha_{CO_2/CH_4} = \frac{P'_{CO_2}}{P'_{CH_4}} \quad (4.6)$$

## CHAPTER 5

### RESULTS AND DISCUSSIONS

This chapter describes the characterization of silicone rubber membranes, effect of pressure, temperature on permeability and ideal selectivity of pure gases  $\text{CO}_2$  and  $\text{CH}_4$  and effect of pressure, temperature and feed composition on permeability and selectivity of binary mixture of gases ( $\text{CO}_2+\text{CH}_4$ ).

#### 5.1. Membrane Characterization

Various analytical instruments were used to characterize silicone rubber membrane. These include SEM, EDX, TGA, and DSC. Figure 5.1 shows SEM image of silicone rubber membrane. It shows that silicone rubber membranes used in this study is a homogenous non-porous symmetric membrane. EDX analysis shows that silicone rubber membrane contains 38.37 weight % elemental (Si). TGA analysis indicates that the thermal degradation temperature of the silicone rubber membrane is  $474.761^\circ\text{C}$ . The analysis is shown in Figure 5.2. Glass transition temperature was determined by DSC and was found to be  $-43.147^\circ\text{C}$ . The analysis is shown in Figure 5.3.

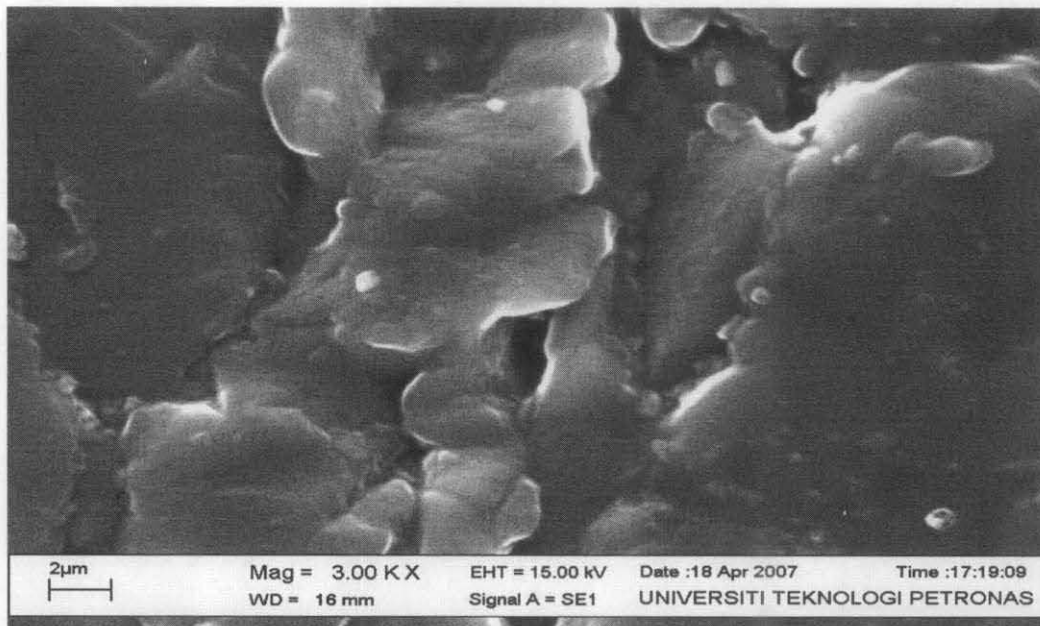


**Figure 5.1:** SEM image of silicone rubber membrane.

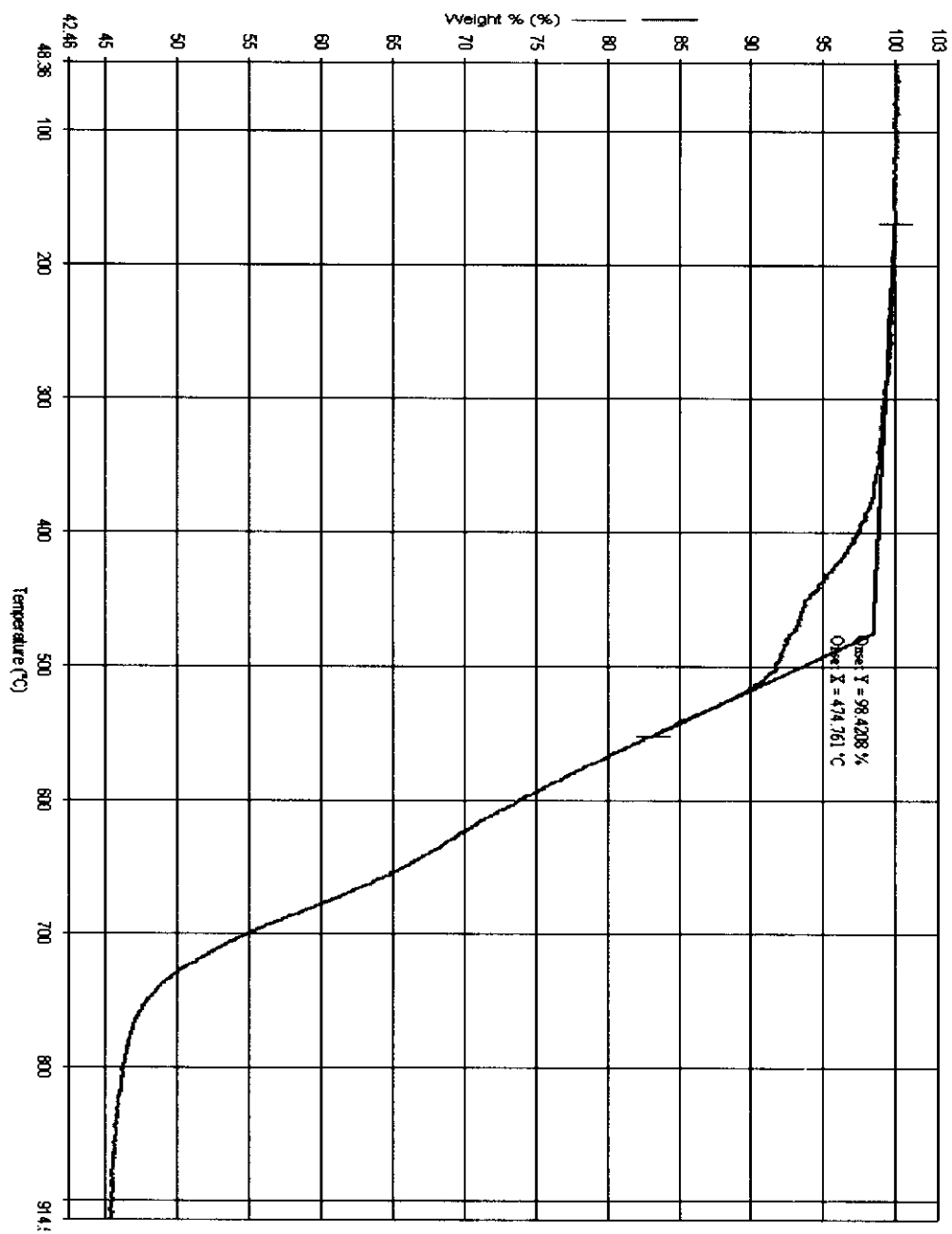


**Figure 5.2:** TGA analysis showing thermal degradation temperature of silicone rubber membrane.

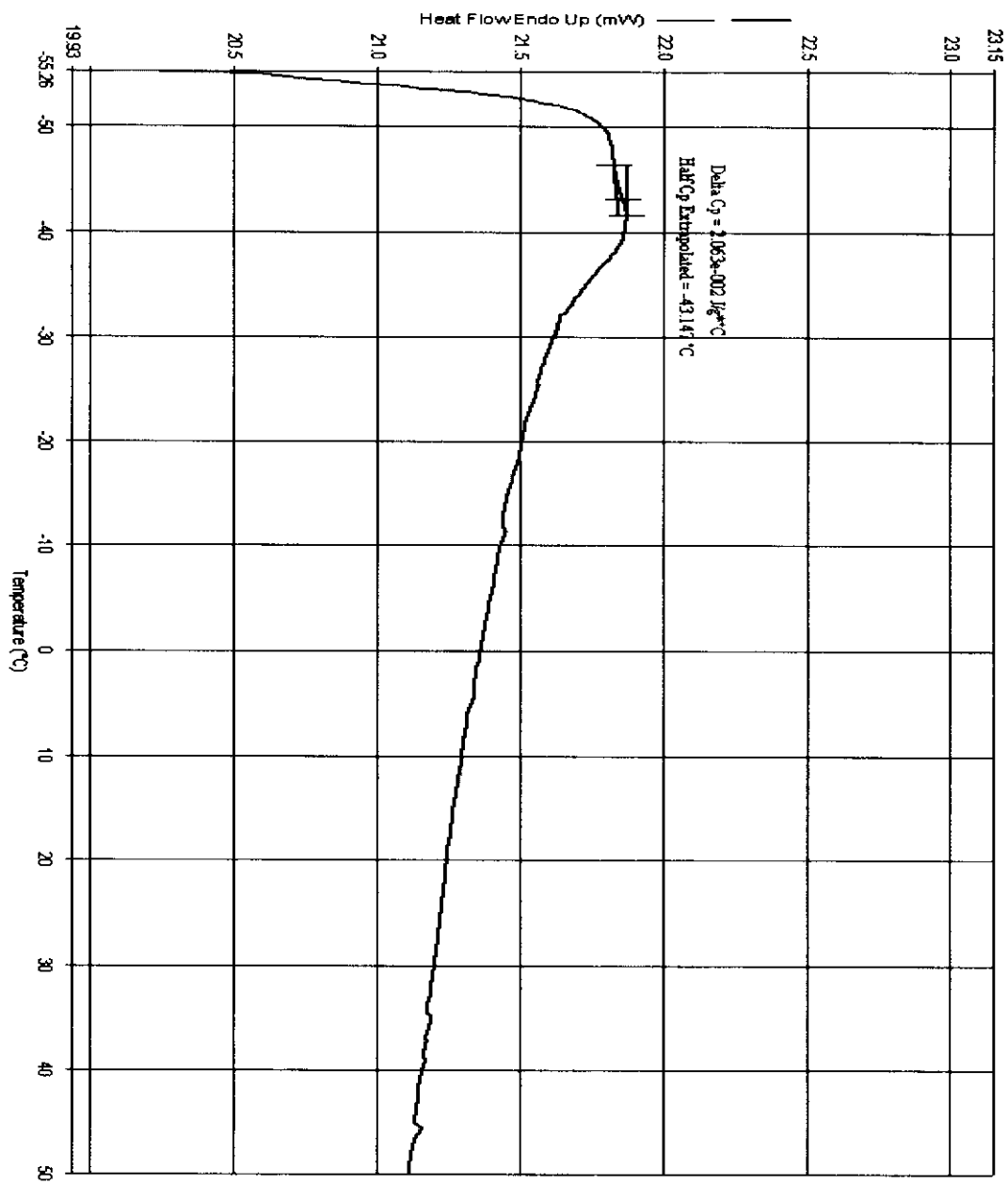


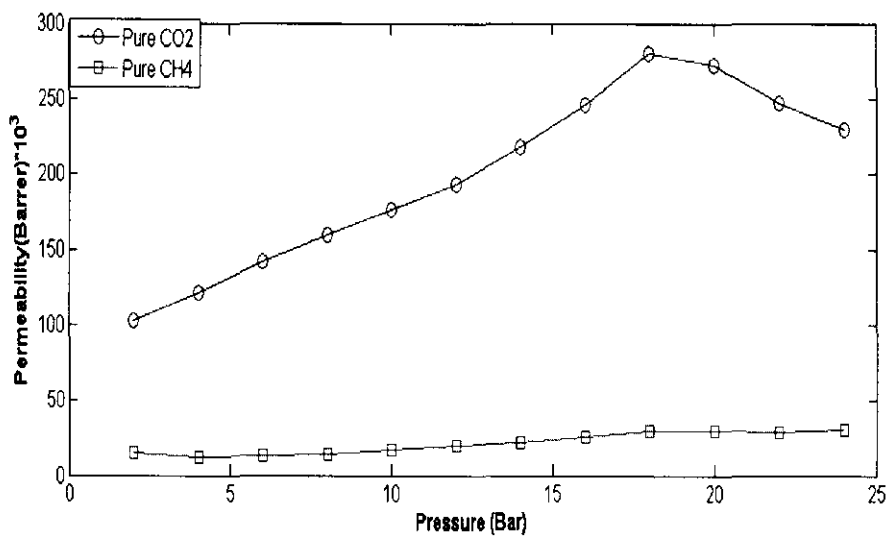
**Figure 5.3:** DSC analysis of silicone rubber membrane showing glass transition temperature of silicone rubber membrane.

## 5.2 Permeability of Pure Gases

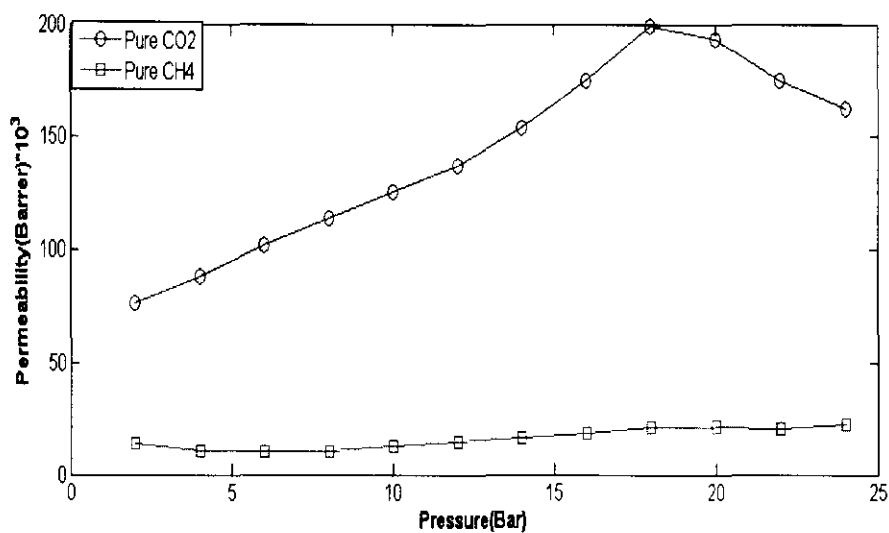
### 5.2.1 Effect of Feed Pressure on Permeability

Figure 5.4 shows the effect of feed pressure on the permeability of pure CO<sub>2</sub> and CH<sub>4</sub> across membrane M<sub>1</sub> at 25°C. Result shows that CO<sub>2</sub> permeability increases with the increase of pressure difference across membrane M<sub>1</sub>, but when pressure reaches 17 bar the permeability of carbon dioxide convex towards pressure axis due to hydrostatic compression effects. While for CH<sub>4</sub> the permeability first slightly decreases with pressure and then increases. Because of the compression effects, the free volume of the polymer decreases (Jordan and Koros, 1990). It appears that the free volume reduction is strong enough only to restrict passage of carbon dioxide to a limited extent. Methane, having a smaller size, can however move through the free volume with out appreciable hindrance. Figure 5.5 and 5.6 show the permeability of CO<sub>2</sub> and CH<sub>4</sub> against pressure across membrane M<sub>2</sub> and M<sub>3</sub> respectively. The same trends were observed as described in Figure 5.1. The permeability of these gases follow the order CO<sub>2</sub> > CH<sub>4</sub>.

The permeability data agree reasonably well with the data reported by Jordan and Koros (Jordan and Koros, 1990). The slight difference between their data and the data of this study can be attributed to the fact that their silicone rubber membrane contains 4.9% silica. In general the gas permeation through dense polymeric membrane is typically described by the solution diffusion model, that is the permeability of gas is determined by the solubility and diffusivity of gas in the membrane (Wijaman and Baker 1995). Silicone rubber has weak inter molecular sieves ability due to its weak inter molecular forces, resulting in broad distribution of intersegmental gap sizes responsible for gas diffusion. The diffusion co-efficient of penetrants often change less than the solubility co-efficient so that more soluble pentrants are more permeable. In 1994 Stern investigated the solubility and diffusivity co-efficient of carbon dioxide in PDMS and found that CO<sub>2</sub> solubility co-efficient increases with pressure and diffusivity slightly decreases with pressure due to hydrostatic compression effects of silicone rubber membranes.



**Figure 5.4:** Permeability of pure CO<sub>2</sub> and pure CH<sub>4</sub> permeability through M<sub>1</sub> silicone rubber membrane against different pressure at 25°C.



**Figure 5.5:** Permeability of pure CO<sub>2</sub> and pure CH<sub>4</sub> permeability through M<sub>2</sub> silicone rubber membrane against different pressure at 25°C.

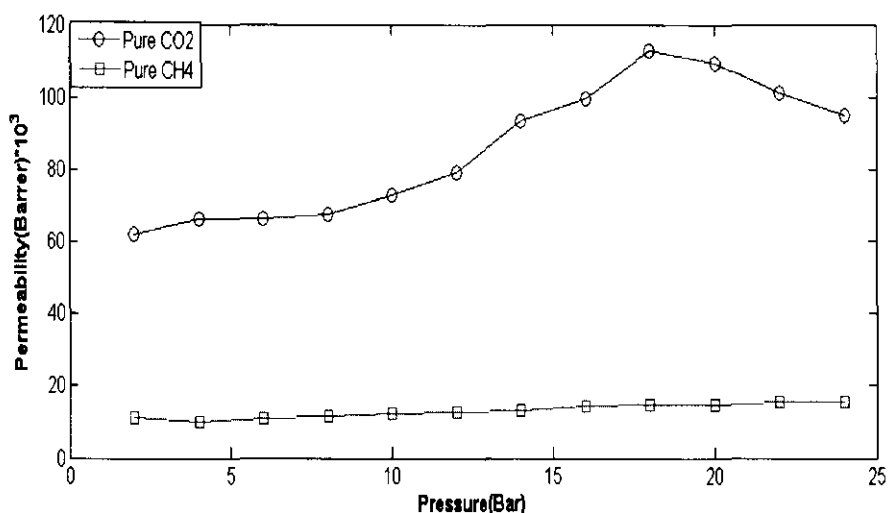


**Figure 5.6:** Permeability of pure CO<sub>2</sub> and pure CH<sub>4</sub> permeability through M<sub>3</sub> silicone rubber membrane with different pressure at 25°C.

Figure 5.7 shows the comparison of permeability of carbon dioxide against pressure across silicone rubber membrane M<sub>1</sub>, M<sub>2</sub> and M<sub>3</sub>. Results show that the permeability of CO<sub>2</sub> across silicone rubber membrane M<sub>1</sub> is the highest followed by membrane M<sub>2</sub> and membrane M<sub>3</sub> respectively. This is due to the effect of membrane thickness. M<sub>1</sub> has the lowest thickness allowing more permeation of CO<sub>2</sub> as compared to membrane M<sub>2</sub> and M<sub>3</sub>. The thicknesses of the membrane are given in chapter 4 in section 4.1. This is in line with solution diffusion model (Wijamins and Baker 1995). Figure 5.8 shows the permeability of CH<sub>4</sub> across silicone rubber membranes M<sub>1</sub>, M<sub>2</sub> and M<sub>3</sub>. Similar trends for CH<sub>4</sub> permeability across membrane M<sub>1</sub>, M<sub>2</sub> and M<sub>3</sub> were observed as described in Figure 5.7.

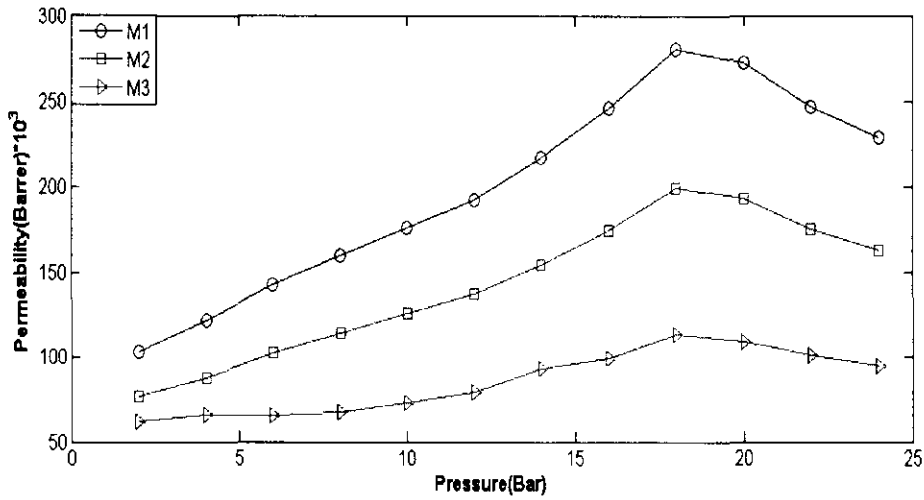


**Figure 5.7 :** Comparison of CO<sub>2</sub> permeability against pressure across silicone rubber membranes M<sub>1</sub>, M<sub>2</sub> and M<sub>3</sub>.

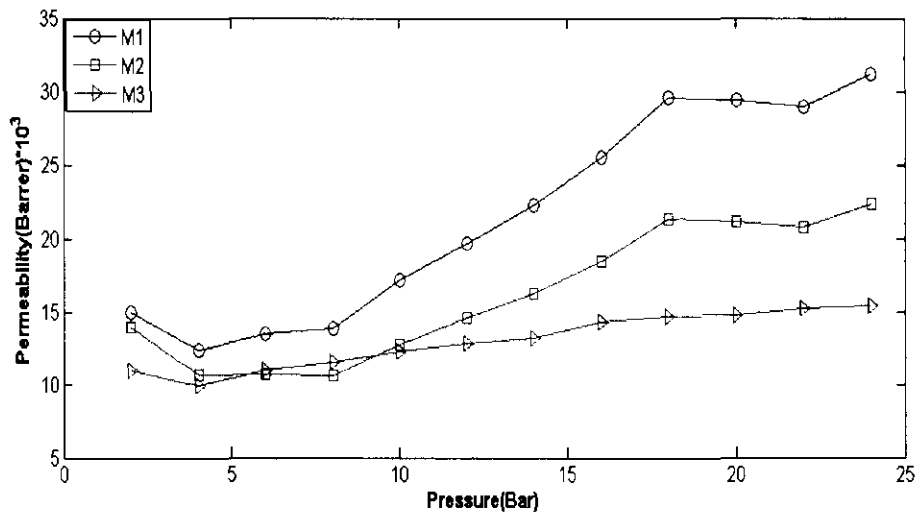
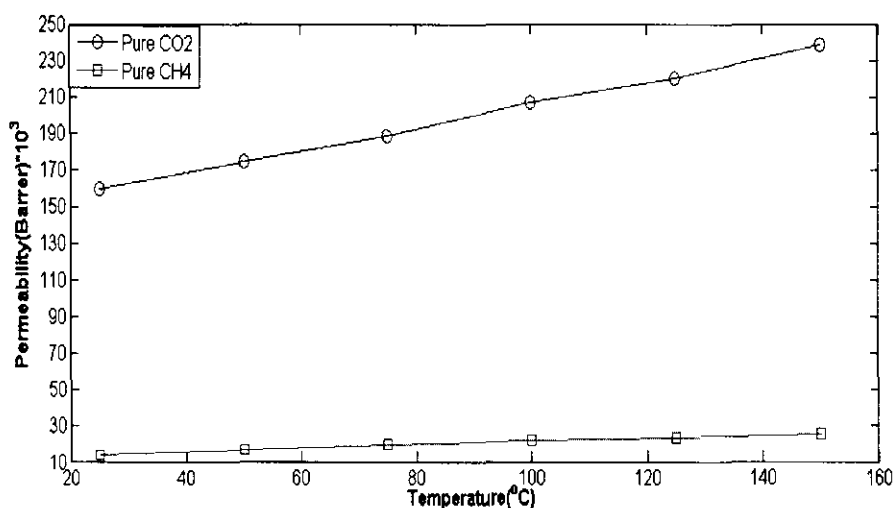


**Figure 5.8 :** Comparison of CH<sub>4</sub> permeability against pressure across silicone rubber membranes M<sub>1</sub>, M<sub>2</sub> and M<sub>3</sub>.

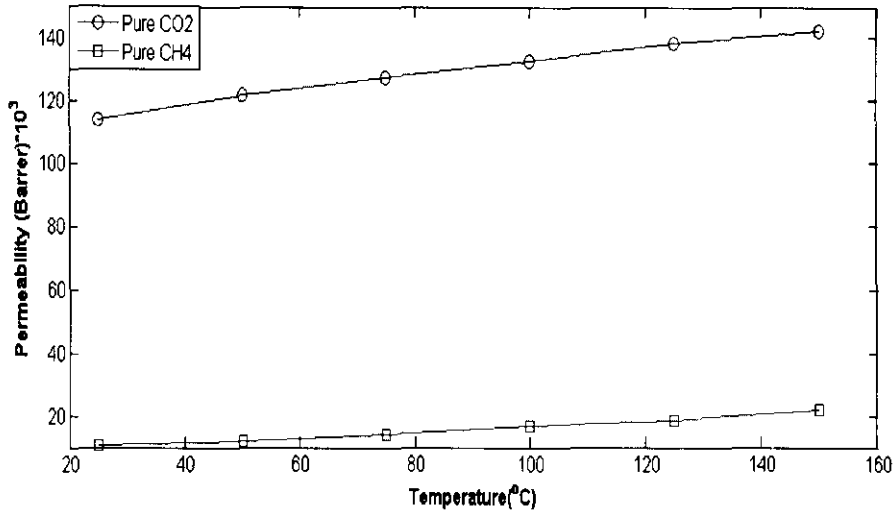
### 5.2.2 Effect of Temperature on Permeability

Figure 5.9 shows the permeability of pure CO<sub>2</sub> and CH<sub>4</sub> against temperature through silicone rubber membrane M<sub>1</sub> at constant pressure of 8 bar. It has been observed that with increasing temperatures the permeability of carbon dioxide and methane increases. But this increase in permeability with temperature is more for carbon dioxide than methane.

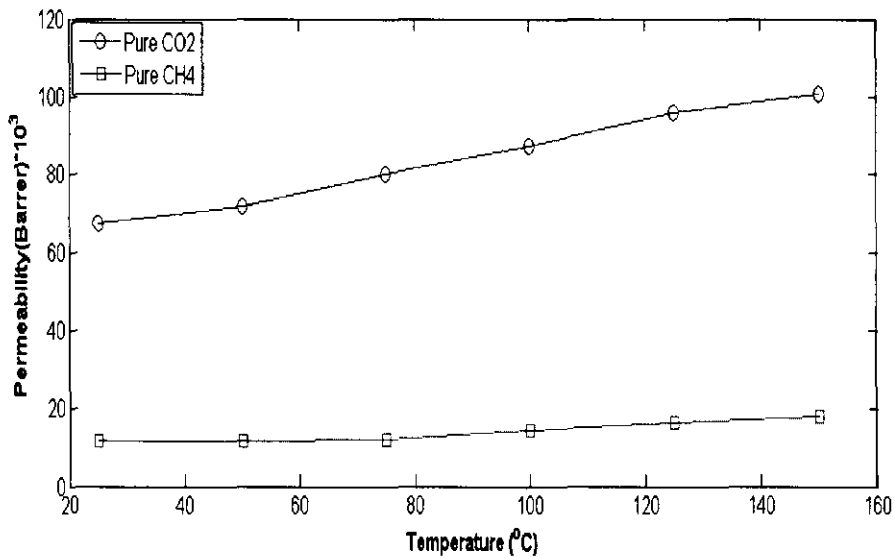
The effect of temperature on permeability of carbon dioxide and methane through silicone rubber membrane has two aspects. The free volume of silicone rubber depends on temperature. Lower temperature results in less free volume and consequently lowers the permeability of carbon dioxide and methane. Similar results have also been observed by (Burnside and Giannelis, 1995). Since the mobility of polymer chain of silicone rubber is high at higher temperature and high mobility of the polymer chains enhances the diffusion of carbon dioxide and methane molecules. Consequently, the permeability of CO<sub>2</sub> and CH<sub>4</sub> increases with increasing temperature. Diffusivity greatly depends on the size of the gas molecule. Since the size of carbon dioxide is smaller than the size of the CH<sub>4</sub> gas molecule, the diffusivity of CO<sub>2</sub> through silicone rubber membrane M<sub>1</sub> is faster compared to CH<sub>4</sub>, resulting in a higher increase in permeability of CO<sub>2</sub> compared to CH<sub>4</sub>. Figures 5.10 and 5.11 show the permeability of pure CO<sub>2</sub> and CH<sub>4</sub> against temperature through silicone rubber membrane M<sub>2</sub> and M<sub>3</sub> at constant pressure of 8 bar respectively. The same trends were observed as described in Figure 5.9.



**Figure 5.9:** Permeability of pure CO<sub>2</sub> and CH<sub>4</sub> through M<sub>1</sub> silicone rubber membrane against temperature at 8 bar.



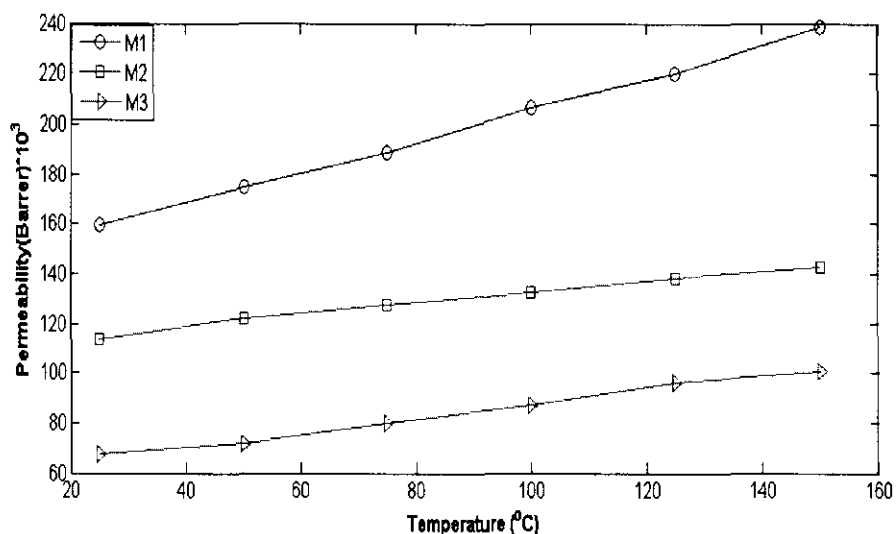
**Figure 5.10:** Permeability of pure CO<sub>2</sub> and CH<sub>4</sub> through M<sub>2</sub> silicone rubber membrane against temperature at 8 bar.



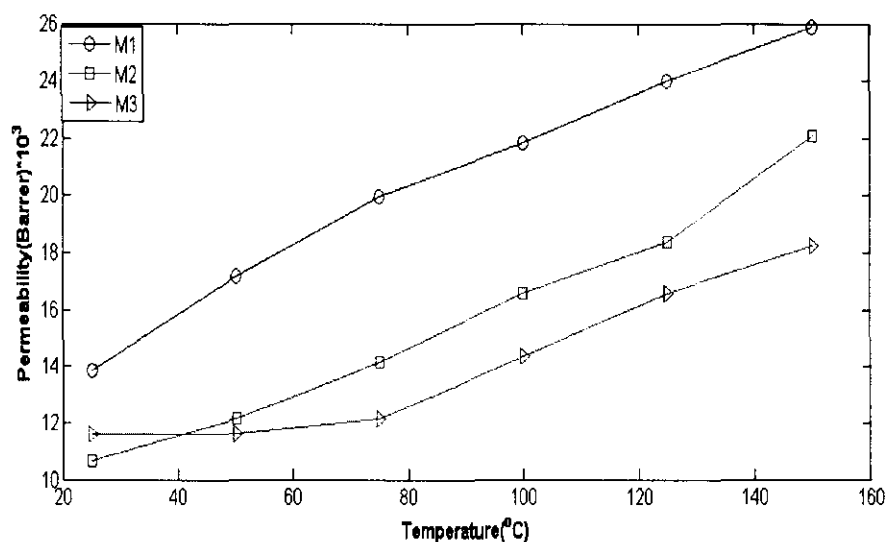
**Figure 5.11:** Permeability of pure CO<sub>2</sub> and CH<sub>4</sub> through M<sub>3</sub> silicone rubber membrane against temperature at 8 bar.

Figure 5.12 shows the comparison of permeability of CO<sub>2</sub> against temperature across silicone rubber membrane M<sub>1</sub>, M<sub>2</sub> and M<sub>3</sub>. It has been observed that permeability of CO<sub>2</sub> against temperature across membrane M<sub>1</sub> is the highest followed by membrane M<sub>2</sub> and M<sub>3</sub> respectively. This is due to the effect of membrane thickness. M<sub>1</sub> has the lowest thickness allowing more permeation of CO<sub>2</sub> as compared to membrane M<sub>2</sub> and M<sub>3</sub>. The thicknesses of the membrane are given in section 4.1 in chapter 4. This is in

line with solution diffusion model (Wijamins and Baker, 1995). Figure 5.13 shows the permeability of CH<sub>4</sub> across silicone rubber membranes M<sub>1</sub>, M<sub>2</sub> and M<sub>3</sub>. Similar trends for CH<sub>4</sub> permeability across membrane M<sub>1</sub>, M<sub>2</sub> and M<sub>3</sub> were observed as described in Figure 5.12.



**Figure 5.12:** Comparison of CO<sub>2</sub> permeability against temperature across silicone rubber membranes M<sub>1</sub>, M<sub>2</sub> and M<sub>3</sub>.



**Figure 5.13 :** Comparison of CH<sub>4</sub> permeability against temperature across silicone rubber membranes M<sub>1</sub>, M<sub>2</sub> and M<sub>3</sub>.

### 5.3 Permeability of Binary Mixture of CO<sub>2</sub>/CH<sub>4</sub>

#### 5.3.1 Effect of Feed Composition

Figure 5.14 shows permeability of carbon dioxide in binary mixture of CO<sub>2</sub>/CH<sub>4</sub> through silicone rubber membrane M<sub>1</sub> against pressure. Carbon dioxide permeability ascends with the increase of carbon dioxide concentration in the binary mixtures of carbon dioxide and methane. This is consistent with previous results (Wu et al, 2006). Figure 5.15 and 5.16 show the permeability of CO<sub>2</sub> in binary mixture of CO<sub>2</sub>/CH<sub>4</sub> against pressure across silicone rubber membrane M<sub>2</sub> and M<sub>3</sub> respectively. The same trends have been observed as described in Figure 5.14.

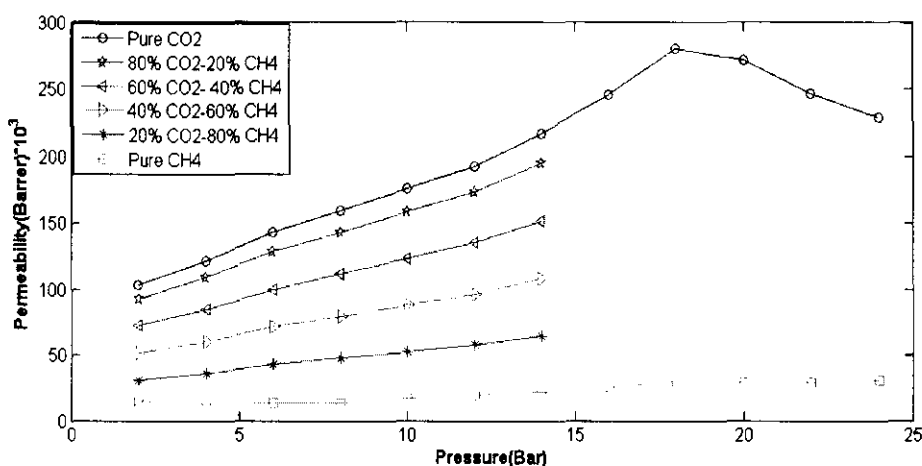


Figure 5.14 : Permeability of CO<sub>2</sub> through silicone rubber membrane M<sub>1</sub> in binary mixture of CO<sub>2</sub>/CH<sub>4</sub> against pressure at 25°C.

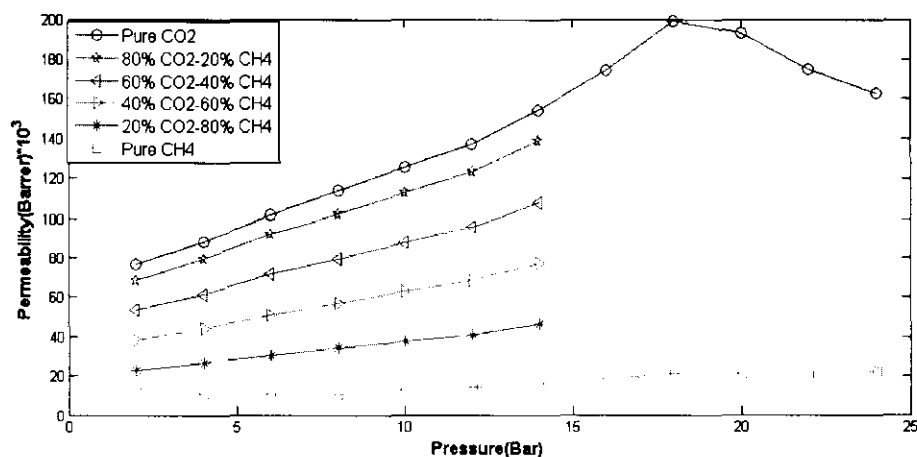
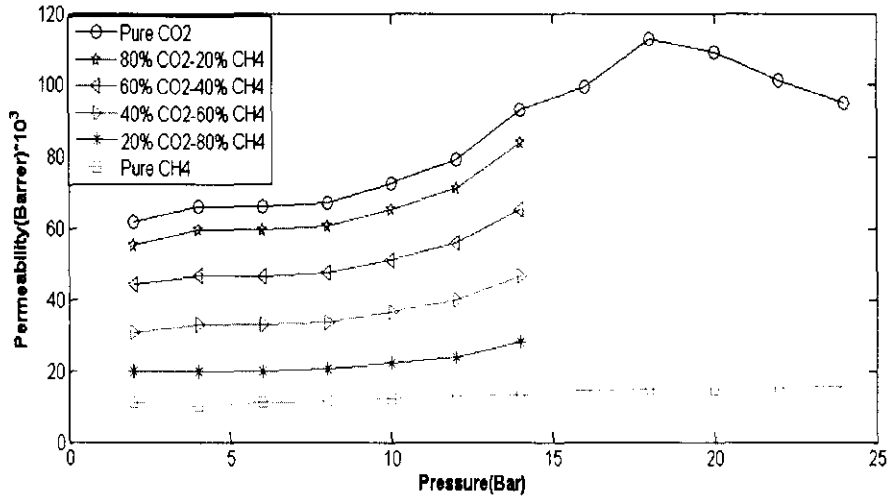
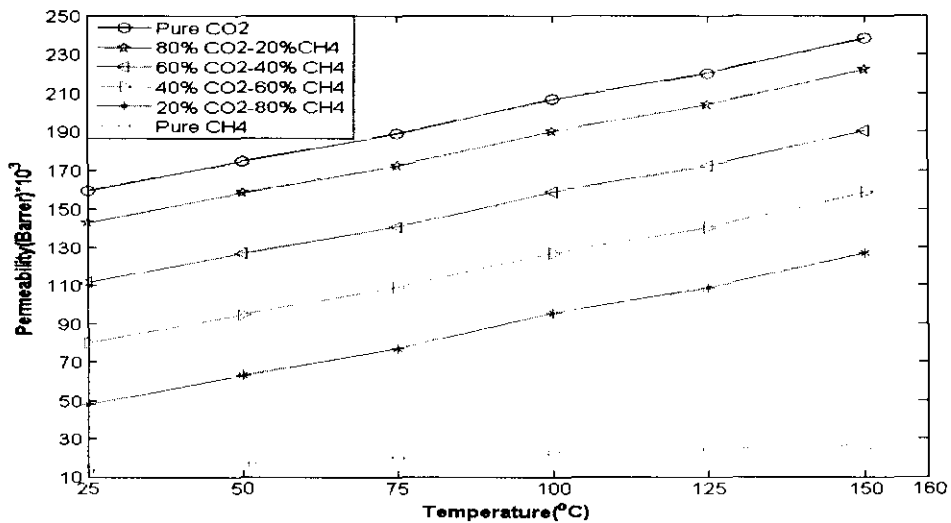


Figure 5.15: Permeability of CO<sub>2</sub> through silicone rubber membrane M<sub>2</sub> in binary mixture of carbon dioxide and methane against pressure at 25°C.

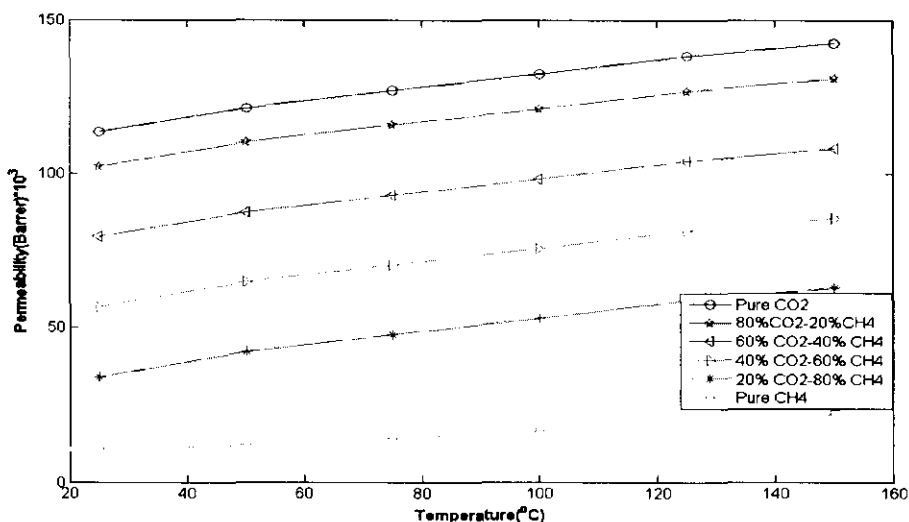


**Figure 5.16 :** Permeability of CO<sub>2</sub> through silicone rubber membrane M<sub>3</sub> in binary mixture of carbon dioxide and methane against at 25°C.

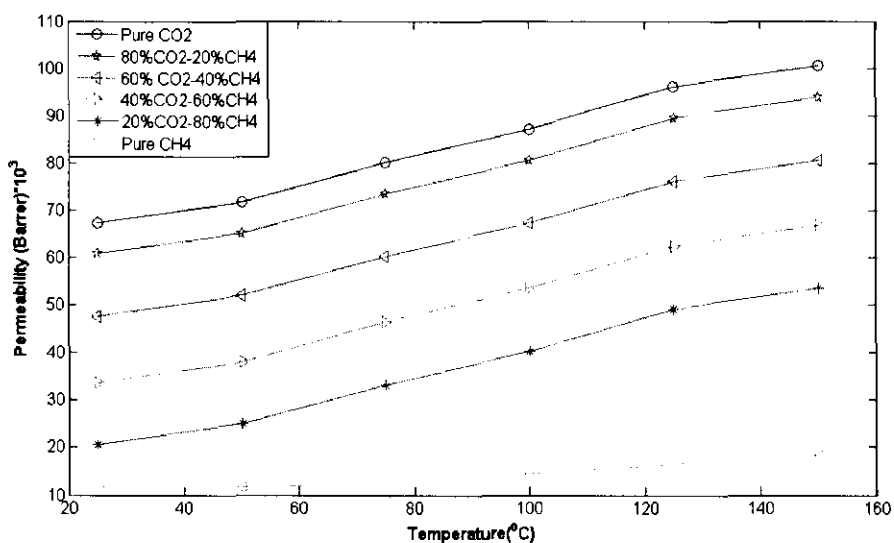
Figure 5.17 shows the permeability of CO<sub>2</sub> in binary mixtures of CO<sub>2</sub>/CH<sub>4</sub> against temperature across silicone rubber membrane M<sub>1</sub>. It has been observed that with the enhancement of the proportion of the carbon dioxide in the binary mixture of CO<sub>2</sub>/CH<sub>4</sub>, the permeability of carbon dioxide increases. Figure 5.18 and 5.19 show the permeability of CO<sub>2</sub> in binary mixtures of CO<sub>2</sub>/CH<sub>4</sub> against temperature across silicone rubber membrane M<sub>2</sub> and M<sub>3</sub>. The same behaviour has been observed as described in Figure 5.17.



**Figure 5.17:** Permeability of CO<sub>2</sub> through M<sub>1</sub> silicone rubber membrane in binary mixture of carbon dioxide and methane against temperature at 8 bar.



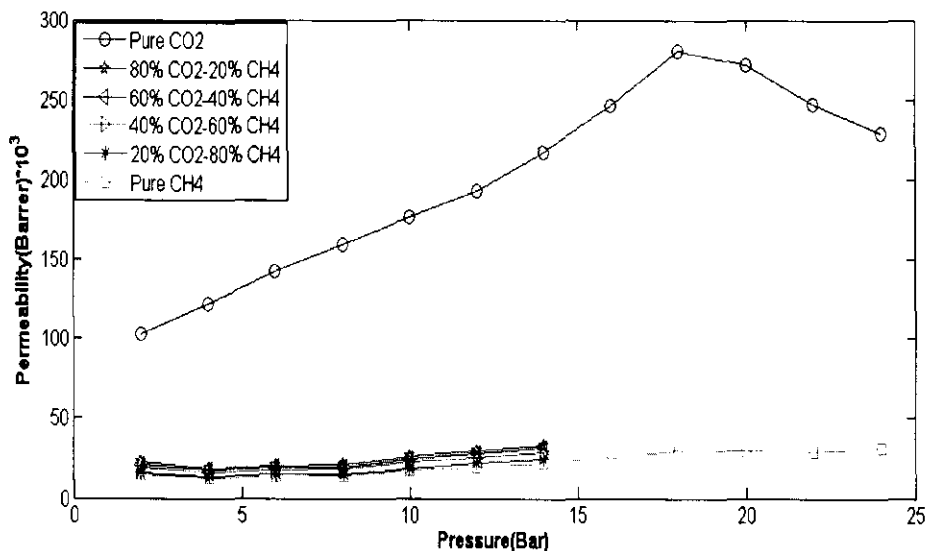
**Figure 5.18:** Permeability of CO<sub>2</sub> through M<sub>2</sub> silicone rubber membrane in binary mixture of carbon dioxide and methane against temperature at 8 bar.



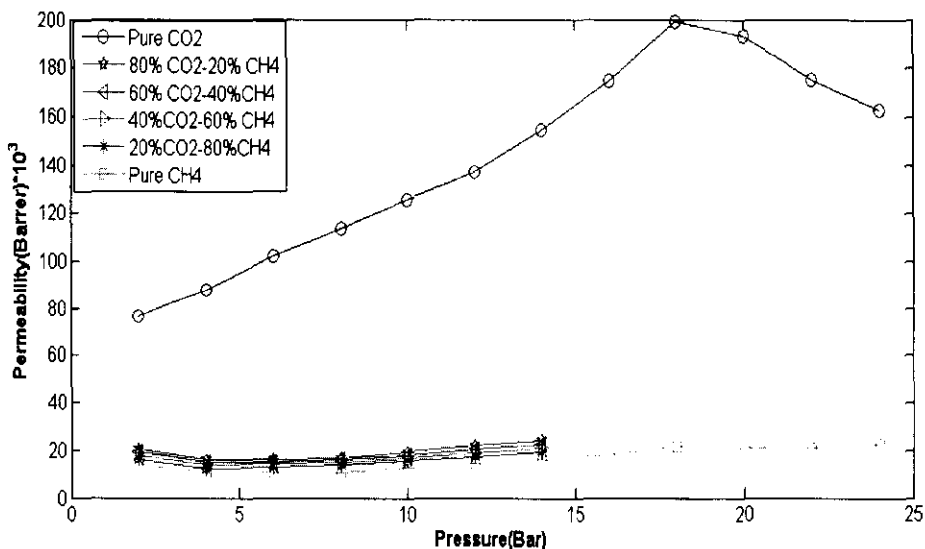
**Figure 5.19:** Permeability of CO<sub>2</sub> through M<sub>3</sub> silicone rubber membrane in binary mixture of carbon dioxide and methane against temperature at 8 bar.

Figure 5.20 shows the permeability of CH<sub>4</sub> against pressure in binary mixture of CO<sub>2</sub>/CH<sub>4</sub> across silicone rubber membrane M<sub>1</sub>. It has been observed that the permeability of methane is significantly enhanced by the presence of carbon dioxide in the feed stream. CO<sub>2</sub> swelling overcomes methane's tendency to compress the polymer, thus the permeability and mobility of CH<sub>4</sub> is increased by the presence of carbon dioxide. Similar behaviour has also been reported by Jordan and Koros

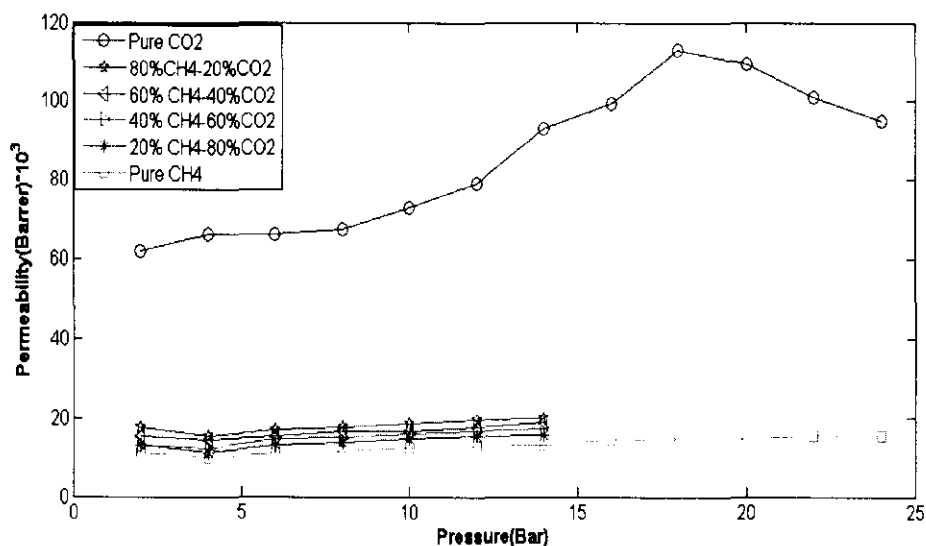
(1990). The observed trends indicate that the higher permeable component is dominating the permeation process and the increase of pressure difference is favorable to the enrichment of the faster component in the permeated stream. Figure 5.21 and 5.22 show the permeability of CH<sub>4</sub> against pressure in binary mixture of CO<sub>2</sub>/CH<sub>4</sub> across silicone rubber membrane M<sub>2</sub> and M<sub>3</sub> respectively. The same trends have been observed as indicated in Figure 5.20.



**Figure 5.20 :** Permeability of CH<sub>4</sub> through M<sub>1</sub> silicone rubber membrane in binary mixtures of carbon dioxide and methane against pressure at 25°C.

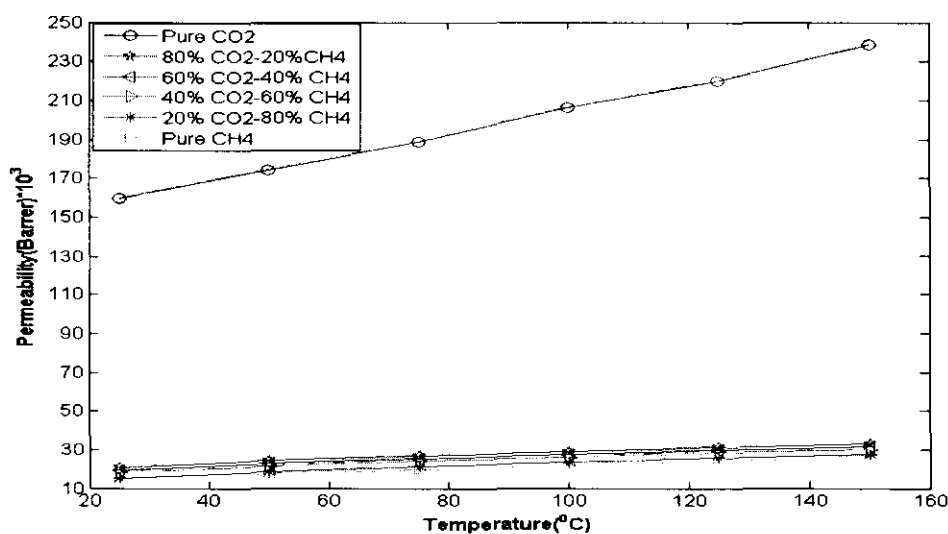


**Figure 5.21:** Permeability of CH<sub>4</sub> through M<sub>2</sub> silicone rubber membrane in binary mixtures of carbon dioxide and methane against pressure at 25°C.

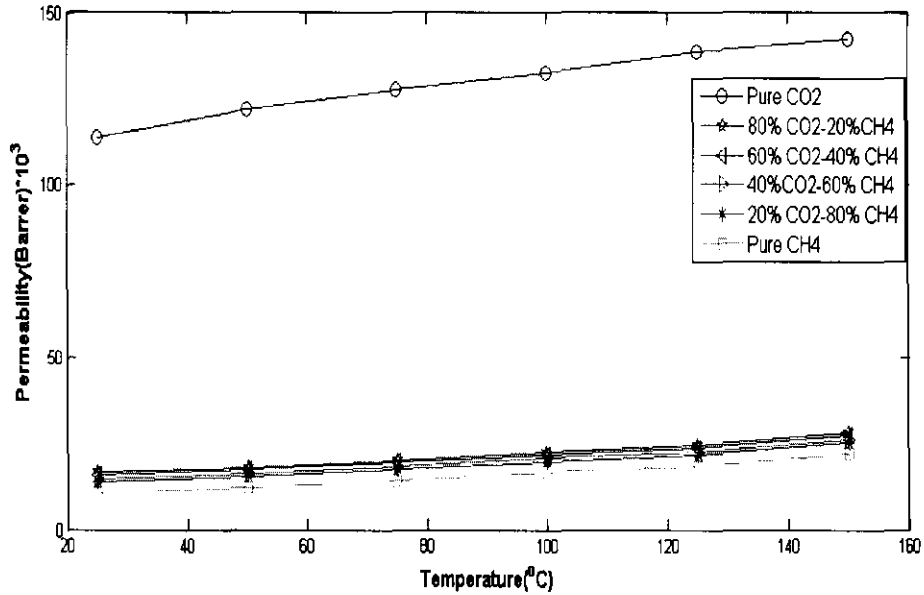


**Figure 5.22 :** Permeability of CH<sub>4</sub> through M<sub>3</sub> silicone rubber membrane in binary mixtures of carbon dioxide and methane against pressure at 25°C.

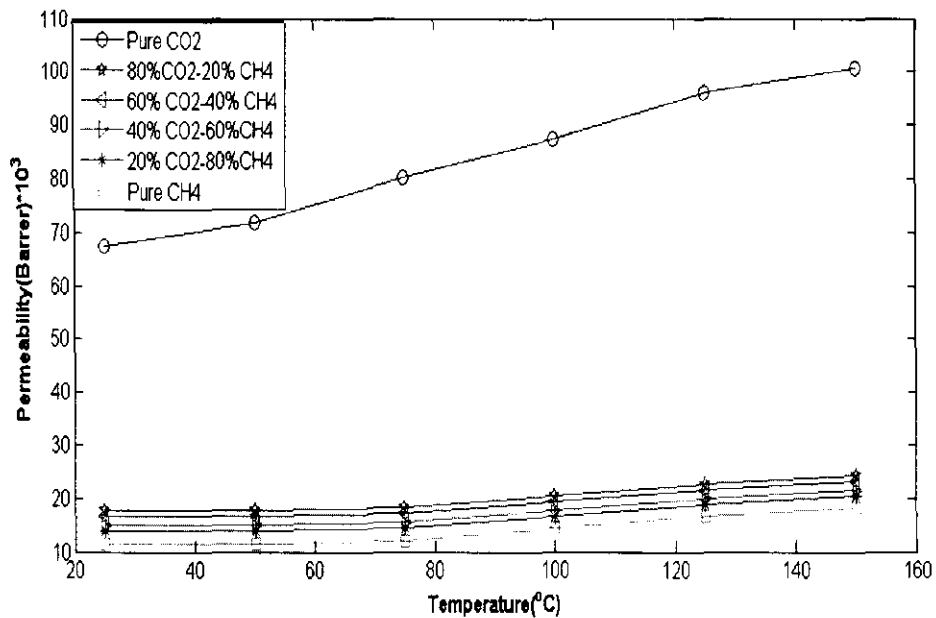
Figure 5.23 shows the permeability of CH<sub>4</sub> in binary mixtures of CO<sub>2</sub>/CH<sub>4</sub> against temperatures across silicone rubber membrane M<sub>1</sub>. It has been observed that with the enhancement of the proportion of the carbon dioxide, the faster component, the permeability of CH<sub>4</sub> increases. Figure 5.24 and 5.25 show the permeability of CH<sub>4</sub> in binary mixtures of CO<sub>2</sub>/CH<sub>4</sub> against temperatures across silicone rubber membrane M<sub>1</sub>, M<sub>2</sub> and M<sub>3</sub>. The same behaviour has been observed as reported in Figure 5.23.



**Figure 5.23:** Permeability of CH<sub>4</sub> through M<sub>1</sub> silicone rubber membrane in binary mixture of carbon dioxide and methane against temperature at 8 bar.



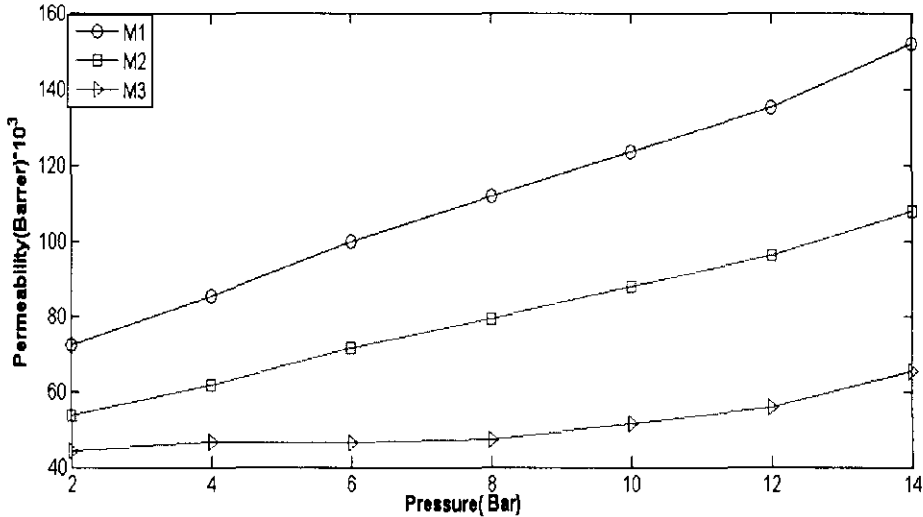
**Figure 5.24:** Permeability of  $\text{CH}_4$  through  $\text{M}_2$  silicone rubber membrane in binary mixture of carbon dioxide and methane against temperature at 8 bar.



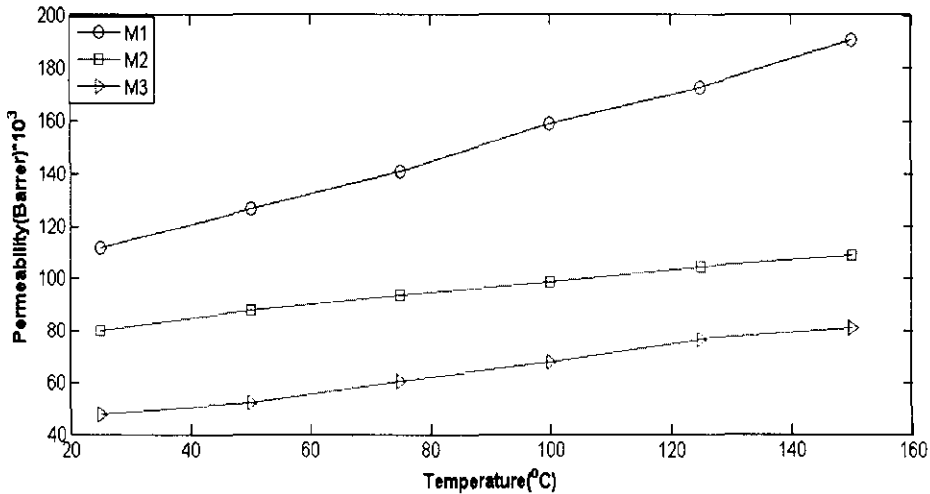
**Figure 5.25:** Permeability of  $\text{CH}_4$  through  $\text{M}_3$  silicone rubber membrane in binary mixture of carbon dioxide and methane with different temperature at 8 bar.

Figure 5.26 and 5.27 show the permeability of  $\text{CO}_2$  in binary mixture (60%  $\text{CO}_2$ -40% $\text{CH}_4$ ) across silicone membranes  $\text{M}_1, \text{M}_2$  and  $\text{M}_3$  against pressure and temperature respectively. It has been observed that the permeability of  $\text{CO}_2$  is

decreasing with increasing the thickness of the membrane. The amount of CO<sub>2</sub> that diffuses through the silicone rubber membrane does depend on the thickness, meaning that thicker membrane result in less total CO<sub>2</sub> diffusion, resulting a lesser CO<sub>2</sub> permeability (Wijamans and Baker, 1995). Figure 5.28 and 5.29 show the permeability of CH<sub>4</sub> in binary mixture (60% CO<sub>2</sub>-40% CH<sub>4</sub>) across silicone membranes M<sub>1</sub>, M<sub>2</sub> and M<sub>3</sub> against pressure and temperature respectively. The same trends has been observed as described in Figure 5.25 and 5.26.



**Figure 5.26:** Comparison of CO<sub>2</sub> permeability against pressure in binary mixture (60% CO<sub>2</sub> - 40%CH<sub>4</sub>) across silicone rubber membranes M<sub>1</sub>, M<sub>2</sub> and M<sub>3</sub>.



**Figure 5.27:** Comparison of CO<sub>2</sub> permeability against temperature in binary mixture (60% CO<sub>2</sub> - 40%CH<sub>4</sub>) across silicone rubber membranes M<sub>1</sub>, M<sub>2</sub> and M<sub>3</sub>.

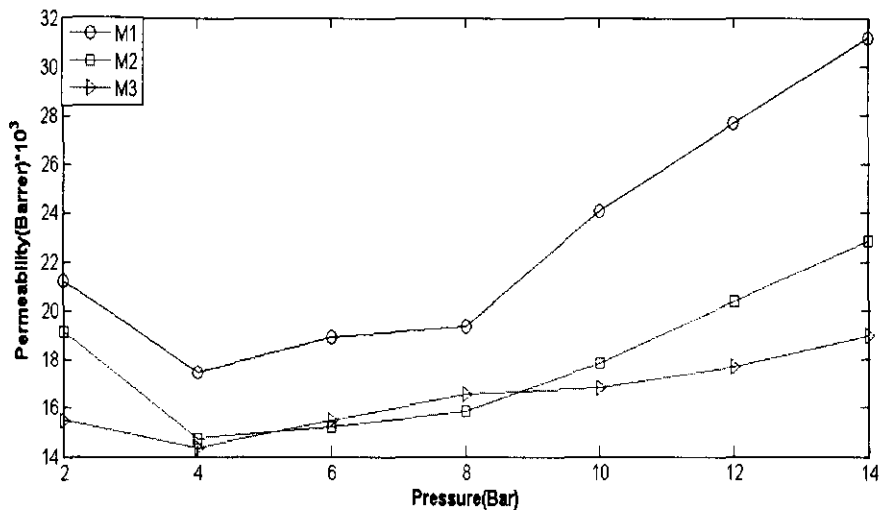


**Figure 5.28:** Comparison of CH<sub>4</sub> permeability against pressure in binary mixture (60% CO<sub>2</sub> - 40%CH<sub>4</sub>) across silicone rubber membranes M<sub>1</sub>, M<sub>2</sub> and M<sub>3</sub>.

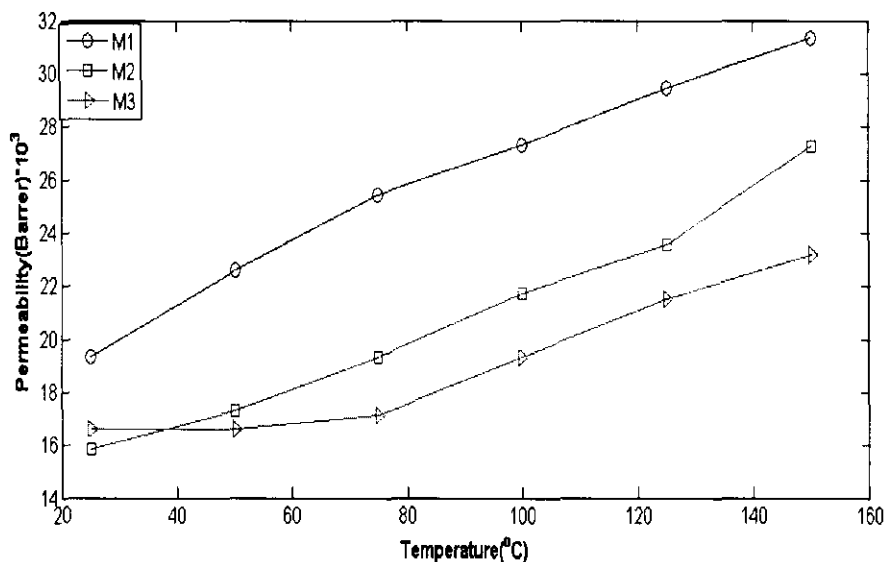


**Figure 5.29:** Comparison of CH<sub>4</sub> permeability against temperature in binary mixture (60% CO<sub>2</sub> - 40%CH<sub>4</sub>) across silicone rubber membranes M<sub>1</sub>, M<sub>2</sub> and M<sub>3</sub>.

## 5.4. Separation Study Through Silicone Rubber Membrane

### 5.4.1. Effect of Pressure, Temperature and Feed Composition on Selectivity

For a binary gas mixture permeating through a polymer membrane, the selectivity of a polymer membrane towards two different penetrant gases, CO<sub>2</sub> and CH<sub>4</sub>, is commonly expressed in terms of the ideal selectivity or ideal perm selectivity,  $\alpha$ .

when the downstream pressure is negligible relative to the upstream pressure,  $\alpha$  can be written as the ratio of permeabilities.

$$\alpha = P_{CO_2} / P_{CH_4} \quad (5.1)$$

Table 5.1 presents the calculated selectivities of pure CO<sub>2</sub> over pure CH<sub>4</sub> and CO<sub>2</sub> over CH<sub>4</sub> in CO<sub>2</sub>/CH<sub>4</sub> binary mixtures in relationship with pressure changes through silicone rubber membrane M<sub>1</sub>. Increasing trends in ideal selectivity with pressure can be observed upto 8 bar, because of the compressive nature of CH<sub>4</sub> in silicone rubber membrane, above 8 bar there is a slight decrease in selectivity because of the increasing permeation rate of methane. Table 5.1 shows that selectivities estimated from pure gas varied slightly with an increase in the feed pressure but reach a max value of 11.494. With 20% CO<sub>2</sub> in the feed stream, the selectivity is two to three times lower than that of pure components over the whole pressure range. High selectivities are obtained at 80% CO<sub>2</sub> in the feed stream.

**Table 5.1** Selectivity of CO<sub>2</sub> over CH<sub>4</sub> through silicone rubber membrane M<sub>1</sub> at different pressure.

Pressure (Bar)	Ideal Selectivity P <sub>CO<sub>2</sub></sub> /P <sub>CH<sub>4</sub></sub>	80% CO <sub>2</sub> - 20%CH <sub>4</sub> Selectivity P <sub>CO<sub>2</sub></sub> /P <sub>CH<sub>4</sub></sub>	60% CO <sub>2</sub> - 40%CH <sub>4</sub> Selectivity P <sub>CO<sub>2</sub></sub> /P <sub>CH<sub>4</sub></sub>	40% CO <sub>2</sub> - 60%CH <sub>4</sub> Selectivity P <sub>CO<sub>2</sub></sub> /P <sub>CH<sub>4</sub></sub>	20% CO <sub>2</sub> - 80%CH <sub>4</sub> Selectivity P <sub>CO<sub>2</sub></sub> /P <sub>CH<sub>4</sub></sub>
2	6.88	4.11	3.41	2.68	1.92
4	9.75	5.85	4.87	3.75	2.66
6	10.55	6.30	5.27	4.03	2.89
8	11.49	6.87	5.77	4.40	3.13
10	10.24	6.14	5.12	3.92	2.81
12	9.76	5.85	4.88	3.75	2.66
14	9.74	5.84	4.87	3.74	2.66

Table 5.2 and Table 5.3 shows the selectivities of pure CO<sub>2</sub>, over pure CH<sub>4</sub> and CO<sub>2</sub> over CH<sub>4</sub> in binary mixture of CO<sub>2</sub>/CH<sub>4</sub> in relationship with pressure changes through silicone rubber membrane M<sub>2</sub> and M<sub>3</sub> respectively. The same trends have been observed as described in Table 5.1.

**Table 5.2** Selectivity of CO<sub>2</sub> over CH<sub>4</sub> through silicone rubber membrane M<sub>2</sub> at different pressure.

Pressure (Bar)	Ideal Selectivity PCO <sub>2</sub> /PCH <sub>4</sub>	80% CO <sub>2</sub> - 20%CH <sub>4</sub> Selectivity PCO <sub>2</sub> /PCH <sub>4</sub>	60% CO <sub>2</sub> - 40%CH <sub>4</sub> Selectivity PCO <sub>2</sub> /PCH <sub>4</sub>	40% CO <sub>2</sub> - 60%CH <sub>4</sub> Selectivity PCO <sub>2</sub> /PCH <sub>4</sub>	20% CO <sub>2</sub> - 80%CH <sub>4</sub> Selectivity PCO <sub>2</sub> /PCH <sub>4</sub>
2	5.47	3.32	2.81	2.17	1.40
4	8.24	5.00	4.18	3.24	2.12
6	9.45	5.67	4.69	3.59	2.40
8	10.65	6.18	5.02	3.85	2.47
10	9.79	5.89	4.93	3.77	2.46
12	9.39	5.65	4.71	3.60	2.36
14	9.46	5.69	4.73	3.67	2.37

**Table 5.3** Selectivity of CO<sub>2</sub> over CH<sub>4</sub> through silicone rubber membrane M<sub>3</sub> at different pressure.

Pressure (Bar)	Ideal Selectivity PCO <sub>2</sub> /PCH <sub>4</sub>	80% CO <sub>2</sub> - 20%CH <sub>4</sub> Selectivity PCO <sub>2</sub> /PCH <sub>4</sub>	60% CO <sub>2</sub> - 40%CH <sub>4</sub> Selectivity PCO <sub>2</sub> /PCH <sub>4</sub>	40% CO <sub>2</sub> - 60%CH <sub>4</sub> Selectivity PCO <sub>2</sub> /PCH <sub>4</sub>	20% CO <sub>2</sub> - 80%CH <sub>4</sub> Selectivity PCO <sub>2</sub> /PCH <sub>4</sub>
2	5.6	3.12	2.86	2.33	1.5
4	6.67	3.86	3.23	2.73	1.8
6	6	3.52	3	2.25	1.5
8	5.80	3.44	2.87	2.26	1.48
10	5.89	3.52	3.05	2.31	1.52
12	6.14	3.66	3.17	2.4	1.55
14	7.02	4.22	3.45	2.69	1.8

Table 5.4 shows effect of temperature on the ideal selectivity for pure CO<sub>2</sub> and CH<sub>4</sub> through silicone rubber membrane M<sub>1</sub>. Table 5.4 also shows the effect of feed composition on the selectivity of binary mixture CO<sub>2</sub>/CH<sub>4</sub> at different temperature through silicone rubber membrane M<sub>1</sub>. With 20% CO<sub>2</sub> in the feed stream, the selectivity is two to three times lower than that of pure components over the whole temperature range. High selectivities are obtained at 80% CO<sub>2</sub> in the feed stream.

Similar results has also been observed by (Ghosal and Freeman, 1993). Gas diffusion coefficients typically increase appreciably with increasing temperature (Ghosal and Freeman, 1993). The temperature changes also affect the solubility selectivity, which

is governed primarily by the chemical nature of the penetrant and polymer-penetrant interactions. For both CO<sub>2</sub>, CH<sub>4</sub> gases, as temperature increases, the solubilities increase. Since carbon dioxide is more condensable component to methane its solubility increase with temperature is higher than methane. The solubility selectivity, therefore, will vary depending on the extent of the temperature effect on each component in the gas mixture (Costello and Koros, 1994). Table 5.5 and 5.6 show the selectivities of pure CO<sub>2</sub>, CH<sub>4</sub> and CO<sub>2</sub>/CH<sub>4</sub> pairs in relationship with temperature changes through silicone rubber membrane M<sub>2</sub> and M<sub>3</sub> respectively. The same trends have been observed as described in Table 5.4.

**Table 5.4** Selectivity of CO<sub>2</sub> over CH<sub>4</sub> through silicone rubber membrane M<sub>1</sub> at different temperature.

Temperature (°C)	Ideal Selectivity PCO <sub>2</sub> /PCH <sub>4</sub>	80% CO <sub>2</sub> - 20%CH <sub>4</sub> Selectivity PCO <sub>2</sub> /PCH <sub>4</sub>	60% CO <sub>2</sub> - 40%CH <sub>4</sub> Selectivity PCO <sub>2</sub> /PCH <sub>4</sub>	40% CO <sub>2</sub> - 60%CH <sub>4</sub> Selectivity PCO <sub>2</sub> /PCH <sub>4</sub>	20% CO <sub>2</sub> - 80%CH <sub>4</sub> Selectivity PCO <sub>2</sub> /PCH <sub>4</sub>
25	11.49	6.85	5.77	4.40	3.13
50	10.18	6.55	5.61	4.43	3.39
75	9.45	6.39	5.54	4.50	3.60
100	9.46	6.59	5.82	4.86	4.08
125	9.17	6.57	5.85	4.97	4.26
150	9.21	6.75	6.08	5.27	4.65

**Table 5.5** Selectivity of CO<sub>2</sub> over CH<sub>4</sub> through silicone rubber membrane M<sub>2</sub> at different temperature.

Temperature (°C)	Ideal Selectivity PCO <sub>2</sub> /PCH <sub>4</sub>	80% CO <sub>2</sub> - 20%CH <sub>4</sub> Selectivity PCO <sub>2</sub> /PCH <sub>4</sub>	60% CO <sub>2</sub> - 40%CH <sub>4</sub> Selectivity PCO <sub>2</sub> /PCH <sub>4</sub>	40% CO <sub>2</sub> - 60%CH <sub>4</sub> Selectivity PCO <sub>2</sub> /PCH <sub>4</sub>	20% CO <sub>2</sub> - 80%CH <sub>4</sub> Selectivity PCO <sub>2</sub> /PCH <sub>4</sub>
25	10.65	6.18	5.02	3.85	2.46
50	10.03	6.12	5.06	4	2.75
75	8.99	5.78	4.81	3.85	2.75
100	8	5.39	4.52	3.66	2.68
125	7.52	5.22	4.42	3.62	2.72
150	6.45	4.68	3.9	3.26	2.48

**Table 5.6** Selectivity of CO<sub>2</sub> over CH<sub>4</sub> through silicone rubber membrane M<sub>3</sub> at different temperature.

Temperature (°C)	Ideal Selectivity P <sub>CO<sub>2</sub></sub> /P <sub>CH<sub>4</sub></sub>	80% CO <sub>2</sub> - 20%CH <sub>4</sub> Selectivity P <sub>CO<sub>2</sub></sub> /P <sub>CH<sub>4</sub></sub>	60% CO <sub>2</sub> - 40%CH <sub>4</sub> Selectivity P <sub>CO<sub>2</sub></sub> /P <sub>CH<sub>4</sub></sub>	40% CO <sub>2</sub> - 60%CH <sub>4</sub> Selectivity P <sub>CO<sub>2</sub></sub> /P <sub>CH<sub>4</sub></sub>	20% CO <sub>2</sub> - 80%CH <sub>4</sub> Selectivity P <sub>CO<sub>2</sub></sub> /P <sub>CH<sub>4</sub></sub>
25	5.81	3.44	2.87	2.26	1.48
50	6.19	3.69	3.13	2.56	1.8
75	6.59	4.03	3.51	3	2.31
100	6.08	3.95	3.49	3.03	2.43
125	5.8	3.95	3.54	3.14	2.62
150	5.52	3.86	3.48	3.10	2.62

### 5.5. Mixed Gas Permeability from Pure gases permeability by Analytical Model

From the permeation behaviour of pure and carbon dioxide and methane, a simple and practical mathematical model expressed in terms of pressure and feed composition was derived to predict quantitatively the permeability at different feed composition. A similar co-relation has been used by (Wu et al 2006). The pure CO<sub>2</sub> and CH<sub>4</sub> permeability is correlated to binary mixture of carbon dioxide and methane through following empirical co-relation.

$$P_{CO_2 \text{ mix}} = m p_{CO_2 \text{ pure}} + n y p_{CO_2 \text{ pure}} + l(1 - y) p_{CH_4 \text{ pure}} \quad (5.2)$$

$$P_{CH_4 \text{ mix}} = m p_{CH_4 \text{ pure}} + n y p_{CH_4 \text{ pure}} + l(1 - y) p_{CO_2 \text{ pure}} \quad (5.3)$$

where  $P_{CO_2 \text{ mix}}$  and  $P_{CH_4 \text{ mix}}$  are the permeability of carbon dioxide and methane in binary mixture of carbon dioxide and methane,  $y$  is the volumetric composition of carbon dioxide in binary mixture of carbon dioxide and methane,  $p_{CO_2 \text{ pure}}$  is the permeability of carbon dioxide at its partial pressure,  $p_{CH_4 \text{ pure}}$  is the permeability of methane at its partial pressure and  $m$ ,  $n$  and  $l$  are the co-efficient. The  $p_{CO_2 \text{ pure}}$  and  $p_{CH_4 \text{ pure}}$  are computed from linear fitting equations using Matlab Version 7.1 and

are shown in Table 5.7 for membrane  $M_1, M_2$  and  $M_3$ . The computed values  $p_{CO_2 \text{ pure}}$  and  $p_{CH_4 \text{ pure}}$  are shown in Table 5.8 and 5.9 respectively for membrane  $M_1$ .

**Table 5.7** Linear fitting equations for pure  $CO_2$  and pure  $CH_4$  permeability at different pressure across silicone rubber membrane  $M, M_1, M_3$ .

Membrane	Linear fitting equation	
$M_1$	$CO_2$	$CH_4$
	$P=9.3 \times p+85$ Norms of residuals = 4.8	$P=0.72 \times p+11$ Norms of residuals= 4.5
$M_2$	$P=6.3 \times p+63$ Norms of residuals = 3.57	$P=0.3 \times p+10$ Norms of residuals = 4.4
$M_3$	$P=2.3 \times p+54$ Norms of residuals = 10.8	$P=0.25 \times p+9.8$ Norms of residuals = 1.1

**Table 5.8** Permeability of carbon dioxide at its partial pressure through silicone rubber membrane  $M_1$ .

Composition	Pressure	Partial pressure	$P_{CO_2 \text{ pure}}$
80% $CO_2$ -20% $CH_4$	2	1.6	99.88
	4	3.2	114.76
	6	4.8	129.64
	8	6.4	144.52
	10	8	159.4
	12	9.6	174.28
	14	11.2	189.16
60% $CO_2$ -40% $CH_4$	2	1.2	96.16
	4	2.4	107.32
	6	3.6	118.48
	8	4.8	129.64
	10	6	140.8
	12	7.2	151.96
	14	8.4	163.12
20% $CO_2$ -80% $CH_4$	2	0.4	88.72
	4	0.8	92.44
	6	1.2	96.16
	8	1.6	99.88
	10	2	103.6
	12	2.4	107.32
	14	2.8	111.04

**Table 5.9** Permeability of methane at its partial pressure through silicone rubber membrane M<sub>1</sub>.

Composition	Pressure	Partial pressure	P <sub>CH<sub>4</sub> pure</sub>
80% CO <sub>2</sub> -20%CH <sub>4</sub>	2	0.4	11.288
	4	0.8	11.576
	6	1.2	11.864
	8	1.6	12.152
	10	2	12.44
	12	2.4	12.728
	14	2.8	13.016
60% CO <sub>2</sub> -40%CH <sub>4</sub>	2	0.8	11.576
	4	1.6	12.152
	6	2.4	12.728
	8	3.2	13.304
	10	4	13.88
	12	4.8	14.456
	14	5.6	15.032
20% CO <sub>2</sub> -80%CH <sub>4</sub>	2	1.6	12.152
	4	3.2	13.304
	6	4.8	14.456
	8	6.4	15.608
	10	8	16.76
	12	9.6	17.912
	14	11.2	19.064

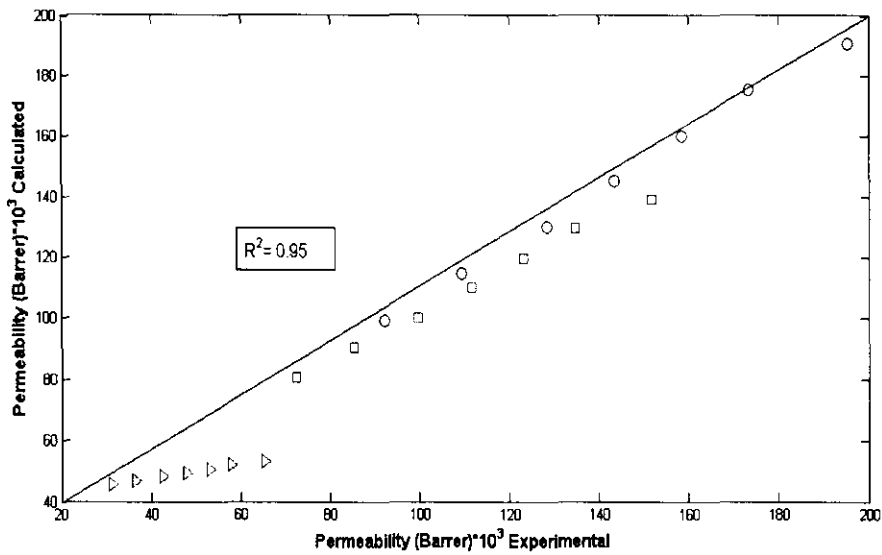
Equation 5.2 and 5.3 are linear equation with one dependent and three independent variables. Using polymath a multiple linear regression is carried out to solve equation 5.2. The co-efficients  $m, n,$  and  $l$  at which the co-relation is best fitted to the experimental permeability of binary mixtures are obtained from the multiple linear regression and are tabulated in Tables 5.10.

**Table 5.10** Polymath results for co-efficients  $m, n,$  and  $l$  for CO<sub>2</sub> permeability through silicone rubber membrane M<sub>1</sub>.

Co-efficients	Value
$m$	0.52
$n$	0.63
$l$	-1.22

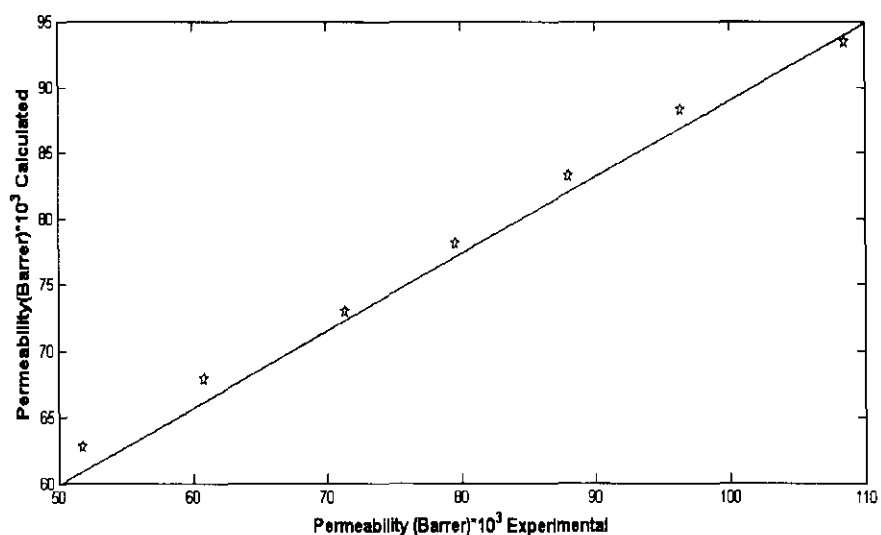
The comparison of carbon dioxide experimental permeability through silicone rubber membrane M<sub>1</sub> with the calculated permeability at different pressures is shown in

Figure 5.30. A regression co-efficient ( $R^2 = 0.95$ ) was obtained showing that the co-relation is best fitted to the experimental data.



**Figure: 5.30** Comparison of experimental and calculated permeabilities of CO<sub>2</sub> through M<sub>1</sub> silicone rubber membrane in binary mixtures of methane and carbon dioxide at different pressure.

In order to test the validity of the co-relation, the co-efficients  $m, n, l$  are used to test the experimental data of binary mixture other than those that are used in multiple linear regression to find these co-efficients. In Figure 5.31 the comparison of experimental and calculated permeability of carbon dioxide in binary mixture of carbon dioxide and methane (40% CO<sub>2</sub>-60%CH<sub>4</sub>) is shown. The percentage errors between experimental permeability and calculated permeability are shown in Table 5.11..



**Figure: 5.31** Comparison of experimental and calculated permeabilities of CO<sub>2</sub> through M<sub>1</sub> silicone rubber membrane in binary mixture (40% CO<sub>2</sub>-60% CH<sub>4</sub>) at different pressure.

**Table 5.11:** Percentage error between experimental permeability and calculated permeability of carbon dioxide through silicone rubber membrane M<sub>1</sub>.

Experimental Permeability (Barrer) × 10 <sup>3</sup>	Calculated Permeability (Barrer) × 10 <sup>3</sup>	Percentage ± Error
51.76957148	62.74964	21.20
60.81365324	67.86647	11.59
71.31310449	72.9833	2.34
79.68147899	78.10013	-1.98
88.07064449	83.21696	-5.51
96.36625052	88.3338	-8.33
108.5289812	93.45063	-13.89

Similarly for silicone rubber membrane M<sub>2</sub> and M<sub>3</sub>, the  $p_{\text{CO}_2 \text{ pure}}$  and  $p_{\text{CH}_4 \text{ pure}}$  are computed from linear fitting equations shown in Table 5.7 and are tabulated in Table 5.12 to 5.15.

**Table 5.12:** Permeability of carbon dioxide at its partial pressure through silicone rubber membrane M<sub>2</sub>.

Composition	Pressure	Partial pressure	$P_{CO_2 \text{ pure}}$
80% CO <sub>2</sub> -20%CH <sub>4</sub>	2	1.6	73.08
	4	3.2	83.16
	6	4.8	93.24
	8	6.4	103.32
	10	8	113.4
	12	9.6	123.48
	14	11.2	133.56
60% CO <sub>2</sub> -40%CH <sub>4</sub>	2	1.2	70.56
	4	2.4	78.12
	6	3.6	85.68
	8	4.8	93.24
	10	6	100.8
	12	7.2	108.36
	14	8.4	115.92
20% CO <sub>2</sub> -80%CH <sub>4</sub>	2	0.4	65.52
	4	0.8	68.04
	6	1.2	70.56
	8	1.6	73.08
	10	2	75.6
	12	2.4	78.12
	14	2.8	80.64

**Table 5.13:** Permeability of methane at its partial pressure through silicone rubber membrane M<sub>2</sub>.

Composition	Pressure	Partial pressure	$P_{CH_4, pure}$
80% CO <sub>2</sub> -20%CH <sub>4</sub>	2	0.4	10.12
	4	0.8	10.24
	6	1.2	10.36
	8	1.6	10.48
	10	2	10.6
	12	2.4	10.72
	14	2.8	10.84
60% CO <sub>2</sub> -40%CH <sub>4</sub>	2	0.8	10.24
	4	1.6	10.48
	6	2.4	10.72
	8	3.2	10.96
	10	4	11.2
	12	4.8	11.44
	14	5.6	11.68
20% CO <sub>2</sub> -80%CH <sub>4</sub>	2	1.6	10.48
	4	3.2	10.96
	6	4.8	11.44
	8	6.4	11.92
	10	8	12.4
	12	9.6	12.88
	14	11.2	13.36

**Table 5.14:** Permeability of carbon dioxide at its partial pressure through silicone rubber membrane M<sub>3</sub>.

Composition	Pressure	Partial pressure	$P_{CO_2 \text{ pure}}$
80% CO <sub>2</sub> -20%CH <sub>4</sub>	2	1.6	57.68
	4	3.2	61.36
	6	4.8	65.04
	8	6.4	68.72
	10	8	72.4
	12	9.6	76.08
	14	11.2	79.76
60% CO <sub>2</sub> -40%CH <sub>4</sub>	2	1.2	56.76
	4	2.4	59.52
	6	3.6	62.28
	8	4.8	65.04
	10	6	67.8
	12	7.2	70.56
	14	8.4	73.32
20% CO <sub>2</sub> -80%CH <sub>4</sub>	2	0.4	54.92
	4	0.8	55.84
	6	1.2	56.76
	8	1.6	57.68
	10	2	58.6
	12	2.4	59.52
	14	2.8	60.44

**Table 5.15:** Permeability of methane at its partial pressure through silicone rubber membrane M<sub>3</sub>.

Composition	Pressure	Partial pressure	$P_{CH_4, pure}$
80% CO <sub>2</sub> -20%CH <sub>4</sub>	2	0.4	9.9
	4	0.8	10
	6	1.2	10.1
	8	1.6	10.2
	10	2	10.3
	12	2.4	10.4
	14	2.8	10.5
60% CO <sub>2</sub> -40%CH <sub>4</sub>	2	0.8	10
	4	1.6	10.2
	6	2.4	10.4
	8	3.2	10.6
	10	4	10.8
	12	4.8	11
	14	5.6	11.2
20% CO <sub>2</sub> -80%CH <sub>4</sub>	2	1.6	10.2
	4	3.2	10.6
	6	4.8	11
	8	6.4	11.4
	10	8	11.8
	12	9.6	12.2
	14	11.2	12.6

Similarly, the comparison of carbon dioxide experimental permeability through silicone rubber membrane M<sub>2</sub> and M<sub>3</sub> with the calculated permeability of carbon dioxide at different pressures is shown in Figure 5.32 and 5.33 respectively. A regression co-efficient ( $R^2$ ) was obtained showing that the co-relation is best fitted to the experimental data. The coefficients  $m, n$ , and  $l$  are shown in Table 5.16 and Table 5.17 for silicone rubber membrane M<sub>2</sub> and M<sub>3</sub> respectively

**Table 5.16:** Polymath results for co-efficients  $m, n$ , and  $l$  for CO<sub>2</sub> permeability through silicone rubber membrane M<sub>2</sub>.

Co-efficients	Value
$m$	0.52
$n$	0.62
$l$	-1.21

**Table 5.17:** Polymath results for co-efficients  $m$ ,  $n$ , and  $l$  for CO<sub>2</sub> permeability through silicone rubber membrane M<sub>3</sub>.

Co-efficients	Value
$m$	0.11
$n$	0.95
$l$	4.87

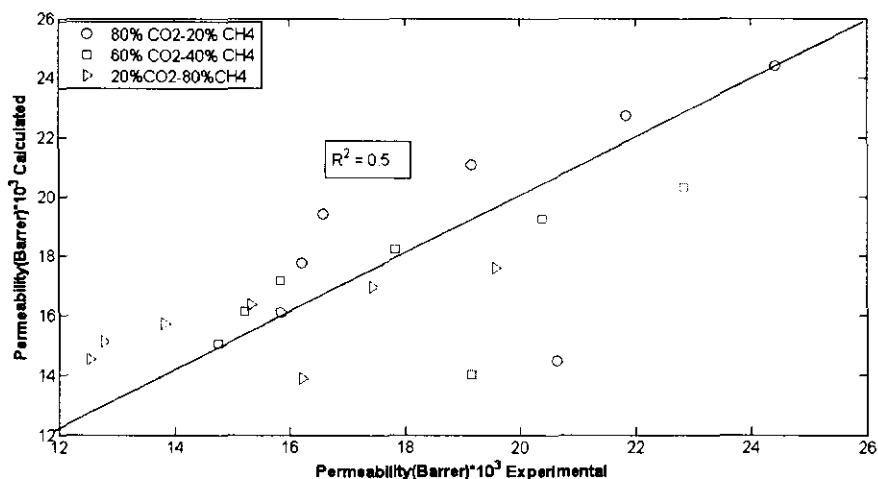


**Figure: 5.32:** Comparison of experimental and calculated permeabilities of CO<sub>2</sub> through M<sub>2</sub> silicone rubber membrane in binary mixtures of methane and carbon dioxide at different pressure.

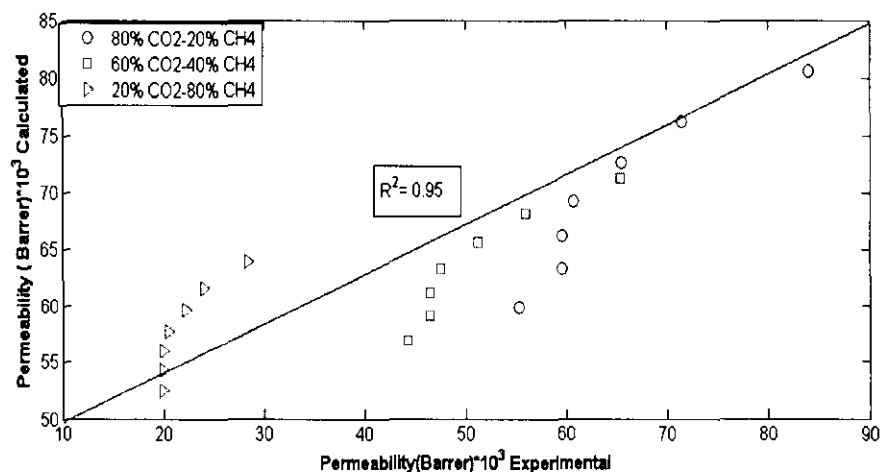


**Figure: 5.33:** Comparison of experimental and calculated permeabilities of CO<sub>2</sub> through M<sub>3</sub> silicone rubber membrane in binary mixtures of methane and carbon dioxide at different pressure.

Similarly the validity of these co-efficients are tested at experimental data other than those that are used in multiple linear regressions to find these co-efficients. The comparison between experimental permeability of carbon dioxide in binary mixture (40% CO<sub>2</sub>-60%CH<sub>4</sub>) and calculated permeability of carbon dioxide in binary mixture (40% CO<sub>2</sub>-60%CH<sub>4</sub>) are shown in Figure 5.34 and 5.35 for silicone rubber membrane M<sub>2</sub> and M<sub>3</sub> respectively. The percentage error between experimental permeability and calculated permeability is shown in Table 5.18 and Table 5.19 for silicone rubber membrane M<sub>2</sub>,M<sub>3</sub> respectively.

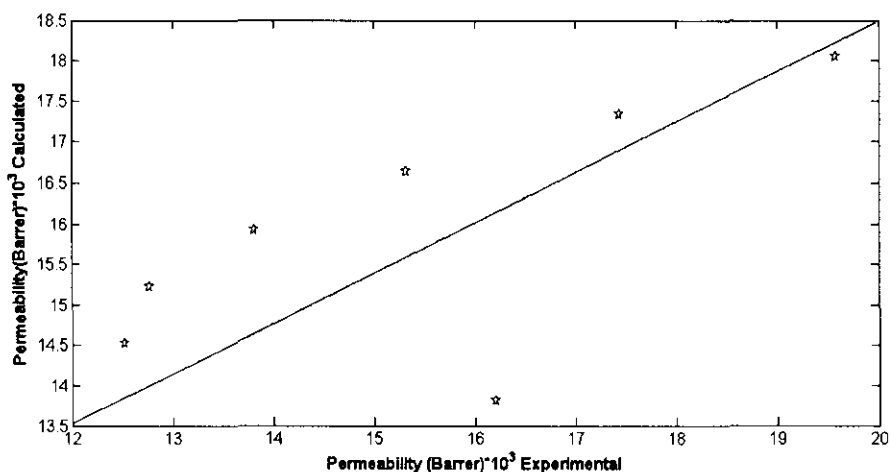


**Figure: 5.34:** Comparison of experimental and calculated permeabilities of CO<sub>2</sub> through M<sub>2</sub> silicone rubber membrane in binary mixture (40% CO<sub>2</sub>-60% CH<sub>4</sub>) at different pressure.

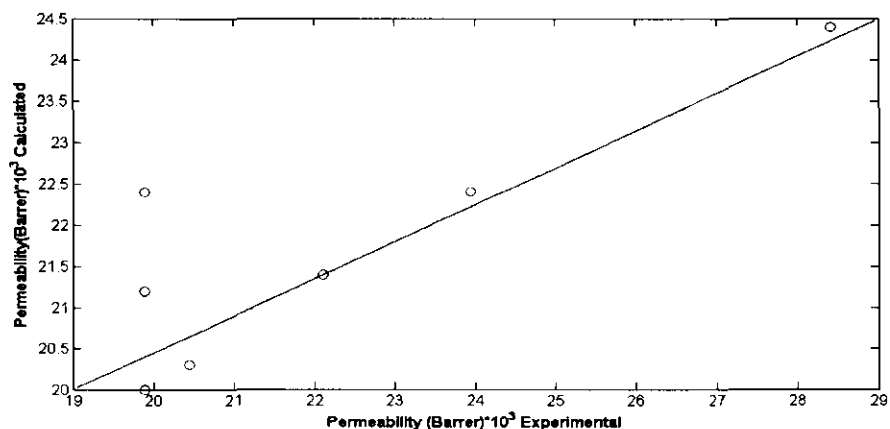


**Figure: 5.35:** Comparison of experimental and calculated permeabilities of CO<sub>2</sub> through M<sub>3</sub> silicone rubber membrane in binary mixture (40% CO<sub>2</sub>-60% CH<sub>4</sub>) at different pressure.

**Table 5.18:** Percentage error between experimental permeability and calculated permeability of carbon dioxide through siliconerubber membrane M<sub>2</sub>.

Experimental Permeability (Barrer)×10 <sup>3</sup>	Calculated Permeability (Barrer)×10 <sup>3</sup>	Percentage± Error
16.20715	13.81978	14.73
12.52371	14.52464	-15.97
12.76927	15.2295	-19.26
13.81291	15.93437	-15.35
15.32313	16.63923	-8.58
17.43497	17.34409	0.52
19.57487	18.04895	7.79

**Table 5.19:** Percentage error between experimental permeability and calculated permeability of carbon dioxide through siliconerubber membrane M<sub>3</sub>.

Experimental Permeability (Barrer)×10 <sup>3</sup>	Calculated Permeability (Barrer)×10 <sup>3</sup>	Percentage± Error
19.8906	20	-0.55
19.8906	21.2	-6.58
19.8906	22.4	-12.61
20.44311	20.3	0.70
22.10066	23.4	-5.87
23.94238	22.4	6.44
28.41514	24.4	14.13

Similarly for co-relating the methane experimental permeability through silicone rubber membrane M<sub>1</sub> with the calculated permeability a multiple linear regression was carried out to solve equation 5.3 using ploymath. The comparison between experimental and calculated permeability of methane through silicone rubber membrane M<sub>1</sub> are shown in Figure 5.36. A regression co-efficient ( $R^2 = 0.79$ ) is obtained, showing a close fit to the experimental permeability. The co-efficients  $m, n, l$  obtained from multiple regression analysis are shown in Table 5.20.

**Table 5.20:** Polymath results for co-efficients  $m$ ,  $n$ , and  $l$  for CH<sub>4</sub> permeability through silicone rubber membrane M<sub>1</sub>.

Co-efficients	Value
$m$	-2.56
$n$	18.63
$l$	0.129

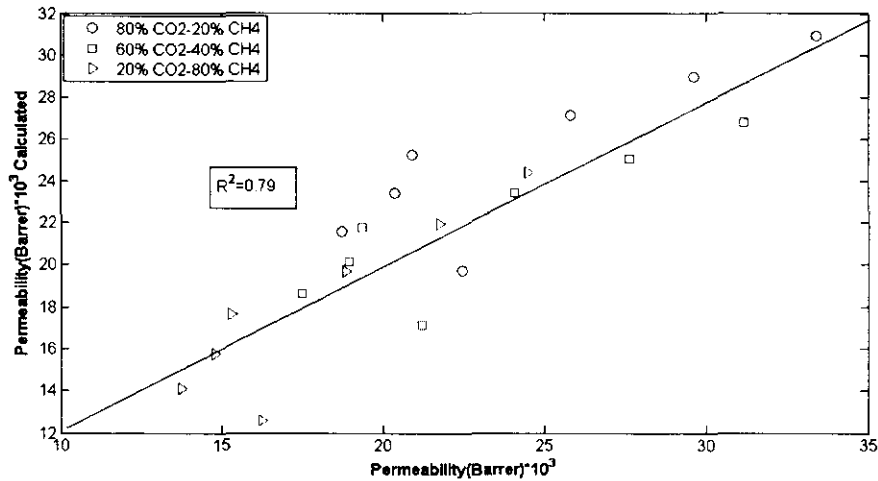


**Figure: 5.36:** Comparison of experimental and calculated permeabilities of CH<sub>4</sub> through M<sub>1</sub> silicone rubber membrane in binary mixture of methane and carbon dioxide at different pressure.

Similarly the validity of these co-efficients are tested at experimental data other than those that are used in multiple linear regressions to find these co-efficients. The comparison between experimental permeability of methane in binary mixture (40% CO<sub>2</sub>-60%CH<sub>4</sub>) and calculated permeability of methane in binary mixture (40% CO<sub>2</sub>-60%CH<sub>4</sub>) are shown in Figure 5.37. The percentage error between experimental permeability and calculated permeability of methane is shown in Table 5.21.

**Table 5.21:** Percentage error between experimental permeability and calculated permeability of methane through silicone rubber membrane M<sub>1</sub>.

Experimental Permeability (Barrer)×10 <sup>3</sup>	Calculated Permeability (Barrer)×10 <sup>3</sup>	Percentage± Error
19.33562	16.23576	16.03
16.21697	17.43646	-7.51
17.67234	18.63715	-5.45
18.08816	19.83785	-9.67
22.45427	21.03855	6.30
25.67688	22.23924	13.38
28.95888	23.43994	19.05

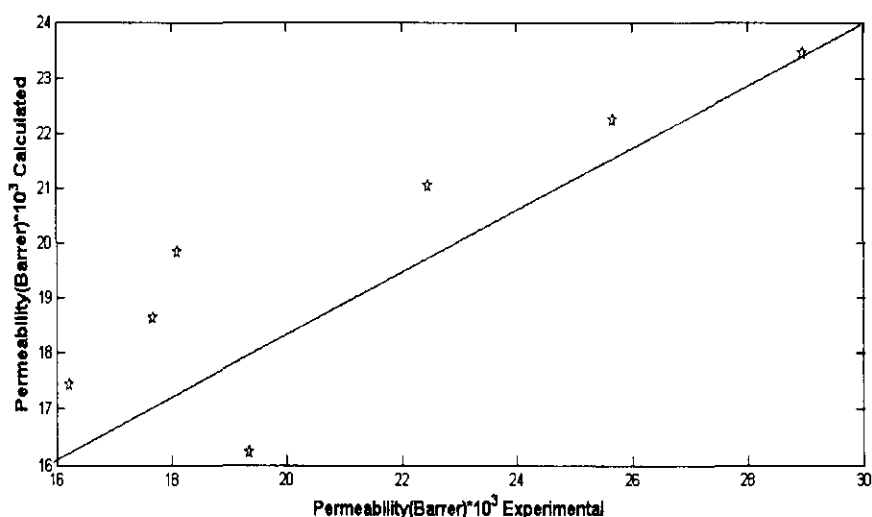


**Figure: 5.37:** Comparison of experimental and calculated permeabilities of CH<sub>4</sub> through M<sub>1</sub> silicone rubber membrane in binary mixture (40% CO<sub>2</sub>-60% CH<sub>4</sub>) at different pressure.

Similarly, the comparison of methane experimental permeability through silicone rubber membrane M<sub>2</sub> and M<sub>3</sub> with the calculated permeability of methane at different pressures is shown in Figure 5.38 and 5.39 respectively. A regression co-efficient (R<sup>2</sup>) was obtained showing that the co-relation is best fitted to the experimental data. The coefficients *m, n* and *l* are shown in Table 5.22 and Table 5.23 for silicone rubber membrane M<sub>2</sub> and M<sub>3</sub> respectively.

**Table 5.22:** Polymath results for co-efficients  $m$ ,  $n$ , and  $l$  for CH<sub>4</sub> permeability through silicone rubber membrane M<sub>2</sub>.

Co-efficients	Value
$m$	1.014
$n$	0.20
$l$	0.10

**Table 5.23:** Polymath results for co-efficients  $m$ ,  $n$ , and  $l$  for CH<sub>4</sub> permeability through silicone rubber membrane M<sub>3</sub>.

Co-efficients	Value
$m$	0.73
$n$	0.38
$l$	0.17

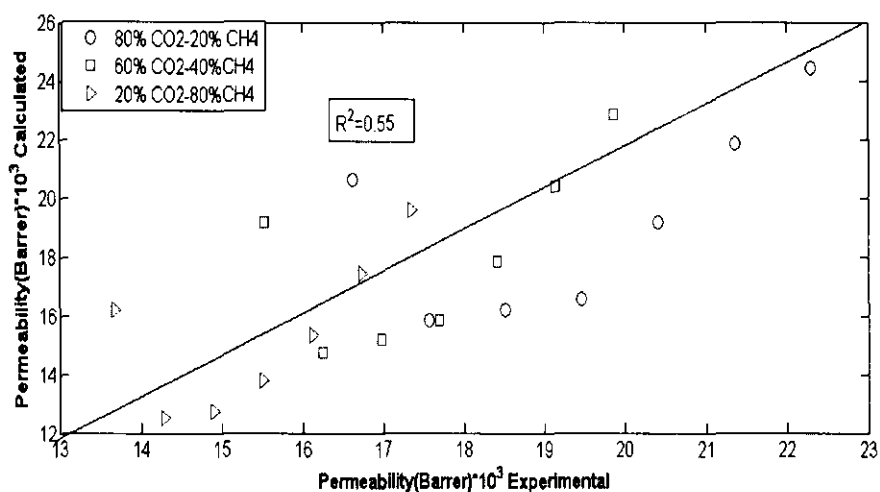


**Figure: 5.38:** Comparison of experimental and calculated permeabilities of CH<sub>4</sub> through M<sub>2</sub> silicone rubber membrane in binary mixture of methane and carbon dioxide at different pressure.

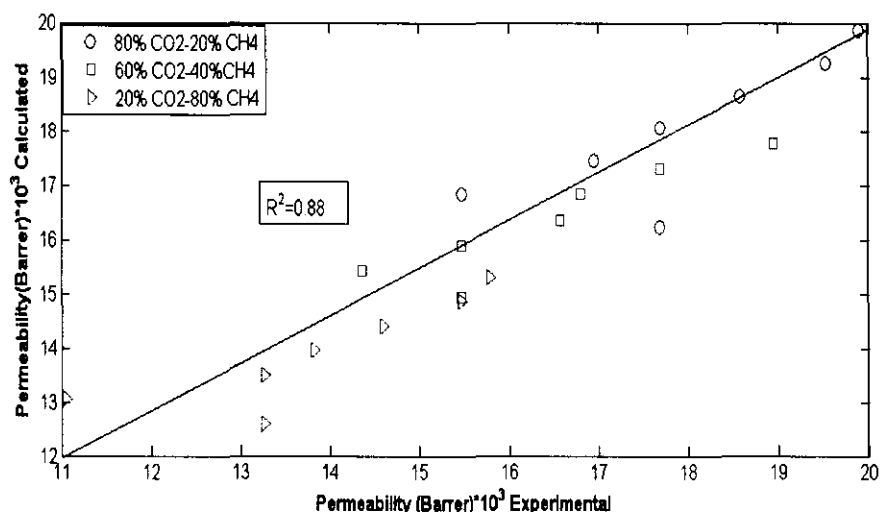


**Figure:5.39:** Comparison of experimental and calculated permeabilities of CH<sub>4</sub> through M<sub>3</sub> silicone rubber membrane in binary mixture of methane and carbon dioxide at different pressure.

Similarly the validity of these co-efficients are tested at experimental data other than those that are used in multiple linear regressions to find these co-efficients. The comparison between experimental permeability of methane in binary mixture (40% CO<sub>2</sub>-60%CH<sub>4</sub>) and calculated permeability of methane in binary mixture (40% CO<sub>2</sub>-60%CH<sub>4</sub>) are shown in Figure 5.40 and 5.41 for silicone rubber membrane M<sub>2</sub> and M<sub>3</sub> respectively. The percentage errors between experimental permeability and calculated permeability are shown in Table 5.24 and Table 5.25 for silicone rubber membrane M<sub>2</sub> and M<sub>3</sub> respectively.

**Table 5.24:** Percentage error between experimental permeability and calculated permeability of methane through silicone rubber membrane M<sub>2</sub>.

Experimental Permeability (Barrer)×10 <sup>3</sup>	Calculated Permeability (Barrer)×10 <sup>3</sup>	Percentage± Error
17.68053	14.53396	17.79683
13.62874	15.14788	-11.1466
14.24265	16.21036	-13.8156
14.73377	16.83886	-14.2875
16.64916	17.46736	-4.91434
19.03113	18.09586	4.914445
21.04825	18.72436	11.0408

**Table 5.25:** Percentage error between experimental permeability and calculated permeability of methane through silicone rubber membrane M<sub>3</sub>.

Experimental Permeability (Barrer)×10 <sup>3</sup>	Calculated Permeability (Barrer)×10 <sup>3</sup>	Percentage± Error
13.2604	13.73382	-3.57
12.15536	14.15463	-16.44
14.73377	15.40028	-4.52
14.91795	15.84422	-6.20
15.91248	16.28816	-2.36
16.5755	16.73209	-0.94
17.36481	17.17603	1.08

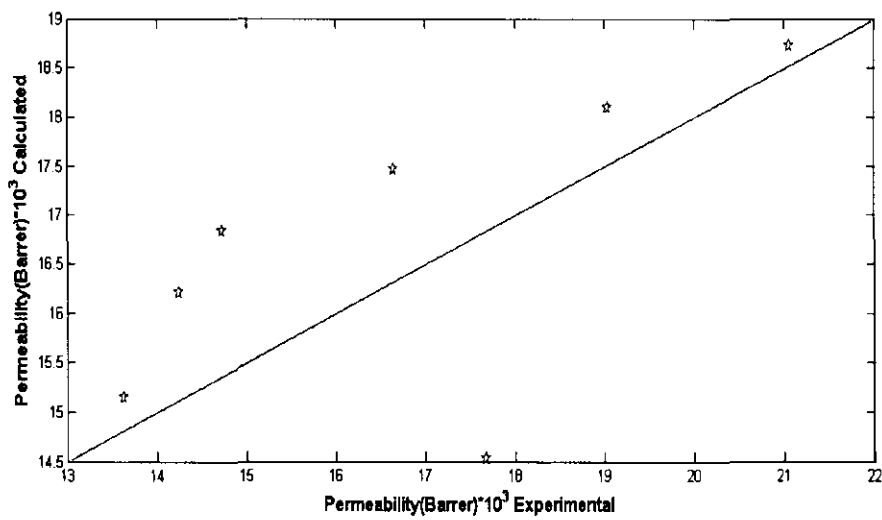


**Figure: 5.40:** Comparison of experimental and calculated permeability of CH<sub>4</sub> through M<sub>2</sub> silicone rubber membrane in binary mixture (40% CO<sub>2</sub>-60% CH<sub>4</sub>) at different pressure.

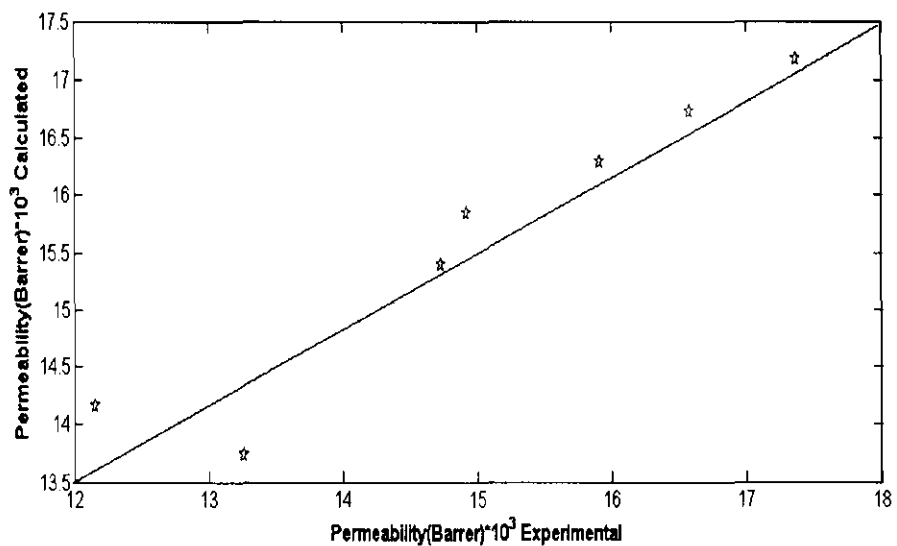


**Figure: 5.41:** Comparison of experimental and calculated permeability of CH<sub>4</sub> through M<sub>3</sub> silicone rubber membrane in binary mixture (40% CO<sub>2</sub>-60% CH<sub>4</sub>) at different pressure.

## CHAPTER 6

### CONCLUSIONS AND RECOMMENDATIONS

#### 6.1. Conclusions

The separation of carbon dioxide and other impurities from natural gas was systematically studied theoretically and experimentally. Pore flow model with capillary condensation mechanism was able to predict separation of carbon dioxide and other gases from natural gas by a nano-porous membrane. Methane was chosen as the representative component of the natural gas.

The Kelvin equation was used to calculate the condition for capillary condensation for predicting the separation of carbon dioxide from  $\text{CO}_2/\text{CH}_4$ , propane from  $\text{C}_3\text{H}_8/\text{CH}_4$ , butane from  $\text{C}_4\text{H}_{10}/\text{CH}_4$ , nitrogen from  $\text{N}_2/\text{CH}_4$ , and hydrogen sulfide from  $\text{H}_2\text{S}/\text{CH}_4$  binary mixtures respectively. The computed results have established that lowering the pore size lowers the condensation pressure required to cause capillary condensation inside the pore at a particular temperature. The effect of pore size on permeability of condensed component in binary mixture of  $\text{CO}_2/\text{CH}_4$ ,  $\text{C}_3\text{H}_8/\text{CH}_4$ ,  $\text{C}_4\text{H}_{10}/\text{CH}_4$ ,  $\text{N}_2/\text{CH}_4$ ,  $\text{H}_2\text{S}/\text{CH}_4$  was also been studied. It has been established that lowering the pore size lowers the permeability. A balance should be struck between the capillary condensation pressure and permeability to decide upon the optimum pore size.

The separation factor of these binary mixtures of gases was analyzed based on the principle that one component would condense preferentially. The separation of  $\text{N}_2/\text{CH}_4$  was found to be the highest with 439 followed by the separation of  $\text{H}_2\text{S}/\text{CH}_4$  and  $\text{CO}_2/\text{CH}_4$ , respectively.

The separation characteristics of pure carbon dioxide, methane and binary mixture of carbon dioxide and methane through silicone rubber membranes of different thickness have been investigated systematically. The analysis has been presented in terms of variations in the permeabilities of both gases, as well as their selectivities. Experimental results showed that the permeability of  $\text{CO}_2$  was found to depend strongly on operating pressure, temperature and membrane thickness as compared to the permeability of  $\text{CH}_4$ . It was also found that the permeability of  $\text{CO}_2$  was higher

than the permeability of CH<sub>4</sub>. It was also found that CO<sub>2</sub> permeability decreases at pressure above 17 bar due to hydrostatic compression effects.

Generally, the permeability of binary mixture of gases followed the same trends as the permeability of pure gases. However, the magnitude of the permeability was determined by the amount of CO<sub>2</sub> composition present in the feed. This is consistent with the previous literatures. Analysis of the selectivities estimated from pure gas permeabilities shows that silicone rubber membrane has the highest selectivity of 11.4 over the pressure range of 2 to 24 bar. For gas mixture, lower values of the selectivities are obtained at low CO<sub>2</sub> vol % composition.

An analytical model expressed in terms of feed pressure and feed composition was developed to predict quantitatively the permeability of binary mixture of gases from pure gas permeability. The model is expressed in terms of two controllable feed parameters, while a common permeation model depends on some intrinsic factors such as the diffusion co-efficient and solubility co-efficient. Comparison of the experimental data with the calculated values shows an excellent agreement. This model is practical in choosing the optimal separation conditions of gas mixture.

The present work is expected to be useful for utilization of high CO<sub>2</sub> natural gas which has been a global challenge including Malaysia. Undeveloped resources of high CO<sub>2</sub> gas fields ( 28-87 mol% of CO<sub>2</sub> ) in Malaysia have potential to contribute up to 13 TSCF (Trillion Standard Cubic Feet) of net hydrocarbon gas which can be translated into value creation of USD 26 billion in terms of gross revenue.

Further more, the simulation technique developed in this study may be used for pre-treatment of natural gas for removal of lower hydrocarbon (C<sub>3</sub> to C<sub>4</sub>) and other minor constituents before membrane separation using polymeric membrane module. It may be mentioned here that a few novel polymeric membranes have been developed and put to use for CO<sub>2</sub> separation. However, lower hydrocarbons and other minor constituents must be removed to prevent plasticization of the polymeric membranes. Thus a nano-porous ceramic membrane system using capillary condensation mechanism may find use for pre-treatment of natural gas if a combination of ceramic

and polymeric membrane module is found convenient depending upon the composition of the feed and the desired quality of the product gas.

## 6.2. Recommendations

Based on this work, some recommendations as future works that may provide further insight into separation of carbon dioxide and other gases from natural gas are listed below.

- i) In order to study the the separation of carbon dioxide and other gases from natural gas using capillary condensation, an experimental set up should be constructed for permeability, capillary condensation and solubility measurements. In addition, a nano-pore size ceramic membrane should be developed and permeability test should be carried using the developed membrane.
- ii) A statistical and Monte Carlo approach should also be studied for the calculation of capillary condensation.
- iii) Mixed gas permeability tests may be conducted for some other polymeric membrane films that have shown high  $\text{CO}_2/\text{CH}_4$  ideal selectivity. Finally, mixed matrix membrane should be developed by incorporating in-organic material such as zeolite and carbon molecular sieve (CMS) in polymeric membrane and  $\text{CO}_2/\text{CH}_4$  mixed gas permeability study should be carried out for enhancing the performance of membrane in removing  $\text{CO}_2$  from natural gas.

## REFERENCES

Abdi, M A., Golkar, M. M., Meisen, A. Improve contaminant control in amine systems, *Hydrocarbon Process*, 80(2001),1020-1021.

Ahmad, F., Mukhtar, H., Man, Z., Dutta, B.K., Predicting separation of carbon dioxide from natural gas by capillary condensation using a nano-porous membrane, 20th Symposium of Malaysian Chemical Engineers, (2006),635-645.

Ahmad, F., Mukhtar, H., Man, Z., Dutta, B.K., Separation of lower hydrocarbon from natural gas through nano-porous membrane using capillary condensation, *Chem. Eng. Technol.* 9 (2007), 1266– 1273.

Ahmad, F., Mukhtar, H., Z.Man, Dutta, B.K., Purification of natural gas using membrane: The current status and research trends, 20th Symposium of Malaysian Chemical Engineers, (2006),645-654.

Ahmad, F., Mukhtar, H., Man, Z., Dutta, B.K., A theoretical analysis for non-chemical removal of hydrogen sulfide from natural gas through nano-porous membrane using capillary condensation, accepted for publication in *Chem. Eng. & processing* (In press).

Alexopoulos, J.B., Barrie, J.A., and Machin, D., The Time lag for the diffusion of gas mixtures, *Polym. J.* 10, 265 (1969).

Baker, R.W., *Membrane Technology and Application*, McGraw-Hill, New York, USA, 2004.

Baker, R.W., Cussler, E.L., Eykamb, W., Koros, W.J., Riley, R.L., and Strathmann, H., *Membrane separation systems: Recent development and future directions*, Noyes Data Corporation, 1991.

Bord, N., Cre' tier, G., Rocca, J.-L., Bailly, C., and Souchez, J.-P., Determination of diethanolamine or N-methyldiethanolamine in high ammonium concentration matrices by capillary electrophoresis with indirect UV detection: application to the analysis of refinery process waters, *Anal Bioanal Chem* 380 (2004), 325–332.

Bhurisa, Thitakamol and Amornvadee Veawab, Foaming behavior in CO<sub>2</sub> absorption process using aqueous solutions of single and blended alkanolamines, *Ind. Eng. Chem. Res.* 47(2008), 216-225.

Bird, R.D., Stewart, W.E and Lightfoot, E.N., *Transport phenomena*, 4<sup>th</sup> edition, John Wiley and Son, New York, 1960.

Burnside, S.D., and E. P. Giannelis, E.P., *Chemistry of materials*, 7(1995), 1597.

Bitter, J.G.A., *Transport mechanisms in membrane separation processes*, Plenum Chemical Engineering Series, Plenum Press, 1991.

Bryk, P., Rzyzko, W., Malijevsky, A., Sokolowski, S., Capillary condensation in pores with rough walls: a density functional approach, *J. Colloid Interface Sci.* 313 (2007), 41-52.

Banerjee, T., Lipscomb, G.G., Mixed gas sorption in elastic solids, *J. Membr. Sci.* 96, 241 (1994).

Boddeker, K.W., editor, *The early History of Membrane Science: Selected papers*, *J. Membr. Sci.* 1, 100 (1995).

Burgraaf, A.J. and Cot, L., *Fundamentals of inorganic membrane science and technology*, Elsevier, Amsterdam, 1996

Cooley, T.E., The use of membrane for natural gas purification, Proc.Eur.Ch.Cont.Meet. -Gas process. Assoc., Biarritz, FRA, (1990),17.

Cornesa, A., Fernando, A., Pitarch, J.A., Vicente-Mingaro, I., Rodriguez, M.A., Separation of binary gas mixtures by means of sol-gel modified ceramic membranes, prediction of membrane performance, J.Membr.Sci.107(1995),1-21.

Crank, J., and Park, G.S., (editors), Diffusion in polymers, Academic Press, 1968.

Costello,L.M., and Koros, W.J., thermally stable polyimide isomers for membrane-based gas separations at elevated temperatures, J.Poly.Sci. : Part B: Polymer Physics, 33,135 (1995).

DiBenedetto, T., Molecular properties of amorphous high polymers. II. An interpretation of gaseous diffusion through polymers, J. Poly.Sci: Part-A, 1, 3477 (1963).

Deetz, D.D Stabilized ultra thin liquid membrane for gas separation, in: Noble, R.D., and J.D.Way (Eds.), Liquid membranes: Theory and application, ACS Symp.Ser., No.347, American Chemical Society, Washington, DC, Chap.11, 1987.

Dortmundt, D., and Doshi, K., Recent developments in CO<sub>2</sub> removal membrane technology, UOP LLC, USA, 1999.

Dhingra,S.S., and Marand, E., Mixed gas transport through polymeric membranes, J. Membr. Sci. 141 (1998),45-63.

Elkamel, A., Noble, R.D., A statistical mechanics approach for the separation of nitrogen using capillary condensation in a micro-porous membrane, J.Membr.Sci. 65(1992),163-172.

Elkamel, A., and Noble, R.D., Prediction of capillary condensation in small cylindrical pores using the local density approximation and a full Leonard–Jones 6-12 Potential, *J.Phys.Chem.*95(1991),10076-10080.

Echt, W., Hybrid systems: Combining technologies lead to more efficient gas conditioning, Laurence Reid Gas Conditioning Conference (2002), [www.uop.com](http://www.uop.com).

Ettouney, H., and Majeed, U., Permeability functions for pure and mixture gases in silicone rubber and polysulfone membranes: dependence on pressure and composition, *J. Membr. Sci.* 135 (1997),251–261.

F.Wu,Lei Li, Z.Xu, S.Tan, Z.Zhang, Transport study of pure and mixed gases through PDMS membrane, *Chem. Eng. J.* 117 (2006),51-59.

Freeman, B.D., and Pinnau, Polymeric membranes for gas and vapor separation, Oxford University Press, USA (1999).

Galiatsatou, P., Kanellopoulos, N.K., and Petropoulos, J.H., Characterization of the transport properties of membranes of uncertain macroscopic structural homogeneity, *J.Membr.Sci.*280 (2006),634-642.

Gas Malaysia Sdn.Bhd. 2003.

Gas Malaysia Sdn.Bhd. 2005.

Ghosal, K., and Freeman,B.D., Gas Separation Using Polymer Membranes: An overview, *Polym. Adv. Technol.* 5, 673 (1994).

Haraya, Shindo, Y., Hakuta, T., and Yoshitome,H., Separation of H<sub>2</sub>-CO mixtures with porous glass membranes in the intermediate flow region, *J.Chem.Eng. Jpn.*19(1986), 186-190.

Hugman, R.H., Vidas, E.H., Springer, P.S., Chemical composition of discovered and undiscovered natural gas in the United States, (Update, GRI-93/0456) (1993).

Hu, C.C., Chang, C.S., Ruaan, R.C., and J.Y. Lai, Effect of free volume and sorption on membrane gas transport, *J. Membr. Sci.* 226(2003), 51-56.

Hughes, R., and Jiang, B.Q., The permeabilities of carbon dioxide, nitrous oxide and oxygen and their mixtures through silicone rubber and cellulose acetate membranes, *Gas Sep. Purif.* 9 (1995), 27-30.

Ismail, A.F., and Lorna, W., Penetrant-induced plasticization phenomenon in glassy polymers for gas separation membrane: Review article, *Sep. Purif. Tech.* 27(2002), 173-194.

Jaguste, D.N., Bhatia, S.K., Combined surface and viscous flow of condensable vapor in porous media, *Chem. Eng. Sci.* 50 (1995), 167-182.

Jou, F.Y., Otto, F.D., and Mather, A.E., Vapor-liquid equilibrium of carbon dioxide in aqueous mixtures of mono-ethanolamine and methyldiethanolamine, *Ind. Eng. Chem. Res.* 33 (1994).

Javaid, A., Review: Membranes for solubility-based gas separation applications, *Chem. Eng. J.* 112 (2005), 219-226.

Jordan, S.M., and Koros, W.J., Permeability of pure and mixed gases in silicone rubber at elevated pressure, *J. Polym. Sci, Part B: Polym. Phys.* 28 (1990), 795-809.

Jordan, S.S., and Koros, W.J., A free volume distribution model of gas sorption and dilation in glassy polymers, *Macromolecules*, 28, (1995), 2228.

Jordan, S.M., Koros, W.J., and Fleming, G.K., The effects of CO<sub>2</sub> exposure on pure and mixed gas permeation behavior: Comparison of glassy polycarbonate and silicone rubber, *J. Membr. Sci.* 30 (1987),191–212.

Kohl, A. and Riesenfeld, F., *Gas purification*, Gulf Publishing Company, Houston, Texas, 1979.

Kohl, A.L., and Nielsen, R., *Gas purification: 5th edition*, Houston, TX: Gulf Publishing Company, 1997.

Keller II, G.E., Anderson, R.A., and Yon, C.M., Adsorption, in: *Handbook of separation process technology*, Rousseau, R.VV., (Ed), John Wiley & Sons, Inc., 1987.

Keizer, K., Uhlhorn, R.J.R., Van Vuren, R.J., and Burggraaf, A.J., Gas separation mechanism in micro-porous modified Al<sub>2</sub>O<sub>3</sub> membranes, *J. Membr. Sci.* 39(1988),285-300.

Kesting, R.E., and Fritzsche, A.E., *Polymeric gas separation membranes*, John Wiley & Sons, Inc., 1993.

Koros, W.J., and Chern, R.T., Separation of gaseous mixtures using polymer membranes, *Handbook of Separation Process Technology*, edit. R. W. Rousseau, (1987).

Lebaron, P.C., and Pinnavaia, T.J., *Chemistry of Material*, 13, 3760 (2001).

Lee, K., Hwang, S.T., The transport of condensable vapors through a micro-porous Vycor Glass membrane, *J. Colloid Interface Sci.* 110(1986),544-554.

Mc Kee, B., *Solution for 21st Century: Zero Emission Technologies for Fossil Fuels*. International Energy Agencies, France (2002).

Mandal, B.P; Kundu, M; Bandyopadhyay, S.S. Density and viscosity of aqueous solutions of (N-Methyldiethanolamine+Monoethanolamine),(NMethyldiethanolamine + Diethanolamine), (2-Amino-2-methyl-1-propanol + Monoethanolamine), and (2-Amino-2-methyl-1-propanol + Diethanolamine). *J. Chem. Eng. Data* 48, (2003), 703-707.

Meyer, M., Renesme, G., Brefort, B., The processes of gas separation by permeating through polymeric membranes: present and future potential in the gas industry, *Recl. Communic. 108e Congr. Gaz, Montpellier, FRA, September, 2 (1991),17-21.*

Mohammed Awad, A., PhD Thesis, University of Texas at Austin, 2004,AAT 3143353.

Mulder., M, Basic principles of membrane technology, Kluwer academic publishers, 1996 .

Merkel, T.C., Bondar, V.I., Nagai, K., Freeman, B.D., and Pinnau, I., Gas sorption, diffusion, and permeation in poly(dimethylsiloxane), *J.Polym.Sci. Part B: Polym.Phys.*38 (2000), 415–434.

Melrose,J.C., Model calculation for capillary condensation, *AIChEJ.*12(1966)986-994.

Kohan,J.P., Kurna,F., Heterogeneous phase equilibria of the methane-hydrogen sulfide system, 4(1958),211-216.

Nunes, S.P., and Peineman, K.V., Membrane technology in the chemical industry, WILEY-VCH, Germany, 2001.

Neimark, A.V., Ravikovitch, P.I., Vishnyakov,A., Bridging scales from molecular simulations to classical thermodynamics: Density functional theory of capillary condensation in nanopores, *J. Phys. Condens. Matter*, 15 (2003), 347-365.

Nguyen, Q.T., Langevin, D., Bahadori, B., Callebert, F., and Schaetzel,P., Sorption and diffusion of volatile organic components in a membrane made by deposition of

tetramethyl disiloxane in cold remote-plasma J.Membr.Sci. Volume 299, Issues 1-2, 1 August 2007, Pages 73-82.

NATCO, Acid Gas (CO<sub>2</sub>) separation systems with Cynara membranes, NATCO group, 2002.

Petropoulos, J.H., Quantitative Analysis of Gaseous Diffusion in Glassy Polymers, J. Poly. Sci: Part A-2, 8, 1797 (1970).

Petropoulos, J.H., Membranes with Non-Homogenous Sorption and Transport Properties, Adv. Polym. Sci. 64, 93 (1985).

Petropoulos, J.H., On the Dual Mode Gas Transport Model for Glassy Polymers, J. Polym. Sci. : Part B: Poly. Phy. 26, 1009 (1988).

Polasek, J., and Bullin, J.A., Selecting amines for sweetening units, Proceedings GPA Regional Meeting, Sept. 1994. "Process Considerations in Selecting Amine" Tulsa, OK: Gas Processors Association, 1994.

Perry, R.H., and Green, D.W., Perry's Chemical Engineer's Handbook, McGraw Hill, 1999.

Pascoli S.D.; Femia A.; Luzzati T. Natural gas, cars and the environment. A relatively 'clean' and cheap fuel looking for users, Ecological Economics, 38(2001),179-189.

Prabhakar, R.S., Roharjo, R., Toy, L.G., Li, H.Q., Freeman, B.D., Self consistent model of concentration and temperature dependence of permeability in rubbery polymer, Ind. Eng. Chem. Res. 44(2005),1547-1556.

Rhim, H., Hwang, S.T., Transport of capillary condensate, J. Colloid Interface Sci. 52(1975),174-180.

Rao, M.B., Sircar, S., and Golden, T.C., Adsorbent membranes for gas separation, U.S. Pat. , 5,104,425 (1992).

Rojey, A., Jaffret, C., Carnot, S., Durand, B., Julian, S., Valias, Natural gas production processing transport “ Edition Technips, Paris, (1997).

Rooney, P. C.; DuPart, M.S. Corrosion in alkanolamine plants: causes and minimization. proceedings of corrosion 2000; NACE International: Houston, TX, 2000; Paper No.494.

Spillman, R.W., Economics of gas separation membranes 1989 Chem.Eng.Progr. 85(1989),41.

Satterfield, C.N., Heterogeneous catalysis in practice, Mc Graw Hill , New York, NY, 1980.

Sandler, S., Chemical and Engineering Thermodynamics, John Wiley & Sons, Inc., 1989.  
Burnside, S.D., and Giannelis, E.P., Chemistry of materials, 7(1995),1597.

Stern, S.A., Polymers for gas separations: the next Decade, J.Membr.Sci.94,1(1994).

Stepanek, F., Soos, M., Rajniak, P., Characterization of porous media by the virtual capillary condensation method, Colloids Surf.: Physicochemical. Eng. Aspects, 300 (2007),11-20.

Shindo, Y., Hakutta, H., Yoshitome, H., Gas diffusion in micro-porous media in Knudsen's regime, J. Chem. Eng. Jpn.16 (1983),120-126.

Sidhu, P.S., Kussler, E.L., Diffusion and capillary flow in track etched membranes J. Membr Sci. 182 (2000), 91-101.

Sperry, L. Falconer and R. D.Noble, Methanol-hydrogen separation by capillary condensation in organic membranes, J. Membr. Sci. 60 (1991),185-193.

- Spillman, R.W., and M.D.Sherwin, Membranes in life, Chemtech. (1990) 378-384.
- Suhartanto, T., York, A.P.E., Hanif, A., Al-Megren, H., and Green, M.L.H., Potential utilisation of Indonesia's Natuna natural gas field via methane dry reforming to synthesis gas, Catalysis Letters 71 (2001),49-54.
- Sartori, G., and Savage, D.W., Sterically hindered amines for CO<sub>2</sub> removal from gases, Ind. Eng. Chem. Fundam. 22 (1983),239-249.
- Stewart, E. J.; Lanning, R. A. Reduce amine plant solvent losses Part1 .Hydrocarbon Process., 73(1994),67-81.
- Scott,K, Handbook of industrial membranes:2nd edition, Elsevier Advanced Technology, 1998.
- Stern, S.A.,Polymers for gas separation: the next decade, J. Member. Sci. 94 (1994),1-65.
- Stannett,V., The transport of gases in synthetic polymeric membranes- an historic perspective, J.Membr.Sci. 3, 97 (1978).
- Uchytel, P., Petrickovic, R., Seidel-Morgenstern,A., Study of capillary condensation of butane in a Vycor glass membrane, J. Membr. Sci., 264 (2005),27-36.
- Uchytel, P., Petrickovic, R., Seidel-Morgenstern, A., Transport of butane in a porous ProSep, Gas sweetening membrane, ProSep Technologies, Inc., 2000.
- Uchytel, P., Petrickovic, R., Thomas, S., Seidel-Morgenstern, A., Influence of capillary condensation effects on mass transport through porous membranes, Sep Purific. Technol., 33 (2003),273-281.
- Veen, H.M.,M. Bracht, Harmoen, E., P.T. Alderliesten, Feasibility of the application of porous inorganic gas separation membranes in some large-scale chemical processes, in:

- Burgraaf, A.J. and Cot, L., Fundamentals of inorganic membrane science and technology, Elsevier, Amsterdam, 1996.
- Vieth, W.R., Diffusion in and through polymers: Principles and applications, Oxford University Press, 1991.
- Vieth, W.R., Howell, J.M., and Hsieh, J.H., Dual sorption theory: Review Paper, J.Membr.Sci. 1, 177 (1976).
- Warrick, E.L., Pierce, O.R., Polmanteer, K.E., and Saam, J.C., Rubber Chemistry and Technology, 52 (1979), 437.
- Wu, F., Lei Li, Xu, Z., Tan, S., Zhang, Z., Transport study of pure and mixed gases through PDMS membrane, Chem. Eng. J. 17 (2006), 51-59.
- Wijmans, J.G., R. W. Baker, The Solution-diffusion model: A review, J. Membr. Sci. 107 (1995), 1-21.
- Wang, S.S., Zeng, M.Y. and Wang, Z.Z., Carbon membrane for gas separation. Sep. Sci. Tech. 31(1996), 2299-2306.
- Yeom, C.K., Lee, S.H., and Lee, J.M., Study of transport of pure and mixed CO<sub>2</sub>/N<sub>2</sub> gases through polymeric membranes, J. Appl. Polym. Sci. 78 (2000), 179-189.

## Appendix A

### Physical Properties of Acid gases, C3 and C4 at different Temperature

Condensation pressure and permeability of condensed phase has been calculated by using equation 3.1 and 2.13 respectively. The physical properties used in the calculation are listed in the following tables

**Table A-1** Physical properties of carbon dioxide at different temperature.

Temperature $T_1(K)$	Viscosity (Pa.s) $10^{-3}$	Density (Kg/m <sup>3</sup> )	Surface Tension (N/m)	Vapor Pressure (Bar)
220	0.2383	1168	0.01581	6.005
230	0.2059	1130	0.01348	8.964
240	0.1788	1089	0.01123	12.86
250	0.1549	1046	0.009070	17.88
260	0.1331	997.9	0.007012	24.22
270	0.1128	944.6	0.0050	32.08
280	0.09391	882.6	0.00327	41.69
290	0.07650	806	0.00167	53.31
300	0.06076	683.4	0.00035	67.25

**Table A-2** Physical properties of methane at different temperature.

Temperature $T_1(K)$	Viscosity (Pa.s)	Density (Kg/m <sup>3</sup> )	Surface Tension (N/m)	Vapor Pressure(Bar)
100	0.0001562	440.4	0.01584	0.3454
110	0.0001220	426.4	0.01394	0.8845
120	0.0000998	411.6	0.01205	1.920
130	0.0008333	396.8	0.01021	3.681
140	0.0000697	378.7	0.00838	6.422
150	0.0000677	358.9	0.00699	10.42
160	0.0000467	338.6	0.00483	15.94
170	0.0000368	313.2	0.00314	23.32
180	0.0000279	279.7	0.00151	32.91
190	0.0000204	206.4	0.00006	45.12

**Table A-3** Physical properties of n-propane at different temperature.

Temperature $T_1(K)$	Viscosity (Pa.s)	Density (Kg/m <sup>3</sup> )	Surface Tension (N/m)	Vapor Pressure (Bar)
200	0.0002934	618.1	0.01962	0.2008
220	0.0002321	596.6	0.01690	0.6038
240	0.0001867	571.3	0.01425	1.478
260	0.0001510	546.3	0.01167	3.108
280	0.0001218	518.7	0.008185	5.823
300	0.0000973	458.1	0.006803	9.989
310	0.0000865	471.2	0.005658	12.74
320	0.0000765	452.7	0.004549	16.01
330	0.0000678	432.7	0.003483	19.85
340	0.0000590	409.7	0.002468	24.32
350	0.0000617	382.1	0.001516	29.50
360	0.0000445	345.0	0.0006565	35.45

**Table A-4** Physical properties of n-butane at different temperature.

Temperature $T_1(K)$	Viscosity (Pa.s) $\times 10^{-3}$	Density (Kg/m <sup>3</sup> )	Surface Tension (Nm)	Vapor Pressure (Bar)
240	28.51 <sup>3</sup>	636.8	0.01890	0.2412
260	23.53	616.1	0.01641	0.6107
280	19.70	594.2	0.01400	1.330
300	16.50	571.0	0.01166	2.580
310	15.05	558.8	0.01052	3.468
320	13.68	546.1	0.009408	4.569
330	12.38	532.8	0.008318	5.912
340	11.13	518.8	0.007254	7.530
350	9.95	504	0.006218	9.455
360	8.839	488.2	0.005215	11.72
370	7.79	471.2	0.004247	14.37
380	6.811	452.5	0.003319	17.43
390	5.904	431.5	0.002438	20.96
400	5.073	407.1	0.001614	24.96
410	4.319	376.4	0.0008649	29.58

**Table A-5** Physical properties of hydrogen sulfide at different temperature.

Temperature $T_1(K)$	Vapor pressure (Bar)	Density (Kg/m <sup>3</sup> )	Viscosity (Pa.s) $\times 10^{-3}$	Surface tension (N.m)
190	0.2659	980	0.5351	0.02854
200	0.4975	964	0.4755	0.02656
220	1.442	930	0.3427	0.02271
240	3.434	896	0.2313	0.01899
260	7.060	858	0.1536	0.01543
280	12.96	817	0.1040	0.01204
300	21.81	772	0.07360	0.008844
320	34.22	721	0.5351	0.005889
340	50.81	658.2	0.4755	0.003234
350	72.16	568.2	0.3427	0.001011

## APPENDIX B

### Pure Gas Permeability of CO<sub>2</sub> and CH<sub>4</sub> at Different Pressure and at Constant Temperature of 25°C

Permeability of pure CO<sub>2</sub> and CH<sub>4</sub> gases was measured as follow.

Using Lab View soft ware , flow rate of the gas in the permeate stream  $Q$  was recorded. This volumetric flow rate  $Q$  was then corrected to STP conditions (0°C and 1 atm) using the following equation

$$Q_{STP} = \frac{T_{STP}}{T} \times Q \quad (B-1)$$

The effective area of membrane,  $A'$ , is 122.7185 cm<sup>2</sup> and testing temperature is 25°C. Hence the permeability of CO<sub>2</sub> and CH<sub>4</sub> gas through membrane silicone rubber membrane  $M_1$  can be determined as follows:

At 2 bar CO<sub>2</sub> volumetric flow rate,  $Q = 165$  ml/min  
 $= 2.75$  cm<sup>3</sup>/s

This volumetric flow rate,  $Q$ , is corrected to standard temperature and pressure (STP),  $Q_{STP}$ , as follows:

$$\frac{Q_{(STP)}}{Q_{300K}} = \frac{273K}{298K} \quad (B-2)$$

$$\begin{aligned} Q_{STP} &= \frac{273K}{298K} \times 2.75 \\ &= 2.52 \text{ cm}^3 (STP)/s \end{aligned}$$

CO<sub>2</sub> flux,  $J_{CO_2}$ , is therefore,

$$J_{CO_2} = \frac{Q_{STP}}{A'} \quad (B-3)$$

$$= \frac{2.519295}{122.7185}$$

$$= 0.021 \text{ cm}^3(\text{STP})/\text{cm}^2 \cdot \text{s}$$

Once CO<sub>2</sub> flux,  $J_{\text{CO}_2}$  was determined, the CO<sub>2</sub> permeability,  $P$ , can be calculated using the following formula:

$$P = \frac{J_{\text{CO}_2} l}{\Delta p} \quad (\text{B-4})$$

$$= \frac{0.020529 \frac{\text{cm}^3(\text{STP})}{\text{cm}^2 \cdot \text{s}} \cdot 0.0762 \text{cm}}{2 \text{ bar} \times 76 \frac{\text{cmHg}}{\text{bar}}}$$

$$= 4 \frac{\text{cm}^3(\text{STP})}{\text{cm}^2 \cdot \text{cmHg} \cdot \text{s}} \text{cm}$$

$$= 1029154 \text{ Barrer}$$

$$= 102.92 \times 10^3 \text{ Barrer}$$

Similarly, CH<sub>4</sub> permeability,  $P$ , can be calculated using the same method. For M1 silicone rubber membrane, CH<sub>4</sub> permeability obtained is  $14.96951 \times 10^3$  Barrer. CO<sub>2</sub>/CH<sub>4</sub> ideal selectivity,  $\alpha_{\text{CO}_2/\text{CH}_4}$ , can be calculated by dividing CO<sub>2</sub> permeability over CH<sub>4</sub> permeability as follows:

$$\alpha_{\text{CO}_2/\text{CH}_4} \quad (\text{B-5})$$

$$= \frac{P_{\text{CO}_2}}{P_{\text{CH}_4}} = 6.88$$

**Table B-1** Effect of pressure on pure CO<sub>2</sub> permeability through membrane M<sub>1</sub>.

Pressure (Bar)	Pressure (cm Hg)	Volumetric flow rate Q(ml/min)	Volumetric flow rate Q(cm <sup>3</sup> /s)	Volumetric flow rate @ STP Q <sub>STP</sub> (cm <sup>3</sup> /s)	Flux cm <sup>3</sup> (STP/s)/cm <sup>2</sup> .s	Permeability (Barrer)×10 <sup>3</sup>
2	152	165	2.75	2.519295	0.020529	102.92
4	304	390	6.5	5.954698	0.048523	121.62
6	456	686	11.43333	10.47416	0.085351	142.62
8	608	1023	17.05	15.61963	0.12728	159.51
10	760	1413	23.55	21.57433	0.175803	176.26
12	912	1854	30.9	28.30772	0.230672	192.73
14	1064	2436	40.6	37.19396	0.303084	217.05
16	1216	3154	52.56667	48.15671	0.392416	245.90
18	1368	4045	67.41667	61.76091	0.503273	280.33
20	1520	4363	72.71667	66.61628	0.542838	272.13
22	1672	4353	72.55	66.46359	0.541594	246.82
24	1824	4409	73.48333	67.31862	0.548561	229.16

**Table B-2** Effect of pressure on pure CH<sub>4</sub> permeability through membrane M<sub>1</sub>.

Pressure (Bar)	Pressure (cm Hg)	Volumetric flow rate Q(ml/min)	Volumetric flow rate Q(cm <sup>3</sup> /s)	Volumetric flow rate @ STP Q <sub>STP</sub> (cm <sup>3</sup> /s)	Flux cm <sup>3</sup> (STP/s)/cm <sup>2</sup> .s	Permeability (Barrer)×10 <sup>3</sup>	Selectivity PCO <sub>2</sub> /PCH <sub>4</sub>
2	152	24	0.4	0.366443	0.002986	14.96951	6.88
4	304	40	0.666667	0.610738	0.004977	12.4746	9.6
6	456	65	1.083333	0.99245	0.008087	13.51415	10.55
8	608	89	1.483333	1.358893	0.011073	13.87799	11.49
10	760	138	2.3	2.107047	0.01717	17.21494	10.24
12	912	190	3.166667	2.901007	0.02364	19.75144	9.76
14	1064	250	4.166667	3.817114	0.031105	22.27606	9.74
16	1216	327	5.45	4.992785	0.040685	25.49495	9.65
18	1368	427	7.116667	6.519631	0.053127	29.59251	9.47
20	1520	472	7.866667	7.206711	0.058726	29.44005	9.24
22	1672	510	8.5	7.786913	0.063453	28.91838	8.54
24	1824	600	10	9.161074	0.074651	31.18649	7.35

**Table B-3** Effect of pressure on pure CO<sub>2</sub> permeability through membrane M<sub>2</sub>

Pressure (Bar)	Pressure (cm Hg)	Volumetric flow rate Q(ml/min)	Volumetric flow rate Q(cm <sup>3</sup> /s)	Volumetric flow rate @ STP Q <sub>STP</sub> (cm <sup>3</sup> /s)	Flux cm <sup>3</sup> (STP/s)/cm <sup>2</sup> s	Permeability (Barrer)×10 <sup>3</sup>
2	152	104	1.733333	1.587919	0.01294	76.61
4	304	239	3.983333	3.649161	0.029736	88.03
6	456	416	6.933333	6.351678	0.051758	102.15
8	608	618	10.3	9.435906	0.076891	113.81
10	760	852	14.2	13.00872	0.106005	125.53
12	912	1117	18.61667	17.05487	0.138976	137.14
14	1064	1466	24.43333	22.38356	0.182398	154.28
16	1216	1897	31.61667	28.96426	0.236022	174.68
18	1368	2432	40.53333	37.13289	0.302586	199.06
20	1520	2622	43.7	40.03389	0.326225	193.15
22	1672	2616	43.6	39.94228	0.325479	175.19
24	1824	2650	44.16667	40.46141	0.329709	162.68

**Table B-4** Effect of pressure on pure CH<sub>4</sub> permeability through membrane M<sub>2</sub>

Pressure (Bar)	Pressure (cm Hg)	Volumetric flow rate Q(ml/min)	Volumetric flow rate Q(cm <sup>3</sup> /s)	Volumetric flow rate @ STP Q <sub>STP</sub> (cm <sup>3</sup> /s)	Flux cm <sup>3</sup> (STP/s)/cm <sup>2</sup> .s	Permeability (Barrer)×10 <sup>3</sup>	Selectivity PCO <sub>2</sub> /PCH <sub>4</sub>
	152	19	0.316667	0.290101	0.002364	13.99709	5.47
	304	29	0.483333	0.442785	0.003608	10.68199	8.24
	456	44	0.733333	0.671812	0.005474	10.80477	9.45
	608	58	0.966667	0.88557	0.007216	10.68199	10.66
	760	87	1.45	1.328356	0.010824	12.81838	9.79
	912	119	1.983333	1.816946	0.014806	14.61099	9.39
	1064	155	2.583333	2.366611	0.019285	16.31239	9.46
	1216	201	3.35	3.06896	0.025008	18.5093	9.44
	1368	261	4.35	3.985067	0.032473	21.36397	9.32
	1520	288	4.8	4.397315	0.035833	21.21663	9.104
	1672	311	5.183333	4.74849	0.038694	20.8282	8.41
	1824	365	6.083333	5.572987	0.045413	22.40762	7.23

**Table B-5** Effect of pressure on pure CO<sub>2</sub> permeability through membrane M<sub>3</sub>.

Pressure (Bar)	Pressure (cm Hg)	Volumetric flow rate Q(ml/min)	Volumetric flow rate Q(cm <sup>3</sup> /s)	Volumetric flow rate @ STP Q <sub>STP</sub> (cm <sup>3</sup> /s)	Flux cm <sup>3</sup> (STP/s)/cm <sup>2</sup> .s	Permeability (Barrer)×10 <sup>3</sup>
2	152	28	0.466667	0.427517	0.003484	61.88
4	304	60	1	0.916107	0.007465	66.30
6	456	90	1.5	1.374161	0.011198	66.30
8	608	122	2.033333	1.862752	0.015179	67.40
10	760	165	2.75	2.519295	0.020529	72.93
12	912	215	3.583333	3.282718	0.02675	79.19
14	1064	295	4.916667	4.504195	0.036703	93.13
16	1216	360	6	5.496644	0.044791	99.45
18	1368	460	7.666667	7.02349	0.057233	112.95
20	1520	495	8.25	7.557886	0.061587	109.39
22	1672	503	8.383333	7.680034	0.062583	101.06
24	1824	515	8.583333	7.863255	0.064076	94.84

**Table B-6** Effect of pressure on pure CH<sub>4</sub> permeability through membrane M<sub>3</sub>.

Pressure (cm Hg)	Volumetric flow rate Q(ml/min)	Volumetric flow rate Q(cm <sup>3</sup> /s)	Volumetric flow rate @ STP Q <sub>STP</sub> (cm <sup>3</sup> /s)	Flux cm <sup>3</sup> (STP/s)/cm <sup>2</sup> .s	Permeability (Barrer)×10 <sup>3</sup>	Selectivity PCO <sub>2</sub> /PCH <sub>4</sub>
152	5	0.083333	0.076342	0.000622	11.05033	5.6
304	9	0.15	0.137416	0.00112	9.945298	6.67
456	15	0.25	0.229027	0.001866	11.05033	6
608	21	0.35	0.320638	0.002613	11.60285	5.81
760	28	0.466667	0.427517	0.003484	12.37637	5.89
912	35	0.583333	0.534396	0.004355	12.89205	6.14
1064	42	0.7	0.641275	0.005226	13.2604	7.02
1216	52	0.866667	0.79396	0.00647	14.36543	6.92
1368	60	1	0.916107	0.007465	14.73377	7.67
1520	67	1.116667	1.022987	0.008336	14.80744	7.39
1672	76	1.266667	1.160403	0.009456	15.26955	6.62
1824	84	1.4	1.28255	0.010451	15.47046	6.13

## APPENDIX C

### Pure Gas Permeability of CO<sub>2</sub> and CH<sub>4</sub> at Different Temperature and at Constant Pressure of 8 bar

Permeability of pure CO<sub>2</sub> and CH<sub>4</sub> gases was measured as follow.

Using Lab View soft ware, flow rate of the gas in the permeate stream  $Q$  was recorded. This volumetric flow rate  $Q$  was then corrected to STP conditions (0°C and 1 atm) using the following equation

$$Q_{STP} = \frac{T_{STP}}{T} \times Q \quad (C-1)$$

The effective area of membrane,  $A'$ , is 122.7185cm<sup>2</sup> and testing pressure is 8 bar. Hence the permeability of CO<sub>2</sub> and CH<sub>4</sub> gas through membrane silicone rubber membrane M<sub>1</sub> can be determined as follows:

$$\begin{aligned} \text{At } 25^{\circ}\text{C CO}_2 \text{ volumetric flow rate, } Q &= 1023 \text{ ml/min} \\ &= 17.05 \text{ cm}^3/\text{s} \end{aligned}$$

This volumetric flow rate,  $Q$ , is corrected to standard temperature and pressure (STP),  $Q_{STP}$ , as follows:

$$\frac{Q_{(STP)}}{Q_{300.K}} = \frac{273K}{298K} \quad (C-2)$$

$$Q_{STP} = \frac{273K}{298K} \times 17.05$$

$$= 15.61963 \text{ cm}^3 (\text{STP})/s$$

$$Q_{STP} = \frac{273K}{298K} \times 17.05$$

$$= 15.61963 \text{ cm}^3 (\text{STP})/s$$

CO<sub>2</sub> flux,  $J_{CO_2}$ , is, therefore,

$$J_{CO_2} = \frac{Q_{STP}}{A'} \tag{C-3}$$

$$= \frac{15.61963}{122.7185}$$

$$= 0.12728 \text{ cm}^3 (\text{STP})/\text{cm}^2 \cdot s$$

Once CO<sub>2</sub> flux,  $J_{CO_2}$  was determined, the CO<sub>2</sub> permeability,  $P$ , can be calculated using the following formula:

$$P = \frac{J_{CO_2} l}{\Delta p} \tag{C-4}$$

$$= \frac{0.12728 \frac{\text{cm}^3 (\text{STP})}{\text{cm}^2 \cdot s}}{8 \text{ bar} \times 76 \frac{\text{cmHg}}{\text{bar}}} \cdot 0.0762 \text{ cm}$$

$$= 159518.9 \frac{\text{cm}^3 (\text{STP})}{\text{cm}^2 \cdot \text{cmHg} \cdot s} \text{ cm}$$

$$= 159.5189 \times 10^3 \text{ Barrer}$$

$$= 159.5189 \times 10^3 \text{ Barrer}$$

Similarly, CH<sub>4</sub> permeability,  $P$ , can be calculated using the same method. For M1 silicone rubber membrane, CH<sub>4</sub> permeability obtained is  $13.87799 \times 10^3$  Barrer. CO<sub>2</sub>/CH<sub>4</sub>

ideal selectivity,  $\alpha_{CO_2/CH_4}$ , can be calculated by dividing CO<sub>2</sub> permeability over CH<sub>4</sub> permeability as follows:

$$\alpha_{CO_2/CH_4} = \frac{P_{CO_2}}{P_{CH_4}} \quad (C-5)$$

$$= 11.4$$

**Table C-1** Effect of temperature on pure CO<sub>2</sub> permeability through membrane M<sub>1</sub>.

Temperature (°C)	Volumetric flow rate Q(ml/min)	Volumetric flow rate Q(cm <sup>3</sup> /s)	Volumetric flow rate @ STP Q <sub>STP</sub> (cm <sup>3</sup> /s)	Flux cm <sup>3</sup> (STP/s)/cm <sup>2</sup> .s	Permeability (Barrer)×10 <sup>3</sup>
25	1023	17.05	15.61963	0.12728	159.52
50	1120	18.66667	17.10067	0.139349	174.64
75	1210	20.16667	18.47483	0.150546	188.68
100	1325	22.08333	20.2307	0.164855	206.61
125	1412	23.53333	21.55906	0.175679	220.18
150	1530	25.5	23.36074	0.19036	238.58

**Table C-2** Effect of temperature on pure CH<sub>4</sub> permeability through membrane M<sub>1</sub>.

Temperature (°C)	Volumetric flow rate Q(ml/min)	Volumetric flow rate Q(cm <sup>3</sup> /s)	Volumetric flow rate @ STP Q <sub>STP</sub> (cm <sup>3</sup> /s)	Flux cm <sup>3</sup> (STP/s)/c m <sup>2</sup> .s	Permeability (Barrer)×10 <sup>3</sup>	Selectivity P <sub>CO<sub>2</sub></sub> /P <sub>CH<sub>4</sub></sub>
25	89	1.48333	1.35889	0.011073	13.87799	11.49
50	110	1.83333	1.67953	0.013686	17.15257	10.18
75	128	2.13333	1.95436	0.015926	19.95935	9.45
100	140	2.33333	2.13758	0.017419	21.83054	9.46
125	154	2.56666	2.35134	0.01916	24.0136	9.17
150	166	2.76666	2.53456	0.020653	25.88479	9.21

**Table C-3** Effect of temperature on pure CO<sub>2</sub> permeability through membrane M<sub>2</sub>.

Temperature (°C)	Volumetric flow rate Q(ml/min)	Volumetric flow rate Q(cm <sup>3</sup> /s)	Volumetric flow rate @ STP Q <sub>STP</sub> (cm <sup>3</sup> /s)	Flux cm <sup>3</sup> (STP/s)/cm <sup>2</sup> .s	Permeability (Barrer)×10 <sup>3</sup>
25	618	10.3	9.435906	0.076891	113.81
50	662	11.03333	10.10772	0.082365	121.92
75	692	11.53333	10.56577	0.086098	127.44
100	720	12	10.99329	0.089581	132.60
125	752	12.53333	11.48188	0.093563	138.49
150	774	12.9	11.81779	0.0963	142.54

**Table C-4** Effect of temperature on pure CH<sub>4</sub> permeability through membrane M<sub>2</sub>.

Temperature (°C)	Volumetric flow rate Q(ml/min)	Volumetric flow rate Q(cm <sup>3</sup> /s)	Volumetric flow rate @ STP Q <sub>STP</sub> (cm <sup>3</sup> /s)	Flux cm <sup>3</sup> (STP/s)/cm <sup>2</sup> .s	Permeability (Barrer)×10 <sup>3</sup>	Selectivity PCO <sub>2</sub> /PCH <sub>4</sub>
25	58	0.966667	0.88557	0.007216	10.68199	10.66
50	66	1.1	1.007718	0.008212	12.15536	10.03
75	77	1.283333	1.175671	0.00958	14.18126	8.99
100	90	1.5	1.374161	0.011198	16.5755	8
125	100	1.666667	1.526846	0.012442	18.41722	7.52
150	120	2	1.832215	0.01493	22.10066	6.45

**Table C-5** Effect of temperature on pure CO<sub>2</sub> permeability through membrane M<sub>3</sub>.

Temperature (°C)	Volumetric flow rate Q(ml/min)	Volumetric flow rate Q(cm <sup>3</sup> /s)	Volumetric flow rate @ STP Q <sub>STP</sub> (cm <sup>3</sup> /s)	Flux cm <sup>3</sup> (STP/s)/cm <sup>2</sup> .s	Permeability (Barrer)×10 <sup>3</sup>
25	122	2.033333	1.862752	0.015179	67.40
50	130	2.166667	1.984899	0.016174	71.82
75	145	2.416667	2.213926	0.018041	80.11
100	158	2.633333	2.412416	0.019658	87.29
125	174	2.9	2.656711	0.021649	96.13
150	182	3.033333	2.778859	0.022644	100.55

**Table C-6** Effect of temperature on pure CH<sub>4</sub> permeability through membrane M<sub>3</sub>.

Temperature (°C)	Volumetric flow rate Q(ml/min)	Volumetric flow rate Q(cm <sup>3</sup> /s)	Volumetric flow rate @ STP Q <sub>STP</sub> (cm <sup>3</sup> /s)	Flux cm <sup>3</sup> (STP/s)/cm <sup>2</sup> .s	Permeability (Barrer)×10 <sup>3</sup>	Selectivity PCO <sub>2</sub> /PCH <sub>4</sub>
25	21	0.35	0.32063	0.002613	11.60285	5.81
50	21	0.35	0.32063	0.002613	11.60285	6.19
75	22	0.36666	0.33590	0.002737	12.15536	6.59
100	26	0.43333	0.39698	0.003235	14.36543	6.08
125	30	0.5	0.45805	0.003733	16.5755	5.8
150	33	0.55	0.50385	0.004106	18.23305	5.52

## APPENDIX D

### Permeability of CO<sub>2</sub> and CH<sub>4</sub> in Binary Mixture (CO<sub>2</sub>+CH<sub>4</sub>) at Different Pressure and at Constant Temperature 25°C

Permeability of CO<sub>2</sub> and CH<sub>4</sub> in binary mixture of (CO<sub>2</sub>+CH<sub>4</sub>) was measured as follow. Using Lab View soft ware, total flow rate of the binary mixture of (CO<sub>2</sub>+CH<sub>4</sub>) in the permeate stream  $Q$  was recorded along with the % age composition of individual gas. The total flow rate was multiplied with the % age composition of individual gas to get the volumetric flow rate of individual gas.

The volumetric flow rate  $Q$  for component gas was then corrected to STP conditions (0°C and 1 atm) using the following equation.

$$Q_{STP} = \frac{T_{STP}}{T} \times Q \quad (D-1)$$

The effective area of membrane  $A'$  is, 122.7185cm<sup>2</sup> and testing temperature is 25°C. Hence the permeability of CO<sub>2</sub> and CH<sub>4</sub> gas in binary mixture (80%CO<sub>2</sub>-20%CH<sub>4</sub>) through membrane silicone rubber membrane M<sub>1</sub> can be determined as follows:

At 25°C and at 2 bar total volumetric flow rate = 184 ml/min (%CO<sub>2</sub>=80.4, %CH<sub>4</sub>=19.5)

$$\begin{aligned} \text{CO}_2 \text{ volumetric flow rate, } Q &= (184 \times 80.4) = 148 \text{ ml/min} \\ &= 2.46667 \text{ cm}^3/\text{s} \end{aligned}$$

This volumetric flow rate,  $Q$ , is corrected to standard temperature and pressure (STP),  $Q_{STP}$ , as follows:

$$\frac{Q_{(STP)}}{Q_{300K}} = \frac{273K}{298K} \quad (D-2)$$

$$\begin{aligned}
Q_{\text{STP}} &= \frac{273\text{K}}{298\text{K}} \times 2.46667 \\
&= 2.259732 \text{ cm}^3 (\text{STP})/\text{s}
\end{aligned}$$

CO<sub>2</sub> flux,  $J_{\text{CO}_2}$ , is, therefore,

$$J_{\text{CO}_2} = \frac{Q_{\text{STP}}}{A'} \quad (\text{D-3})$$

$$= \frac{2.259732}{122.7185}$$

$$= 0.018414 \text{ cm}^3 (\text{STP})/\text{cm}^2 \cdot \text{s}$$

Once CO<sub>2</sub> flux,  $J_{\text{CO}_2}$  was determined, the CO<sub>2</sub> permeability,  $P$ , can be calculated using the following formula:

$$P = \frac{J_{\text{CO}_2} \cdot l}{\Delta p} \quad (\text{D-4})$$

$$= \frac{0.018414 \frac{\text{cm}^3 (\text{STP})}{\text{cm}^2 \cdot \text{s}}}{2 \text{ bar} \times 76 \frac{\text{cmHg}}{\text{bar}}} \cdot 0.0762 \text{ cm}$$

$$= 923120.01 \frac{\text{cm}^3 (\text{STP})}{\text{cm}^2 \cdot \text{cmHg} \cdot \text{s}} \text{ cm}$$

$$= 92.3120 \times 10^3 \text{ Barrer}$$

Similarly, CH<sub>4</sub> permeability,  $P$ , can be calculated using the same method. For M1 silicone rubber membrane, CH<sub>4</sub> permeability in binary mixture (80%CO<sub>2</sub>-20%CH<sub>4</sub>) obtained is  $22.45427 \times 10^3$  Barrer. CO<sub>2</sub>/CH<sub>4</sub> selectivity,  $\alpha_{\text{CO}_2/\text{CH}_4}$ , can be calculated by dividing CO<sub>2</sub> permeability over CH<sub>4</sub> permeability as follows:

$$\alpha_{\text{CO}_2/\text{CH}_4} = \frac{P_{\text{CO}_2}}{P_{\text{CH}_4}} = 4.11 \quad (\text{D-5})$$

**Table D-1** Effect of Pressure on CO<sub>2</sub> Permeability in Binary Mixture (80%CO<sub>2</sub>-20%CH<sub>4</sub>) Through Membrane M<sub>1</sub>.

Pressure (Bar)	Pressure (cm Hg)	Volumetric flow rate Q(ml/min)	Volumetric flow rate Q(cm <sup>3</sup> /s)	Volumetric flow rate @ STP Q <sub>STP</sub> (cm <sup>3</sup> /s)	Flux cm <sup>3</sup> (STP/s)/cm <sup>2</sup> .s	Permeability (Barrer)×10 <sup>3</sup>
2	152	148	2.466667	2.259732	0.018414	92.31
4	304	351	5.85	5.359228	0.043671	109.46
6	456	618	10.3	9.435906	0.076891	128.48
8	608	920	15.333333	14.04698	0.114465	143.45
10	760	1272	21.2	19.42148	0.15826	158.67
12	912	1668	27.8	25.46779	0.20753	173.39
14	1064	2192	36.53333	33.46846	0.272725	195.31

**Table D-2** Effect of Pressure on CO<sub>2</sub> Permeability in Binary Mixture (60%CO<sub>2</sub>-40%CH<sub>4</sub>) Through Membrane M<sub>1</sub>.

Pressure (Bar)	Pressure (cm Hg)	Volumetric flow rate Q(ml/min)	Volumetric flow rate Q(cm <sup>3</sup> /s)	Volumetric flow rate @ STP Q <sub>STP</sub> (cm <sup>3</sup> /s)	Flux cm <sup>3</sup> (STP/s)/cm <sup>2</sup> .s	Permeability (Barrer)×10 <sup>3</sup>
2	152	116	1.933333	1.771141	0.014433	72.35
4	304	273	4.55	4.168289	0.033966	85.13
6	456	480	8	7.328859	0.059721	99.79
8	608	716	11.93333	10.93221	0.089084	111.64
10	760	989	16.48333	15.1005	0.12305	123.37
12	912	1298	21.63333	19.81846	0.161495	134.93
14	1064	1705	28.41667	26.03272	0.212134	151.92

**Table D-3** Effect of Pressure on CO<sub>2</sub> Permeability in Binary Mixture (40%CO<sub>2</sub>-60%CH<sub>4</sub>) Through Membrane M<sub>1</sub>.

Pressure (Bar)	Pressure (cm Hg)	Volumetric flow rate Q(ml/min)	Volumetric flow rate Q(cm <sup>3</sup> /s)	Volumetric flow rate @ STP Q <sub>STP</sub> (cm <sup>3</sup> /s)	Flux cm <sup>3</sup> (STP/s)/cm <sup>2</sup> .s	Permeability (Barrer)×10 <sup>3</sup>
2	152	83	1.383333	1.267282	0.010327	51.76
4	304	195	3.25	2.977349	0.024262	60.81
6	456	343	5.716667	5.237081	0.042676	71.31
8	608	511	8.516667	7.802181	0.063578	79.68
10	760	706	11.76667	10.77953	0.087839	88.07
12	912	927	15.45	14.15386	0.115336	96.36
14	1064	1218	20.3	18.59698	0.151542	108.52

**Table D-4** Effect of Pressure on CO<sub>2</sub> Permeability in Binary Mixture (20%CO<sub>2</sub>-80%CH<sub>4</sub>) Through Membrane M<sub>1</sub>.

Pressure (Bar)	Pressure (cm Hg)	Volumetric flow rate Q(ml/min)	Volumetric flow rate Q(cm <sup>3</sup> /s)	Volumetric flow rate @ STP Q <sub>STP</sub> (cm <sup>3</sup> /s)	Flux cm <sup>3</sup> (STP/s)/cm <sup>2</sup> .s	Permeability (Barrer)×10 <sup>3</sup>
2	152	50	0.833333	0.763423	0.006221	31.18
4	304	117	1.95	1.786409	0.014557	36.48
6	456	205	3.416667	3.130034	0.025506	42.62
8	608	307	5.116667	4.687416	0.038196	47.87
10	760	424	7.066667	6.473826	0.052753	52.89
12	912	556	9.266667	8.489262	0.069177	57.79
14	1064	731	12.18333	11.16124	0.09095	65.13

**Table D-5** Effect of Pressure on CH<sub>4</sub> Permeability in Binary Mixture (80%CO<sub>2</sub>-20%CH<sub>4</sub>) Through Membrane M<sub>1</sub>.

Pressure (Bar)	Pressure (cm Hg)	Volumetric flow rate Q(ml/min)	Volumetric flow rate Q(cm <sup>3</sup> /s)	Volumetric flow rate @ STP Q <sub>STP</sub> (cm <sup>3</sup> /s)	Flux cm <sup>3</sup> (STP/s)/cm <sup>2</sup> .s	Permeability (Barrer)×10 <sup>3</sup>
2	152	36	0.6	0.549664	0.004479	22.45
4	304	60	1	0.916107	0.007465	18.71
6	456	98	1.633333	1.496309	0.012193	20.37
8	608	134	2.233333	2.045973	0.016672	20.89
10	760	207	3.45	3.16057	0.025755	25.82
12	912	285	4.75	4.35151	0.035459	29.62
14	1064	375	6.25	5.725671	0.046657	33.41

**Table D-6** Effect of Pressure on CH<sub>4</sub> Permeability in Binary Mixture (60%CO<sub>2</sub>-40%CH<sub>4</sub>) Through Membrane M<sub>1</sub>.

Pressure (Bar)	Pressure (cm Hg)	Volumetric flow rate Q(ml/min)	Volumetric flow rate Q(cm <sup>3</sup> /s)	Volumetric flow rate @ STP Q <sub>STP</sub> (cm <sup>3</sup> /s)	Flux cm <sup>3</sup> (STP/s)/cm <sup>2</sup> .s	Permeability (Barrer)×10 <sup>3</sup>
2	152	34	0.566667	0.519128	0.00423	21.20
4	304	56	0.933333	0.855034	0.006967	17.46
6	456	91	1.516667	1.38943	0.011322	18.91
8	608	124	2.066667	1.893289	0.015428	19.33
10	760	193	3.216667	2.946812	0.024013	24.07
12	912	266	4.433333	4.061409	0.033095	27.65
14	1064	350	5.833333	5.34396	0.043546	31.18

**Table D-7** Effect of Pressure on CH<sub>4</sub> Permeability in Binary Mixture  
(40%CO<sub>2</sub>60%CH<sub>4</sub>) Through Membrane M<sub>1</sub>.

Pressure (Bar)	Pressure (cm Hg)	Volumetric flow rate Q(ml/min)	Volumetric flow rate Q(cm <sup>3</sup> /s)	Volumetric flow rate @ STP Q <sub>STP</sub> (cm <sup>3</sup> /s)	Flux cm <sup>3</sup> (STP/s)/cm <sup>2</sup> .s	Permeability (Barrer)×10 <sup>3</sup>
2	152	83	1.383333	1.267282	0.010327	51.76
4	304	195	3.25	2.977349	0.024262	60.81
6	456	343	5.716667	5.237081	0.042676	71.31
8	608	511	8.516667	7.802181	0.063578	79.68
10	760	706	11.76667	10.77953	0.087839	88.07
12	912	927	15.45	14.15386	0.115336	96.36
14	1064	1218	20.3	18.59698	0.151542	108.52

**Table D-8** Effect of Pressure on CH<sub>4</sub> Permeability in Binary Mixture  
(20%CO<sub>2</sub>80%CH<sub>4</sub>) Through Membrane M<sub>1</sub>.

Pressure (Bar)	Pressure (cm Hg)	Volumetric flow rate Q(ml/min)	Volumetric flow rate Q(cm <sup>3</sup> /s)	Volumetric flow rate @ STP Q <sub>STP</sub> (cm <sup>3</sup> /s)	Flux cm <sup>3</sup> (STP/s)/cm <sup>2</sup> .s	Permeability (Barrer)×10 <sup>3</sup>
2	152	26	0.433333	0.39698	0.003235	16.21
4	304	44	0.733333	0.671812	0.005474	13.72
6	456	71	1.183333	1.08406	0.008834	14.76
8	608	98	1.633333	1.496309	0.012193	15.28
10	760	151	2.516667	2.305537	0.018787	18.83
12	912	209	3.483333	3.191107	0.026003	21.72
14	1064	275	4.583333	4.198826	0.034215	24.50

**Table D-9** Effect of Pressure on CO<sub>2</sub> Permeability in Binary Mixture (80%CO<sub>2</sub>-20%CH<sub>4</sub>) Through Membrane M<sub>2</sub>.

Pressure (Bar)	Pressure (cm Hg)	Volumetric flow rate Q(ml/min)	Volumetric flow rate Q(cm <sup>3</sup> /s)	Volumetric flow rate @ STP Q <sub>STP</sub> (cm <sup>3</sup> /s)	Flux cm <sup>3</sup> (STP/s)/cm <sup>2</sup> .s	Permeability (Barrer)×10 <sup>3</sup>
2	152	93	1.55	1.419966	0.011571	68.51
4	304	215	3.583333	3.282718	0.02675	79.19
6	456	374	6.233333	5.710403	0.046533	91.84
8	608	556	9.266667	8.489262	0.069177	102.39
10	760	766	12.76667	11.69564	0.095305	112.86
12	912	1005	16.75	15.3448	0.125041	123.39
14	1064	1319	21.98333	20.13909	0.164108	138.81

**Table D-10** Effect of Pressure on CO<sub>2</sub> Permeability in Binary Mixture (60%CO<sub>2</sub>-40%CH<sub>4</sub>) Through Membrane M<sub>2</sub>.

Pressure (Bar)	Pressure (cm Hg)	Volumetric flow rate Q(ml/min)	Volumetric flow rate Q(cm <sup>3</sup> /s)	Volumetric flow rate @ STP Q <sub>STP</sub> (cm <sup>3</sup> /s)	Flux cm <sup>3</sup> (STP/s)/cm <sup>2</sup> .s	Permeability (Barrer)×10 <sup>3</sup>
2	152	73	1.216667	1.114597	0.009083	53.77
4	304	167	2.783333	2.549832	0.020778	61.51
6	456	291	4.85	4.443121	0.036206	71.45
8	608	432	7.2	6.595973	0.053749	79.56
10	760	596	9.933333	9.1	0.074153	87.81
12	912	782	13.03333	11.93993	0.097295	96.01
14	1064	1026	17.1	15.66544	0.127653	107.97

**Table D-11** Effect of Pressure on CO<sub>2</sub> Permeability in Binary Mixture (40%CO<sub>2</sub>-60%CH<sub>4</sub>) Through Membrane M<sub>2</sub>.

Pressure (Bar)	Pressure (cm Hg)	Volumetric flow rate Q(ml/min)	Volumetric flow rate Q(cm <sup>3</sup> /s)	Volumetric flow rate @ STP Q <sub>STP</sub> (cm <sup>3</sup> /s)	Flux cm <sup>3</sup> (STP/s)/cm <sup>2</sup> .s	Permeability (Barrer)×10 <sup>3</sup>
2	152	52	0.866667	0.79396	0.00647	38.30
4	304	120	2	1.832215	0.01493	44.20
6	456	208	3.466667	3.175839	0.025879	51.07
8	608	308	5.133333	4.702685	0.038321	56.72
10	760	426	7.1	6.504362	0.053002	62.76
12	912	558	9.3	8.519799	0.069426	68.51
14	1064	733	12.21667	11.19178	0.091199	77.14

**Table D-12** Effect of Pressure on CO<sub>2</sub> Permeability in Binary Mixture (20%CO<sub>2</sub>-80%CH<sub>4</sub>) Through Membrane M<sub>2</sub>.

Pressure (Bar)	Pressure (cm Hg)	Volumetric flow rate Q(ml/min)	Volumetric flow rate Q(cm <sup>3</sup> /s)	Volumetric flow rate @ STP Q <sub>STP</sub> (cm <sup>3</sup> /s)	Flux cm <sup>3</sup> (STP/s)/cm <sup>2</sup> .s	Permeability (Barrer)×10 <sup>3</sup>
2	152	31	0.516667	0.473322	0.003857	22.83
4	304	72	1.2	1.099329	0.008958	26.52
6	456	125	2.083333	1.908557	0.015552	30.69
8	608	185	3.083333	2.824664	0.023017	34.07
10	760	256	4.266667	3.908725	0.031851	37.71
12	912	335	5.583333	5.114933	0.04168	41.13
14	1064	440	7.333333	6.718121	0.054744	46.30

**Table D-13** Effect of Pressure on CH<sub>4</sub> Permeability in Binary Mixture (80%CO<sub>2</sub>-20%CH<sub>4</sub>) Through Membrane M<sub>2</sub>

Pressure (Bar)	Pressure (cm Hg)	Volumetric flow rate Q(ml/min)	Volumetric flow rate Q(cm <sup>3</sup> /s)	Volumetric flow rate @ STP Q <sub>STP</sub> (cm <sup>3</sup> /s)	Flux cm <sup>3</sup> (STP/s)/cm <sup>2</sup> .s	Permeability (Barrer)×10 <sup>3</sup>
2	152	28	0.466667	0.427517	0.003484	20.62
4	304	43	0.716667	0.656544	0.00535	15.83
6	456	66	1.1	1.007718	0.008212	16.20
8	608	90	1.5	1.374161	0.011198	16.57
10	760	130	2.166667	1.984899	0.016174	19.15
12	912	178	2.966667	2.717785	0.022146	21.85
14	1064	232	3.866667	3.542282	0.028865	24.41

**Table D-14** Effect of Pressure on CH<sub>4</sub> Permeability in Binary Mixture (60%CO<sub>2</sub>-40%CH<sub>4</sub>) Through Membrane M<sub>2</sub>

Pressure (Bar)	Pressure (cm Hg)	Volumetric flow rate Q(ml/min)	Volumetric flow rate Q(cm <sup>3</sup> /s)	Volumetric flow rate @ STP Q <sub>STP</sub> (cm <sup>3</sup> /s)	Flux cm <sup>3</sup> (STP/s)/cm <sup>2</sup> .s	Permeability (Barrer)×10 <sup>3</sup>
2	152	26	0.433333	0.39698	0.003235	19.15
4	304	40	0.666667	0.610738	0.004977	14.73
6	456	62	1.033333	0.946644	0.007714	15.22
8	608	86	1.433333	1.313087	0.0107	15.83
10	760	121	2.016667	1.847483	0.015055	17.82
12	912	166	2.766667	2.534564	0.020653	20.38
14	1064	217	3.616667	3.313255	0.026999	22.83

**Table D-15** Effect of Pressure on CH<sub>4</sub> Permeability in Binary Mixture (40%CO<sub>2</sub>-60%CH<sub>4</sub>) Through Membrane M<sub>2</sub>.

Pressure (Bar)	Pressure (cm Hg)	Volumetric flow rate Q(ml/min)	Volumetric flow rate Q(cm <sup>3</sup> /s)	Volumetric flow rate @ STP Q <sub>STP</sub> (cm <sup>3</sup> /s)	Flux cm <sup>3</sup> (STP/s)/cm <sup>2</sup> .s	Permeability (Barrer)×10 <sup>3</sup>
2	152	24	0.4	0.366443	0.002986	17.68
4	304	37	0.616667	0.564933	0.004603	13.62
6	456	58	0.966667	0.88557	0.007216	14.24
8	608	80	1.333333	1.221477	0.009953	14.73
10	760	113	1.883333	1.725336	0.014059	16.64
12	912	155	2.583333	2.366611	0.019285	19.03
14	1064	200	3.333333	3.053691	0.024884	21.04

**Table D-16** Effect of Pressure on CH<sub>4</sub> Permeability in Binary Mixture (20%CO<sub>2</sub>-80%CH<sub>4</sub>) Through Membrane M<sub>2</sub>.

Pressure (Bar)	Pressure (cm Hg)	Volumetric flow rate Q(ml/min)	Volumetric flow rate Q(cm <sup>3</sup> /s)	Volumetric flow rate @ STP Q <sub>STP</sub> (cm <sup>3</sup> /s)	Flux cm <sup>3</sup> (STP/s)/cm <sup>2</sup> .s	Permeability (Barrer)×10 <sup>3</sup>
2	152	22	0.366667	0.335906	0.002737	16.20
4	304	34	0.566667	0.519128	0.00423	12.52
6	456	52	0.866667	0.79396	0.00647	12.76
8	608	75	1.25	1.145134	0.009331	13.81
10	760	104	1.733333	1.587919	0.01294	15.32
12	912	142	2.366667	2.168121	0.017667	17.43
14	1064	186	3.1	2.839933	0.023142	19.57

**Table D-17** Effect of Pressure on CO<sub>2</sub> Permeability in Binary Mixture (80%CO<sub>2</sub>-20%CH<sub>4</sub>) Through Membrane M<sub>3</sub>.

Pressure (Bar)	Pressure (cm Hg)	Volumetric flow rate Q(ml/min)	Volumetric flow rate Q(cm <sup>3</sup> /s)	Volumetric flow rate @ STP Q <sub>STP</sub> (cm <sup>3</sup> /s)	Flux cm <sup>3</sup> (STP/s)/cm <sup>2</sup> .s	Permeability (Barrer)×10 <sup>3</sup>
2	152	25	0.416667	0.381711	0.00311	55.25
4	304	54	0.9	0.824497	0.006719	59.67
6	456	81	1.35	1.236745	0.010078	59.67
8	608	110	1.833333	1.67953	0.013686	60.77
10	760	148	2.466667	2.259732	0.018414	65.41
12	912	194	3.233333	2.962081	0.024137	71.45
14	1064	266	4.433333	4.061409	0.033095	83.98

**Table D-18** Effect of Pressure on CO<sub>2</sub> Permeability in Binary Mixture (60%CO<sub>2</sub>-40%CH<sub>4</sub>) Through Membrane M<sub>3</sub>.

Pressure (Bar)	Pressure (cm Hg)	Volumetric flow rate Q(ml/min)	Volumetric flow rate Q(cm <sup>3</sup> /s)	Volumetric flow rate @ STP Q <sub>STP</sub> (cm <sup>3</sup> /s)	Flux cm <sup>3</sup> (STP/s)/cm <sup>2</sup> .s	Permeability (Barrer)×10 <sup>3</sup>
2	152	20	0.333333	0.305369	0.002488	44.20
4	304	42	0.7	0.641275	0.005226	46.41
6	456	63	1.05	0.961913	0.007838	46.41
8	608	86	1.433333	1.313087	0.0107	47.51
10	760	116	1.933333	1.771141	0.014433	51.27
12	912	152	2.533333	2.320805	0.018912	55.98
14	1064	207	3.45	3.16057	0.025755	65.35

**Table D-19** Effect of Pressure on CO<sub>2</sub> Permeability in Binary Mixture (40%CO<sub>2</sub>-60%CH<sub>4</sub>) Through Membrane M<sub>3</sub>.

Pressure (Bar)	Pressure (cm Hg)	Volumetric flow rate Q(ml/min)	Volumetric flow rate Q(cm <sup>3</sup> /s)	Volumetric flow rate @ STP Q <sub>STP</sub> (cm <sup>3</sup> /s)	Flux cm <sup>3</sup> (STP/s)/cm <sup>2</sup> .s	Permeability (Barrer)×10 <sup>3</sup>
2	152	14	0.233333	0.213758	0.001742	30.94
4	304	30	0.5	0.458054	0.003733	33.15
6	456	45	0.75	0.687081	0.005599	33.15
8	608	61	1.016667	0.931376	0.00759	33.70
10	760	83	1.383333	1.267282	0.010327	36.68
12	912	108	1.8	1.648993	0.013437	39.78

**Table D-20** Effect of Pressure on CO<sub>2</sub> Permeability in Binary Mixture (20%CO<sub>2</sub>-80%CH<sub>4</sub>) Through Membrane M<sub>3</sub>.

Pressure (Bar)	Pressure (cm Hg)	Volumetric flow rate Q(ml/min)	Volumetric flow rate Q(cm <sup>3</sup> /s)	Volumetric flow rate @ STP Q <sub>STP</sub> (cm <sup>3</sup> /s)	Flux cm <sup>3</sup> (STP/s)/cm <sup>2</sup> .s	Permeability (Barrer)×10 <sup>3</sup>
2	152	9	0.15	0.137416	0.00112	19.89
4	304	18	0.3	0.274832	0.00224	19.89
6	456	27	0.45	0.412248	0.003359	19.89
8	608	37	0.616667	0.564933	0.004603	20.44
10	760	50	0.833333	0.763423	0.006221	22.10
12	912	65	1.083333	0.99245	0.008087	23.94
14	1064	90	1.5	1.374161	0.011198	28.41

**Table D-21** Effect of Pressure on CH<sub>4</sub> Permeability in Binary Mixture (80%CO<sub>2</sub>-20%CH<sub>4</sub>) Through Membrane M<sub>3</sub>.

Pressure (Bar)	Pressure (cm Hg)	Volumetric flow rate Q(ml/min)	Volumetric flow rate Q(cm <sup>3</sup> /s)	Volumetric flow rate @ STP Q <sub>STP</sub> (cm <sup>3</sup> /s)	Flux cm <sup>3</sup> (STP/s)/cm <sup>2</sup> .s	Permeability (Barrer)×10 <sup>3</sup>
2	152	8	0.133333	0.122148	0.000995	17.68
4	304	14	0.233333	0.213758	0.001742	15.47
6	456	23	0.383333	0.351174	0.002862	16.94
8	608	32	0.533333	0.488591	0.003981	17.68
10	760	42	0.7	0.641275	0.005226	18.56
12	912	53	0.883333	0.809228	0.006594	19.52
14	1064	63	1.05	0.961913	0.007838	19.89

**Table D-22** Effect of Pressure on CH<sub>4</sub> Permeability in Binary Mixture (60%CO<sub>2</sub>-40%CH<sub>4</sub>) Through Membrane M<sub>3</sub>.

Pressure (Bar)	Pressure (cm Hg)	Volumetric flow rate Q(ml/min)	Volumetric flow rate Q(cm <sup>3</sup> /s)	Volumetric flow rate @ STP Q <sub>STP</sub> (cm <sup>3</sup> /s)	Flux cm <sup>3</sup> (STP/s)/cm <sup>2</sup> .s	Permeability (Barrer)×10 <sup>3</sup>
2	152	7	0.116667	0.106879	0.000871	15.47
4	304	13	0.216667	0.19849	0.001617	14.36
6	456	21	0.35	0.320638	0.002613	15.47
8	608	30	0.5	0.458054	0.003733	16.57
10	760	38	0.633333	0.580201	0.004728	16.79
12	912	48	0.8	0.732886	0.005972	17.68
14	1064	60	1	0.916107	0.007465	18.94

**Table D-23** Effect of Pressure on CH<sub>4</sub> Permeability in Binary Mixture (40%CO<sub>2</sub>-60%CH<sub>4</sub>) Through Membrane M<sub>3</sub>.

Pressure (Bar)	Pressure (cm Hg)	Volumetric flow rate Q(ml/min)	Volumetric flow rate Q(cm <sup>3</sup> /s)	Volumetric flow rate @ STP Q <sub>STP</sub> (cm <sup>3</sup> /s)	Flux cm <sup>3</sup> (STP/s)/cm <sup>2</sup> .s	Permeability (Barrer)×10 <sup>3</sup>
2	152	6	0.1	0.091611	0.000747	13.26
4	304	11	0.183333	0.167953	0.001369	12.15
6	456	20	0.333333	0.305369	0.002488	14.73
8	608	27	0.45	0.412248	0.003359	14.91
10	760	36	0.6	0.549664	0.004479	15.91
12	912	45	0.75	0.687081	0.005599	16.57
14	1064	55	0.916667	0.839765	0.006843	17.36

**Table D-24** Effect of Pressure on CH<sub>4</sub> Permeability in Binary Mixture (20%CO<sub>2</sub>-80%CH<sub>4</sub>) Through Membrane M<sub>3</sub>.

Pressure (Bar)	Pressure (cm Hg)	Volumetric flow rate Q(ml/min)	Volumetric flow rate Q(cm <sup>3</sup> /s)	Volumetric flow rate @ STP Q <sub>STP</sub> (cm <sup>3</sup> /s)	Flux cm <sup>3</sup> (STP/s)/cm <sup>2</sup> .s	Permeability (Barrer)×10 <sup>3</sup>
2	152	6	0.1	0.091611	0.000747	13.26
4	304	10	0.166667	0.152685	0.001244	11.05
6	456	18	0.3	0.274832	0.00224	13.26
8	608	25	0.416667	0.381711	0.00311	13.81
10	760	33	0.55	0.503859	0.004106	14.58
12	912	42	0.7	0.641275	0.005226	15.47
14	1064	50	0.833333	0.763423	0.006221	15.78

**Table D-25** Selectivity of CO<sub>2</sub> over CH<sub>4</sub> in membrane M<sub>1</sub> at different pressure.

Composition	Pressure (Bar)	CO <sub>2</sub> Permeability (Barrer)×10 <sup>3</sup>	CH <sub>4</sub> Permeability (Barrer)×10 <sup>3</sup>	Selectivity PCO <sub>2</sub> /PCH <sub>4</sub>
80% CO <sub>2</sub> 20% CH <sub>4</sub>	2	92.31200697	22.45427	4.11
	4	109.4645758	18.71189	5.85
	6	128.488334	20.37517	6.31
	8	143.4578487	20.89495	6.87
	10	158.6768552	25.82241	6.15
	12	173.396878	29.62716	5.85
	14	195.3165244	33.4141	5.85
60% CO <sub>2</sub> 40% CH <sub>4</sub>	2	72.35265412	21.20681	3.41
	4	85.13911454	17.46443	4.88
	6	99.7967643	18.9198	5.27
	8	111.6476301	19.33562	5.77
	10	123.3737499	24.07597	5.12
	12	134.9335417	27.65202	4.88
	14	151.9227528	31.18649	4.87
40% CO <sub>2</sub> 60% CH <sub>4</sub>	2	51.76957148	19.33562	2.68
	4	60.81365324	16.21697	3.75
	6	71.31310449	17.67234	4.03
	8	79.68147899	18.08816	4.41
	10	88.07064449	22.45427	3.92
	12	96.36625052	25.67688	3.75
	14	108.5289812	28.95888	3.74
20% CO <sub>2</sub> 80% CH <sub>4</sub>	2	31.18648884	16.21697	1.92
	4	36.48819195	13.72206	2.66
	6	42.62153475	14.7616	2.89
	8	47.87126037	15.28138	3.13
	10	52.89228508	18.83664	2.81
	12	57.79895932	21.72659	2.66
	14	65.13520955	24.50367	2.66

**TableD-26** Selectivity of CO<sub>2</sub> over CH<sub>4</sub> in membrane M<sub>2</sub> at different pressure.

Composition	Pressure (Bar)	CO <sub>2</sub> Permeability (Barrer)×10 <sup>3</sup>	CH <sub>4</sub> Permeability (Barrer)×10 <sup>3</sup>	Selectivity P <sub>CO<sub>2</sub></sub> /P <sub>CH<sub>4</sub></sub>
80% CO <sub>2</sub> 20% CH <sub>4</sub>	2	68.51205029	20.62728	3.32
	4	79.19403663	15.83881	5
	6	91.8405262	16.20715	5.67
	8	102.3997311	16.5755	6.18
	10	112.8607108	19.15391	5.89
	12	123.3953594	21.8551	5.64
	14	138.8132017	24.41597	5.68
60% CO <sub>2</sub> 40% CH <sub>4</sub>	2	53.77827604	19.15391	2.81
	4	61.51350752	14.73377	4.17
	6	71.45880514	15.2249	4.69
	8	79.56238098	15.83881	5.02
	10	87.81329457	17.82787	4.93
	12	96.01509557	20.38172	4.71
	14	107.9775171	22.83735	4.73
40% CO <sub>2</sub> 60% CH <sub>4</sub>	2	38.30781307	17.68053	2.16
	4	44.20132277	13.62874	3.24
	6	51.07708409	14.24265	3.59
	8	56.72503089	14.73377	3.85
	10	62.76587833	16.64916	3.77
	12	68.51205029	19.03113	3.6
	14	77.14183236	21.04825	3.66
20% CO <sub>2</sub> 80% CH <sub>4</sub>	2	22.8373501	16.20715	1.41
	4	26.52079366	12.52371	2.11
	6	30.69536303	12.76927	2.40
	8	34.07185297	13.81291	2.47
	10	37.7184621	15.32313	2.46
	12	41.13178647	17.43497	2.36
	14	46.30614766	19.57487	2.36

**Table D-27** Selectivity of CO<sub>2</sub> over CH<sub>4</sub> in membrane M<sub>3</sub> at different pressure.

Composition	Pressure (Bar)	CO <sub>2</sub> Permeability (Barrer)×10 <sup>3</sup>	CH <sub>4</sub> Permeability (Barrer)×10 <sup>3</sup>	Selectivity P <sub>CO<sub>2</sub></sub> /P <sub>CH<sub>4</sub></sub>
80% CO <sub>2</sub> 20% CH <sub>4</sub>	2	55.25163	17.68053	3.125
	4	59.67178	15.47046	3.86
	6	59.67178	16.94384	3.521
	8	60.77681	17.68053	3.43
	10	65.41795	18.56456	3.52
	12	71.45880	19.52225	3.66
	14	83.98251	19.8906	4.22
60% CO <sub>2</sub> 40% CH <sub>4</sub>	2	44.20137	15.47046	2.86
	4	46.41139	14.36543	3.23
	6	46.41139	15.47046	3
	8	47.51649	16.5755	2.87
	10	51.27354	16.7965	3.05
	12	55.98831	17.68053	3.177
	14	65.35485	18.94342	3.45
40% CO <sub>2</sub> 60% CH <sub>4</sub>	2	30.94094	13.2604	2.33
	4	33.15098	12.15536	2.73
	6	33.15098	14.73377	2.25
	8	33.70356	14.91795	2.26
	10	36.68709	15.91248	2.30
	12	39.78114	16.5755	2.4
	14	46.72716	17.36481	2.69
20% CO <sub>2</sub> 80% CH <sub>4</sub>	2	19.89052	13.2604	1.5
	4	19.89052	11.05033	1.8
	6	19.89059	13.2604	1.5
	8	20.44311	13.81291	1.48
	10	22.10066	14.58644	1.51
	12	23.94238	15.47046	1.55
	14	28.41513	15.78619	1.8

## APPENDIX E

### Permeability of CO<sub>2</sub> and CH<sub>4</sub> in Binary Mixture (CO<sub>2</sub>+CH<sub>4</sub>) at Different Temperature and at Constant Pressure of 8 bar

Permeability of CO<sub>2</sub> and CH<sub>4</sub> in binary mixture of (CO<sub>2</sub>+CH<sub>4</sub>) was measured as follow. Using Lab View soft ware, total flow rate of the binary mixture of (CO<sub>2</sub>+CH<sub>4</sub>) in the permeate stream  $Q$  was recorded along with the % age composition of individual gas. The total flow rate was multiplied with the % age composition of individual gas to get the volumetric flow rate of individual gas.

The volumetric flow rate  $Q$  for component gas was then corrected to STP conditions (0°C and 1 atm) using the following equation.

$$Q_{STP} = \frac{T_{STP}}{T} \times Q \quad (E-1)$$

The effective area of membrane A' is 122.7185cm<sup>2</sup> and testing pressure is 8 bar. Hence the permeability of CO<sub>2</sub> and CH<sub>4</sub> gas in binary mixture (80%CO<sub>2</sub>-20%CH<sub>4</sub>) through membrane silicone rubber membrane M<sub>1</sub> can be determined as follows:

At 25°C and at 8 bar total volumetric flow rate=1052 ml/min (87.3 %CO<sub>2</sub> =, 12.7 %CH<sub>4</sub>)  
CO<sub>2</sub> volumetric flow rate,  $Q = 918$  ml/min  
 $= 15.3$  cm<sup>3</sup>/s

This volumetric flow rate,  $Q$ , is corrected to standard temperature and pressure (STP),  $Q_{STP}$ , as follows:

$$\frac{Q_{(STP)}}{Q_{300K}} = \frac{273K}{298K} \quad (E-2)$$

$$Q_{STP} = \frac{273K}{298K} \times 15.3$$

$$= 14.016 \text{ cm}^3 \text{ (STP)/s}$$

CO<sub>2</sub> flux,  $J_{CO_2}$ , is, therefore,

$$J_{CO_2} = \frac{Q_{STP}}{A'} \tag{E-3}$$

$$= 0.114216 \text{ cm}^3 \text{ (STP)/cm}^2 \cdot \text{s}$$

Once CO<sub>2</sub> flux,  $J_{CO_2}$  was determined, the CO<sub>2</sub> permeability,  $P$ , can be calculated using the following formula:

$$P = \frac{J_{CO_2} l}{\Delta p} \tag{E-4}$$

$$= \frac{0.114216 \frac{\text{cm}^3 \text{ (STP)}}{\text{cm}^2 \cdot \text{s}}}{8 \text{ bar} \times 76 \frac{\text{cmHg}}{\text{bar}}} \times 0.0762 \text{ cm}$$

$$=$$

$$= 143.1459838 \times 10^3 \text{ Barrer} \quad \text{As } 1 \text{ Barrer} = \frac{10^{10} \text{ cm}^3 \text{ (STP)}}{\text{cm Hg}} \text{ cm}$$

Similarly, CH<sub>4</sub> permeability,  $P$ , can be calculated using the same method. For M<sub>1</sub> silicone rubber membrane, CH<sub>4</sub> permeability in binary mixture (80%CO<sub>2</sub>-20%CH<sub>4</sub>) obtained is 20.89495×10<sup>3</sup> Barrer. CO<sub>2</sub>/CH<sub>4</sub> selectivity, selectivity ( $\alpha$ ), can be calculated by dividing CO<sub>2</sub> permeability over CH<sub>4</sub> permeability as follows:

$$\alpha_{CO_2/CH_4} = \frac{P_{CO_2}}{P_{CH_4}} = 6.85 \tag{E-5}$$

**Table E-1** Effect of Temperature on CO<sub>2</sub> Permeability in Binary Mixture (80%CO<sub>2</sub>-20%CH<sub>4</sub>) Through Membrane M<sub>1</sub> at 8 bar.

Temperature (°C)	Volumetric flow rate Q(ml/min)	Volumetric flow rate Q(cm <sup>3</sup> /s)	Volumetric flow rate @ STP Q <sub>STP</sub> (cm <sup>3</sup> /s)	Flux cm <sup>3</sup> (STP)/cm <sup>2</sup> .s	Permeability (Barrer)×10 <sup>3</sup>
25	918	15.3	14.01644	0.114216	143.15
50	1015	16.91667	15.49748	0.126285	158.27
75	1105	18.41667	16.87164	0.137482	172.31
100	1220	20.33333	18.62752	0.151791	190.24
125	1307	21.78333	19.95587	0.162615	203.80
150	1425	23.75	21.75755	0.177296	222.20

**Table E-2** Effect of Temperature on CO<sub>2</sub> Permeability in Binary Mixture (60%CO<sub>2</sub>-40%CH<sub>4</sub>) Through Membrane M<sub>1</sub> at 8 bar.

Temperature (°C)	Volumetric flow rate Q(ml/min)	Volumetric flow rate Q(cm <sup>3</sup> /s)	Volumetric flow rate @ STP Q <sub>STP</sub> (cm <sup>3</sup> /s)	Flux cm <sup>3</sup> (STP)/cm <sup>2</sup> .s	Permeability (Barrer)×10 <sup>3</sup>
25	716	11.93333	10.93221	0.089084	111.64
50	813	13.55	12.41326	0.101152	126.77
75	903	15.05	13.78742	0.11235	140.80
100	1018	16.96667	15.54329	0.126658	158.74
125	1105	18.41667	16.87164	0.137482	172.31
150	1223	20.38333	18.67332	0.152164	190.71

**Table E-3** Effect of Temperature on CO<sub>2</sub> Permeability in Binary Mixture (40%CO<sub>2</sub>-60%CH<sub>4</sub>) Through Membrane M<sub>1</sub> at 8 bar.

Temperature (°C)	Volumetric flow rate Q(ml/min)	Volumetric flow rate Q(cm <sup>3</sup> /s)	Volumetric flow rate @ STP Q <sub>STP</sub> (cm <sup>3</sup> /s)	Flux cm <sup>3</sup> (STP)/cm <sup>2</sup> .s	Permeability (Barrer)×10 <sup>3</sup>
25	511	8.516667	7.802181	0.063578	79.69
50	608	10.13333	9.283221	0.075646	94.81
75	698	11.63333	10.65738	0.086844	108.96
100	813	13.55	12.41326	0.101152	126.77
125	900	15	13.74161	0.111977	140.33
150	1018	16.96667	15.54329	0.126658	158.73

**Table E-4** Effect of Temperature on CO<sub>2</sub> Permeability in Binary Mixture (20%CO<sub>2</sub>-80%CH<sub>4</sub>) Through Membrane M<sub>1</sub> at 8 bar.

Temperature (°C)	Volumetric flow rate Q(ml/min)	Volumetric flow rate Q(cm <sup>3</sup> /s)	Volumetric flow rate @ STP Q <sub>STP</sub> (cm <sup>3</sup> /s)	Flux cm <sup>3</sup> (STP)/cm <sup>2</sup> .s	Permeability (Barrer)×10 <sup>3</sup>
25	307	5.116667	4.687416	0.038196	47.87
50	404	6.733333	6.168456	0.050265	62.99
75	494	8.233333	7.542617	0.061463	77.03
100	609	10.15	9.29849	0.075771	94.96
125	696	11.6	10.62685	0.086595	108.53
150	814	13.56667	12.42852	0.101277	126.93

**TableE-5** Effect of Temperature on CH<sub>4</sub> Permeability in Binary Mixture (80%CO<sub>2</sub>-20%CH<sub>4</sub>) Through Membrane M<sub>1</sub> at 8 bar.

Temperature (°C)	Volumetric flow rate Q(ml/min)	Volumetric flow rate Q(cm <sup>3</sup> /s)	Volumetric flow rate @ STP Q <sub>STP</sub> (cm <sup>3</sup> /s)	Flux cm <sup>3</sup> (STP)/cm <sup>2</sup> .s	Permeability (Barrer)×10 <sup>3</sup>
25	134	2.233333	2.045973	0.016672	20.895
50	155	2.583333	2.366611	0.019285	24.17
75	173	2.883333	2.641443	0.021524	26.98
100	185	3.083333	2.824664	0.023017	28.85
125	199	3.316667	3.038423	0.024759	31.03
150	211	3.516667	3.221644	0.026252	32.90
25	134	2.233333	2.045973	0.016672	20.89

**Table E-6** Effect of Temperature on CH<sub>4</sub> Permeability in Binary Mixture (60%CO<sub>2</sub>-40%CH<sub>4</sub>) Through Membrane M<sub>1</sub> at 8 bar.

Temperature (°C)	Volumetric flow rate Q(ml/min)	Volumetric flow rate Q(cm <sup>3</sup> /s)	Volumetric flow rate @ STP Q <sub>STP</sub> (cm <sup>3</sup> /s)	Flux cm <sup>3</sup> (STP)/cm <sup>2</sup> .s	Permeability (Barrer)×10 <sup>3</sup>
25	124	2.066667	1.893289	0.015428	19.33
50	145	2.416667	2.213926	0.018041	22.61
75	163	2.716667	2.488758	0.02028	25.41
100	175	2.916667	2.67198	0.021773	27.28
125	189	3.15	2.885738	0.023515	29.47
150	201	3.35	3.06896	0.025008	31.34
25	124	2.066667	1.893289	0.015428	19.33

**Table E-7** Effect of Temperature on CH<sub>4</sub> Permeability in Binary Mixture (40%CO<sub>2</sub>-60%CH<sub>4</sub>) Through Membrane M<sub>1</sub> at 8 bar.

Temperature (°C)	Volumetric flow rate Q(ml/min)	Volumetric flow rate Q(cm <sup>3</sup> /s)	Volumetric flow rate @ STP Q <sub>STP</sub> (cm <sup>3</sup> /s)	Flux cm <sup>3</sup> (STP)/cm <sup>2</sup> .s	Permeability (Barrer)×10 <sup>3</sup>
25	116	1.933333	1.771141	0.014433	18.08
50	137	2.283333	2.091779	0.017045	21.36
75	155	2.583333	2.366611	0.019285	24.16
100	167	2.783333	2.549832	0.020778	26.04
125	181	3.016667	2.763591	0.02252	28.22
150	193	3.216667	2.946812	0.024013	30.09

**Table E-8** Effect of Temperature on CH<sub>4</sub> Permeability in Binary Mixture (20%CO<sub>2</sub>-80%CH<sub>4</sub>) Through Membrane M<sub>1</sub> at 8 bar.

Temperature (°C)	Volumetric flow rate Q(ml/min)	Volumetric flow rate Q(cm <sup>3</sup> /s)	Volumetric flow rate @ STP Q <sub>STP</sub> (cm <sup>3</sup> /s)	Flux cm <sup>3</sup> (STP)/cm <sup>2</sup> .s	Permeability (Barrer)×10 <sup>3</sup>
25	98	1.633333	1.496309	0.012193	15.28
50	119	1.983333	1.816946	0.014806	18.55
75	137	2.283333	2.091779	0.017045	21.36
100	149	2.483333	2.275	0.018538	23.23
125	163	2.716667	2.488758	0.02028	25.42
150	175	2.916667	2.67198	0.021773	27.29
25	98	1.633333	1.496309	0.012193	15.29

**Table E-9** Effect of Temperature on CO<sub>2</sub> Permeability in Binary Mixture (80%CO<sub>2</sub>-20%CH<sub>4</sub>) Through Membrane M<sub>2</sub> at 8 bar.

Temperature (°C)	Volumetric flow rate Q(ml/min)	Volumetric flow rate Q(cm <sup>3</sup> /s)	Volumetric flow rate @ STP Q <sub>STP</sub> (cm <sup>3</sup> /s)	Flux cm <sup>3</sup> (STP)/cm <sup>2</sup> .s	Permeability (Barrer)×10 <sup>3</sup>
25	556	9.266667	8.489262	0.069177	102.39
50	600	10	9.161074	0.074651	110.50
75	630	10.5	9.619128	0.078384	116.03
100	658	10.96667	10.04664	0.081867	121.19
125	690	11.5	10.53523	0.085849	127.08
150	712	11.86667	10.87114	0.088586	131.13

**Table E-10** Effect of Temperature on CO<sub>2</sub> Permeability in Binary Mixture (60%CO<sub>2</sub>-40%CH<sub>4</sub>) Through Membrane M<sub>2</sub> at 8 bar.

Temperature (°C)	Volumetric flow rate Q(ml/min)	Volumetric flow rate Q(cm <sup>3</sup> /s)	Volumetric flow rate @ STP Q <sub>STP</sub> (cm <sup>3</sup> /s)	Flux cm <sup>3</sup> (STP)/cm <sup>2</sup> .s	Permeability (Barrer)×10 <sup>3</sup>
25	432	7.2	6.595973	0.053749	79.56
50	476	7.933333	7.267785	0.059223	87.663
75	506	8.433333	7.725839	0.062956	93.197
100	534	8.9	8.153356	0.066439	98.35
125	566	9.433333	8.641946	0.070421	104.24
150	588	9.8	8.977852	0.073158	108.29

**Table E-11** Effect of Temperature on CO<sub>2</sub> Permeability in Binary Mixture (40%CO<sub>2</sub>-60%CH<sub>4</sub>) Through Membrane M<sub>2</sub> at 8 bar.

Temperature (°C)	Volumetric flow rate Q(ml/min)	Volumetric flow rate Q(cm <sup>3</sup> /s)	Volumetric flow rate @ STP Q <sub>STP</sub> (cm <sup>3</sup> /s)	Flux cm <sup>3</sup> (STP)/cm <sup>2</sup> .s	Permeability (Barrer)×10 <sup>3</sup>
25	308	5.133333	4.702685	0.038321	56.72
50	352	5.866667	5.374497	0.043795	64.82
75	382	6.366667	5.83255	0.047528	70.35
100	410	6.833333	6.260067	0.051012	75.51
125	442	7.366667	6.748658	0.054993	81.40
150	464	7.733333	7.084564	0.05773	85.45

**Table E-12** Effect of Temperature on CO<sub>2</sub> Permeability in Binary Mixture (20%CO<sub>2</sub>-80%CH<sub>4</sub>) Through Membrane M<sub>2</sub> at 8 bar.

Temperature (°C)	Volumetric flow rate Q(ml/min)	Volumetric flow rate Q(cm <sup>3</sup> /s)	Volumetric flow rate @ STP Q <sub>STP</sub> (cm <sup>3</sup> /s)	Flux cm <sup>3</sup> (STP)/cm <sup>2</sup> .s	Permeability (Barrer)×10 <sup>3</sup>
25	185	3.083333	2.824664	0.023017	34.07
50	229	3.816667	3.496477	0.028492	42.17
75	259	4.316667	3.95453	0.032224	47.70
100	287	4.783333	4.382047	0.035708	52.85
125	319	5.316667	4.870638	0.03969	58.75
150	341	5.683333	5.206544	0.042427	62.80

**Table E-13** Effect of Temperature on CH<sub>4</sub> Permeability in Binary Mixture (80%CO<sub>2</sub>-20%CH<sub>4</sub>) Through Membrane M<sub>2</sub> at 8 bar.

Temperature (°C)	Volumetric flow rate Q(ml/min)	Volumetric flow rate Q(cm <sup>3</sup> /s)	Volumetric flow rate @ STP Q <sub>STP</sub> (cm <sup>3</sup> /s)	Flux cm <sup>3</sup> (STP)/cm <sup>2</sup> .s	Permeability (Barrer)×10 <sup>3</sup>
25	90	1.5	1.374161	0.011198	16.57
50	98	1.633333	1.496309	0.012193	18.04
75	109	1.816667	1.664262	0.013562	20.07
100	122	2.033333	1.862752	0.015179	22.46
125	132	2.2	2.015436	0.016423	24.31
150	152	2.533333	2.320805	0.018912	27.99

**Table E-14** Effect of Temperature on CH<sub>4</sub> Permeability in Binary Mixture (60%CO<sub>2</sub>-40%CH<sub>4</sub>) Through Membrane M<sub>2</sub> at 8 bar.

Temperature (°C)	Volumetric flow rate Q(ml/min)	Volumetric flow rate Q(cm <sup>3</sup> /s)	Volumetric flow rate @ STP Q <sub>STP</sub> (cm <sup>3</sup> /s)	Flux cm <sup>3</sup> (STP)/cm <sup>2</sup> .s	Permeability (Barrer)×10 <sup>3</sup>
25	86	1.433333	1.313087	0.0107	15.83
50	94	1.566667	1.435235	0.011695	17.31
75	105	1.75	1.603188	0.013064	19.33
100	118	1.966667	1.801678	0.014681	21.73
125	128	2.133333	1.954362	0.015926	23.57
150	148	2.466667	2.259732	0.018414	27.25

**Table E-15** Effect of Temperature on CH<sub>4</sub> Permeability in Binary Mixture (40%CO<sub>2</sub>-60%CH<sub>4</sub>) Through Membrane M<sub>2</sub> at 8 bar.

Temperature (°C)	Volumetric flow rate Q(ml/min)	Volumetric flow rate Q(cm <sup>3</sup> /s)	Volumetric flow rate @ STP Q <sub>STP</sub> (cm <sup>3</sup> /s)	Flux cm <sup>3</sup> (STP)/cm <sup>2</sup> .s	Permeability (Barrer)×10 <sup>3</sup>
25	80	1.333333	1.221477	0.009953	14.73
50	88	1.466667	1.343624	0.010949	16.20
75	99	1.65	1.511577	0.012317	18.23
100	112	1.866667	1.710067	0.013935	20.62
125	122	2.033333	1.862752	0.015179	22.46
150	142	2.366667	2.168121	0.017667	26.15

**Table E-16** Effect of Temperature on CH<sub>4</sub> Permeability in Binary Mixture (20%CO<sub>2</sub>-80%CH<sub>4</sub>) Through Membrane M<sub>2</sub> at 8 bar.

Temperature (°C)	Volumetric flow rate Q(ml/min)	Volumetric flow rate Q(cm <sup>3</sup> /s)	Volumetric flow rate @ STP Q <sub>STP</sub> (cm <sup>3</sup> /s)	Flux cm <sup>3</sup> (STP)/cm <sup>2</sup> .s	Permeability (Barrer)×10 <sup>3</sup>
25	75	1.25	1.145134	0.009331	13.81
50	83	1.383333	1.267282	0.010327	15.28
75	94	1.566667	1.435235	0.011695	17.31
100	107	1.783333	1.633725	0.013313	19.70
125	117	1.95	1.786409	0.014557	21.54
150	137	2.283333	2.091779	0.017045	25.23

**Table E-17** Effect of Temperature on CO<sub>2</sub> Permeability in Binary Mixture (80%CO<sub>2</sub>-20%CH<sub>4</sub>) Through Membrane M<sub>3</sub> at 8 bar.

Temperature (°C)	Volumetric flow rate Q(ml/min)	Volumetric flow rate Q(cm <sup>3</sup> /s)	Volumetric flow rate @ STP Q <sub>STP</sub> (cm <sup>3</sup> /s)	Flux cm <sup>3</sup> (STP)/cm <sup>2</sup> .s	Permeability (Barrer)×10 <sup>3</sup>
25	110	1.833333	1.67953	0.013686	60.77
50	118	1.966667	1.801678	0.014681	65.19
75	133	2.216667	2.030705	0.016548	73.48
100	146	2.433333	2.229195	0.018165	80.66
125	162	2.7	2.47349	0.020156	89.50
150	170	2.833333	2.595638	0.021151	93.92

**Table E-18** Effect of Temperature on CO<sub>2</sub> Permeability in Binary Mixture (60%CO<sub>2</sub>-40%CH<sub>4</sub>) Through Membrane M<sub>3</sub> at 8 bar.

Temperature (°C)	Volumetric flow rate Q(ml/min)	Volumetric flow rate Q(cm <sup>3</sup> /s)	Volumetric flow rate @ STP Q <sub>STP</sub> (cm <sup>3</sup> /s)	Flux cm <sup>3</sup> (STP)/cm <sup>2</sup> .s	Permeability (Barrer)×10 <sup>3</sup>
25	86	1.433333	1.313087	0.0107	47.52
50	94	1.566667	1.435235	0.011695	51.93
75	109	1.816667	1.664262	0.013562	60.22
100	122	2.033333	1.862752	0.015179	67.40
125	138	2.3	2.107047	0.01717	76.25
150	146	2.433333	2.229195	0.018165	80.67

**Table E-19** Effect of Temperature on CO<sub>2</sub> Permeability in Binary Mixture (40%CO<sub>2</sub>-60%CH<sub>4</sub>) Through Membrane M<sub>3</sub> at 8 bar.

Temperature (°C)	Volumetric flow rate Q(ml/min)	Volumetric flow rate Q(cm <sup>3</sup> /s)	Volumetric flow rate @ STP Q <sub>STP</sub> (cm <sup>3</sup> /s)	Flux cm <sup>3</sup> (STP)/cm <sup>2</sup> .s	Permeability (Barrer)×10 <sup>3</sup>
25	61	1.016667	0.931376	0.00759	33.70
50	69	1.15	1.053523	0.008585	38.12
75	84	1.4	1.28255	0.010451	46.41
100	97	1.616667	1.48104	0.012069	53.59
125	113	1.883333	1.725336	0.014059	62.43
150	121	2.016667	1.847483	0.015055	66.85

**Table E-20** Effect of Temperature on CO<sub>2</sub> Permeability in Binary Mixture (20%CO<sub>2</sub>-80%CH<sub>4</sub>) Through Membrane M<sub>3</sub> at 8 bar.

Temperature (°C)	Volumetric flow rate Q(ml/min)	Volumetric flow rate Q(cm <sup>3</sup> /s)	Volumetric flow rate @ STP Q <sub>STP</sub> (cm <sup>3</sup> /s)	Flux cm <sup>3</sup> (STP)/cm <sup>2</sup> .s	Permeability (Barrer)×10 <sup>3</sup>
25	37	0.616667	0.564933	0.004603	20.44
50	45	0.75	0.687081	0.005599	24.86
75	60	1	0.916107	0.007465	33.15
100	73	1.216667	1.114597	0.009083	40.33
125	89	1.483333	1.358893	0.011073	49.17
150	97	1.616667	1.48104	0.012069	53.59

**Table E-21** Effect of Temperature on CH<sub>4</sub> Permeability in Binary Mixture (80%CO<sub>2</sub>-20%CH<sub>4</sub>) Through Membrane M<sub>3</sub> at 8 bar.

Temperature (°C)	Volumetric flow rate Q(ml/min)	Volumetric flow rate Q(cm <sup>3</sup> /s)	Volumetric flow rate @ STP Q <sub>STP</sub> (cm <sup>3</sup> /s)	Flux cm <sup>3</sup> (STP)/cm <sup>2</sup> .s	Permeability (Barrer)×10 <sup>3</sup>
25	32	0.533333	0.488591	0.003981	17.68
50	32	0.533333	0.488591	0.003981	17.68
75	33	0.55	0.503859	0.004106	18.23
100	37	0.616667	0.564933	0.004603	20.44
125	41	0.683333	0.626007	0.005101	22.65
150	44	0.733333	0.671812	0.005474	24.31
25	32	0.533333	0.488591	0.003981	17.68

**Table E-22** Effect of Temperature on CH<sub>4</sub> Permeability in Binary Mixture (60%CO<sub>2</sub>-40%CH<sub>4</sub>) Through Membrane M<sub>3</sub> at 8 bar.

Temperature (°C)	Volumetric flow rate Q(ml/min)	Volumetric flow rate Q(cm <sup>3</sup> /s)	Volumetric flow rate @ STP Q <sub>STP</sub> (cm <sup>3</sup> /s)	Flux cm <sup>3</sup> (STP)/cm <sup>2</sup> .s	Permeability (Barrer)×10 <sup>3</sup>
25	30	0.5	0.458054	0.003733	16.57
50	30	0.5	0.458054	0.003733	16.57
75	31	0.516667	0.473322	0.003857	17.12
100	35	0.583333	0.534396	0.004355	19.33
125	39	0.65	0.59547	0.004852	21.54
150	42	0.7	0.641275	0.005226	23.20
25	30	0.5	0.458054	0.003733	16.57

**Table E-23** Effect of Temperature on CH<sub>4</sub> Permeability in Binary Mixture (40%CO<sub>2</sub>-60%CH<sub>4</sub>) Through Membrane M<sub>3</sub> at 8 bar.

Temperature (°C)	Volumetric flow rate Q(ml/min)	Volumetric flow rate Q(cm <sup>3</sup> /s)	Volumetric flow rate @ STP Q <sub>STP</sub> (cm <sup>3</sup> /s)	Flux cm <sup>3</sup> (STP)/cm <sup>2</sup> .s	Permeability (Barrer)×10 <sup>3</sup>
25	27	0.45	0.412248	0.003359	14.91
50	27	0.45	0.412248	0.003359	14.91
75	28	0.466667	0.427517	0.003484	15.47
100	32	0.533333	0.488591	0.003981	17.68
125	36	0.6	0.549664	0.004479	19.89
150	39	0.65	0.59547	0.004852	21.54
25	27	0.45	0.412248	0.003359	14.91

**Table E-24** Effect of Temperature on CH<sub>4</sub> Permeability in Binary Mixture (20%CO<sub>2</sub>-80%CH<sub>4</sub>) Through Membrane M<sub>3</sub> at 8 bar.

Temperature (°C)	Volumetric flow rate Q(ml/min)	Volumetric flow rate Q(cm <sup>3</sup> /s)	Volumetric flow rate @ STP Q <sub>STP</sub> (cm <sup>3</sup> /s)	Flux cm <sup>3</sup> (STP)/cm <sup>2</sup> .s	Permeability (Barrer)×10 <sup>3</sup>
25	25	0.416667	0.381711	0.00311	13.81
50	25	0.416667	0.381711	0.00311	13.81
75	26	0.433333	0.39698	0.003235	14.36
100	30	0.5	0.458054	0.003733	16.57
125	34	0.566667	0.519128	0.00423	18.78
150	37	0.616667	0.564933	0.004603	20.44

**Table E-25** Selectivity of CO<sub>2</sub> over CH<sub>4</sub> at different temperature for membrane M<sub>1</sub>.

Composition	Temperature	CO <sub>2</sub> Permeability (Barrer)×10 <sup>3</sup>	CH <sub>4</sub> Permeability (Barrer)×10 <sup>3</sup>	Selectivity (PCO <sub>2</sub> )/(PCH <sub>4</sub> )
80% CO <sub>2</sub> 20% CH <sub>4</sub>	25	143.1459838	20.89495	6.85
	50	158.2714309	24.16953	6.55
	75	172.3053509	26.97631	6.39
	100	190.2375819	28.8475	6.59
	125	203.8037046	31.03056	6.57
	150	222.203733	32.90175	6.75
	25	143.1459838	20.89495	6.85
60% CO <sub>2</sub> 40% CH <sub>4</sub>	25	111.6476301	19.33562	5.77
	50	126.7730771	22.6102	5.61
	75	140.8069971	25.41699	5.54
	100	158.7392282	27.28818	5.82
	125	172.3053509	29.47123	5.85
	150	190.7053793	31.34242	6.08
	25	111.6476301	19.33562	5.77
40% CO <sub>2</sub> 60% CH <sub>4</sub>	25	79.68147899	18.08816	4.40
	50	94.80692608	21.36274	4.43
	75	108.8408461	24.16953	4.50
	100	126.7730771	26.04072	4.86
	125	140.3391998	28.22377	4.97
	150	158.7392282	30.09496	5.27
	25	79.68147899	18.08816	4.40
20% CO <sub>2</sub> 80% CH <sub>4</sub>	25	47.87126037	15.28138	3.13
	50	62.99670746	18.55596	3.39
	75	77.03062744	21.36274	3.60
	100	94.96285853	23.23393	4.08
	125	108.5289812	25.41699	4.26
	150	126.9290096	27.28818	4.65
	25	47.87126037	15.28138	3.13

**Table E-26** Selectivity of CO<sub>2</sub> over CH<sub>4</sub> at different temperature for membrane M<sub>2</sub>

Composition	Temperature	CO <sub>2</sub> Permeability (Barrer)×10 <sup>3</sup>	CH <sub>4</sub> Permeability (Barrer)×10 <sup>3</sup>	Selectivity (PCO <sub>2</sub> )/(PCH <sub>4</sub> )
80% CO <sub>2</sub> 20% CH <sub>4</sub>	25	102.3997311	16.5755	6.18
	50	110.5033069	18.04887	6.12
	75	116.0284723	20.07477	5.78
	100	121.1852933	22.46901	5.39
	125	127.078803	24.31073	5.22
	150	131.1305909	27.99417	4.68
	25	102.3997311	16.5755	6.17
60% CO <sub>2</sub> 40% CH <sub>4</sub>	25	79.56238098	15.83881	5.02
	50	87.66595683	17.31218	5.06
	75	93.19112217	19.33808	4.81
	100	98.34794316	21.73232	4.52
	125	104.2414529	23.57404	4.42
	150	108.2932408	27.25748	3.9
	25	79.56238098	15.83881	5.02
40% CO <sub>2</sub> 60% CH <sub>4</sub>	25	56.72503089	14.73377	3.85
	50	64.82860673	16.20715	4
	75	70.35377207	18.23305	3.85
	100	75.51059306	20.62728	3.66
	125	81.40410277	22.46901	3.62
	150	85.45589069	26.15245	3.26
	25	56.72503089	14.73377	3.85
20% CO <sub>2</sub> 80% CH <sub>4</sub>	25	34.07185297	13.81291	2.46
	50	42.17542881	15.28629	2.75
	75	47.70059416	17.31218	2.75
	100	52.85741514	19.70642	2.68
	125	58.75092485	21.54814	2.72
	150	62.80271277	25.23159	2.48
	25	34.07185297	13.81291	2.46

**Table E-27** Selectivity of CO<sub>2</sub> over CH<sub>4</sub> at different temperature for membrane M<sub>3</sub>

Composition	Temperature	CO <sub>2</sub> Permeability (Barrer)×10 <sup>3</sup>	CH <sub>4</sub> Permeability (Barrer)×10 <sup>3</sup>	Selectivity (PCO <sub>2</sub> )/(PCH <sub>4</sub> )
80% CO <sub>2</sub> 20% CH <sub>4</sub>	25	60.77681881	17.68053	3.44
	50	65.19695108	17.68053	3.69
	75	73.4846991	18.23305	4.03
	100	80.66741405	20.44311	3.95
	125	89.50767861	22.65318	3.95
	150	93.92781088	24.31073	3.86
	25	60.77681881	17.68053	3.4375
60% CO <sub>2</sub> 40% CH <sub>4</sub>	25	47.51642198	16.5755	2.87
	50	51.93655425	16.5755	3.13
	75	60.22430227	17.12801	3.51
	100	67.40701722	19.33808	3.49
	125	76.24728178	21.54814	3.54
	150	80.66741405	23.20569	3.48
	25	47.51642198	16.5755	2.87
40% CO <sub>2</sub> 60% CH <sub>4</sub>	25	33.70350861	14.91795	2.26
	50	38.12364089	14.91795	2.56
	75	46.41138891	15.47046	3
	100	53.59410386	17.68053	3.03
	125	62.43436841	19.8906	3.14
	150	66.85450069	21.54814	3.10
	25	33.70350861	14.91795	2.26
20% CO <sub>2</sub> 80% CH <sub>4</sub>	25	20.44311178	13.81291	1.48
	50	24.86324406	13.81291	1.8
	75	33.15099208	14.36543	2.31
	100	40.33370703	16.5755	2.43
	125	49.17397158	18.78556	2.62
	150	53.59410386	20.44311	2.62

## APPENDIX F

### Paper Published and Presented in International Journal and Conference

#### F-1 Papers Published in International Journal

- i) F.Ahmad, H. Mukhtar, Z .Man, B. K.Dutta, Separation of lower hydrocarbon from natural gas through nano-porous membrane using capillary condensation, Chem. Eng. Technol. 9 (2007), 1266– 1273.
- ii) F.Ahmad, H. Mukhtar, Z .Man, B. K.Dutta, A theoretical analysis for non-chemical removal of hydrogen sulfide from natural gas through nano-porous membrane using capillary condensation, accepted for publication in Chem. Eng. & processing (In press).

#### F-2 Paper Presented in Conference

- i) F.Ahmad, H.Mukhtar, Z.Man, B.K.Dutta, Purification of natural gas using membrane: The current status and research trends, 20th Symposium of Malaysian Chemical Engineers, (2006) 645-654.
- ii) F.Ahmad, H.Mukhtar, Z.Man, B.K.Dutta, Predicting separation of carbon dioxide from natural gas by capillary condensation using a nano-porous membrane, 20th Symposium of Malaysian Chemical Engineers, (2006) 635-645.